

Synthesis of multifunctional
glyco-pseudodendrimers and glyco-dendrimers
and their investigation as anti-Alzheimer agents

DISSERTATION

Zur Erlangung des akademischen Grades

Doctor rerum naturalium

(Dr. rer. nat.)

vorgelegt

dem Bereich Mathematik und Naturwissenschaften

der Technischen Universität Dresden

von

M.Tech. Shamila Firdaus

geboren am 08.09.1987 in Jamshedpur, Indien

Eingereicht am 7. Juli 2022

Verteidigt am 8. November 2022

Erster Gutachter: Prof. Dr. Brigitte Voit

Zweiter Gutachter: Prof. Dr. Barbara Klajnert-Maculewicz

Die Dissertation wurde in der Zeit von November 2017 bis Juli 2022
am Leibniz-Institut für Polymerforschung Dresden e. V. angefertigt.

This dissertation was accomplished under the scientific supervision of:
Prof. Dr. Brigitte Voit and Prof. Dr. Albena Lederer

To my father

Table of Contents

	<i>Page</i>
Abstract	v
List of Tables	vii
List of Figures	ix
Abbreviations	xvii
1 Introduction	1
1.1 Objectives of the work	2
1.2 Thesis overview	3
2 Fundamentals and Literature	5
2.1 Alzheimer’s Disease and its impact	5
2.1.1 Neurological diagnosis of AD	7
2.1.2 Histopathology of AD	8
2.1.3 Amyloid precursor protein (APP) and its role in AD	8
2.2. Amyloid Beta (A β) peptide	10
2.2.1 A β peptide	10
2.2.2. Location and function	10
2.2.3 Amyloid hypothesis	11
2.2.4 The mechanism of A β aggregation	13
2.2.5 Amyloid fibrils	16
2.2.6 Toxicity of A β	19
2.3 Research methods to study A β aggregates	20
2.3.1 Models to study the mode of action of aggregates	20
2.3.2 Endogenous A β aggregates and synthetic aggregates	20
2.3.3 Strategies to alter aggregation of amyloids	23
2.4 Treatment and therapeutics	23
2.4.1 Current therapeutics	24
2.4.2 Current therapeutic research	24
2.4.2.1 Reduction of A β production	25
2.4.2.2 Reduction of A β plaque accumulation	25
2.4.2.2.1 Anti-amyloid aggregation agents	25
2.4.2.2.2 Metals	26
2.4.2.2.3 Immunotherapy	26
2.4.2.2.4 Dendrimers as potential anti-amyloidogenic agent	27
2.6 Dendrimers	28
2.6.1 Definition	28
2.6.2 Structure	29

2.6.3 Synthesis	30
2.6.4 Properties	31
2.7 Pseudodendrimers - a sub-class of hyperbranched polymer	32
2.7.1 Definition	32
2.7.2 Structure	34
2.7.3 Synthesis	35
3 Analytical Techniques	39
3.1 Size Exclusion Chromatography Coupled to Light Scattering (SEC-MALS)	39
3.2 Asymmetric Flow Field Flow Fractionation (AF4)	41
3.3 Dynamic Light Scattering	43
3.4 Molecular Dynamics Simulation	43
3.5 Nuclear Magnetic Resonance Spectroscopy	44
3.6 Thioflavin T fluorescence	44
3.6.1 Kinetic analysis	45
3.7 Circular Dichroism Spectroscopy	47
3.8 Atomic Force Microscopy	49
3.9 Cytotoxic assay	51
3.9.1 MTT assay	51
3.9.2 Determining the level of reactive oxygen species	51
3.9.3 Changes in mitochondrial transmembrane potential	52
3.9.4 Flow cytometric detection of phosphatidyl serine exposure	52
4 Experimental Details and Methodology	53
4.1 Details of chemicals/components used	53
4.1.1 Other materials	54
4.1.2 Peptide preparation	54
4.1.3 Buffer preparation	54
4.1.4 Fibril growth conditions	54
4.2 Synthesis and characterization of polymers	55
4.2.1 Synthesis and characterization of pseudodendrimers and dendrimers	55
4.2.1.1 Synthesis of hyperbranched polymer (1)	55
4.2.1.2 Synthesis of protected monomer	55
4.2.1.2.1 bis-MPA acetonide (2)	55
4.2.1.2.2 bis-MPA-acetonide anhydride (3)	56
4.2.1.3 Synthesis of protected pseudodendrimers (4, 6 and 8) and protected dendrimers (10, 12, and 14)	56
4.2.1.4 Deprotection of pseudodendrimers (5,7, and 9) and dendrimers (11,13 and 15)	57
4.2.2 Synthesis of glyco-pseudodendrimers and glyco-dendrimers	57
4.2.2.1 Pentynoic anhydride (16)	58
4.2.2.2 Synthesis of pentinate modified pseudodendrimers (17, 18 and 19) and dendrimers (20, 21 and 22)	58
4.2.2.3 3-Azido-1-propanol (23)	59
4.2.2.4 Mannose propyl azide tetraacetate (24)	59

4.2.2.5 Mannosepropylazide (25)	59
4.2.2.6 Glyco-pseudodendrimers (GI-P) (26, 27 and 28) and glyco- dendrimers (GI-D) (29, 30 and 31)	60
4.3 Analytical techniques and their general details	61
4.3.1 SEC-MALS - Instrumentation, software and analysis	61
4.3.2 AF4 - Instrumentation, software and analysis	61
4.3.2.1 Sample preparation	62
4.3.2.2 Method development for analysis of GI-P and GI-D	62
4.3.2.3 Method development for analysis of A β 40 and its interaction with GI-P and GI-D	63
4.3.3 Batch DLS - Instrumentation, software and analysis	64
4.3.3.1 Sample preparation	65
4.3.4 Theoretical calculations and molecular dynamics simulations	65
4.3.4.1 Ab-initio calculations	65
4.3.4.2 Modelling of the polymer structures	65
4.3.4.2.1 Pseudodendrimers	65
4.3.4.2.2 Dendrimers	66
4.3.4.2.3 Modification of the polymers with special end groups	66
4.3.4.2.4 Preparing of the THF solvent box	66
4.3.4.2.5 Solvation of the polymer structures	66
4.3.4.3 Molecular dynamics simulations	67
4.3.4.3.1 Evaluation of the simulation trajectories	67
4.4 Investigation of interaction of GI-P and GI-D with amyloid beta (A β 40)	67
4.4.1 ThT Assay - Instrumentation and software	67
4.4.1.1 Sample preparation	68
4.4.1.2 Kinetics based on ThT assay- software and data analysis	68
4.4.2 CD spectroscopy - Instrumentation and software	69
4.4.2.1 Sample preparation	69
4.4.3 AFM - Instrumentation and software	70
4.4.3.1 Substrate and sample preparation	71
4.4.3.2 Height determination and counting procedures	71
4.4.3.3 Topography and diameter.	71
4.5 Cytotoxicity	72
4.5.1 Zeta potential	72
4.5.2 Cell culturing	72
4.5.3 Sample preparation	72
4.5.4 MTT assay.	72
4.5.5 Changes in mitochondrial transmembrane potential (JC-1 method).	73
4.5.6 Flow cytometric detection of phosphatidyl serine exposure (Annexin V and PI method)	73
5 Results and Discussion.	75
5.1 Synthesis and characterization of glyco-pseudodendrimers and glyco- dendrimers.	76
5.1.1 Synthesis and characterization of hyperbranched polyester.	78

5.1.2 Synthesis and characterization of pseudodendrimers P-G1-OH, P-G2-OH and P-G3-OH	80
5.1.3 Synthesis and characterization of dendrimers D-G4-OH, D-G5-OH and D-G6-OH.	91
5.1.4 Synthesis and characterization of GI-P and GI-D	96
5.1.4.1 Molecular size determination of GI-P and GI-D using SEC	107
5.1.4.2 Particle size determination using batch DLS	109
5.1.4.3 Apparent densities.	110
5.1.4.4 Molecular size determination of GI-P and GI-D using AF4	111
5.1.5 Molecular dynamics simulation	114
5.2 Investigation of interaction of GI-P and GI-D with amyloid beta (A β 40)	118
5.2.1 ThT Assay.	118
5.2.1.1 Kinetics based on ThT assay.	121
5.2.2 CD spectroscopy	124
5.2.3 Time dependent AF4.	127
5.3.2.1 Separation of A β 40 by AF4.	127
5.3.2.2 A β 40 amyloid aggregation in the presence of GI-P and GI-D	128
5.2.4 AFM	131
5.2.4.1 Height.	133
5.2.4.2 Topography and diameter	136
5.2.4.3 Length.	136
5.2.4.4 Morphology	137
5.2.5 Cytotoxicity.	138
5.2.5.1 MTT assay	139
5.2.5.2 Changes in mitochondrial transmembrane potential	140
5.2.5.3 Flow cytometric detection of phosphatidyl serine exposure.	141
6 Conclusions and Outlook.	143
7 Bibliography	147
Appendix.	169
Acknowledgements.	182
Versicherung	187

Abstract

As the world population is aging, the cases of Alzheimer's Disease (AD) are increasing. AD is a disorder of the brain which is characterized by the aggregation of amyloid beta ($A\beta$) plaques. This leads to the death of numerous brain cells thus affecting the cognitive and motor functions of the individual. Till date, no cure for the disease is available. $A\beta$ are peptides with 40/42 amino acid residues but, their exact mechanism(s) of action in AD is under debate. Having different amino acid residues makes them susceptible to form hydrogen bonds. Dendrimers with sugar units are often referred to as glycopolymers and have been shown to have potential anti-amyloidogenic activity. However, they also have drawbacks, the synthesis involves multiple tedious steps, and dendrimers themselves offer only a limited number of functional units. Pseudodendrimers are another class of branched polymers based on hyperbranched polymers. Unlike the dendrimers, they are easy to synthesize with a dense shell of functional units on the surface. One of the main goals in this dissertation is the synthesis and characterization of pseudodendrimers and dendrimers based on 2,2-bis(hydroxymethyl)-propionic acid (bis-MPA), an aliphatic polyester scaffold, as it offers biocompatibility and easy degradability. Furthermore, they are decorated with mannose units on the surface using a 'click' reaction forming glyco-pseudodendrimers and glyco-dendrimers. A detailed characterization of their structures and physical properties was undertaken using techniques such as size exclusion chromatography, asymmetric flow field flow fractionation (AF4), and dynamic light scattering.

The second main focus of this work has been to investigate the interaction of synthesized glyco-pseudodendrimers and glyco-dendrimers with $A\beta$ 40 peptides. For this task, five different concentrations of the synthesized glycopolymers were tested with $A\beta$ 40 using the Thioflavin T assay. The results of the synthesized polymers which produced the best results of showing maximum anti-aggregation behavior against $A\beta$ 40 were confirmed with circular dichroism spectroscopy. AF4 was also used to investigate $A\beta$ 40-glycopolymer aggregates, which has never been done before and constitutes the highlight of this dissertation. Atomic force microscopy was used to image $A\beta$ 40-glycopseudodendrimer aggregates.

A basic but important step in the development of drug delivery platforms is to evaluate the toxicity of the drugs synthesized. In this work, preliminary studies of the cytotoxicity of glyco-pseudodendrimers were performed in two different cell lines. Thus, this study comprises a preliminary investigation of the anti-amyloidogenic activity of glyco-pseudodendrimers synthesized on an aliphatic polyester backbone.

List of Tables

	<i>Page</i>
2.1 An overview of different species formed during A β fibrillogenesis. Low molar mass oligomers define A β 40/42 dimer to hexamer. High molar mass oligomers represent A β 40/42 aggregates larger than 600 kDa	22
4.1 Details of chemicals and components used	53
4.2 Quantities used in the synthesis of protected pseudodendrimers and dendrimers.	57
4.3 Quantities used in the deprotection of protected pseudodendrimers and dendrimers.	57
4.4 Quantities used in the post-modification of pseudodendrimers and dendrimers	58
4.5 Quantities used in the synthesis of mannose functionalized glyco-pseudodendrimers and glyco-dendrimers	60
5.1 Results of the model calculation of hb-G0-OH	80
5.2 Molecular characteristics of pseudodendrimers G0-G3	89
5.3 Molecular characteristics of dendrimers G4-G6.	94
5.4 Molecular characteristics of glyco-pseudodendrimers and glyco-dendrimers.	108
5.5 Rh values for glyco-pseudodendrimers and glyco-dendrimers determined from Batch DLS in DMAC and PBS	110
5.6 Molar masses of the glyco-pseudodendrimers and glyco-dendrimers determined from AF4 and SEC	113
5.7 Theoretical molecular characteristics of the systems in this work, from molecular dynamics simulations. Both unmodified and mannose-modified pseudodendrimers and dendrimers are simulated with generation number, number of end groups in THF and water.	114
5.8 Rate constant values from Amylofit software obtained for A β 40 at five different concentrations of P-G2-Man.	122
5.9 IC50 and IC70 values [μ M] of glyco-pseudodendrimers in non-cancer HMEC-1 and cancer HeLa human cell lines.	140
Appendix	
1 Mass fraction of aggregates determined from RI detector signals in AF4	184
2 Total number of atoms from MD simulations	184

List of Tables

List of Figures

	<i>Page</i>
2.1 History of Alzheimer's disease: a) The "first" AD-patient Auguste Deter, and b) neurofibrillary tangles, drawings by Dr. Alois Alzheimer.	5
2.2 Molecular design of APP (amyloid precursor protein). Schematic representation of human APP isoforms and the APP-like proteins (APLP), APLP1 and APLP2. APP695 is the most abundant form in human brain, it does not contain KPI domain (Kunitz type serine protease inhibitory)	9
2.3 Human APP proteolytic pathways displaying amyloidogenic and non-amyloidogenic pathways	10
2.4 A paraffin section of brain of an AD patient suffering from progressive dementia for 6 years displaying lesions by Bielschowsky Silver Stain. Neurofibrillary tangles are shown as dark stained structures in contrast to golden brown cytoplasm of adjacent normal neurons (arrows). The letter A in the center shows a senile plaque of amyloid which is surrounded by a circularly arranged abnormal neurites (triangles)	11
2.5 Amyloid cascade hypothesis. Representing a sequence of pathogenic events leading to AD as explained by Selkoe and Hardy. A β (mature fibrils) and oligomers imbalance can injure the synapses and thus cause dementia.	13
2.6 An assembly and possible structures of A β 42 monomers model, low molar mass oligomers, high molar mass oligomers, unit-protofibrils, and protofibrils/fibril	14
2.7 a) The 3D structure of an A β 42 fibril, with the A β 17-42 amino acid residues. Amino acids with positively, negatively, hydrophobic charges and polar residues are displayed blue, red, yellow and blue, respectively. b) Certain families with AD history showed APP mutations within A β sequence	15
2.8 The model of A β 40 fibrils proposed by Petkova et al. (down the fibril axis). a) The β -strands with residues 9–24 and 30–40, hairpin bend from residues 25–29. Aspartate 23 and lysine 28 forms a salt bridge (dotted line). These hairpins stack to form two parallel β -sheets. b) Two hairpin stacks together to form the protofilaments. Thicker fibrils can be formed when two or more protofilaments pack together	17
2.9 a) A schematic of fibrillogenesis process. b) A schematic energy landscape for protein misfolding and aggregation showing different energy states of the protein conformations moving towards its native or misfolded condition	19
2.10 Structural components of a dendrimer where G1, G2 and G3 show the successive generations with T as terminal and D as dendritic units	29
2.11 Dendrimer examples a) second generation PAMAM and, b) fourth generation bis-MPA	30
2.12 Divergent versus convergent growth approaches for the synthesis of a typical fourth generation dendrimer	31

2.13	a) Synthesis of glycerol pseudodendrimers by Haag et al. b) Schematic representation of a hyperbranched polymer with $A\beta_2$ monomer having different branching units terminal (T), dendritic (L) and linear (L). c) A schematic representation of the modification of an AB_2 type hyperbranched polymer by AB_2^* protected monomers to form pseudodendrimer of the first generation.	33
2.14	a) Synthesis of acetonide-protected bis-MPA anhydride chemistry, b) Synthesis of multivalent, dendrimer using click chemistry by Malkoch	36
3.1	Schematic of theoretical background of multi angle laser light scattering	39
3.2	Basic principle of AF4: a) Action of different flows in a channel, b) mechanism during elution. Species having higher diffusion coefficient elute faster	42
3.3	Details of ThT fluorescence a) ThT dye with its specific dimension b) A typical sigmoid ThT curve from the formation of amyloid fibrils c) Scheme of ThT interaction within the fibrils along the fibril axis (left) and perpendicular to it (right) d) Green and orange circles stand for hydrophobic residues able to interact with aromatic rings of the ThT	45
3.4	Basic principle of CD spectroscopy. a) circularly polarized light. b) Plane polarized light, made of 2 components the left handed (L) and right handed (R), c) The relationship between absorption and CD spectra. Band 1 shows a positive CD signal with L absorbed more; band 2 shows a negative CD signal with R absorbed more; band 3 shows no CD signal due to achiral chromophore. d) Far-UV CD spectra showing various types of secondary structure. Solid line, α -helix; long dashed line, anti-parallel β -sheet; dotted line, type I β -turn; cross dashed line extended 3 ₁ -helix or poly (Pro) II helix; short dashed line, irregular structure	47
4.1	Scheme of SEC-MALS-dRI used in this work, comprising of the SEC column coupled to 2 detectors i.e. MALS and dRI. Important quantities obtained are assigned below the respective detectors	61
4.2	Scheme of AF4 setup used in this work coupled to MALS and dRI with online DLS detector. Red box shows the sample preparation involved in this experiment, thermoshaker was used to incubate samples	62
4.3	Graphical representation of the optimized flow profile for GI-Ps and GI-Ds	63
4.4	Graphical representation of the optimized flow profile for $A\beta$ 40 amyloid and its interaction with GI-P/GI-D	64
4.5	Scheme of batch DLS setup	64
4.6	Scheme of the ThT fluorescence setup: the solid arrows indicate the excitation light path, the dashed arrows determine the emission light path.	68
4.7	A schematic representation of CD spectropolarimeter	69
4.8	A schematic representation of AFM instrumentation	70
5.1	Outline of the synthesis strategy for glyco-pseudodendrimers used in this work	76
5.2	Outline of the synthesis strategy for glyco-dendrimers used in this work, performed in the same way as glyco-pseudodendrimers	77
5.3	Synthesis of hyperbranched polyester hb-G0-OH (1) as which serves as a core for next steps	78

5.4	The molecular structure of the hb-G0-OH with terminal (T), linear (L) and dendritic (D) repeating units and the focal group (F)	78
5.5	¹ H NMR structure of hb-G0-OH displaying terminal (T), linear (L) and dendritic (D) methyl groups. Solvent signals have been greyed out.	79
5.6	Reaction scheme for the formation of protected monomer from bis-MPA first forming bis-MPA acetonide (2) and then forming bis-MPA acetonide anhydride (3) (AB* ₂)	80
5.7	¹ H NMR spectrum of the acetonide-protected bis-MPA anhydride (AB* ₂)	81
5.8	¹³ C NMR spectrum of the acetonide-protected bis-MPA anhydride (AB* ₂)	82
5.9	Reaction scheme for the formation of first-generation pseudodendrimer (P-G1-OH) forming bis-MPA acetonide (2) and then forming bis-MPA acetonide anhydride (3) (AB* ₂).	83
5.10	¹ H NMR spectrum showing methyl regions for P-G1-pro in CDCl ₃	84
5.11	¹ H NMR spectrum of the first-generation pseudodendrimer (P-G1-OH). The solvent signal is greyed out	84
5.12	A section of ¹ H NMR spectrum of the first-generation pseudodendrimer (P-G1-OH); peak due to linear units has decreased	85
5.13	Reaction scheme for the formation of second-generation pseudodendrimer (P-G2-OH) involving two steps: first the protection of OH groups of P-G1-OH forming a protected pseudodendrimer P-G2-pro followed by a deprotection step resulting in the formation of pseudodendrimer (P-G2-OH).	86
5.14	¹ H NMR spectrum of the second-generation pseudodendrimer (P-G2-OH)	87
5.15	Reaction scheme for the formation of third-generation pseudodendrimer (P-G3-OH)	87
5.16	¹ H NMR spectrum of the third generation pseudodendrimer (P-G3-OH)	88
5.17	Chromatograms of OH functionalized hb-G0-OH to P-G3-OH, measured with SEC coupled to MALS and dRI detector in DMAC for determination of molar mass (MALS signal at 90°)	90
5.18	Fourth generation dendrimer D-G4-OH displaying 48 OH functional units	91
5.19	Reaction scheme for the formation of fourth-generation dendrimer (D-G4-OH), involving two steps: first the protection of OH groups of PFD-G3-TMP-OH (starting polymer) forming a protected dendrimer D-G4-pro and a deprotection step resulting in dendrimer formation (D-G4-OH)	92
5.20	¹ H NMR of D-G4-pro displaying concerned signals	93
5.21	¹ H NMR of D-G4-OH showing focal (1), terminal (2), linear (3) and dendritic (4) groups	94
5.22	Chromatograms of the three generations of OH functionalized dendrimers D-G4-OH, D-G5-OH and D-G6-OH measured with SEC coupled to MALS and dRI detector in DMAC	95
5.23	Reaction scheme for the synthesis of pentynoic anhydride.	96
5.24	¹ H NMR spectrum of 4-pentynoic anhydride along with ¹³ C NMR spectrum in the inset	97
5.25	Reaction of pseudodendrimers (P-G _x ; x=1 to 3) with 4-pentynoic anhydride forming corresponding generations of pentinate modified pseudodendrimers (P-G _x -pent)	98

5.26	¹ H NMR spectrum of the first generation pentinate (P-G1-pent)	98
5.27	Reaction of dendrimers (D-Gx; x=4 to 6) with 4-pentynoic anhydride forming corresponding generations of pentinate modified dendrimers (D-Gx-pent)	99
5.28	¹ H NMR spectrum for D-G4-pent	100
5.29	Reaction for the synthesis of azidopropanol (23) from 3-bromo-1-propanol and sodium azide	101
5.30	Reaction of α-D-mannose pentaacetate with 3-azido-1-propanol forming mannose propylazide tetraacetate (24)	101
5.31	¹ H NMR spectrum of mannose propylazide tetraacetate (24)	102
5.32	¹³ C NMR spectrum of mannose propylazide tetraacetate (24).	103
5.33	Deprotection of α-D-mannose propylazide tetraacetate (24) to form α-D-mannose tetrahydroxyl propylazide (25) in presence of Amberlite resin.	103
5.34	¹ H NMR spectrum for mannose tetrahydroxyl propylazide (25)	104
5.35	Copper catalyzed click reaction for pseudodendrimers. All post-modified pseudodendrimers (P-Gx-pent) were used with mannose propylazide in THF:water (1:1) in the presence of CuSO ₄ .5H ₂ O and sodium ascorbate forming three generations of glyco-pseudodendrimers (P-Gx-Man; x=1, 2, 3)	105
5.36	¹ H NMR spectrum of P-G1-Man.	106
5.37	Chromatograms of mannose functionalized P-G1-Man, P-G2-Man and P-G3-Man in DMAC with SEC coupled to a LS and RI detectors	107
5.38	Chromatograms of mannose functionalized D-G4-Man, D-G5-Man and D-G6-Man in DMAC with SEC coupled to a LS and RI detectors	108
5.39	DLS in DMAC using 0.2 μm filter for a) G1-Ps b) G1-Ds	109
5.40	DLS in PBS using 0.2 μm filter for a) G1-Ps b) G1-Ds	110
5.41	Comparison of apparent densities of G1-Ps and G1-Ds, showing that G1-Ds have lower densities than G1-Ps for almost similar number of mannose groups on the surface.	111
5.42	AF4 fractograms of a) G1-Ps and b) G1-Ds in PBS buffer showing detector signals (dashed line-RI) and molar masses (symbol) depending on elution time	112
5.43	A comparison of R _h values obtained from online DLS (AF4) between G1-Ps and G1-Ds obtained with AF4 in PBS buffer	113
5.44	Molecular dynamics simulations for different generations of pseudodendrimers (with OH groups) and glyco-pseudodendrimers (with mannose groups).	115
5.45	Molecular dynamics simulations for different generations of dendrimers (with OH groups) and glyco-dendrimers (with mannose groups)	115
5.46	R _g values for a) unmodified pseudodendrimers and glyco-pseudodendrimers b) unmodified dendrimers and glyco-dendrimers; radial distribution function of c) unmodified pseudodendrimers d) unmodified dendrimers e) glyco-pseudodendrimers and f) glyco-dendrimers, as determined from simulation studies in THF	117
5.47	ThT assay of Aβ 40 (50 μM) with different concentrations of a) P-G1-Man b) D-G4-Man. Control data refers to zero concentration of glycopolymer.	119
5.48	ThT assay of Aβ 40 (50 μM) with different concentrations of a) P-G2-Man b) D-G5-Man. Control data refers to zero concentration of glycopolymer.	120

5.49	ThT assay of A β 40 (50 μ M) with different concentrations of a) P-G3-Man b) D-G6-Man. Control data refers to zero concentration of glycopolymer	120
5.50	a) Global fitting by chemical kinetics analysis reveals inhibition through secondary nucleation and elongation. In a perturbed system, to show the main mechanism of inhibition, the results from ThT assay were normalized and fitted under the constraint that deviation was allowed in only one microscopic step. Each column represents one mode of kinetic step and each row represents the repeats of experiments. b) Proposed behavior based on the results of global fitting of kinetic analysis as the fits are better in case of two microscopic processes i.e., inhibition of secondary nucleation and inhibition of elongation at 50 μ M A β 40 (representation of amyloids and pseudodendrimers are not to scale)	123
5.51	CD spectroscopy a) Summary of samples; spectra over different time intervals with heparin in 1 mM PBS buffer b) control (A β 40 at 50 μ M) c) P-G1-Man d) P-G2-Man e) P-G3-Man f) D-G4-Man g) D-G5-Man and h) D-G6-Man	125
5.52	Summary of the secondary structure distributions for A β 40 in presence and absence of Gl-Ps and Gl-Ds, obtained by BeStSel software at 0 h, 1 h, 5 h and 24 h (a) A β 40 (50 μ M) with heparin (0.041mg/ml) (Control), A β 40 (50 μ M) with heparin after addition of (b) P-G1-Man (1 μ M), (c) P-G2-Man (10 μ M), (d) P-G3-Man (2 μ M), (e) D-G4-Man (1 μ M), (f) D-G5-Man (5 μ M) and (g) D-G6-Man (5 μ M) and h) content of β sheets and α helix together	126
5.53	Time dependent separation by AF4 of A β 40 without heparin at room temperature in PBS, normalized RI signals of differently incubated samples vs. elution time showing that the elution behavior changes very slow without the presence of heparin in PBS	128
5.54	a) Fractogram of A β 40 (with heparin) after 5 h of incubation, and b) Mass fraction A β 40 (with heparin) determined at different time interval. The bar encircled with red box highlights the mass fraction of the corresponding fractogram (a).	129
5.55	Percentage mass fraction of the two aggregate fractions for each sample at different time interval determined from RI signal (a) A β 40 (50 μ M) (control) (b) A β 40+P-G1-Man (1 μ M) (c) A β 40+P-G2-Man (10 μ M) (d) A β 40+ P-G3-Man (2 μ M) (e) A β 40+D-G4-Man (1 μ M) (f) A β 40+D-G5-Man (5 μ M) (g) A β 40+D-G1-Man (5 μ M). All the samples contained final concentration of 50 μ M A β 40, 0.041 mg/ml heparin (pH 5.5) and respective final concentrations of Gl-P/Gl-D	130
5.56	Trends of aggregates deduced from AF4 at different elapsed time for Gl-Ps and Gl-Ds along with control A β 40. Solid lines are polynomial fit (order 4)	131
5.57	Interaction of P-G2-Man with A β 40 a) ThT, b) CD and c) AF4. A nice correlation can be seen for the results with P-G2-Man at 10 μ M concentration in all the three experiments	132
5.58	AFM images of a-d) Control of A β amyloid (50 μ M). e-h) A β amyloid with P-G2-Man, with increasing incubation time; we sectioned across white line on single fibrils and calculated the mean diameter: i) Mean heights of A β amyloid at different incubation times, j) mean heights of A β amyloid mixed with P-G2-Man	133

List of Figures

5.59	AFM analysis of P-G2-Man (10 μ M) treated A β amyloid (50 μ M) with increasing incubation time: a-d) AFM images of control with A β amyloid (50 μ M), e-h) AFM images of A β amyloid with P-G2-Man; i) cross section profiles of A β amyloid aggregate on images a–d) (white dotted lines), j) cross section profiles of A β amyloid aggregate with P-G2-Man on images e-h) (white dotted lines); Roughness was calculated with squares of 1 μ m ² at four parts of an AFM image a-h), k) roughness for A β amyloid aggregate, l) roughness for A β amyloid with P-G2-Man.	135
5.60	AFM images a) Higher magnification peak force error image of amyloid fibrils after 20 h of incubation, showing twists pattern in fibrils, b) A β 40 (control) after 20 h incubation showing diameter of 9 nm and (c) A β 40 with P-G2-Man after 20 h incubation showing a diameter of 5 nm.	136
5.61	AFM images for A β 40 solution a) 0 h, b) 2 h, c) 5 h, d) 20 h, and A β 40 solution with P-G2-Man e) 0 h, f) 2 h, g) 5 h, h) 20 h	137
5.62	AFM images showing morphology at 2 h of a) A β 40 and b) A β 40 with P-G2-Man; a) and b) show entanglement marked with red. c) peak force error image for A β 40 showing clumped fibrils. d) Peak force error image for A β 40 with P-G2-Man.	137
5.63	Zeta potential measurements of glyco-pseudodendrimers and glyco-dendrimers in 10 mM phosphate buffer (pH 7.4)	138
5.64	Influence of P-G1-Man, P-G2-Man and P-G3-Man glyco-pseudodendrimers on the viability of a) HMEC-1 and b) HeLa cells after 24-hour incubation	139
5.65	Changes in mitochondrial membrane potential based on cell viability using JC-1 assay, after treatment of a) HMEC-1 and b) HeLa cells with glyco-pseudodendrimers	141
5.66	Influence of glyco-pseudodendrimers on the apoptosis induction in cell lines, estimated by annexin V/propidium iodide assay for HMEC-1 at a) 3 h, b) 24h and for HeLa at c) 3 h, d) 24 h. Quantitative results of the effect of polymers on the level of live, necrotic and apoptotic cells are represented by the mean \pm standard deviation (S.D.) for three independent experiments	142

Appendix

1	¹ H NMR spectrum of bis-MPA acetonide (2)	169
2	¹³ C NMR spectrum of the bis-MPA acetonide (2).	169
3	¹ H NMR spectrum of P-G2-pro	170
4	¹ H NMR spectrum of P-G3-pro	170
5	¹ H NMR spectrum of D-G5-pro	171
6	¹ H NMR spectrum of D-G6-pro	171
7	¹ H NMR spectrum of D-G5-OH.	172
8	¹ H NMR spectrum of D-G6-OH.	172
9	¹ H NMR spectrum of P-G2-pent.	173
10	¹ H NMR spectrum of P-G3-pent.	173
11	¹ H NMR spectrum of D-G4-pent	174
12	¹ H NMR spectrum of D-G5-pent	175
13	¹ H NMR spectrum of D-G6-pent	176

14	Calculation of degree of modification for P-Gx-pent (x=1, 2, 3)	177
15	Calculation of degree of modification for D-Gx-pent (x=4, 5, 6)	178
16	¹ H NMR spectrum of azidopropanol	179
17	¹³ C NMR spectrum of azidopropanol	179
18	¹ H NMR spectrum of P-G2-Man.	180
19	¹ H NMR spectrum of P-G3-Man.	181
20	¹ H NMR spectrum of D-G4-Man	182
21	¹ H NMR spectrum of D-G5-Man	183
22	¹ H NMR spectrum of D-G6-Man	183

List of Figures

Abbreviations

AD	Alzheimer's disease
A β	Amyloid beta
PAMAM	Poly(amidoamine)
BBB	Blood Brain Barrier
PPI	Poly(propyleneimine)
AF4	Asymmetric flow field flow fractionation
CD	Circular Dichroism
ThT	Thioflavin T
AFM	Atomic Force Microscopy
RI	Refractive Index
APOE	Apolipoprotein
ADAS	AD Assessment Scale
MMSE	Mini-mental state examination
PET	Positron Emission Tomography
CSF	Cerebrospinal fluid
CT	Computed tomography
MRI	Magnetic resonance imaging
PHFs	Paired helical filaments
NFT	Neurofibrillary tangle
CERD	Consortium to Establish a Registry for AD
RIP	Regulated intramembrane proteolysis
APP	Amyloid precursor protein
AICD	APP intracellular domain
ADAM	A disintegrin and metalloproteinase
BACE	β -secretase
PS1/2	Presenilin-1/2
APH1b	Anterior pharynx-defective 1
PEN2	Presenilin enhancer 2
ER	Endoplasmic reticulum
NMDA/R	N-methyl-D-aspartate agonists receptor
AChR	Acetylcholinesterase inhibitors
R _h	Hydrodynamic radius
GNAs	Granular non-fibrillar aggregates
ELISA	Enzyme-linked Immunosorbent Assay
bis-MPA	2,2-bis (hydroxymethyl) propionic acid
hb	Hyperbranched polymer
pd	Pseudodendrimer
n	Number of repeating units
AB* ₂	bis-MPA-acetonide anhydride
pro	Protected
pent	Pentinate (terminal alkyne)
Man	Mannose units
G1-pro	Protected first generation pseudodendrimer

Abbreviations

G2-pro	Protected second generation pseudodendrimer
G3-pro	Protected third generation pseudodendrimer
hb-G0-OH	Hyperbranched polymer (zero generation)
P-G1-OH	First generation pseudodendrimer
P-G2-OH	Second generation pseudodendrimer
P-G3-OH	Third generation pseudodendrimer
P-G1-Pent	First generation pentinate
P-G2-Pent	Second generation pentinate
P-G3-Pent	Third generation pentinate
P-G1-Man	First generation glyco-pseudodendrimer
P-G2-Man	Second generation glyco-pseudodendrimer
P-G3-Man	Third generation glyco-pseudodendrimer
PFD-G3-TMP	Polymer Factory Dendrimer-third generation-Trimethylpropane
G3-pro	Protected third generation pseudodendrimer
G4-pro	Protected fourth generation pseudodendrimer
G5-pro	Protected Fifth generation pseudodendrimer
D-G4-OH	Fourth generation dendrimers
D-G5-OH	Fifth generation pseudodendrimers
D-G6-OH	Sixth generation pseudodendrimers
P-G4-Pent	Fourth generation pentinate
P-G5-Pent	Fifth generation pentinate
P-G6-Pent	Sixth generation pentinate
D-G4-Man	Fourth generation glyco-dendrimer
D-G5-Man	Fifth generation glyco-dendrimer
D-G6-Man	Sixth generation glyco-dendrimer
NMR	Nuclear magnetic resonance
MDS	Molecular dynamics Simulation
p-TSA	para-Toluenesulfonic acid
DMAC	N,N-dimethylacetamide
DMSO	Dimethylsulfoxide
DMP	Dimethoxypropane
DCM	Dichloromethane
DCC	Dicyclohexylcarbodiimide
DPTS	Di(2-pyridyl)trisulphide
DCU	Dicyclohexylurea
DMAP	4-Dimethylaminopyridine
THF	Tetrahydrofuran
PBS	Phosphate Buffer Saline
MTT	3-[4,5-dimethylthiazole-2-yl]-2,5-diphenyltetrazolium bromide
ROS	Reactive oxygen species
DHE	Dihydroethidium
DNA	Deoxyribonucleic acid
H ₂ DCF-DA	Diacetate dihydrodichlorofluorescein
BeStSel	Beta Structure Selection Software
PI	Propodium Iodide

1 Introduction

A perfectly healthy brain has approximately 100 billion neurons, with multiple branching and extensions. They carry signals and messages to through the brain, which forms the basis for our memories, emotions, thoughts, sensations, movements and skills. Now, let us imagine not being able to perform any of these. Difficulty in recollecting recent conversations, names or events are often an early clinical symptoms of Alzheimer's disease (AD). Symptoms which occur at the later stages can be impaired communication, confusion, behavioral changes, disorientation, ultimately difficulty in speaking, swallowing and walking. The hallmark pathology of AD is the accumulation of amyloid beta ($A\beta$) plaques covering the neurons in the brain. These $A\beta$ plaque accumulations over many years lead to death of neurons as well as damage to other parts of brain tissue ultimately causing neurological deficit.^[1]

In the past decades, great progress has been achieved towards an improved understanding of the pathogenesis of AD along with its mitigation. Several strategies have been explored in the recent years to intervene with accumulation of $A\beta$ plaques but are unable to go beyond clinical trials. Dendrimers^[2] have been shown to have tremendous potential as anti-amyloidogenic agents but are yet to go into clinical trials. For example, PAMAM^[3,4] and phosphorous dendrimers^[5] have been shown to successively alter amyloid formation. However, they have inherent drawbacks with regards to cytotoxicity due to a high cationic charge density. which interacts strongly with the negative charges on the cell membrane.^{[6][7]} As an alternative, use of glycopolymers and dendritic structures have been studied as they have neutral charges on the surface and have hydrogen bonding tendency.^[8] Functionalization with sugar units on the outer shell of the polymer gives an opportunity for several different kinds of biological interactions due to their ability to form hydrogen bonds. As a result, glyco-dendrimers have been found to be effective as anti-prion protein aggregation agents.^[9] Glyco-dendrimers based on poly-(propylene imine) (PPI), after modification with maltose enables a high functionality with reduced cytotoxicity, which can successfully cross blood-brain-barrier (BBB),^[10] but was not found to be effective towards AD in transgenic mice.^[11] Another PPI dendrimer with maltose units along with further incorporation of histidine molecules^[12,13], showed a significant improvement in biocompatibility and successfully crossed BBB along with prevention of memory decline in AD transgenic mice.^[13] Despite several advantages, dendrimers suffer from certain limitations. First, they have multiple arduous steps in synthesis which costs a king's ransom per ounce. Second, the achievable molar mass and the density of functional groups are limited. This likely affects the protein polymer interaction thereby requiring additional functionalization which further complicates the synthesis. Moreover, dendrimers have limitations with regards to applicability as well as are rather not economically viable. Pseudodendrimers are based on hyperbranched (statistically branched) polymers. Contrary to dendrimers, pseudodendrimers are rather simple to construct from synthetic point of view. Moreover, due to statistical branching, a significantly high molar mass can be achieved along with a dense shell of functional units on the surface. Furthermore, glycopolymers based on pseudodendrimers are more likely to show improved biological interactions owing to high

density of sugar units. A corresponding increase of neutral or negative charges is expected which is advantageous considering the cytotoxicity. Thus, this synthetic strategy could open a new window in the search for practical neuroprotective properties and anti-amyloidogenic agents, being effective yet easy to synthesize with low cost.

The synthesis and functionalization of desired glyco-pseudodendrimers, as well as their bioactivity necessitates a careful choice of the polymer backbone. Polyester scaffolds offer a number of advantages such as easy degradability and biocompatibility and do not display cytotoxicity or immunogenicity. An important class of dendrimers based on 2,2-bis(hydroxymethyl)-propionic acid (bis-MPA) was introduced in early 1990s^[14,15] but they were mainly used for coating applications. Recently, bis-MPA dendrimers and their derivatives have been employed in radiolabeling, bioimaging and catalysis.^[16,17] However, due to their small size, even at higher generations they have limited potential in drug delivery platforms.^[16]

Several synthetic strategies have been proposed to attain large sized bis-MPA dendritic architecture, including the concept of pseudodendrimers, and to have sugar units using the synthetic strategy^[18-22] of ‘click’ reaction to obtain glyco-pseudodendrimers. A combination of these of synthetic strategies^[23] can give rise to bis-MPA pseudodendritic architectures having potential anti-amyloidogenic property. The key point is to synthesize dendritic-like highly branched structure which mimics the properties of dendrimers, but at the same time is relatively easier as well as cheaper to synthesize and which also offers increased biocompatibility.

1.1 Objectives of the work

The present work focuses on the synthesis and characterization of large-sized, high-functionality glyco-pseudodendrimers with a polyester basis having mannose on the surface, as prospective anti-amyloidogenic agents. A combination of different analytical techniques was used to confirm their structure and as well as their ability to interact with synthetic A β 40. The main objectives of this work have been:

1. To synthesize bis-MPA based mannose-decorated glycopolymers: glyco-pseudodendrimers along with glyco-dendrimers for comparison.
2. To undertake a detailed characterization of their structures and physical properties using size exclusion chromatography (SEC) as well as asymmetric flow field flow fractionation (AF4) and dynamic light scattering (DLS).
3. To investigate the interaction of synthesized glycopolymers with A β 40 peptide using different techniques: Thioflavin T (ThT) assay, circular dichroism (CD) spectroscopy, AF4 and atomic force microscopy (AFM).
4. To study the cytotoxicity of the synthesized glyco-pseudodendrimers.

The synthesis of bis-MPA glyco-pseudodendrimers and investigation of their interaction with synthetic A β 40 are the two main aspects discussed in this thesis. Apart from ThT assay, CD spectroscopy and AFM, a highlight of this work is the first-time application of specialized AF4 technique to investigate A β 40-glyco-pseudodendrimers aggregates. An extensive kinetics analysis undertaken based on ThT results shows that glyco-pseudodendrimers alter the amyloid

aggregation by interfering at secondary nucleation and elongation phases. Finally, the toxic behavior of glyco-pseudodendrimers was also studied in two different cell lines-human microvascular endothelial cells (HMEC) and cervical cancer cells (HeLa) showing relatively weak cytotoxicity because of the residual negative charges. Thus, higher generations of novel glyco-pseudodendrimers were successfully synthesized and characterized, and found to be promising as anti-amyloidogenic agents. Moreover, a better understanding of the anti-amyloidogenic activity of such glyco-pseudodendrimers was developed which shall hopefully pave the way for further research and innovation towards an effective cure of AD.

1.2 Thesis Overview

This work primarily focuses on the development of a new subclass of dendrimers i.e. the pseudodendrimers, modification of their structures and decoration of their surface with mannose forming glyco-pseudodendrimers, along with development of their corresponding glyco-dendrimers for comparison. The second focus of this work was to study the interaction of these synthesized pseudodendrimers with amyloid peptide (A β 40), one of the culprits of Alzheimer's. The thesis is divided into 5 chapters. The ongoing chapter, Chapter 1, introduces this work with its specific objectives and provides an overview of the thesis.

Chapter 2 deals with the fundamentals and literature of the important topics involved. It focuses on the impact of Alzheimer disease (AD) in current day and age, its history and pathological role. It also discusses AD's biology in brief, focusing more on the amyloid proteins. Understanding the mechanism of amyloid is important which can further help in the development of futuristic drug candidates. Briefly, it also discusses different current therapeutics research and dendrimers that have been under study recently. It also focuses on explaining the structural aspects of dendrimers and pseudodendrimers.

Chapter 3 involves the different analytical techniques used. It deals with the analytical techniques utilized in this work and their basic principles. Techniques like NMR, SEC-MALS and DLS are used for the synthesis and characterization of polymers synthesized in this work. MDS provides a three-dimensional view of the samples. This work was performed by Dr. Peter Friedel at IPF Dresden. Techniques like ThT fluorescence, CD spectroscopy, AF4 and AFM were used to investigate the interaction of synthesized polymers with A β 40. CD spectroscopy was performed in close collaboration with Dr. Martin Müller and Birgit Urban at IPF Dresden. In AFM, the samples were measured by Dr. Andreas Janke at IPF Dresden. It also, very briefly, discussed the different techniques involved in the cytotoxicity of synthesized pseudodendrimers. Cytotoxicity experiments were performed by Dr. Anna Janaszewska in Department of General Biophysics, Lodz, Poland. The Chapter 4 includes the general experimental details of all the techniques and procedures used in this work.

Chapter 5 deals with the results and discussion in this work. The chapter opens up with a synthesis and characterization of the polymers, three generations of glyco-pseudodendrimers and glyco-dendrimers and intermediate stages using NMR and SEC-MALS. It discusses the results from its interaction with A β 40. ThT fluorescence assay confirms their interaction with

A β 40. AF4-MALS-dRI has been used for the first time to investigate it, which is a novelty to date. CD spectroscopy also confirms the similar behavior.

In summary, three generations of glyco-pseudodendrimers and glyco-dendrimers were successfully synthesized and characterized. Their interaction with A β 40 was also confirmed, with AF4 being involved, for the first time in such study towards clinical application.

This work was carried out under official principal supervision of Professor Brigitte Voit and co-supervision of Professor Albena Lederer. It was also supervised in part by Dr. Dietmar Appelhans. This work was carried out at the Leibniz Institute of Polymer Research Dresden e.V., Germany. This PhD work was funded by the Scholarship Program for the Promotion of Early-Career Female Scientists of TU Dresden. Cytotoxicity experiments were performed at the Department of General Biophysics, Lodz, Poland.

2 Fundamentals and Literature

2.1 Alzheimer's Disease and its impact

When I was a child I always wondered why my grandmother kept forgetting things. Over summer holidays visits, we had to remind her who we are, and on some occasions, she would even address us by her siblings' name. She was able to recall things from her childhood but would forget things that happened a day before. When I was at the university, whenever I visited home I witnessed her condition deteriorate from not being able to recall who I was to forgetting what day it was to becoming completely quiet. During the later stages of her illness and death, I came to know about Alzheimer's disease (AD). I always wondered how it feels when your brain which has stored data for many years starts to lose all the information gradually.

Alois Alzheimer was the first scientist to observe and extensively study a presenile form of dementia in 1901 during his examinations of Auguste Deter. She was a 50-year old woman who showed a strong cognitive impairment. She was disoriented and also suffered from hallucinations. After her death, Alzheimer not only examined her brain histologically but also described several characteristic hallmarks, namely reduction of the cerebral cortex volume together with the presence of extracellular amyloid plaques and intercellular neurofibrillary tangles (NFTs) (Figure 2.1).^[24,25]

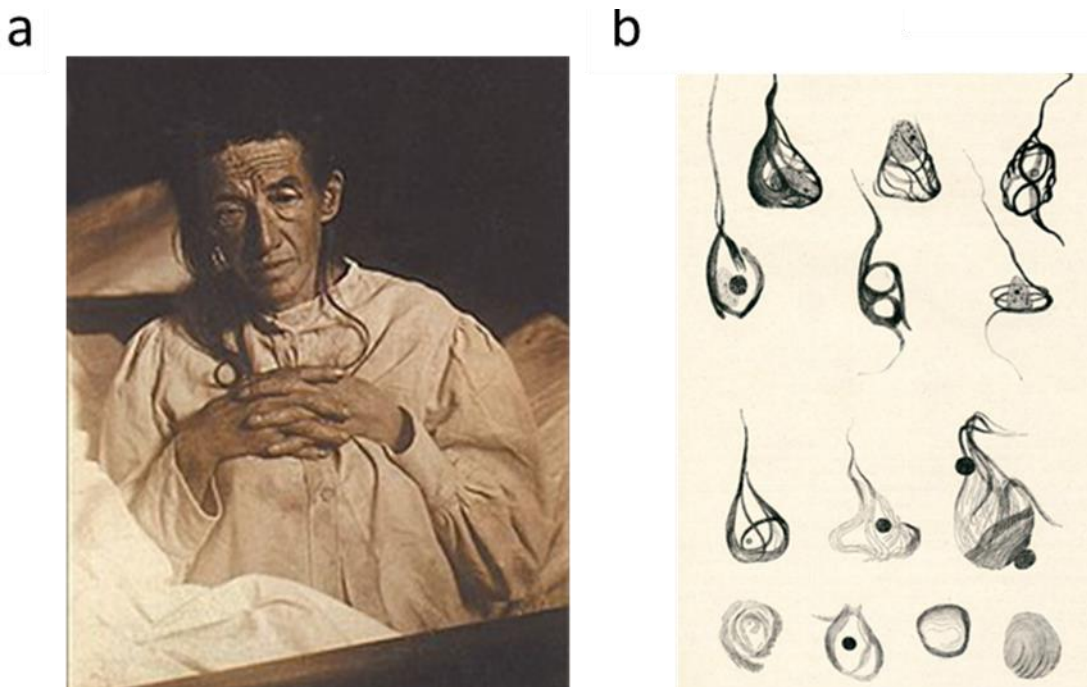


Figure 2.1: History of Alzheimer's disease: a) The "first" AD-patient Auguste Deter. *Reprinted with permission from ref.^[26], Copyright (1997), from Elsevier,* and b) neurofibrillary tangles, drawings by Dr. Alois Alzheimer. *Reprinted with permission from ref.^[27], Copyright (2006), from Elsevier.*

According to World Health Organization (2020), AD and other dementias are the 7th leading cause of death worldwide. Worldwide over 55 million people have been diagnosed, while many others who are unaccounted due to lack of awareness about the disease, geographical or even cultural biases, inaccessible resources and lack of trained professionals. AD is one of the most common cause of dementia in population over the age of 65 or older,^[28,29] and may contribute to 60-70% of all the dementia cases. As per the World Alzheimer Report 2021, the number of people diagnosed with dementia is expected to increase to 78 million in 2030 to 139 million in 2050.^[30]

AD is understood to be developed as a result of multiple factors like genetic, environmental and lifestyle factors, rather than a single cause. Uncommon genetic changes also heavily increase the risk of AD especially the apolipoprotein e4 gene (APOE-e4).^[31,32] Every individual inherits one of the three forms (alleles) of the APOE gene i.e., e2, e3 or e4, from each parent. Having the e4 form of APOE increase one's risk of developing AD compared with having the e3 form, but does not guarantee it. Those possessing the e2 form may decrease the risk compared to those having the e3 form. Those who possess one copy of the e4 form are three times more susceptible to develop AD than those with 2 copies of e3 form, whereas those who come under the maximum risk are the ones with two copies of the e4 form with almost an 8-12 times risk.^[33-35] Different racial and ethnic groups have different combinations of these genes.^[36] Additionally, people with the e4 form are more likely to develop beta amyloid (A β) accumulation, a hallmark of the disease and AD early in life than those with the e2 or e3 forms.^[37] Having a family history of AD is another risk factor, however, it is not requisite for a person to develop the disease.^[38] The importance of any of these factors in risk assessment of development of AD can vary from person to person.

It is important to mention that AD is not a normal part of aging.^[39] People diagnosed with AD exhibit specific symptoms, including memory loss, disorientation, confrontational behavior, language and speech problems and an array of physical and sometimes mental issues altering vision and mobility. For each patient with AD, these symptoms can present in different ways. The development of AD can go through seven stages of cognitive and functional impairment.^[40]

Stage 1: No cognitive decline

In this stage no memory deficit shows up in clinical interview and there are no complaints by the patient.

Stage 2: Age associated memory impairment

In this early stage, patient behaves rather normally and carries out all his/her/their conceptual daily activities, viz., housekeeping, paying bills, etc., but he/she/they develops recent recalls or loss of short-term memory such as difficulty in remembering activities done or event(s) occurred a few days ago or even a few minutes ago and tend to repeat it.

Stage 3: Mild cognitive impairment

In the 3rd stage of AD, cognitive dysfunction is mild in nature. Although patient appears normal, but his/her/their executive functions tend to deteriorate. For example, he/she/they may tend to get lost during driving and shows poor performance at work. These patients become aware of their symptoms and get frustrated but are often reluctant to take help from the family or friends, even when offered.

Stage 4: Mild dementia

In the 4th stage, cognitive dysfunction becomes significant. Patient may forget their own personal history sometimes, are not able to travel or handle finances, and become unable to deal with challenging situations. Again, denial becomes a dominant mechanism in their behavior.

Stage 5: Moderate dementia

In the 5th stage, cognitive dysfunction is severe. Patient cannot take care of themselves without some assistance. They may forget the phone numbers, names of grandchildren, or the name of their high school.

Stage 6: Moderately severe dementia

The patient forgets the name of their caregiver (spouse/children) and remains unaware of the recent events. They still have some sketchy knowledge of their childhood. Sleep pattern is changed along with personality and emotional changes. Patient becomes delusional, and shows anxiety, agitation, and in some cases a violent behavior can also occur, as well as loses willpower.

Stage 7: Severe dementia

In this stage the patient becomes quiet, requires assistance for eating, as well as suffers from incontinence and irregular bowel movements. Motor skills are lost and the brain can no longer function properly.

After an AD diagnosis, the average life expectancy is about seven years (National Institute on Aging, USA).^[41]

2.1.1 Neurological diagnosis of AD

The diagnosis of AD and its differentiation from other forms of dementias is quite challenging because it shows symptoms of general decline of cognitive functions of the brain due to aging.^[42,43] *Ante mortem*, there are different methods or approaches and tools which physicians use to make a diagnosis. Approaches include recording a thorough medical and family history of cognitive and behavioral changes, carrying out problem-solving tests, memory and other cognitive tests (AD Assessment Scale-Cognitive, ADAS), as well as physical and neurologic examinations (“mini-mental state examination”, MMSE).^[44] The physicians also conduct blood tests and brain imaging tests to exclude other potential causes of dementia symptoms, such as a brain tumor or certain vitamin deficiencies. In some circumstances, Positron Emission Tomography (PET) of the brain has been used to determine if the patients have high percentage

of A β .^[45] With the use of a lumbar puncture, the levels of A β and certain types of tau (protein responsible for neurofibrillary tangles) in cerebrospinal fluid (CSF) can be determined.^[46] Computed tomography (CT) and/or magnetic resonance imaging (MRI) can be used to rule out other treatable causes for cognitive decline. *Post mortem* diagnosis is briefly discussed in the following section.

Lack of knowledge and awareness about the disease by general public are the two most significant roadblocks in obtaining a diagnosis of dementia. There are very few countries who have a public awareness campaigns for AD. Nevertheless, there has been an increasing media attention in the recent years.

2.1.2 Histopathology of AD

A histological examination *post mortem*, is the only way to confirm AD. In this method, the brain is examined for the presence of intracellular NFT and extracellular amyloid plaques. Both are lesions comprising of protein fibrils with a high amount of β -pleated sheet structures, which have the predisposition to further aggregate, resulting in microscopic amorphous protein deposits. These protein deposits can be identified histologically using β -sheet-sensitive stains such as Congo Red or Thioflavin S/T.^[47-49] These extracellular deposits of amyloid plaques are mainly made up of short peptide of ~40 amino acids amyloid beta (A β), whereas the intracellular deposits are paired helical filaments (PHFs) which later grow to form intracellular NFTs, comprising of tau (τ) proteins.^[1,50] The occurrence and the density of these lesions serves to assess the different forms of cognitive decline as well as the severity of the disease.

As mentioned earlier the definite diagnosis of AD is only possible *post mortem*. The most common tests are the Braak stages and CERAD-diagnosis (“Consortium to Establish a Registry for AD”).^[51] The resemblance in these diagnostic methods is their dependence on semi-quantitative estimation of the relative content of neuritic plaques and tangles compared to age-matched controls.^[51-53]

2.1.3 Amyloid precursor protein (APP) and its role in AD

Over the last few decades, molecular biological research has enriched our understanding of the pathological basis of AD. Although different genetic origins of the disease have been identified as discussed earlier, all findings point to a common culprit - an increased production and accumulation of A β peptide. This accumulation of A β peptide is derived from proteolytic cleavage of a larger glycoprotein named amyloid precursor protein (APP).^[54,55] A β is formed via post-translational proteolysis from APP^[56] in a process, which is known as ‘regulated intramembrane proteolysis’ (RIP).^[57] The APP gene is found on chromosome 21 that encodes a glycosylated type 1 transmembrane protein with a large N-terminal ectodomain and a short-terminal cytoplasmic domain.^[56] Furthermore, by alternative splicing, the three isoforms of this transmembrane protein are formed with lengths of 695, 751 and 770 amino acids^[58,59] of which the shortest form APP₆₉₅ is expressed in neurons (Figure 2.2).^[60]

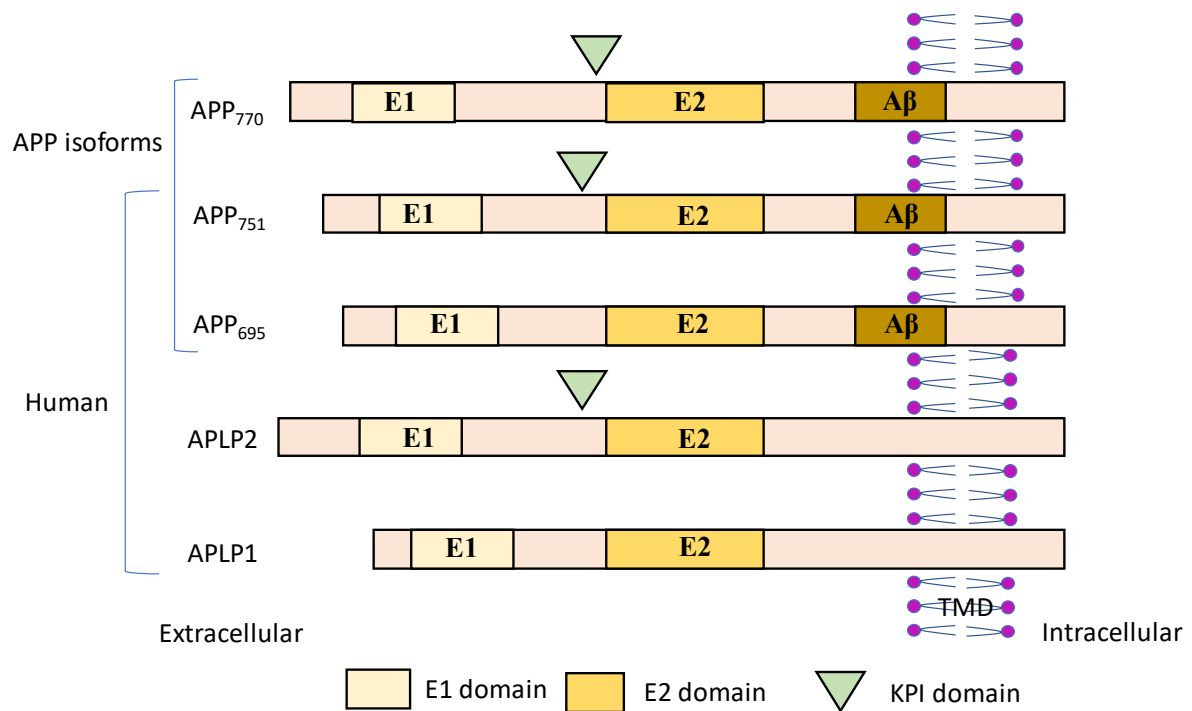


Figure 2.2: Molecular design of APP (amyloid precursor protein). Schematic representation of human APP isoforms and the APP-like proteins (APLP), APLP1 and APLP2. APP695 is the most abundant form in human brain, it does not contain KPI domain (Kunitz type serine protease inhibitory). *Adapted with permission from ref.^[1], Copyright (2017) Springer Nature.*

A β peptides are the product of regulated intramembrane proteolysis. There are two alternative pathways that exist for this: firstly, the non-amyloidogenic pathway, which produces harmless or even neuroprotective peptides^[61] and secondly the amyloidogenic pathway, which produces the aggregation prone A β peptides, the neurotoxic species.^[62] APP is cleaved by at least three enzymes, secretases, in two consecutive steps.^[63] In RIP, a type 1 transmembrane protein is first cleaved at the ectodomain (outside the cell-neuron) and released into the extracellular fluids. The remaining membrane part is then further cleaved into two, forming a second extracellular and a third intracellular fragment.

Firstly, APP is cleaved either by α -secretase (non-amyloidogenic^[64]) between amino acids 16-17 or by sequential cleavages by β - and γ -secretase (amyloidogenic^[65]) at two different sites, which generate α - or β -C-terminal fragments (CTFs), respectively as shown in Figure 2.3. The α -secretase cleaves APP and releases sAPP α from cell surface and leaves behind an 83 amino acid CTF APP fragment (C83). Next, the γ -secretase cleaves C83 by forming P3 and the APP intracellular domain (AICD). The amyloidogenic cleavage of APP by β -secretase releases sAPP β and leaves behind a 99 amino acid CTF (C99). The remnant membrane part C99, is later cleaved by the same enzyme (the γ -secretase complex) at multiple sites to generate different fragments of amino acids that are further cleaved to the main A β forms, the 40- amino acid (A β 40) and the 42-amino acid (A β 42) residues in endocytic part.^[66,67] Several researches have been done on α , β and γ - secretases involved in this proteolysis of APP which lead to the development of different therapeutics as it gives unique targets.^[68]

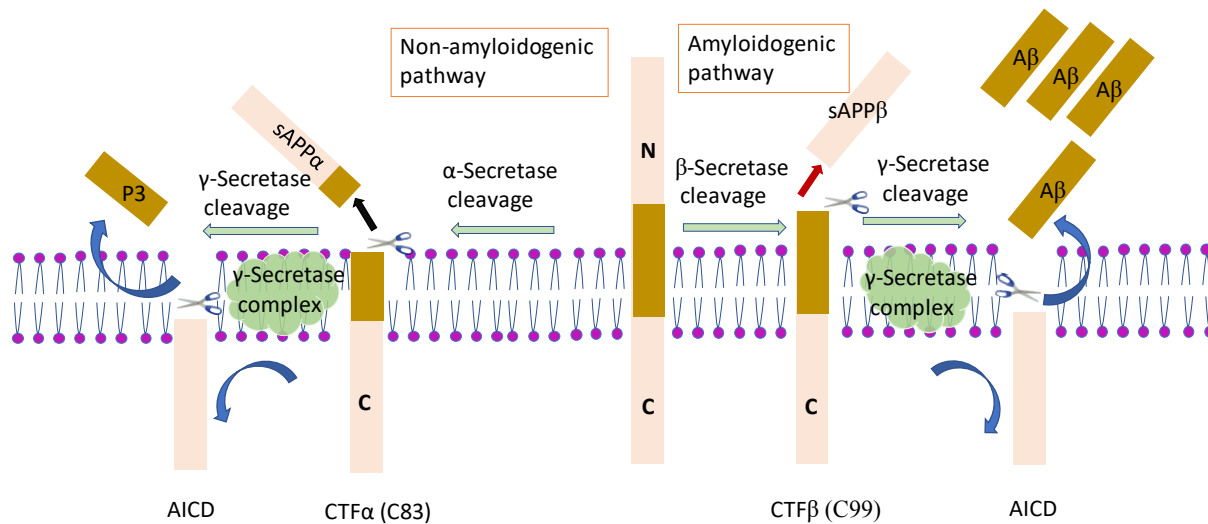


Figure 2.3: Human APP proteolytic pathways displaying amyloidogenic and non-amyloidogenic pathways. Adapted with permission from ref.^[1], Copyright (2017), Springer Nature.

2.2 Amyloid Beta (A β) peptide

2.2.1 A β peptide

Aforementioned A β peptide is a fragment of the protein which is snipped from the APP by different enzymes in the brain. Extracellular amyloid plaques and intracellular NFTs are the two fundamental features of brain afflicted with AD. Almost 90% of the amyloid plaques consist of the aggregated form of A β and is the hallmark of AD.^[69] The amyloid peptides A β 40 and A β 42 are the two main abundant isoforms of A β . The A β 40 is more abundant; however, A β 42 forms fibrils more rapidly and hence its toxicity is much greater than A β 40. Studies of the kinetics aggregation indicate that A β 42 nucleates more rapidly. Despite its lower toxicity, the γ -secretase produces A β 40 10-times more than A β 42. In addition to known forms, shorter fragments have also been identified in CSF. However, this involves a different APP processing pathway. The sequence of A β 40/42 is as follows:

D₁AEFRH₆DSGYEVH₁₃H₁₄QKLVFFAEDVGSNK₂₈GAIIGLMVGGVV₄₀IA₄₂

The A β has a *hydrophobic C-terminal* and a *hydrophilic N-terminal*; the residues 1-10 are disordered; residues 10-12, residues 13-17, and residues 17-21 form the hydrophobic cluster in center and residues 30-40 have a hydrophilic cluster.^[70] NMR studies have revealed a *hairpin like structure* which is discussed later in Section 2.2.4.

2.2.2 Location and function

Most peripheral cells express APP and A β is present in plasma as well as CSF. A β is produced in the endoplasmic reticulum (ER) and Golgi system and then transferred to the plasma membrane where it is cleaved and secreted in the extracellular matrix. The unprocessed part of APP is taken up by endosome where it is cleaved by β -secretases (BACE1) where it is further processed to A β or shuttled back to ER and further to plasma membrane, again to be cleaved.

The extracellular A β can bind to cell surface receptors (NMDA receptors or AChR) and the receptor-A β complex can be internalized into endosomes. These receptors are also an important site for therapeutics. Multivesicular bodies and lysosome accumulates A β intracellularly. A β also accumulates in mitochondria, ER and Golgi bodies where it influences proteasome function.

The level of A β 40 and A β 42 in plasma is normally under 200 pM and 60 pM, respectively. The level of both are higher in patients with AD. A concentration of A β lower than 500 pg/ml (0.1 nM) suggests that A β is accumulating instead of circulating in the brain (CSF).

2.2.3 Amyloid hypothesis

As stated earlier, A β peptides are the major part of amyloid plaques, one of the pathohistological hallmarks of AD (Figure 2.4). Previous studies confirmed that A β peptides are released in extracellular matrix and have a different propensity to aggregate and thus differ in their ability to build up the insoluble amyloid plaques i.e., fibrillar A β 42 and A β 40.^[71] The aggregation propensities of different A β residues (A β 42>>A β 40>>A β 38) correlates with their extracellular appearance in the histopathological lesions.^[72–75] But as outlined earlier, production of A β *per se*^[76] or their intracellular presence in early endosomes^[77–79] is a physiological process in human brain. Therefore, the extracellular A β peptide is responsible for the disease.

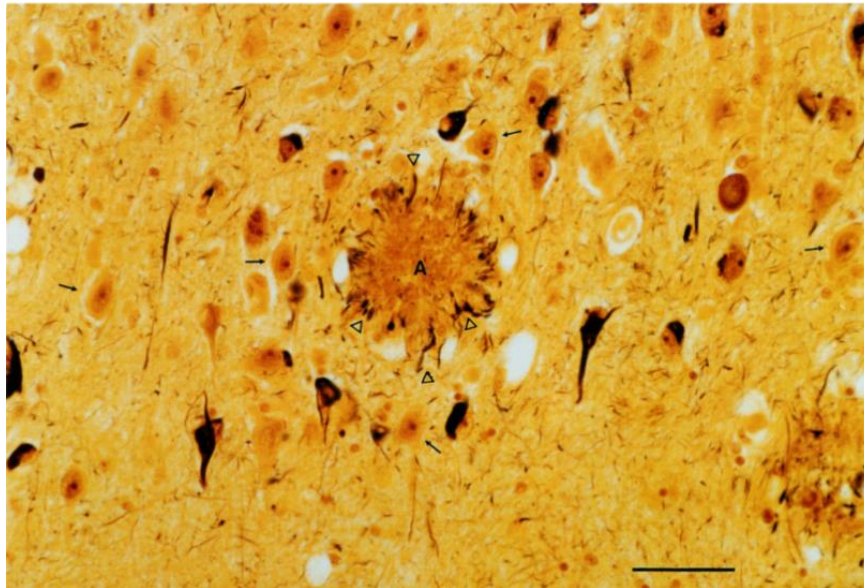


Figure 2.4: A paraffin section of brain of an AD patient suffering from progressive dementia for 6 years displaying lesions by Bielschowsky Silver Stain. Neurofibrillary tangles are shown as dark stained structures in contrast to golden brown cytoplasm of adjacent normal neurons (arrows). The letter A in the center shows a senile plaque of amyloid which is surrounded by a circularly arranged abnormal neurites (triangles). *Reprinted with permission from ref. ^[80], Copyright (1991), Elsevier.*

Nevertheless, overproduction of either all A β peptides, or an increased ratio of A β 42/A β 40, is sufficient to cause AD.^[81] This was proven by several genetic studies, as APP is coded on chromosome 21 and is related to the gene dose, with higher incidence of AD associated with

higher expression levels of APP and A β .^[54,82] Firstly, a few families having been identified as carrying a duplication of the APP-locus alone, also suffer from early-onset AD.^[83] Secondly, in case of familial AD,^[81] mutations in APP, presenilin 1 or 2 (PS1 or PS2) either (i) increase the relative amount of A β 42 generated (PS1 and PS2 mutations or APP mutations at the C-terminus of A β), or (ii) increase the total amount of A β peptides generated (APP mutations at the N-terminus of A β), or (iii) increase the ability of the A β peptides to aggregate (APP mutations in the central part of A β ^[84]).

Overall, amyloid hypothesis positions the aggregating A β peptide as the prime suspect in the pathogenesis of AD (Figure 2.5).^{[80],[85]} However, one weak point arises in amyloid hypothesis, which is the lack of correlation between the amount of A β deposits analyzed *post mortem* and the severity of the disease as assessed by cognitive tests such as MMSE^[86] and ADAS-cog.^[87,88] Sometimes, insoluble A β plaques are even considered to be inert and might play a role in the induction of neuroinflammatory processes as mentioned earlier due their binding behavior to different receptors.^[89] Their presence signifies that the patient has accumulated reserves of proteins which are potentially damaging to the brain and overall health. So, one cannot view them to be neuroprotective.

So, many researches are focused on mature fibrils, the water soluble, oligomeric A β aggregates which are increased in AD patients.^[90] Of these, oligomeric species had shown the best correlation to neuropsychiatric analysis and synapse loss.^[88] These results increased appreciation of importance of soluble, premature A β aggregates in the disease progression of AD. Additionally, the kinetics of A β aggregation was examined to identify the toxic species after it is generated from APP and during the progression until the end stage deposition in amyloid plaques. Even after the knowledge of existence of oligomeric A β ,^[91] the scientific discourse that which A β species is pertinent in AD and other forms of dementia, is still controversial. This probably due to the dynamic and non-linear nature of aggregation and partly due to methodological limitations hampering the identification of natural A β aggregates and partly because of its difference from synthetic ones.^[92,93]

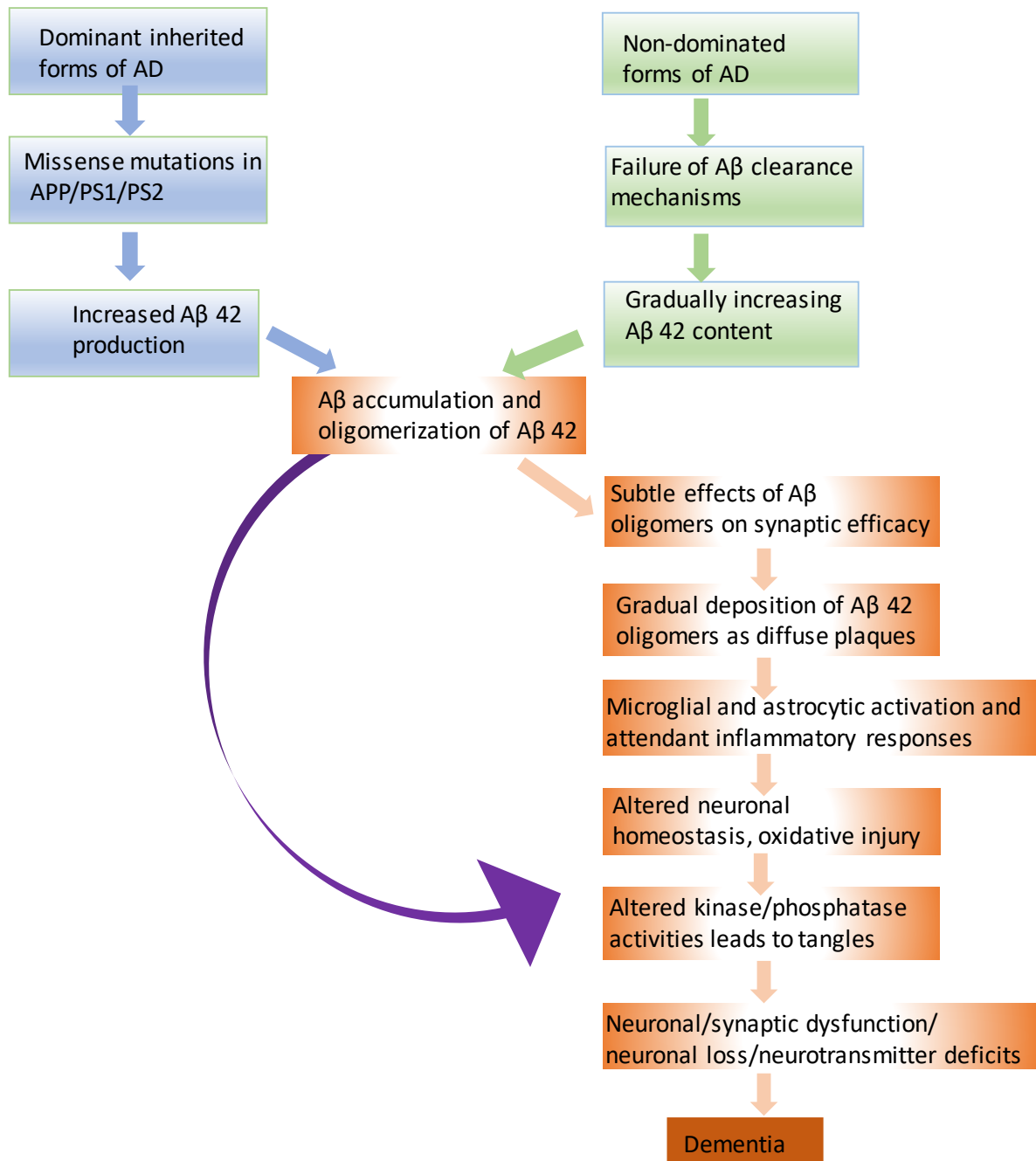


Figure 2.5: Amyloid cascade hypothesis. Representing a sequence of pathogenic events leading to AD as explained by Selkoe and Hardy. Aβ (mature fibrils) and oligomers imbalance can injure the synapses and thus cause dementia. *Adapted from ref. [94], Copyright (2016) John Wiley and Sons.*

2.2.4 The mechanism of Aβ aggregation

A stepwise self-assembly of Aβ aggregation is shown in Figure 2.6, in which the monomer homo-dimerizes, trimerizes and also forms molecules of higher order, termed ‘oligomeric Aβ’, [75,90,95–97] finally leading to mature amyloid fibrils. The Aβ oligomers can be divided into at least two classes: low molecular weight (LMW) and high molecular weight (HMW) oligomers, which could grow to protofibrillar aggregates. [48,91,98–100] Protofibrils are water soluble, metastable and thus can collapse back to oligomeric Aβ or further mature to fibrils,

which are the building blocks for the insoluble amyloid plaques.^[101–104] The mature amyloid fibrils are long unbranched fibers having a repeating substructure of β strand that run perpendicular to the fiber axis. This forms a cross β sheet of unlimited and variable lengths.^[105] Like most other proteins, this “protein misfolding” leads to formation of well-ordered amyloid aggregates.^[106,107]

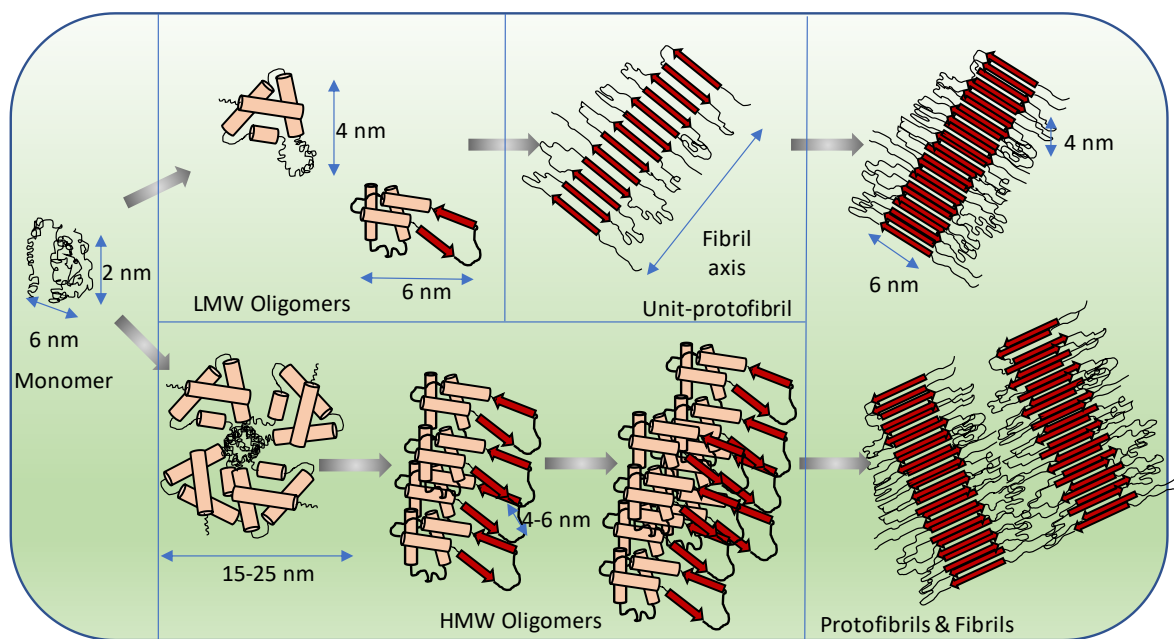


Figure 2.6: An assembly and possible structures of A β 42 monomers model, low molar mass oligomers, high molar mass oligomers, unit-protofibrils, and protofibrils/fibril. Adapted with permission from ref. ^[108], Copyright (2006), from Elsevier.

Kinetic studies have revealed that A β aggregation follows a time dependence of a nucleation dependent process in which nucleating seeds are generated at the beginning of the process.^[95] After a certain threshold concentration has been achieved by these nucleating seeds they begin to propagate faster and fibrillization begins. The growth of these fibrils can be reasonably fast (~ 10 nm/s).^[109–111] Although Figure 2.6 implies an ordered aggregation process from monomeric over oligomeric to fibrillar A β , oligomerization and fibrillization can also occur in separated pathways and coexist.^[112] Kinetic studies have also revealed that because of high kinetic barriers associated with the self-assembly, protein native states may be only metastable with regard to amyloid fibrils.^[113] Monomeric A β 40 and A β 42 have a predominately random coil structure, with short α -helical fragments.^[114] However, a conformational change at C-terminus can transition it into two β -pleated sheet structures, which are separated through a hairpin-like structure (Figure 2.7). The N-terminus is quite flexible.^[108,115,116]

longer needs to be stabilized via salt bridges and thus aggregates faster.^[122] Some of these mutations result in A β peptides which show a higher resistance to proteolytic degradation.^[123,124] Additionally, there are further A β variants which differ at the N-terminus.^[125–127] The loss of N-terminal charge again increases the propensity to aggregate.^[128–130] All these studies suggest that a higher propensity of A β to aggregate predicts a higher pathogenicity in inducing AD, even though the fibrils are not the neurotoxic species.

2.2.5 Amyloid fibrils

As mentioned before, A β is a cleavage product of APP. Amyloid fibrils are basically β -sheet rich peptide and their parallel stacking of β -sheets perpendicular to the axis of the fibril is the characteristic feature. X-ray diffraction reflections of *Ex vivo* fibrils of A β appear at 4.76 and 10–11 Å^[73] and fibrils formed *in vitro* show a diffraction pattern corresponding to cross- β . The signal at 4.7 Å corresponds to the hydrogen bonding between the 15 strands in each sheet and other signal indicates the spacing between different interacting sheets.^[131] A myriad of studies, on shorter segments of A β have been performed revealing their structure and properties.^[74,75,132–136] These studies have revealed that the structure of A β fibrils are affected by peptide sequence, fragment length, and physiological conditions (pH, temperature, etc.). It may also be composed of parallel or antiparallel sheets, extended and/or contain turns, and multiple stacking of variable orders are also likely. Methods like solid-state NMR and cryo-electron microscopy have further helped in characterizing the fibril structure from a number of proteins and peptides.

A fibril model of A β 40 based on solid-state NMR (ssNMR) experiments was proposed by Petkova et al. in 2002.^[135] The ssNMR data revealed that 1–10 amino acid residues are disordered (and are omitted in Figure 2.8). Parallel β -sheets are formed by residues 12–24 and 30–40 via intermolecular hydrogen bonding and residues 25–29 forms a ‘hairpin’ bend in the chain. This hairpin structure brings the side chains of the 2 strands into proximity (Figure 2.9a). These hairpins stack parallel and constitutes the length of the fibril, resulting in a cross- β sheet pattern. Hydrophobic interactions between C-terminal strands determine this parallel packing of hairpins two stacks of hairpins pack to form a protofilament (Figure 2.8b). Mass-per-unit-length measurements suggests that there are 2 peptides within each 4.8 “layers” of the protofilament and by electron microscopy measurements of the smallest fibril diameters of 50±10 Å. They also suggested a mechanism for fibrils with larger diameters (Figure 2.8b). Mature fibrils are made up of about 2–6 protofilaments, slightly twisted around each other, form long unbranched fibers, 7–12 nm in diameter.

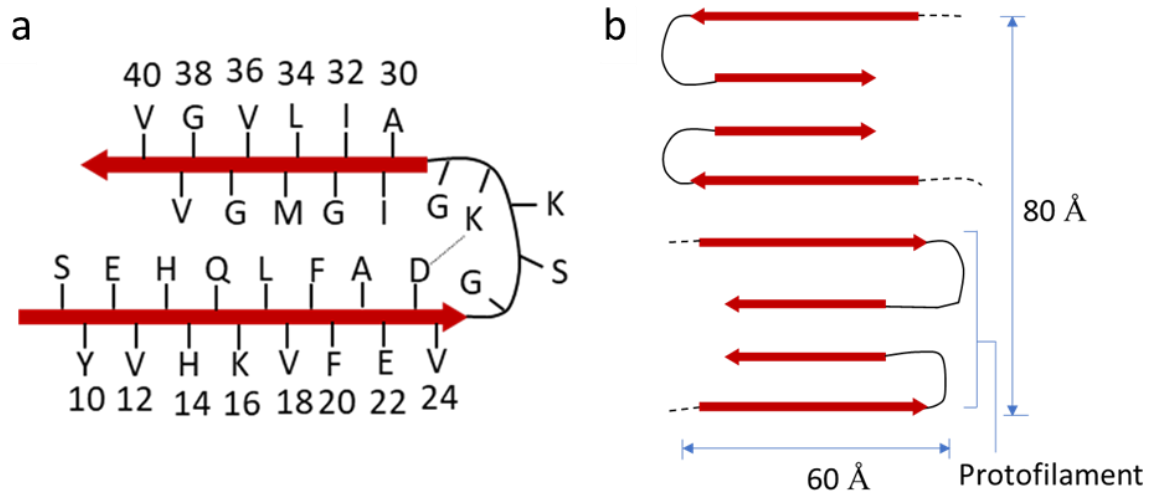


Figure 2.8: The model of A β 40 fibrils proposed by Petkova et al. (down the fibril axis). a) The β -strands with residues 9–24 and 30–40, hairpin bend from residues 25–29. Aspartate 23 and lysine 28 forms a salt bridge (dotted line). These hairpins stack to form two parallel β -sheets. b) Two hairpin stacks together to form the protofilaments. Thicker fibrils can be formed when two or more protofilaments pack together. Adapted with permission from ref. ^[135], Copyright (2002) National Academy of Sciences.

Formation of mature fibrils can be simply described by a sigmoid curve, suggesting a three stage process of nucleation, elongation and equilibrium (Figure 2.9a).^[137] Figure 2.9a shows a schematic of the fibrillogenesis process. During the nucleation the soluble species, usually monomers, associate to form nuclei and the soluble native structures transform to oligomeric species. This is discussed in more detail in Section 2.2.6. During the exponential phase or growth phase the soluble species are arranged at the ends of preformed β sheets leading to the formation of protofibrils which are the initial stable elements in the fibril formation pathway. This is a multiple step process which takes place progressively and is thermodynamically favorable. This phenomenon depends mainly on hydrophobic interactions, backbone hydrogen bonding, stacking interactions irrespective of the specific amino acid residues. Generally speaking, fibril growth mechanisms are of two types: β -sheet elongation and lateral addition. In former type, the fibril extends by adding individual peptides to the end of each β -sheet, and the latter takes place by, adding a preformed β -sheet to the sides. In fibril development both of these mechanisms play an equally important role. The lateral growth of oligomers is followed by longitudinal growth into mature fibrils.^[138] In equilibrium, “or saturation phase”, stable fibers are formed by associating together the already formed fibrils resulting in mature and more stable fibers.^[139] Sometimes the elongation and saturation phases are combined and together referred as “elongation phase”.

Net charge, secondary structure, hydrophobicity and aromatic interactions are the factors responsible for the propensity of proteins and peptides to form amyloid fibrils.^[140] Figure 2.9b shows a schematic energy landscape for protein misfolding and aggregation. It is also suggested that, the aromatic interactions play a pivotal role in favoring, driving and orienting the amyloid fibril formation. This is because of the aromatic residues like tryptophan, tyrosine and phenylalanine in different amyloid peptides and these aromatic residues form short aromatic peptide fragments and are able to form well-ordered amyloid structures by self-assembly.

Sometimes intermolecular stacking interactions in aromatic residues can accelerate the self-assembly process by giving the direction through energy contribution, leading to aggregates.^[141]

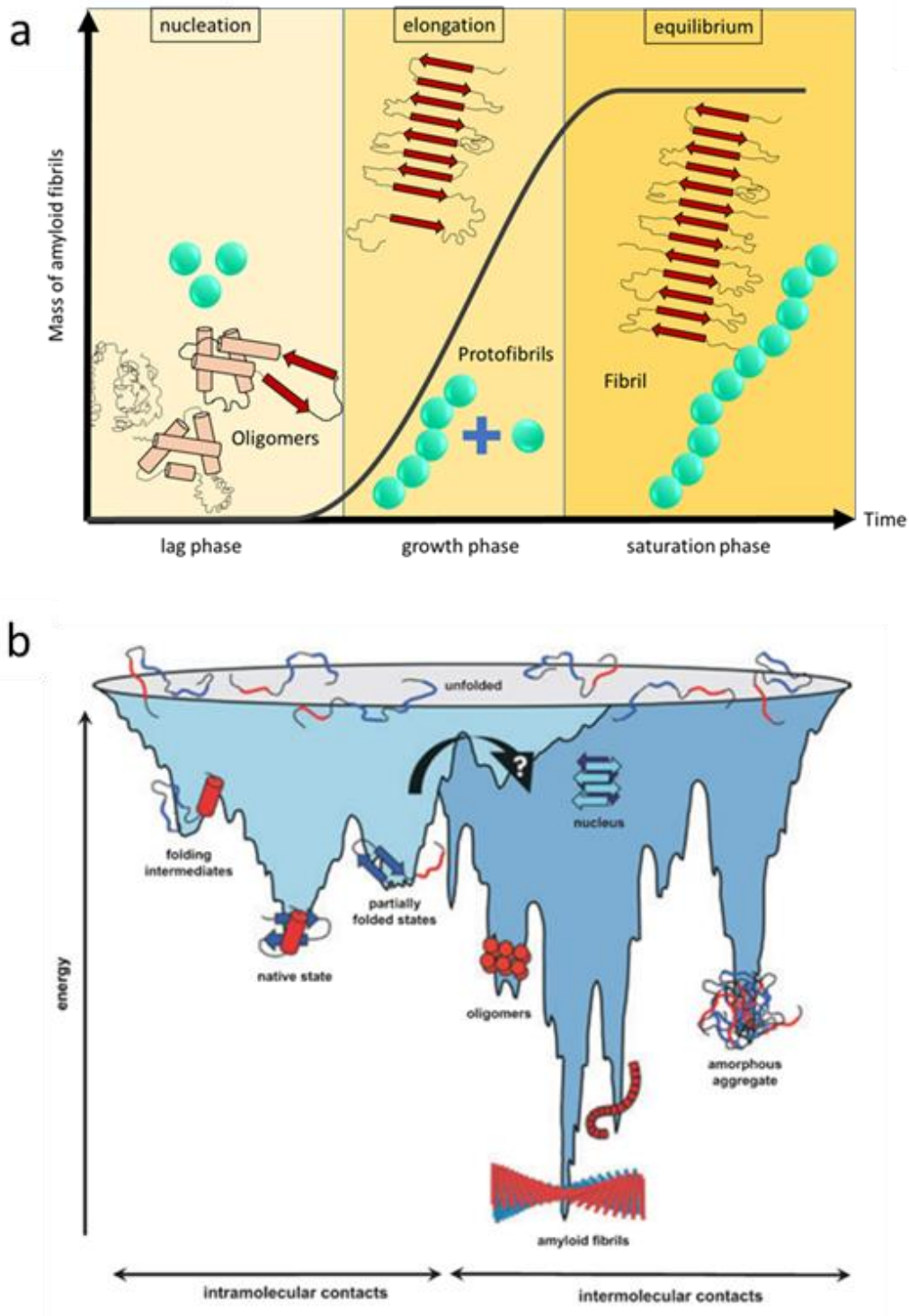


Figure 2.9: a) A schematic of fibrillogenesis process. b) A schematic energy landscape for protein misfolding and aggregation showing different energy states of the protein conformations moving towards its native or misfolded condition. *Reprinted with permission from ref. [142], Copyright (2005), John Wiley and Sons.*

2.2.6 Toxicity of A β

As mentioned earlier, A β is formed during normal cellular metabolism and is present in human brains. Thus, mere presence of A β does not simply cause neurodegeneration, rather neuronal injury takes place because of the ordered self-assembly of A β molecules which becomes neurotoxic.

The role of prefibrillar and fibrillar aggregates in AD pathogenesis is supported by studies based on synthetic A β peptides. Size and relative solubilities are important to differentiate between them. The protofibrils are the true fibrils intermediates so they can both form fibrils and dissociate to low molar mass species. These lower mass species along with protofibrils are often referred to be neurotoxic.^[98,143,144]

A β follows a misfolding pathway in AD to form fibrils which in turn is related to the formation for toxic species. The nucleating event i.e., the lag phase that triggers the fibrillogenesis may follow four proposed pathways:

1. α -helix formation
2. Folding nucleus formation
3. Micelle formation
4. Paranuclei formation

In the first pathway of α -helix formation, soluble A β exists in equilibrium with α -helix and β -sheet secondary structure. The nucleating factor is the change to β -sheet structure, i.e., the fibrils will only be formed after the β -sheet structure has been obtained.^[145]

As per the second pathway i.e., folding nucleus formation, an intramolecular nucleation step in both A β 40 and 42 is implied, where Val24-Lys28 forms a “folding nucleus” by undergoing a turn.^[146]

In the micelle formation pathway, the nucleation will occur through micelles if a critical A β 40 monomeric concentration is reached or exceeded, with a hydrodynamic radii (R_h) of 7 nm. These micelles might act as sites of nucleation and below this critical concentration micelles are not formed and subsequently, nucleation is heterogeneous, with multiple nucleation pathways, perhaps by growing on impurities.^[109] Hence, the last step i.e., paranuclei formation, will always take place irrespective of the micelle formation.

Thereon the oligomers and fibers are formed when the nuclei grow by a series of elongation steps to low molar mass oligomers. Electron microscopy and solid-state NMR have shown that fibrils grown under quiescent conditions can have diameter of 9 ± 1 nm with a periodic twist and are toxic to neuronal cell cultures.^[147] On the other hand, fibrils grown under agitated conditions had a diameter of 5 ± 1 nm, non-twisting and were not toxic to cell cultures.^[147] Once formed, the fibrils further associate to form senile plaques in brains with AD.

The nature by which A β species is toxic was greatly debated initially, but now, thanks to recent advances in AD pathogenesis studies, it is confirmed that the oligomeric species, protofibrils are more toxic and not the fibrils.^[148] However, there is not always a link between the presence of amyloid plaques and cognitive decline. In 2012, Benseny-Cases et al. showed that granular

non-fibrillar aggregates (GNAs) are possible toxic species in AD.^[149] They proposed that A β interacts with oxidized membranes, which are marked by the presence of negative charges on the membrane structure, and therefore a local acidification takes place. This leads to the formation of GNAs, which are capable of disrupting the membrane surface of cells and are potentially toxic.^[149]

However, the relevant mechanisms of their toxicity have still not been fully established.

2.3 Research methods to study A β aggregates

There several methods to study A β aggregates depending on what information is required. The following subsections discusses some of the methods.

2.3.1 Models to study the mode of action of aggregates

In preclinical studies, three different approaches can be carried out to identify the oligomeric species and to address the pathophysiological of A β . First, it can be endogenously extracted and size separated from a deceased AD patient or cerebrospinal fluid.^[90,150,151] A second approach is to develop A β overexpressing mice and cell lines, from which endogenous oligomeric A β can extracted and /or purified.^[152,153] Third, synthetic A β peptide is used in order to allow aggregation to be induced *in vitro* by varying ionic strength, pH and temperature.^[75,96,97,154,155]

2.3.2 Endogenous A β aggregates and synthetic A β aggregates

The presence of soluble A β in AD patients have been demonstrated using buffers in different conditions. Even with saline extraction, A β was detected, mainly in monomeric and dimeric forms.^[156,157] Kuo et al., later extracted A β with a more rigorous centrifugal separation of AD- and control brain samples in a Tris based buffer, free of detergents or chaotropic agents.^[90] Soluble A β ranging in sizes from < 10kD to >100kD was shown by improving methods using different cut-off filters and ultrafiltration combined with ELISA.^[90] Also, using SEC different A β species could be detected in non-denaturing gel electrophoresis and in western blotting.^[158] These “apparent dimer or trimer” decrease dendritic spine density^[159], inhibit long-term potentiation^[160] and impair memory in rats.^[161] Few research works have proved the presence of endogenous A β in transgenic mice. For example, the behavior of tg2576-mouse showed a cognitive decline after six months, which was confirmed by the presence of 56 kDa oligomeric A β species.^[162] Due to the challenges in extraction procedure of “natural” aggregates, synthetic A β aggregates comes in more handy. Hence, only little structural information about “natural” A β aggregates has been reported.

Different synthetic A β aggregates have been described in many works, with regards to different peptide species,^[84,122,158,163] solubilization and aggregation conditions.^[144,164,165] These parameters can lead to different intra and intermolecular interactions, favoring entirely different structural conformations and consequently, different aggregates.^[108,165] Table 2.1 summarizes different methods of preparation from different sources and characterization.^[91,93,166] After identifying the primary sequence of A β , several research groups started working on the synthetic A β peptides to address the aggregation process *in vitro*. In the past, several methods

have been described to obtain A β fibrils,^[74] protofibrils^[48,100] and oligomers.^[96,97,154,155,164] Not only the water insoluble A β fibrils have been identified but the water soluble protofibrils were also identified. However, due to their metastability, these observations turned out to be difficult to reproduce. This metastability, of A β aggregates not only hampers the elucidation of the aggregate structure but also affects the empirical testing of pathological effects.^[99] Kinetic analysis have revealed that the secondary nucleation pathway plays a key role in the proliferation of amyloid fibrils.^[167] Owing to an altered environment (e.g. buffer change, dilution, temperature) a change in molecular interactions can result in a rapid rearrangement of previously characterized A β aggregates.^[158,165,168] Several studies have been made to identify and characterize these soluble intermediates giving rise to a range of molecular sizes, depending on the methods used for their evaluation such as gel electrophoresis,^[96,97] SEC,^[97,169] ultracentrifugation and gel filtration followed by static light scattering methods.^[169] Due to the metastability of A β intermediates, many studies were made on A β mature fibrils using SEC.^[170] Small-angle scattering technique in combination with solid-state NMR have also been used to elucidate the structure of amyloid fibrils.^[171,172] AF4 presents itself as a more gentle and recoverable technique when it comes to polymer/protein separation technologies especially in comparison to SEC, but to the best of our knowledge so far there has only been one known study involving amyloids with AF4.^[173]

To summarize, a huge amount of effort has been made to identify and decipher distinct A β aggregates from synthetic versions to “natural” aggregates. Many of these methods uses purification procedure which later affects the aggregation behavior, e.g., the use of denaturing agents such as SDS or matrix interaction SEC. Imaging methods such as AFM and TEM offer structural information on a molecular scale, but require a high protein concentration and purity. Therefore, it is important to critically evaluate the experimental paradigm to determine whether they affect aggregation per se. Only when stability of the characterized A β aggregate is assured for the duration of the experiment, a deduction to a pathogenic mechanism can be drawn.

Table 2.1: An overview of different species formed during A β fibrillogenesis ^[2,93]. Low molar mass oligomers define A β 40/42 dimer to hexamer. High molar mass oligomers represent A β 40/42 aggregates larger than 600 kDa.

Species	Origin	Preparation/ purification	Characterization	MW (kDa)	Height (nm)	Diameter (nm)	Structure Morphology	Meta- stability	Bioactivity
A β 40, A β 42 ^[108]	S	Freshly dissolved or HFIP dissolved	stAFM, SDS-PAGE, SEC	4	1	-	Unfolded/ hairpin	yes	inactive
A β 38-42 ^[151,160,174]	E	Cell culture (7PA2); AD	SEC-SDS PAGE	4	-	-	-	-	inactive
Pentamers/hexamers ^[165,175]	S	Aqueous A β 42	TEM, stAFM; MS		1.5, 2.5	10-15	Disc-shaped	yes	neurotoxic
Paranucleus ^[163]	S	Crosslinked A β 42	TEM, SDS-PAGE, SEC; DLS	20-24	-	5	spheroidal	yes	neurotoxic
Dimer/ Tetramer ^[144,174]	E	Cell culture (7PA2); AD tissue	SEC, SDS-PAGE	8-16	-	-	-	-	Synaptotoxic: inhibit NMDAR-dependent LTP; impair cognition in vivo
A β *56 ^[153]	E	Mice brain tissue (tg2576)	SEC; SDS-PAGE	~56	-	-	-	-	Impair cognition in vivo
Globulomer ^[155] ^[176]	S	SDS induced aggregation of A β 42 in PBS	SDS-PAGE	~60	-	-	spheroidal	no	Neurotoxic, inhibit LTP
A β O ^[177]	S	HFIP solubilized A β 42 in water	SEC, TEM	~90	-	2-5	spheroidal	no	Neurotoxic, alter CA ²⁺ conductivity
ADDL ^[169]	S	DMSO solubilized A β 42 in Ham's F12	AFM, TEM, SEC-MALS	30-1000	2-7	-	spheroidal	no	Neurotoxic, inhibit NMDAR-dependent LTP; impair cognition in vivo
ASPD ^[178,179]	E	Rotated A β 40/42 solutions	AFM, TEM, AU	150-700	10-15	10-15	spheroidal	no	Neurotoxic by presynaptic mechanism
	S	Immune-purified AD tissue	TEM	-	-	-	-	-	-
Annulus ^[180,181]	S	A β 40, A β 40 _{E22G} in PBS	SEC, TEM, AU	150-250	7-10	7-10	annular	yes	Pore formation
Protofibril ^[48,99,168] (reversed)	S	A β 40, A β 42 in PBS	AFM, TEM, SEC-MALS	>250	3-5, 250	3-5, 250	curvilinear	yes	Neurotoxic, impair neurotransmission in vitro and in vivo
GNA ^[149]	S	A β 40, Hepes buffer+ 0.02%NH ₃ at pH 12	AFM, gel electrophoresis; FTR-IR		0-30 (length)		Amorphous aggregates	pH 5.5-6.5	Neurotoxic (Oxidative stress vascular events, amyloid peptides)

E=from the brain; S= synthetic; ADDL =amyloid derived diffusible ligands; ASPD= amyloid spheroids; GNA = Granular Non-Fibrillar Aggregates

2.3.3 Strategies to alter aggregation of amyloids

As mentioned earlier, the most common variants of A β are A β 40 and A β 42. It is known that A β 42 is more toxic^[182] and faster aggregation as compared to A β 40.^[183] Certain biochemical and molecular simulations studies have shown A β 40 can inhibit aggregation mechanisms.^[175,184] Recent clinical experiments revealed that A β 42/40 ratio was more relevant to the AD pathogenesis than the amount of either A β 42 or A β 40.^[158,185–188] However, in order to fully understand the structure and aggregation mechanism of different A β isoforms, more detailed biophysical evidences are required. A β 40, being slower in aggregation offers a reasonable time window to plan such experiments, which can even be altered on addition of heparin.^[4,189]

An ultimate cure to AD is yet to be ascertained, in spite of the several intensive efforts to face its challenges and the remarkable advances in understanding the mechanisms underlying the pathogenesis that has been made. Protein misfolding and aggregation are the main events on which different therapeutic strategies are currently being investigated, which can be summarized as follows:

1. Inhibition of the amyloidogenic form of proteins by stabilizing the native conformation or by reducing in the formation of misfolded/unfolded structures like certain BACE1 inhibitors^[190–192], acetylcholinesterase inhibitors^[193–195] and N-methyl-D-aspartate receptor agonists (NMDAR).^[196,197]
2. Inhibition of peptide self-assembly in oligomers and fibrils by chaperons^[198,199], natural molecules^[200–202] for example, Polyphenols^[203] and short chain amino acids/peptides,^[201,202,204–207] conjugated polymers^[208,209], polymeric nanoparticles^[210] and dendritic polymers.^{[4,9,211][212–214]}
3. Enhancement in the clearance of toxic aggregates.^[215]

2.4 Treatment and therapeutics

A combination of different factors like age, genetic makeup, diet, environment, and overall general health, is likely to cause AD and not just a single factor. Currently, there are no treatments available which can delay or halt the progression of the disease. As of 2021, there are more than 2700 clinical trials^[216] which are being tested for identification of a possible treatment. But it is not clear if these intervention strategies will prove to be promising in the future. A healthy life style, exercise and a balance diet with a mentally challenging, middle life are preventive measures, but there is a lack of scientific evidence as to whether these recommendations can actually reduce neurodegeneration. Nevertheless, an early diagnosis can help manage the disease better.

2.4.1 Current therapeutics

Currently there is no cure for AD. But there are medicines available that can temporarily give some relief to the patients. There are five drugs for treatment of AD, approved by regulatory agencies such as the U.S. Food and Drug Administration (FDA) and the European Medicines Agency (EMA). Three of which are acetylcholinesterase (AChE) inhibitors^[217] – Donepezil (Pfizer, New York, USA), Galantamine (Janssen, Beerse, Belgium) and Rivastigmine (Novartis, Basel, Switzerland). Acetylcholinesterase inhibitors were developed based on cholinergic hypothesis, i.e., a decrease in acetylcholine – a major neurotransmitter in brain, leads to cholinergic lesions in the neurons. This dysfunction in cholinergic networks interacts with other important physio pathologic aspects of AD – including A β plaques. The AChE inhibitors have proven to be clinically useful by increasing the availability of acetylcholine at synapses. There is a wealth of clinical literature which supports the use of acetylcholinesterase inhibitors. Early start of AChE inhibitors is preferred, for which early diagnosis is required. However, use of AChE inhibitors is associated certain side effects including an increase in rate of heart, etc.

A fourth drug Memantine^[218] (Lundbeck, Valby, Denmark) is an NMDAR antagonist. Neuronal dysfunction and degeneration arise because of NMDAR mediated glutamate excitotoxicity leading to neuronal death characteristic to AD. Glutamate is another most abundant neurotransmitter in the body, and is bound at chemical synapses by the NMDAR, on the membranes of post-synaptic neurons. High levels of calcium ions enter the cells due to excess of glutamate, a number of enzymes are activated, leading to cell death. Thus, NMDAR antagonists prevents excess glutamate binding and subsequent excitotoxicity. Several clinical investigations have shown improvement in cognition and behaviors in patients with moderate to severe AD after 6 months of NMDAR antagonist use.^[218] However, adverse events have also been reported like dizziness, headache and confusion.^[219]

Certain clinical studies on a group of patients with moderate to severe AD showed a significant improvement with use of a combination drugs – memantine (a NMDAR antagonist) and donepezil (a centrally acting reversible acetylcholinesterase inhibitor and structurally unrelated to other anticholinesterase agents). However, the efficacy was not found reproducible in patients with mild to moderate AD.^[220]

It is of interest to note that the drugs currently used for the treatment of AD have weak beneficial effects on cognitive improvement or may offer only some relief to psychological symptoms. There are certain drugs available for the palliative treatment of behavioral and psychological symptoms in AD.^[221] Therefore, the discovery/development of drugs having an effective intervention in the early stages of AD are a ‘medical necessity’.

2.4.2 Current therapeutic research

Since 2003, FDA has not approved any new drug for AD despite many long and expensive clinical trials. Very late starting of therapies, wrong main target of the treatment, inappropriate drug dosage and to some account, misleading understanding of the pathophysiology of AD are some of the possible reasons for such failures. In the near future we can expect an improvement in clinical trials because of global thrust, novel biomarkers, enrollment of patients in early stages of the disease and innovative trial designs.

From previous sections, we now have an understanding that in AD, A β is the prime target for disease modifying therapies. Another target is tau protein but, in this work, it has not been discussed. There is a website to search for different drugs under clinical trials. A search for phases 1, 2, and 3 “recruiting” or “active but not recruiting” clinical trials for AD in clinicaltrials.gov (accessed March 30, 2022) showed 661 outcomes.^[216] The last annual review of the drug development pipeline for AD examined clinicaltrials.gov in May, 2021 (126 agents in 152 trials) and enlists information available for different drug trials at that time: 28 drugs in phase 3 trials, 74 drugs in phase 2 trials, and 24 drugs in phase 1 trials.^[222]

2.4.2.1 Reduction of A β production

As mentioned previously, the inhibition of enzymes such as BACE1 and γ -secretase which leads to the sequential cleavage of APP are considered as a major therapeutic target. Unfortunately, γ -secretase is also associated with other substances and also cleaves various other transmembrane proteins. This fact is responsible for the recent failure in clinical trials with γ -secretase inhibitors: semagacestat,^[223] avagacestat^[224] and tarenflurbil.^[225] So far, no γ -secretase inhibitors are currently being studied in clinical trials.^[226]

Elenbecestat (E2609) in phase 2 and umibecestat (CNP520) in phase 3 are two BACE inhibitors still under study, along with the use of neuroimaging biomarkers.^[226] However, due to unexpected difficulties BACE inhibitors lanbecestat,^[227] verubecestat^[228] and atabecestat^[229] have been discontinued. Etazolate (EHT0202) works by stimulating the nonamyloidogenic α -secretase pathway acting as a selective modulator of γ -aminobutyric (GABA) receptors.^[230] Initially phase 2 trial has shown that the agent was safe and well tolerated in patients with mild to moderate AD. However, further assessment of etazolate in phase 3 trials has not proceeded.

2.4.2.2 Reduction of A β plaque accumulation

2.4.2.2.1 Anti-amyloid aggregation agents

An oral agent scyllo-inositol (ELND005) was the last A β aggregation inhibitor that was tested. It went in phase 2 clinical trials but the results from this study did not provide enough benefit. On the contrary, severe toxicity issues caused infections in some patients, hence the study was discontinued.^[231]

Recently, peptidomimetics are under investigations. Peptidomimetics are specific agents in the form of short peptides that inhibit and partially reverse the aggregation of A β are tested in TEM studies. KLVFF is a peptide sequence that resembles the central hydrophobic part of A β and it mainly prevents the aggregation of A β 42 and can also dissolve oligomers to a limited extent.^[232] The γ -AA peptides are another recently developed peptidomimetics. γ -AA26, appear almost 100-fold as efficient as KLVFF. The *in vivo* studies of these compounds are still in progress.^[233]

2.4.2.2.2 Metals

Metal ions such as iron, copper and zinc and its abnormal accumulation has also been associated with the pathophysiology of AD.^[234] An iron chelating agent, Deferiprone is studied in phase 2 trials in patients with mild and prodromal AD.^[226]

A second generation metal protein–attenuating compound, 5,7-Dichloro-2-((dimethylamino)methyl)quinoline-8-ol / (PBT2) has recently progressed to phase 2 AD trials, because of its promising efficacy in preclinical studies.^[235] In phase 2 study, it succeeded in a 13% reduction of CSF A β and an executive function improvement in a dose-related pattern in people with early AD.^[236]

2.4.2.2.3 Immunotherapy

During the last 15 years, immunotherapy has been one of the strategies that is being studied by pharmaceutical companies.^[237] There are different mechanisms by which it works: first, by direct disassembly of plaques by conformation selective antibodies; second, by antibody-induced activation of microglial cells which can cause dissolution of A β plaques (digestion by cells). Third, by neutralizing toxic soluble oligomers and finally, immunoglobulin M (IgM)-mediated hydrolysis. These approaches can be brought about by active (vaccination) and passive (monoclonal antibodies) immunization. The reasons of failure for active vaccination using human A β 42 (AN1792) in phase 2 trials was the occurrence of meningoencephalitis in 6% of tested patients.^[238] It had mixed response, thereby encouraging more clinical trials. In a recent study of antibody treatment, patients who were administered a primary and booster vaccination in the first year after primary vaccination provided further support for continuation of the investigation. Five other vaccines are being tested for antibodies to bind to A β are CAD-106 (phase 2 and phase 3),^[239] A β vac40 (phase 2),^[240] GV001 (phase 2),^[241] ACC-001 (phase 2a),^[242] UB-311 (phase2)^[243] and LuAF20513 (phase1).^[244]

Due to the adverse effects of active immunization and the variable response to vaccines, passive immunization channeled towards different domains of A β emerged as an alternative immunology treatment. Elan/Wyeth trial of AAB-001 monoclonal antibody (bapineuzumab) entered the phase 3 trial in 2007. Significant benefits were seen in a subgroup of patients who did not have e4 gene. Another passive vaccination LY2062430 (solanezumab) was directed at A β central domain, a humanized monoclonal antibody. Many monoclonal antibodies trials are in phase 3, including aducanumab, gantenerumab and BAN2401 in mild AD.^[245]

Finally, human anti-A β immunoglobulins G (IgG) have been found, intravenous immunoglobulins (IVIg) from blood plasma of healthy donors. This approach went in phase 3 trials in 2009 and displayed good tolerability but lack of efficacy. However, passive vaccination requires repeated infusions and is very expensive, so active vaccinations are always taken into consideration.^[246]

Another strategy which is being explored is the transportation of accumulated A β plaques through BBB. Plasma exchange (PE) with albumin replacement, causing the shift of the existing dynamic equilibrium between plasma and A β in brain is a recent therapeutic method. This is based in the following facts: (1) In AD patients, there are high levels of A β aggregation in brain

and low levels of A β in CSF, (2) the main protein transporter in human body is albumin, (3) albumin has A β -binding ability and albumin can bind up to 90% of A β . Thus, albumin-bound A β would increase the shift of free A β from CSF to plasma to rectify the imbalance between brain and blood A β levels.^[247] PE with several replacement volumes of albumin, is in a phase 3 trial known as AMBAR (Alzheimer's Management by Albumin Replacement).

2.4.2.2.4 Dendrimers as potential anti-amyloidogenic agent

Since the last two decades there has been a growing interest in dendrimers in biomedical field due to their unique control over molecular structure and large number of functional groups.^[248–252] They have shown to be capable of interfering with the formation of amyloid aggregated structures leading to AD and prion diseases, *in vitro*.^[3,5,9,213,253–260] This makes them potentially valuable in the search of anti-amyloidogenic agents. This breakthrough study was done by group of Klajnert showing that PAMAM, phosphorous dendrimers and PPI dendrimers could interfere with aggregation behavior of two amyloid model peptides: A β 28 and A β 40. In this work, the PAMAM dendrimers were used against aggregation of A β 28 and PrP 185-208 peptide using ThT assay complimented with electron microscopy.^[3] According to the ThT assay, at low dendrimer/peptide ratio there is a clear shortening of the nucleation phase, which means that the presence of dendrimer accelerates nuclei formation, but it does not stop it completely. This means that the peptide will still form fibrils at the end of the process. They also used cryo-TEM to see the effect at the end of the process. The results confirmed that low dendrimer/peptide ratio and no dendrimer leads to the formation of fibrils. However, at high dendrimer/peptide ratios, no fibrillar structures were present but only amorphous aggregates were formed, these are “granular non-fibrillar aggregates”.^[149] The intrinsic cell toxicity of these dendrimers, due to high positive electrical charge density, makes it difficult to further check the cell toxicity of these dendrimer/peptide complexes.^[3,4,255,256,261–263]

Another point to be mentioned is that A β 28 and PrP 28 are not toxic to the cells themselves. Not only they are easier to handle in comparison to A β 40, but they serve as a good model for such studies. But studies on A β 40/A β 42 have always been challenging. Significant effort has been done to study the cytotoxicity of these dendrimers by Janaszewska et al.^[264] Later on, similar studies were performed on A β 40 variant as well which showed similar results.^[265]

In general, cationic dendrimers are more haemolytic and cytotoxic than neutral and anionic dendrimers. Therefore, by substituting the cationic charge with hydrogen bond forming oligosaccharides units is one idea of designing the biocompatible dendrimers with anti-amyloid activity.^[213] These dendrimers substituted with oligosaccharides are called glycopolymers/glyco-dendrimers, which have already shown remarkable results concerning cell toxicity.^[214] An example of which is fourth generation maltose PPI dendrimer.^[6] Klementieva et al. studied the aggregation behavior of A β 40 with maltose and maltotriose modified PPI dendrimer which showed similar results as shown by PAMAM and phosphorus dendrimers on A β 28 and PrP185-208.^{[9][266]} Recently, studies with dendrimers are proceeding *in vivo* as well. Lactose coated 5th generation PPI dendrimers in mice was carried out, which showed the preferred retention of dendritic glyco-dendrimers in liver.^[7] Another study, in which a 4th generation maltotriose modified PPI dendrimer was examined in rats to check its predisposition to cross blood brain barrier (BBB).^[267] In a very recent study by Janszewska et

al., the fibrillation mechanism of A β 40 was studied in presence of Cu(II) ions with 4th generation PPI maltose modified dendrimer having sulfate groups.^[268] Another recent work, showed that 4th generation histidine-maltose modified PPI dendrimers significantly improves biocompatibility and their ability to cross the BBB.^[269] Recently, Benseny-Cases et al. showed that there was a significant decrease of early stage oligomeric/granular aggregates by administering an APP/PS1 mice with PPI dendrimers with histidine-maltose shell.^[13] All this point to a common viewpoint that biocompatibility of the dendrimers owing to its structure and its interaction ability with the A β amyloid, are two very important aspects in the search of anti-amyloidogenic agents.

2.6 Dendrimers

2.6.1 Definition

The word ‘dendron’ in Greek means ‘tree like’. Dendrimers have tree-like branches, and are radially symmetrical, Nano-sized, well defined, homogenous and monodisperse. These were first discovered by Vögtle in 1978, Tomalia and co-workers in the early 1980s, and by Newkome, but independently, also in 1980s.^[270–273] They are built around a linear core or a small molecule having symmetric branching units. Dendrimers have a carefully tailored architecture with a compact molecular structure with high end-groups, which can be functionalized, thus modifying their physicochemical or biological properties.^[248,274–279] They are synthesized from branched monomer units in stepwise manner. By choosing appropriate building/branching units and surface end-groups one can have precise control over their molecular shape, dimension, size, density, solubility, polarity and flexibility. This mélange of properties makes them extremely sought after.

Until now, dendrimers have been applied in many fields, such as supramolecular chemistry^[280] or host-guest chemistry^[281], electrochemistry and photochemistry^[282], nanoparticle synthesis^[283], pollution management^[284], dye decolorization^[285], preparation of monomolecular membranes^[286], curing of epoxy resins, catalysis^[287], drug delivery^[288,289], and gene transfection.^[290]

Dendrimers have rather open conformations with internal cavities which makes it possible to encapsulate hydrophobic drug molecules.^[291] As mentioned earlier, their much higher surface functional group density allows to enhance the solubility of many dyes and drugs.^[292,293] Furthermore, dendrimers have also been exploited as neuroprotectors where they are found to significantly suppress the aggregation of prion and amyloid proteins, which has been discussed earlier (Section 2.4.2.2.4).

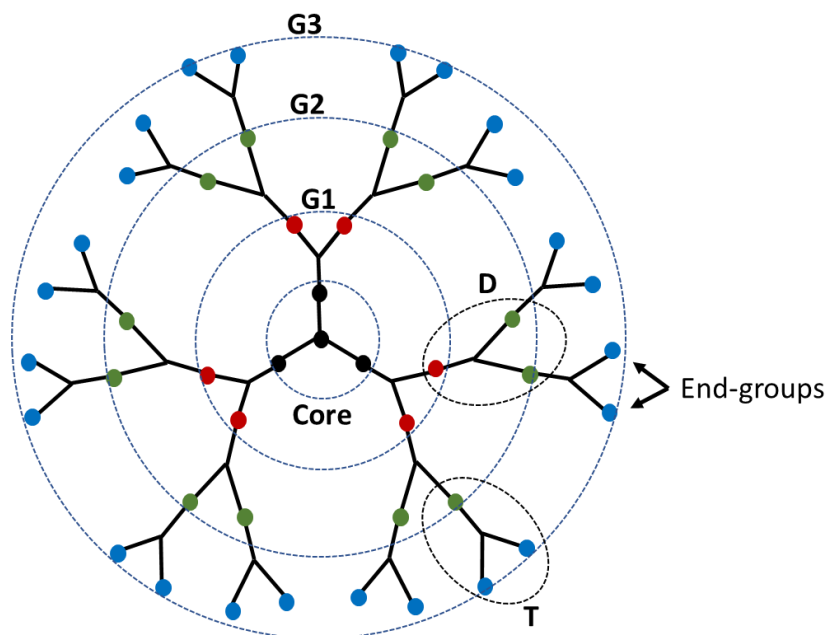


Figure 2.10: Structural components of a dendrimer where G1, G2 and G3 show the successive generations with T as terminal and D as dendritic units. Adapted with permission from ref. ^[23], Copyright (2009), The Royal Society of Chemistry.

2.6.2 Structure

The dendrimers are made up of a central atom or a group of atoms labeled as the core. The core molecule can have different functionality N_c . The functionality each branching site N_b depends on the monomer functionality. These essential data can predict the development of the dendrimer structure. From this central core, the branches called ‘dendrons’ grow through a variety of chemical reactions, resulting in layers of repeat units which are branched. The number of layer when going from the core to the periphery, is the generation number, usually represented by ‘G’. Figure 2.10 shows the structural components of a dendrimer. The number of end groups z increases according to:

$$z = N_c N_b^G \quad (1)$$

The number of repeating units N_r is given by:

$$N_r = N_c \frac{N_b^{G+1} - 1}{N_b - 1} \quad (2)$$

And the molar mass M increases exponentially with every generation:

$$M = M_c + N_c \left(N_r \frac{N_b^{G+1} - 1}{N_b - 1} + M_t N_b^{G+1} \right) \quad (3)$$

where M_c is the mass of the core and M_t the mass of terminal units.

In a branched polymer there are different branching units as terminal (T), linear (L) and dendritic (D), but a dendrimer has only dendritic (D) and terminal (T) units only. They have a theoretical mass distribution of 1 and a degree of branching of 100% corresponding to the presence of only D and T end groups. However, if there are defects certain heterogeneity can occur.

The ‘dendrons’ are a crucial entity of dendrimers, which are monodisperse and wedge-shaped. One can say, a dendrimer is made of at least 2 or more dendrons. Each functional group gives rise to one dendron and these dendrons of higher generations (G4 onwards) can be seen as dendrimers but with an active core that can further be functionalized. Some examples of dendrimers: Tomalia-type PAMAM (Figure 2.11 a)^[294], Frechét-type poly(benzylether)^[294], Newkome’s arborol dendrimers^[273], phosphorus-containing dendrimers^[295] and poly(2,2-bis(hydroxymethyl)propionic acid) (bis-MPA) dendrimer (Figure 2.11b).^[296]

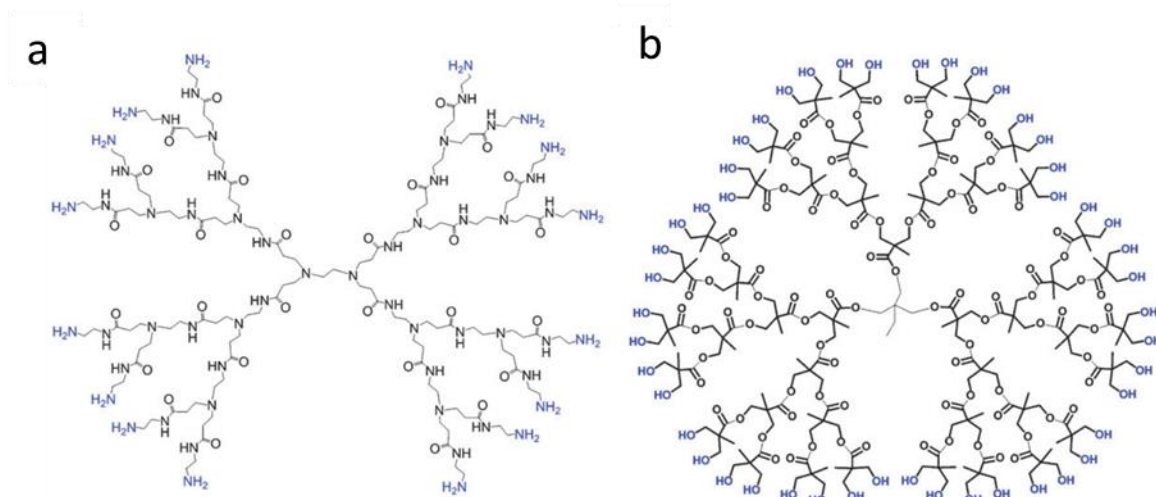


Figure 2.11: Dendrimer examples a) second generation PAMAM and, b) fourth generation bis-MPA. Reprinted with permission from ref.^[231], Copyright (2009), The Royal Society of Chemistry.

2.6.3. Synthesis

Dendrimers are generally prepared using either a divergent route or a convergent route. In divergent route, the dendrimers grow outwards from multifunctional core molecule. The first-generation dendrimer is formed when this core molecule reacts with monomer molecules having one reactive and two dormant groups. After this the new boundary of the resulting molecule is activated for reactions with more molecules. The step is repeated for several generations and eventually, a dendrimer is constructed in a stratified manner. Divergent route is successful for the production of large quantities of dendrimers. Structural defects can occur due to incomplete reactions of end groups and side reactions. To prevent side reactions and to force reactions competition a large excess of reagents is required. It imposes difficulties in the purification procedure of the final product.^[279] In the convergent route, firstly the individual dendrons are synthesized and then coupled to a core molecule. The dendrons are built in the same way as the dendrimers in divergent route using similar protection and deprotection steps, once they have reached the desired generation they can be coupled to the core. Since the dendrons can be much more carefully monitored as their structure is much less complicated, this method has an

advantage over divergent route. However, the coupling to the core can be potentially difficult owing to the steric hindrance. It also does not allow the formation of high generations. The purification steps are easier as the chances of having small sized side products are more due to dendrons. Convergent route serves an important advantage in the preparation of bifunctional dendrimers.

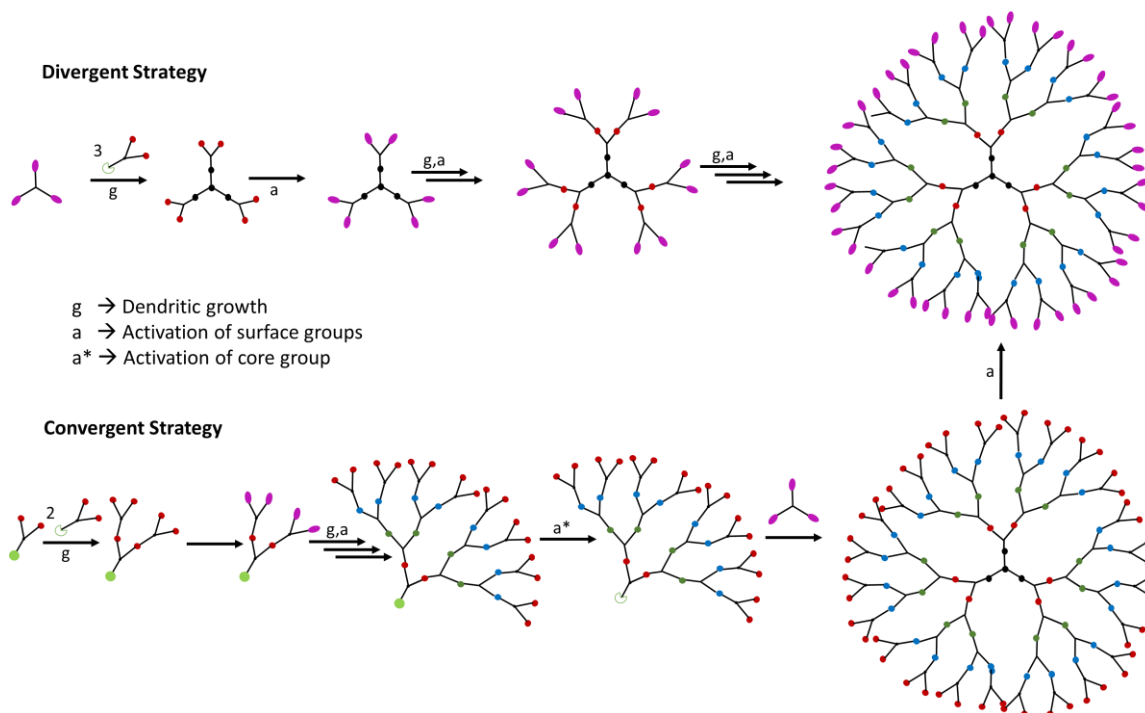


Figure 2.12: Divergent versus convergent growth approaches for the synthesis of a typical 4th generation dendrimer. Adapted with permission from ref. [23], Copyright (2009), The Royal Society of Chemistry.

The dendrimers based on 2,2-bis(hydroxymethyl)-propionic acid (bis-MPA) was introduced by Hult et al. in the 1990s.^[14,296,297] They are one of the most established dendrimers from a synthetic point of view.

2.6.4 Properties

Dendrimers are monodispersed macromolecules; their size and mass can be specifically controlled during synthesis. When compared to traditional linear polymers, dendrimers show improved physical and chemical properties due to their molecular structure. In solution, linear chains exist as flexible coils; in contrast, dendrimers form a tightly packed ball. Dendrimer solutions have significantly lower viscosity than linear polymers. The solubility of dendrimers depends on the surface functional groups, dendrimer generation, repeating units, and even the core.^[248,293] The high density of surface functional groups have potential applications in enhancing the solubility of hydrophobic drugs by electrostatic interactions^[280] and in covalent conjugation of numerous drugs.^[248,298]

A very important feature concerning the synthetic design of dendrimers comes from the idea of comparing these with proteins, and hence, dendrimers are often referred to as ‘artificial proteins’.^[299,300] For over hundreds of millions of years, proteins have always proved to be biocompatible and aids in systemic functions in multicellular organisms, have been even more

beneficial to decorate their surfaces with oligosaccharides (complex carbohydrates). Thus, it is clear, that these ‘sugars’ help in achieving molecular recognition over short distances, such as interactions with the extracellular matrix and with neighboring cells, as well as providing system wide communication (all protein hormones are glycosylated).^[301] These sugar-coated dendrimers are called glyco-dendrimers. Many examples of sugar-coated dendrimers like PPI-mal have potential application as anti-amyloidogenic agents.^[302,303] However, dendrimers has some limitations. On one hand, they are expensive to manufacture involving costly multiple steps, and on the other hand, the achievable molar mass and the possible density of functional end groups is limited.^[304] So, several other low-cost alternative dendritic polymers are being explored.

2.7 Pseudodendrimers - a sub-class of hyperbranched polymers

2.7.1 Definition

The high number of functional groups combined with a special geometry of dendrimers gives many possibilities of potential applications. One such amalgamation is pseudodendrimers, a class of dendritic hybrid, which possesses perfectly branched dendritic units coupled to the end functionalities of a hyperbranched polymers. In the 1990s, hyperbranched polymers became the focus of many researches owing to their easy synthesis in a ‘one pot polymerization’ which can mimic the properties of tediously synthesized dendrimers. The key difference between dendrimers and hyperbranched polymers (hb) lies in their one-pot synthesis method, which limits the control on molar mass and branching accuracy, forming products which are heterogenous with a distribution in molar mass and branching. Several excellent reviews have precisely summed up the different approaches concerning synthesis strategies, properties and application of hb polymers.^[23,305,306] They have excellent thermal stability, solubility when compared to linear polymers, and also have low solution viscosity, modified rheology, and high functionality.^[307,308] Traditionally, hb polymers have commercial interest in coatings, resin formulations and polymer additives.^[309] Their advantages lie in the irregular but dense, highly branched structure, and high level of terminal end groups. This unique feature also gives a possibility for new applications such as in thin films, and therapeutics.^[310,311] Polyesters are of paramount importance, because of the relatively easy availability e.g., Perstorp “Boltorn” products, based on bis(4-hydroxyphenyl) pentanoic acid (BHPPA).^[307] Few more examples of hb polymers suited for coatings and resin application are poly(ethyleneimine)s, polyurethanes^[312] and polyesters from BASF SE.^[313] Hyperbranched polyglycerols,^[314] and self-assembling nanocapsules by Nanotransport Systems^[315] have potential in biomedical applications. Hyperbranched polyester based on bis-MPA by Polymer Factory^[316] also has potential biomedical applications.

Unlike the dendrimers, hb polymers possess a lower degree of branching, fewer functional groups, and lower segmental density, but without a doubt, they are easier to prepare. It would be beneficial to have a high segmental density with a high density of functional groups in hb polymers, close to those of dendrimers.^[306] There are different strategies for increasing number of functional groups as well as the degree of branching, using dendrons,^[317,318] core

molecules,^[319–321] designing special architectures for tandem reactions,^[322] special monomer design^[323] or after complete post-synthetic modification of the functional groups. The latter approach could lead to 100% branching and was used by Frey et al. for polycarbosilanes.^[324] Haag et al. expanded this strategy to polyglycerols and introduced the term pseudodendrimers in 2000 (Figure 2.13a).^[325,326] However, these modifications were limited in the synthesis of first generation.

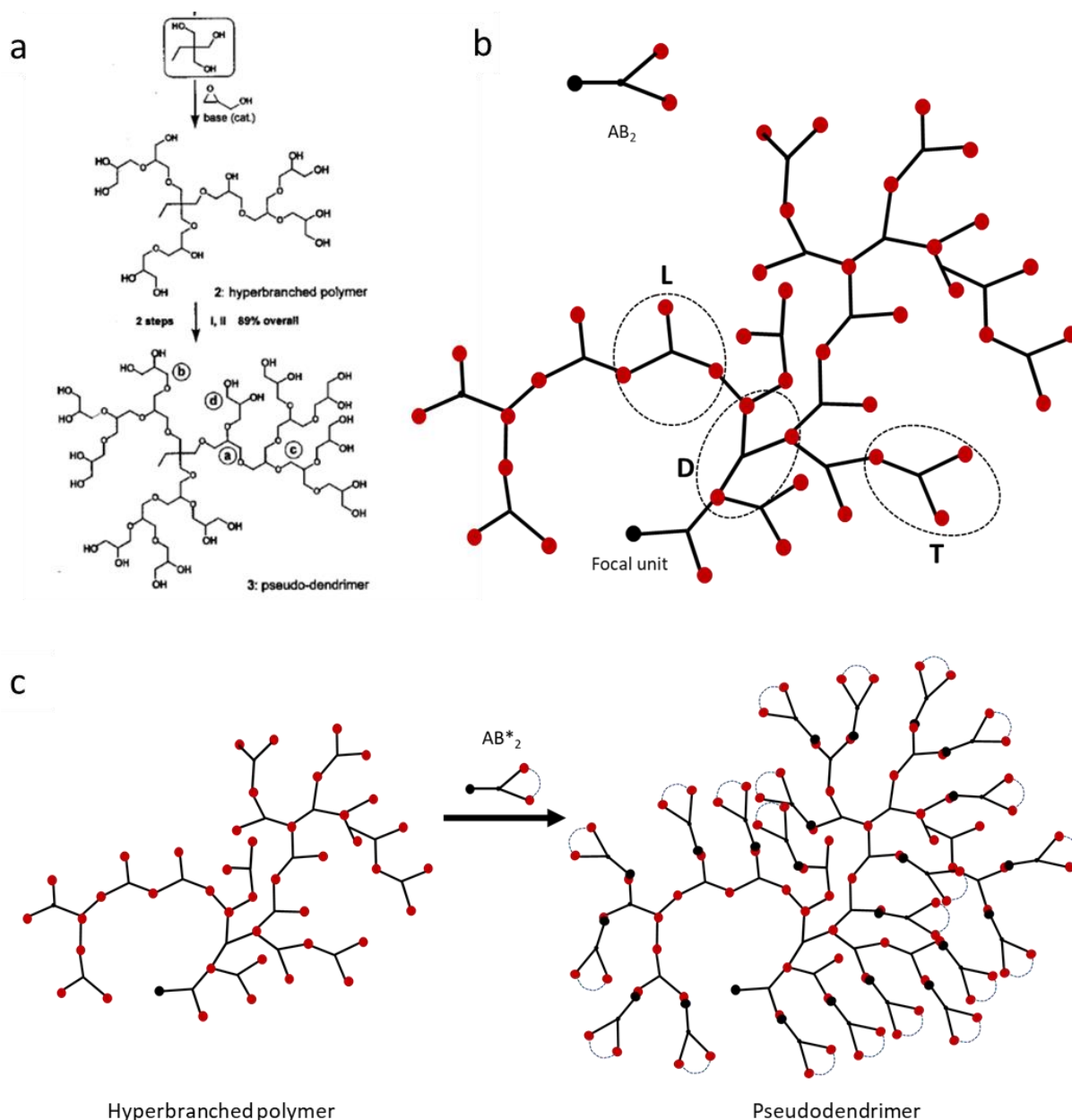


Figure 2.13: a) Synthesis of glycerol pseudodendrimers by Haag et al. Reprinted from ref. ^[326], with permission from *Journal of the American Chemical Society*. b) Schematic representation of a hyperbranched polymer with AB_2 monomer having different branching units terminal (T), dendritic (L) and linear (L). c) A schematic representation of the modification of an AB_2 type hyperbranched polymer by AB_2^* protected monomers to form pseudodendrimer of the first generation. Used with permission of *Royal Society of Chemistry*, from ref. ^[306], Copyright (2015).

A decade later, Lederer et al. developed a method to form higher generations by repeating the modification procedure in a stepwise manner similar to the divergent approach giving a rise in branching up to 100%.^[327] They used 4,4 bis(4'-hydroxyphenyl)pentanoic acid by polycondensation in solution to form the hb core and AB*₂ monomer in which B-functionality were protected with TBDMS forming first-fourth generation pseudodendrimers with approximately 100%-84% degree of branching, respectively. In the succeeding work, they proved the structural differences of these pseudodendritic structures as compared to dendrimers, having a high segmental density, high compactness and high functionality.^[328] Therefore, these type of materials are quite interesting from drug delivery and molecular recognition aspect and form the basis of the work herein from a synthesis point of view.

2.7.2 Structure

As outlined earlier, pseudodendrimers are an amalgamation of dendrimers and hb polymers. It is important to understand the key structural parameters of a hb polymer. In the 1950s, Flory found that highly branched structures are formed with a certain branching degree, before reaching the gel point and produced many great works for its statistics.^[329] If there is a monomer of AB_x (x ≥ 1) type, the combination of both reacting units should prevent gelation under three conditions:

1. If A reacts only with B,
2. No cyclization or side reactions occur,
3. Reactivity of B is independent of the degree of polymerization

When x=2, in monomer AB₂ the one pot synthetic route leads to the formation of three branching units unlike in dendrimers, i.e., terminal (T), linear (L) and dendritic (D), as shown in Figure 2.13b. When the above three conditions are fulfilled, the fraction of three types of polymer units at high conversion are:

$$\frac{L}{L+D+T} \approx 0.5, \frac{D}{L+D+T} \approx 0.25, \frac{T}{L+D+T} \approx 0.25 \quad (4)$$

$$L + D + T \approx DP_n \quad (5)$$

Under ideal conditions, 75% of the polymer units contain B-units, which corresponds to free functional units approximately equal to degree of polymerization (DP_n):

$$z = DP_n - 1 \quad (6)$$

Applying these assumptions on a polycondensation reaction gave rise to statistical branching. Considering a monomer with functionality *f*, in this case A=1 and B=*f*-1. The conversion of the reaction *P_a* and degree of branching was defined as:

$$\alpha = \frac{P_a}{f - 1} \quad (7)$$

Where α is the extent of reaction. However, number of branching units deviates from ideal values due to unwanted side products and cyclization. This leads to a deviation in degree of branching (DB). Based on different types of branching units D, L and T, Kim and Webster^[330] and Hawker et al.^[331] proposed a method to estimate the DB:

$$DB_{Kim} = DB_{Frechet} = \frac{\sum T + \sum D}{\sum T + \sum D + \sum L} \quad (8)$$

So, in case of dendrimers, perfect branching occurs, i.e. DB=1, because dendrimers have no L units. This can describe DB for high molar mass polymer with high degree of polymerization where T is equal to D. But if the polymer is linear, DB would still be high. Another, simplified form for calculation of DB suitable for both high and low molar masses was put forth by Frey et al.^[319] and Yan et al.^[332]:

$$DB_{Frey} = \frac{2 \sum D}{2 \sum D + \sum L} \quad (9)$$

As outlined above, a dendrimer has no L units, so the DB becomes equal to unity. Since, hyperbranched polymers have both L and T units, Larry et al.^[333] found an indirect method to determine DB based on analytical methods to measure the relative amount of these units in their architecture. Several investigations followed NMR spectroscopic methods to identify different branching units and used in the above equations.

The degree of branching for hyperbranched polymers based on ideal conditions and for equal reactivity of B groups in AB₂ is always 0.5. To increase the DB, the L units have to be modified with another AB₂* monomer (functional units are protected or protected monomer) in the next step of synthesis as shown in Figure 2.13c. This strategy will give rise to a branched polymer with high DB and high molar mass and are thus called pseudodendrimers.

Although irregular, this type of modification leads to a complete branching, simultaneously leading to a high number of functional groups showing properties very similar to dendrimers. They are like the ‘ugly cousins’ to the dendrimers. Pseudodendrimers based on polyglycerol architectures were also reported by Lach and Frey, and Caldéron et al. investigated their potential in bio applications.^[305,334,335] Therefore, the pseudodendrimers can possibly overcome the drawbacks of dendrimers with regards to synthesis and functionalization. As with several ‘sugar’ decorated dendrimers have improved biocompatibility, the pseudodendrimers with ‘sugar’ functionality could be show protein interaction.^[336] Glycopolymers based on pseudodendrimers can potentially offer significantly improvements towards alteration of cytotoxic aggregates and thus lead to a more efficient anti-amyloidogenic agent.

2.7.3 Synthesis

In this work pseudodendrimers and dendrimers based on 2,2-bis(hydroxymethyl)propionic acid (bis-MPA) have been explored because of their easy availability from synthetic point of view. Also, they offer a number of advantages such as degradability and biocompatibility along with long shelf life and do not show cytotoxicity or immunogenicity to human cancer cells.^[301,337]

The bis-MPA scaffold in dendrimers and their derivatives show slow degradation at high generations despite the presence of hydrolytic susceptible ester bonds.^[338] This is the reason for successful implementation of dendritic polyesters in radiolabeling, bioimaging and catalysis.^[16,17] Decoration with different sugar units makes them quite useful in bio applications as inhibitory agents towards sugar-recognizing membrane protein, viruses, and bacteria. Previous work on PPI glyco-dendrimers has shown that larger size (5-7 nm diameters) are promising as anti-amyloidogenic agents. Dendrimers based on bis-MPA are commercially available from Polymer Factory, Sweden.

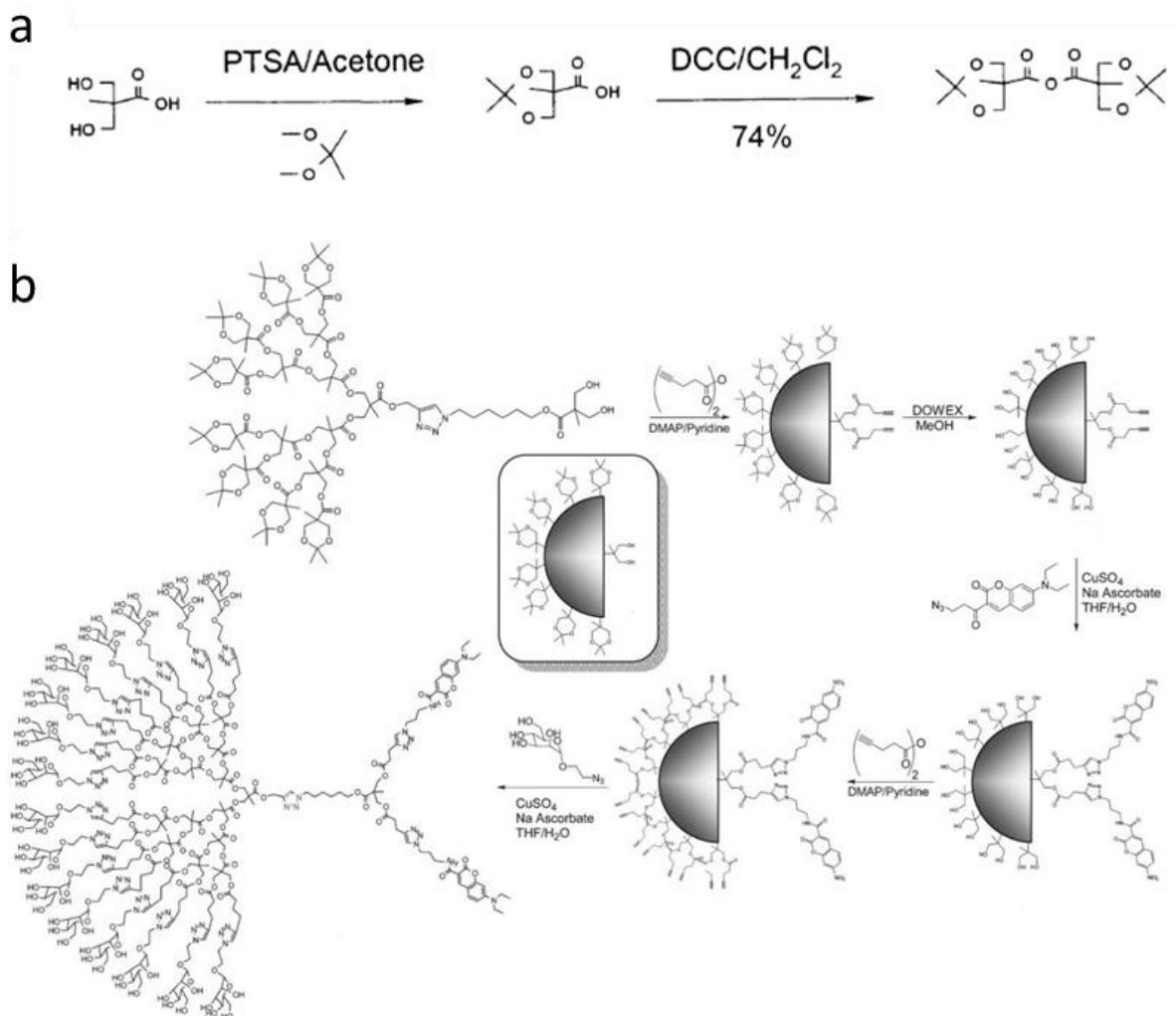


Figure 2.14: a) Synthesis of acetonide-protected bis-MPA anhydride chemistry. Reprinted with permission from ref. ^[19]. Copyright (2002) American Chemical Society. b) Synthesis of multivalent dendrimer using click chemistry by Malkoch. Reprinted with permission from ref. ^[18], Copyright (2002) Royal Society of Chemistry.

In literature, pseudodendrimers until third (first, second and third) generation based on bis-MPA were synthesized using the pioneering work of anhydride chemistry, by Malkoch et al.^[339] Dendrimer of the third generation based on bis-MPA was bought from Polymer Factory, Sweden and the next three generations (fourth, fifth and sixth) were synthesized using the same anhydride chemistry. The reason for choosing higher generations of dendrimers as compared to pseudodendrimers was their similar molar masses, e.g. molar mass distribution of the first

generation pseudodendrimers was similar to molar mass of fourth generation dendrimer, so on and so forth.

To get first insights, both of these bis-MPA architectures (dendritic and pseudodendritic) with high functionality were modified with sugar using well established synthetic route via “click” reaction introduced by Hult, Malkoch (Figure 2.14), and other groups.^[18,20,22,340] Among sugars, mannose was chosen because mannose receptors are present in the surface of monocyte macrophages, alveolar macrophages, astrocytes in brain, etc. Recently, targeting drugs with mannose is a new strategy for mannosylated PPI dendrimer against HIV.^[341] There are enough evidences to show the protein binding nature of mannose,^[342,343] one such great example comes from nature itself, mannose binding lectin (MBL) – a protein produced in the liver, responsible to generate anti-inflammation response in infection and injury.^[344] MBL is also hypothesized to play a role in brain homeostasis and which can also lead to clearance of A β aggregates. Using the above-mentioned advantages of mannose combined with easy synthetic procedures of pseudodendrimers based on bis-MPA, we were able to successfully synthesize three generation of mannose coated pseudodendrimers and prove its affinity to a plant protein, Concanavalin A.^[336]

3 Analytical Techniques

3.1 Size Exclusion Chromatography Coupled to Light Scattering (SEC-MALS)

In case of highly branched polymers, the methods for the determination of molar mass based on colligative properties fail because of increasing molar mass these techniques reach their limits. Size exclusion chromatography (SEC) with different detectors such as light scattering (LS), concentrations, usually refractive index (RI) and viscosity detectors can be used to obtain a vast array of information. The ability of a molecule to scatter light is related to the polarizability, which is directly proportion to the specific refractive index increment (dn/dc).

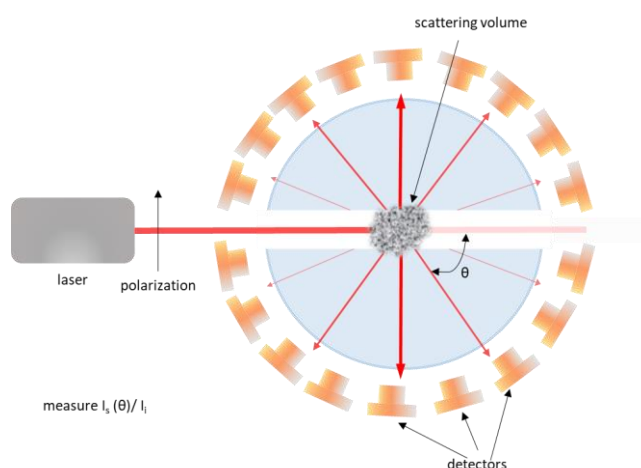


Figure 3.1: Schematic of theoretical background of multi angle laser light scattering (MALS).

$$I(\theta)_{scattered} \propto M_c \left(\frac{dn}{dc}\right)^2 P(\theta) \quad (10)$$

From above equation, the intensity of the scattered light $I(\theta)$ is proportional to the molar mass of the scatterer (M), the particle concentration (c), the refractive index increment (dn/dc) and a form factor of the angular dependency $P(\theta)$. The dn/dc in this setup is determined by the batch method for polymer (0.150) and is a constant value (0.185) for proteins.

The basis for molar mass determination by LS detection is based on the property of particles to scatter light as a function of their size at a certain scattering angle. The most basic equation behind static light scattering principle was put forth by Zimm.^[345] An important point to mention is that the extent of scattering is based on the size of the particles in solution. In particular, if the molecule is small with respect to laser wavelength, it acts as “isotropic scatterer” i.e. emits light with the same intensity in all directions. However, if the molecule is large, different points within the same molecule scatter the individual photons from laser. These scattered photons vary in phase and cause interference with each other, so that the resulting

intensity depends on the angle from which it is measured, “angular dependence”. This behavior leads to stronger scattering intensity at $\theta = 0$ and decreasing scattering intensity with increasing angle because of destructive interference. For molecules with size smaller than 1/20 of the wavelength of the irradiated light (isotropic scatterer), this behavior is determined by the so-called Rayleigh scattering. The intensity of the scattered light on the molar mass of the molecules also depends on constant wavelength constant, equipment and sample parameters. The reduced Rayleigh scattering or the contrast of the scattered light of the molecules in solution with the pure solvent, which also called the Rayleigh ratio, is defined as follows:

$$R = \frac{4\pi^2 \cdot n_0^2 \cdot \left(\frac{dn}{dc}\right)^2}{\lambda^4 \cdot N_A} \cdot c \cdot M = K \cdot C \cdot M \quad (11)$$

where:

K= optical constant

n_0 = refractive index of pure solvent

Λ = wavelength of incident light

N_A = Avogadro’s constant

dn/dc = refractive index increments of the polymer

C = concentration of the polymer

M = molar mass of the polymer

Using this relationship one can determine the molar mass with known dn/dc and known concentration of the polymer. Most instruments have wavelengths between 633 nm and 670 nm so the limit of isotropic scattering is between 15-17 nm. This is why R_g , radius of gyration, also known as root mean square radius determination, is not possible in this work.

Multi angle light scattering (MALS) solves this angular dependence issues, and measures the intensity of scattered light at different angles, current state of the art offers up to 21 angles. The calculation of the average molar mass, radius of gyration and the second virial coefficient can thereby be calculated using different models and most are measured at different angles. Light scattering intensities are then interpreted by the Zimm plot. This determination works for particles with sizes higher than 1/20 of the wavelength, which scatter anisotropically. In this study the molecules are smaller in sizes. Therefore, this approach was not implemented in the present work. The drawback of SEC-MALS is the interaction of the samples with the column material which can falsify results especially for samples with high functionality. In addition, the sample must not show too strong tendency to aggregate, as this can cause filter effects with the SEC separation, which in the worst case will block the system. These aggregates can pass through the column and this may lead to the distortion of the average molar mass of the polymer, as the light scattering detector will recognize the molar masses of the aggregates and not of the polymer.

3.2 Asymmetric Flow Field Flow Fractionation (AF4)

From the previous section we know that highly branched structures along with high functionality are difficult to characterize. To support our findings from SEC-MALS, in this work we used another advanced size separation technique to overcome the difficulties encountered with SEC. And as mentioned earlier, AF4 has not been used much in literature when it comes to study the A β amyloid behavior.

Field flow fractionation is a type of elution technique introduced by Giddings in late 1960s.^{[346][347]} In contrast to SEC, FFF is implemented in a thin, open, channel, which does not contain any stationary phase as shown in Figure 3.2. The eluent is pumped in through the inlet (flow IN) and transports to sample solution to the end of the channel (flow OUT). After separation the eluted fractions are detected, and the choice of the detector is similar to SEC. The laminar flow of mobile phase and perpendicular force field allows the size separation in the channel. Depending on what information is required such as molar mass, size, charge or chemical composition, different type of force-field can be applied e.g., temperature, centrifugal force or flow stream. The channel consists of two walls, an upper wall and a lower, accumulation wall. The choice of channel-length, width and material depends on the characteristics of the probe. Most exploited FFF method is asymmetrical flow FFF (AF4) having an extremal cross-flow stream as the separation force. Figure 3.2 shows a typical AF4 channel as well as the separation mechanism.

The AF4 channel has a trapezoidal geometry with the upper wall that is impermeable whereas the accumulation wall is made of porous frit material, permeable to eluent but impermeable to the analytes. An ultrafiltration membrane covers the accumulation wall, with a certain cut-off which can be chosen depending on the samples. The two walls are separated by a spacer generally having thickness of 100-500 μm .

The working principle involves two modes: focus and elution. The sample is introduced into the channel during focusing, during this the flow is entering the channel from both inlet and outlet. After the sample is focused, and relaxed in a narrow band on the membrane. At this point the concentration of sample is 10 times higher than the starting concentration of the sample. This is another advantage of AF4 over SEC. All components of the sample will reach steady state equilibrium, placing the different components of the sample with different diffusion coefficients at different distances from the accumulation wall. Sample components with high diffusion coefficients will be placed at larger distance from the accumulation wall than components with lower diffusion coefficients. After focusing, elution mode follows during which the sample components are transported in the direction of the channel outlet towards the detectors by the laminar flow of the eluent in a parabolic flow profile. The application of a cross-flow stream perpendicular to channel flow pushes the sample components towards the membrane, and the Brownian motion of the molecules generates a counteracting diffusion back to the center of the channel: smaller molecules with high diffusion coefficient form equilibrium states in the middle of the channel, where the laminar flow rates are higher, and therefore elute before the larger molecules as opposed to SEC elution behavior.

The concentration profile is given by:

$$C(x) = C_0 e^{(-x/\lambda w)} \quad (12)$$

Where x is the position of the sample component in the channel, C_0 is the concentration at accumulation wall ($x=0$), w is spacer thickness, λ is a physical parameter representing the distance of the sample from accumulation wall and is given by:

$$\lambda = \frac{D V_c}{w^2 V_x} \quad (13)$$

where D is the molecular diffusion opposing the cross-flow velocity (V_x) and V_c is the channel flow rate. The retention time t_r can be calculated based on different equations in the FFF method.

$$t_r = \frac{w^2}{6D} \ln \left(1 + \frac{V_x}{V_c} w^2 \right) \quad (14)$$

Using the Stokes–Einstein equation:

$$D = \frac{K_B * T}{6\pi * \eta * R_h} \quad (15)$$

where η is the dynamic viscosity of the carrier fluid, the hydrodynamic radius (R_h) can be directly calculated from retention data.

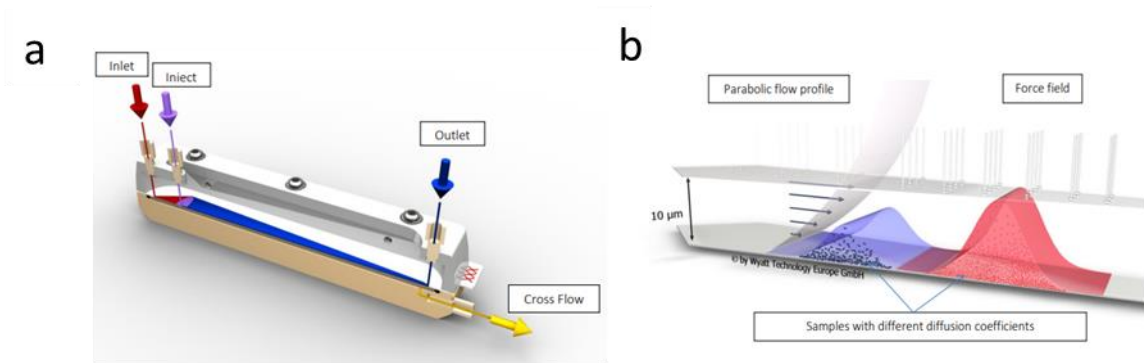


Figure 3.2: Basic principle of AF4: a) Action of different flows in a channel. b) mechanism during elution. Species having higher diffusion coefficient elutes faster. *Reprinted with permission from Eclipse Channel User’s Guide, Copyright (2019) Wyatt Technology Corporation.*

Based on the known parameters t_0 , V_x , V_c , w and the experimentally determined t_r , the diffusion coefficient can be directly determined. By using Stokes-Einstein equation, hydrodynamic radius can be assessed as shown in the equation.

Therefore, AF4 not only enables fractionation but also can be used for a direct determination of the particle size based on the measurement of the retention time t_r . However, the reliability of the t_r values determined is not only dependent on the particle size, but also on sample-channel

interactions, meaning that differently-sized particles could reveal similar retention times. Therefore, MALS was combined with AF4 for size-separation and concomitant determination of the molar mass, using the MALS detector coupled to AF4 system (Equations 12-15) and using the known dn/dc value and the known concentration of the solution polymers and protein. Since the samples are polydisperse except the dendrimers, the MALS measurement detects a summed scattering intensity and therefore an averaged molar mass is obtained. The details of the selection parameters for optimized in order to also investigate the interaction of amyloid with the synthesized polymers on the same parameters, it becomes easy to tell the difference after their interaction. The specific details are discussed in the Results and Discussion chapter.

3.3 Dynamic Light Scattering

This method is used to determine the R_h of synthesized polymers. Particles in solution are forced by Brownian motion to move in a random pattern which corresponds to their diffusion coefficient (D_t). As light is scattered by particles in solution, the motion of these particles imparts, randomness to the phase of the scattered light, resulting in constructive and destructive interference. A fast photon counter measures the time-dependent fluctuations of the scattered light. The fluctuations are analyzed over a second order correlation function and the Stokes-Einstein relation determines the hydrodynamic radius (R_h) of the sample. ^[348]

$$R_h = \frac{kT}{6\pi\eta D_t}$$

where, k is Boltzmann constant, T is the temperature and η is the solvent viscosity.

To ensure sufficient and accurate detection the samples should have sufficient concentration as well as free from large aggregates. For this, different types of filters are used. In case of interaction with amyloids, unfortunately, this method could not be used because of the presence of massive aggregates which would lead to a significant underestimation of smaller species.

3.4 Molecular Dynamics Simulation

A powerful tool which enables to follow up and understand structural dynamics is molecular dynamics (MD) simulation method. ^{[349][350]} Newton's equations of motion for a system allows the calculation of force between interacting particles and respective potential energy based on the physical movements of atoms and molecules. MD simulations are based on different algorithms and parameters which can be chosen based on the structure of molecules. Through this one can develop a comparison between macroscopic properties and microscopic simulations. By correlating macroscopic properties to the distribution and motion of atoms and the equation of motion of particles, giving rise to complex mathematical expressions, this connection can be made. However, the primary limitation of simulation methods is that they are approximate. Thus, experimental data are important because comparisons with experimental data gives the accuracy of the calculated results and provides a base to improve the methodology.

In this work MD simulations have been included to have a 3-dimensional view of the polymers synthesized, so that one can see the whole molecule which in turn can help us understand the difference in behaviors toward amyloid protein.

3.5 Nuclear Magnetic Resonance Spectroscopy

NMR spectroscopy is a powerful and the most widely used method for structure determination in chemistry. The NMR observes odd mass nuclei having fractional spins ($I=1/2$) (angular momentum). When an NMR active nucleus is subjected to an external magnetic field, a characteristic electromagnetic interaction takes place. The main principle of NMR spectroscopy based on spectral lines of different atomic nuclei that are excited when a strong magnetic field and a radiofrequency waves are applied. It is sensitive to the features of molecular/chemical structure because signals from individual nuclei are influenced by its neighboring atoms and as a result whole structure of the molecule can be discerned.^[351] The measured values are resonances which leads to signals in chemical shifts, splitting and integrals in the Fourier transform spectrum. The chemical shift comes when NMR nuclei absorbs, and depends on the electron density as the measured resonance values are heavily influenced by shielding effects of the nuclei from its surroundings. This shielding effect depends on electronegativity, magnetic anisotropy of π -electrons and hydrogen bonding. A high electron density requires a lower frequency of applied magnetic field and so, resonances of nuclei will absorb at high frequency and signals of chemical shift will appear in high field region of NMR spectrum. Different spectra are possible based on different type of nucleus. However, the most commonly used technique for the structural elucidation of organic molecules is ^{13}C NMR and, more importantly, ^1H NMR.

3.6 Thioflavin T fluorescence

Thioflavin T (ThT) assay is one of the most commonly used methods to study aggregation processes and effect of aggregation inhibitors. It is a fluorescent spectroscopy method reported for the first time by Vassar and Culling in 1959.^[352] ThT is a 2-arylbenzothiazole dye is the most widely used staining dye for amyloid fibrils. This characteristic behavior of ThT dye lies in its structure which contains a di-methyl aniline and benzothiazole ring connected by carbon-carbon bond. The low emission arises from the free rotation of the two parts (di-methyl aniline and benzothiazole ring) about their common axis in solution. This led to the change from locally excited (LE) state to a non-radiative charge transfer state. This free rotation is hindered when it binds to amyloid fibrils leading to more populated LE state which leads to higher fluorescence yield. Besides, it also shows a strong bathochromic shift of the excitation and emission maxima when bound to fibrils (from 385 nm to 450 nm and from 445 nm to 480 nm, respectively).^[353]

ThT fluorescence displays a typical sigmoid curve, in the beginning low ThT fluorescence corresponds to nucleation phase where A β peptides are in monomeric form. The steep increase in ThT signal indicates the elongation phase during which the protofibrils rich β sheet are formed. And in the end a plateau is obtained indicating an equilibrium between the fibrils and

other prefibrillar species. Thus, it is possible to study time-dependent fibrillization of A β peptides *in vitro* and give us information on the kinetic behavior of amyloids and inhibitors.

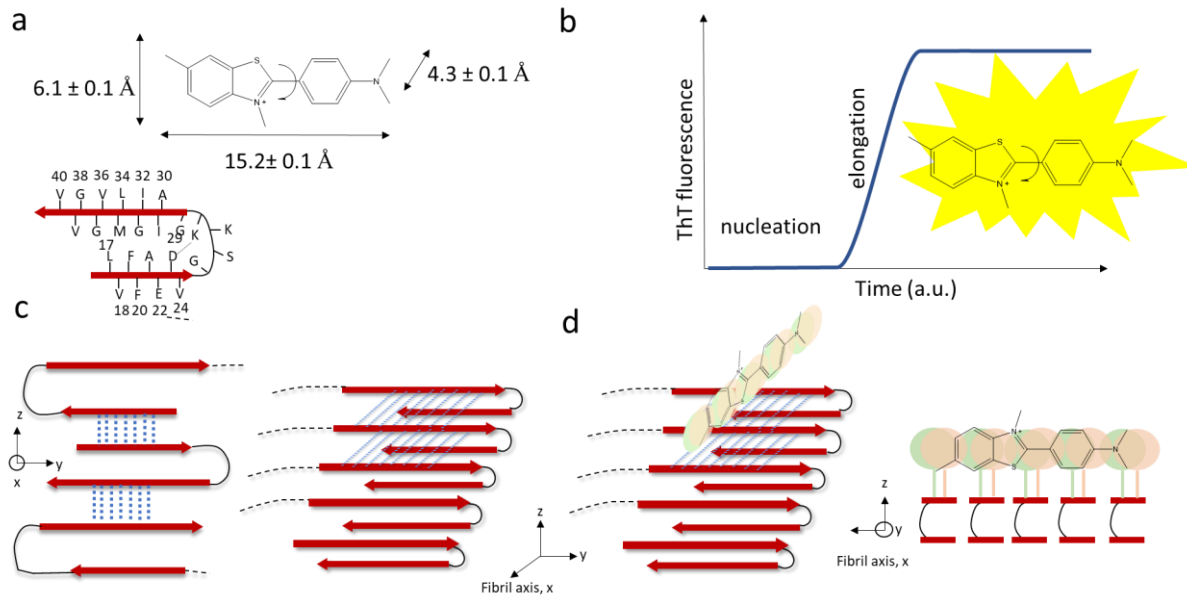


Figure 3.3: Details of ThT fluorescence a) ThT dye with its specific dimension b) A typical sigmoidal ThT curve from the formation of amyloid fibrils c) Scheme of ThT interaction within the fibrils along the fibril axis (left) and perpendicular to it (right) d) Green and orange circles stand for hydrophobic residues able to interact with aromatic rings of the ThT. *Republished with permission from ref. [354], Copyright (2013) Royal Society of Chemistry.*

Despite being the most commonly method for study aggregation processes, it suffers certain drawbacks, specifically interference of ThT fluorescence with aggregation process, self-quenching when used in too large concentrations or in presence of certain ions and cannot distinguish between several different amyloid fibrils (α -synuclein, prion proteins etc.).

In this study different concentrations of synthesized glycopolymers were used to see their effect on the aggregation of A β 40 amyloid as anti-aggregating agents. By using experimental kinetic data obtained from ThT assay, important information about the reaction rate constants is obtained (see Section 5.2.1.1).

3.6.1 Kinetic analysis

As mention earlier, aggregation of A β occurs via secondary nucleation mechanism.^[167] The ThT data can be further analyzed in order to calculate the rate constants. The experimental data is fitted to such a model using the following equations by using the online fitting software AmyloFit, following the referred protocol.^[355] This software allows the detection of amyloid fibril growth profile based on different models that has been described in different literature. In this work ‘secondary nucleation dominated’ was used, with reaction orders set to 2 and under the constraint of allowing deviations in only one parameter at a time to investigate which microscopic step is most likely affected by the synthesized glycopolymers.

In this work the focus was to see the change in microscopic steps on addition of glycopolymers to a specific concentration of A β 40 peptide, however, the software was developed by using the studies based on pure A β 42.

The differential equations describing^[355] the secondary nucleation are:

$$\frac{dP}{dt} = k_n m(t)^{n_c} + k_2 m(t)^{n_2} M(t) \quad (16)$$

$$\frac{dM}{dt} = 2m(t)k_+ P(t) \quad (17)$$

The approximate analytical solution is:

$$\frac{M}{M_\infty} = 1 - \left(1 - \frac{M_0}{M_\infty}\right) e^{-k_\infty t} \cdot \left(\frac{B_- + C_+ e^{-\kappa t}}{B_+ + C_+ e^{-\kappa t}} \cdot \frac{B_+ + C_+}{B_- + C_+}\right)^{\frac{k_\infty}{\kappa \bar{k}_\infty}} \quad (18)$$

Where the definitions of the parameters are

$$\kappa = \sqrt{2m_0 k_+ m_0^{n_2} k_2} \quad (19)$$

$$\lambda = \sqrt{2k_+ k_n m_0^{n_c}} \quad (20)$$

$$C_\pm = \frac{k_+ P_0}{\kappa} \pm \frac{k_+ M_0}{2m_0 k_+} \pm \frac{\lambda^2}{2\kappa^2} \quad (21)$$

$$k_\infty = \sqrt{(2k_+ P(0))^2 + \frac{4k_+ k_n m_0^{n_c}}{n_c} + \frac{4k_+ k_2 m_{tot} m_0^{n_c}}{n_2} + \frac{4k_+ k_2 m_0^{n_2+1}}{n_2 + 1}} \quad (22)$$

$$\bar{k}_\infty = \sqrt{k_\infty^2 - 2C_+ C_- \kappa^2} \quad (23)$$

$$B_\pm = \frac{k_\infty \pm \bar{k}_\infty}{2\kappa} \quad (24)$$

Where, M_∞ represents the mass at long times and m_{tot} , represents the total protein mass concentration. This solution is understood to be more accurate than ones involving fragmentation, i.e. very close to the numerical integration of the differential equations, however, it only applies to negligible off rates $k_{off} \ll k_+ m_0$.

3.7 Circular Dichroism Spectroscopy

Jean-Baptiste Biot, Augustin Fresnel and Aime Cotton discovered the phenomenon of Circular Dichroism (CD) based on the optical activity of a compound.^[356] The CD is observed in compounds which are optically active. CD spectroscopy is a valuable method for determining the secondary structures, folding and binding of proteins.^[357] This involves differential absorption of left-handed and right handed circularly polarized light by the asymmetric molecules. The principle is explained in Figure 3.4b. When light passes through a sample and there is equal absorption or no absorption, θ is 0, generates a plane polarized light (bold line circle). But, if L and R are absorbed to different extents, the resulting radiation would be said to possess elliptical polarization (dashed ellipse). This differential absorption produces positive and negative bands in the CD spectrum (Figure 3.4c). In proteins, the main chromophores are the peptide bonds and which absorb L and R components differentially and produces a characteristic signal in the CD spectrum. Usually, they absorb light in the far-UV wavelength region (180- 240 nm).^[358]

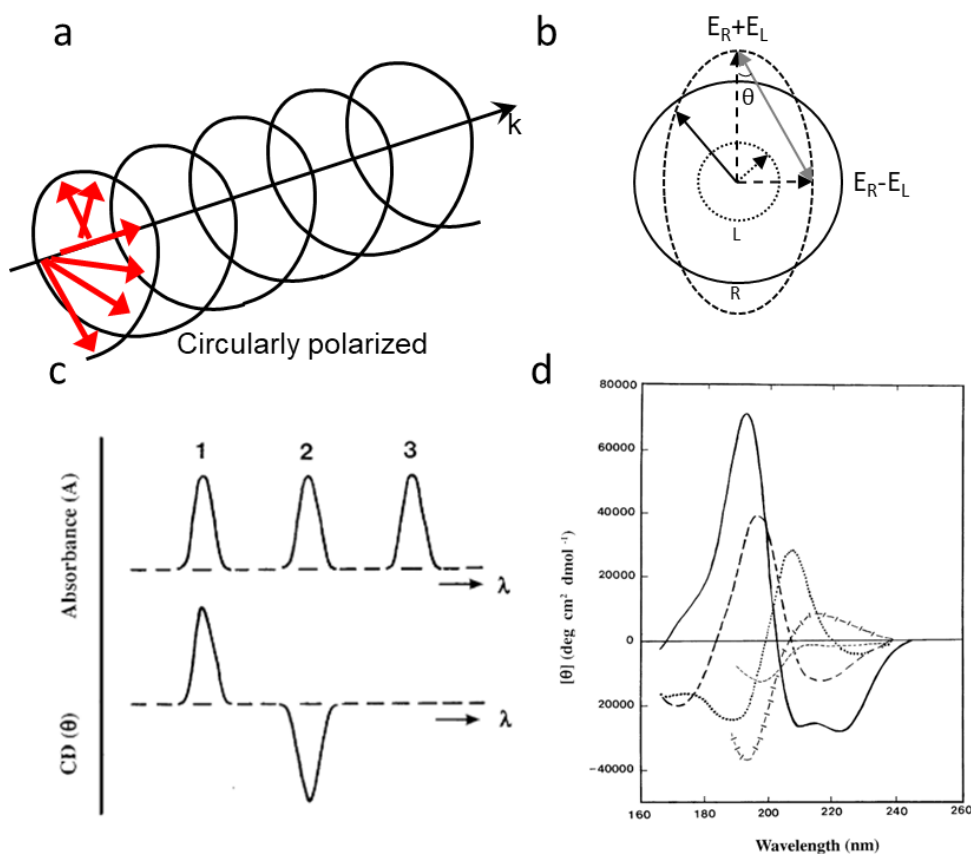


Figure 3.4: Basic principle of CD spectroscopy. a) circularly polarized light. b) Plane polarized light is made of 2 components the left handed (L) and right handed (R), c) The relationship between absorption and CD spectra. Band 1 shows a positive CD signal with L absorbed more; band 2 shows a negative CD signal with R absorbed more; band 3 shows no CD signal due to achiral chromophore. d) Far-UV CD spectra showing various types of secondary structure. Solid line, α -helix; long dashed line, anti-parallel β -sheet; dotted line, type I β -turn; cross dashed line, extended 31-helix or poly (Pro) II helix; short dashed line, irregular structure. Reprinted with permission from ref. ^[359], Copyright (2005) Elsevier.

CD instruments measure the difference in absorbance (ΔA) between the L and R circularly polarized components and expressed in terms of molar ellipticity ($[\theta]$) in degrees.

$$\Delta A = A_L - A_R \quad (25)$$

By using Beer's law:

$$\Delta A = (\epsilon_L - \epsilon_R) C * l \quad (26)$$

ϵ_L and ϵ_R are the molar extinction coefficients for L and R circularly polarized light, C is the molar concentration and l is the path length in centimeters (cm).

The molar circular dichroism, $\Delta\epsilon$ is:

$$\Delta\epsilon = (\epsilon_L - \epsilon_R) \quad (27)$$

It should be noted that:

$$\tan \theta = \frac{E_R - E_L}{E_R + E_L} \quad (28)$$

There is a simple numerical relationship between $\Delta\epsilon$ and molar ellipticity $[\theta]$ (in degrees)

$$[\theta] = 3298.2 \Delta\epsilon \quad (29)$$

The CD spectrum is obtained when the dichroism is measured as a function of wavelength. So, by using the known values of exact concentration of protein and its molar mass, the path length and wavelength molar ellipticity is determined. In biological studies the observed CD signals are very small, i.e., ellipticities are typically in the range 10 mdeg. So, care must be taken while performing such experiments especially concerning the concentration. In case of proteins, the mean residue weight i.e., the average molar mass of the amino acid residues is used. This means that residue ellipticity is useful for comparing the CD of proteins of different molar masses.

The different secondary structures of protein have characteristic spectra base on the optical transitions of the peptide backbone of the protein (Figure 3.4d). Since the CD spectra of proteins are so dependent on their conformation, it is often used to estimate the structure of unknown protein, monitor conformational changes over time, mutations, effect of temperature and binding interactions. Another advantage of CD spectroscopy is that it is relatively fast method and proteins can be analyzed in solution under physiological conditions. However, it does not give information on the secondary structure of specific amino acid residues unlike x-ray crystallographic and ssNMR. Secondary structure can also be estimated from Fourier transform infrared spectroscopy of proteins and Raman spectroscopy. But sometimes, these measurements require high concentrations, protein films or in deuterium oxide.

There are several libraries of reference spectra of known proteins, based on which different online software are developed to predict the secondary structure of proteins.^[360] $\alpha\beta$ are β sheet rich proteins, and β sheets can largely differ in the parallel-antiparallel orientation, in length and number of strands and their twists.^[358] This spectral diversity makes the secondary structure estimate of amyloid difficult in CD spectroscopy. In this work we have used a recently

developed method which accounts for more accurate determination of secondary structures of β -sheet rich proteins, known as BeStSel (Beta Structure Selection).^[361]

3.8 Atomic Force Microscopy

Atomic Force Microscopy (AFM) was invented by Binnig et al. and since then it has undergone much advancement.^[362] AFM has been successful in imaging DNA,^[363] plant cell walls,^[364] a wide range of proteins and many other systems.

AFM allows biomolecules to be imaged under physiological conditions and also during biological processes are working. AFM can obtain detailed topological information for crystalline samples as well as biomolecules which lacks inherent symmetry because of high signal-to-noise (S/N) ratio.

AFM works in the same way as white cane works for blind people. The use of a white cane to “visualize” an object leads brain to deduce its topography while feeling it. AFM give the resolution based on the radius of the tip attached. A sharp stylus (tip) (radius \sim 1-2 nm) is attached to a cantilever, used in the AFM to scan an object point by point and contouring it while a constant small force is applied to the stylus. The forces (van der Waals, electrostatic, magnetic etc.) generated between the stylus and the sample are transmitted to an attached flexible cantilever, causing it to bend (deflections). These deflections are monitored by an optical detector (photodiode) which measures the reflected signal from a laser beam on the cantilever tip. This signal is used by a feedback system to change the force applied to the sample by the tip controlling the movements of piezo crystal. In AFM, the role of the brain is taken over by a computer, while scanning the stylus is accomplished by a piezoelectric tube. The basic advantages of AFM are as follows: 1) almost no limits to samples; (2) high resolution sample morphology in three dimensions; (3) working in various environments, such as vacuum, air, fluid and low temperature; (4) enabling dynamic observation in physiological environment.

There are two modes of operations for an AFM device, static mode (contact) and dynamic modes (non-contact and tapping). In static mode, the cantilever is dragged on the surface of the sample and with its deflections contours of the sample surface is measured. In dynamic mode, the cantilever externally oscillates at or close to its fundamental resonance frequency. This sample-tip interaction gives oscillation amplitude, phase and resonance frequency. And the changes give the characteristic information of the sample under study.

Contact mode is the static mode of operation, as outlined above. There is a feedback loop which keeps the deflections of the cantilever in within a desired value. When the measured deflection is different from the desired value, the feedback amplifier applies a voltage to the piezo crystal to adjust the sample relative to the cantilever to achieve the desired value of deflection. This voltage is the measure of the height of features on the surface of sample.

Non-contact mode, as the name suggests the tip of cantilever does not touch the sample surface. The van der Waals forces between the tip and the samples are detected by hovering the tip over the sample surface. The cantilever vibrates at its resonant frequency and the van der Waals

forces tends to decrease the resonance frequency of the cantilever. A topographic image is created by measuring the tip-to-sample distance at each data point. It is a non-invasive method.

Tapping mode is the most popular mode to obtain the surface morphology by scanning the surface with the cantilever tip up and down, very lightly, close enough to the sample surface, without scratching while it is in contact with the surface. In this mode the cantilever oscillates at or near the resonant frequency using the piezo crystal. When not in contact with the sample surface, the cantilever oscillates with this constant frequency leading to a high amplitude (200 nm). The oscillating tip is then moved toward the surface until it just touches the surface, the interaction of forces causes the amplitude of the cantilever's oscillation to change, generally reduced. This change in amplitude helps control the height of the cantilever above the sample. But when the tip passes over a depression on the sample surface, then the oscillation amplitude is increased. This change in oscillation amplitude is measured by the detector and sent to the AFM software. The digital feedback loop then readjusts the tip-sample distance to maintain a constant amplitude and force.

Like all other microscopic techniques, AFM is susceptible to temperature variation and vibration. These can be overcome by temperature control around the instrument and by installing the device on anti-vibration air table or using active piezo isolation base. Regarding the imaging capabilities, when measuring samples in liquid, the relatively slow rate of scanning during AFM imaging often leads to thermal drift, causing the cantilever to bend due to the difference between the liquid and the liquid cell.

Tip convolution is an image artefact that occurs because of the large size of the AFM probe in relation to the samples. These image artefacts are unavoidable; however, they can be reduced by using an appropriate tip, or a modified operating environment.

The samples for AFM imaging should be immobilized on a rigid support. There are many options for the choice of substrate. Glass cover slips and cleaved mica sheets can be used depending on the type of samples. Biological samples are usually bound on mica or glass. Mica is quite a versatile material for substrate due to its non-conducting-layered nature, atomically flat, clean after cleavage, easy to cut desired sizes, relatively inexpensive, negatively charged but can be modified to make the surface positive.

It is also known that most proteins contain both positively and negatively charged residues at neutral pH and the neutrality can be altered by changing the pH of the buffer solution. Therefore, it seems plausible to assume that electrostatic interaction is responsible for adsorption. However, it must also be realized that most of these charged groups are shielded by counterions in solution. It is unclear whether it is the direct interaction between the oppositely charged groups or the salt bridges between like charged groups that is responsible for surface adsorption.^[365]

Several studies have been done on amyloid proteins like α -synuclein and A β 42 which gives the information on different types of species involved.^[366] However, the focus of this work has been to see the effect of synthesized glycopolymers on A β amyloid, AB 40 specifically. In the present study, AFM measurements are performed to see the changes occurring after the addition

of synthesized glycopolymers which gave the best results in AF4 and CD spectroscopy. The details of the sample preparation and procedure is discussed in Chapter 4.

3.9 Cytotoxic assay

In the drug development process, the testing of new compounds for its toxicity is an essential step. The toxicity of substances can be observed by (a) *in vitro* studies using cells/cell lines (b) studying the accidental exposures to a substance (c) *in vivo* exposure on experimental animals. Screening for toxicity as early as possible may reveal inappropriate drug candidates that should not proceed in the drug development process. Although *in vitro* methods cannot predict the toxicity for compounds as compared to *in vivo* methods, but they are useful tools to compare different treatments, and indicate toxicity at a very basic level.

In this work the toxic effects of glyco-pseudodendrimers on two different cell cultures were assessed.

3.9.1 MTT assay

The MTT (3-[4,5-dimethylthiazole-2-yl]-2,5-diphenyltetrazolium bromide) assay is traditionally the most widely used method of cell viability, developed by Mosmann in 1983.^[367] When dissolved in water, MTT produces a yellow solution. It is a tetrazolium salt. Active mitochondrial dehydrogenase in metabolically active cells will convert MTT to insoluble purple formazan crystals. Dead cells will not show this change of color because all cell organelles are not active anymore. Hence, MTT assay is dependent on the activity of mitochondria and indirectly serves to assess the cellular energy capacity of a cell. The insoluble formazan is solubilized by the addition of cell lysis buffer, and the absorbance at 570 nm wavelength is measured.^[368]

3.9.2 Determining the level of reactive oxygen species

Reactive oxygen species (ROS) are unstable and highly reactive species. When they react with particular substances they form end products which provides information about their presence.^[369] These have the potential to cause a number of deleterious events in a cell including oxidative stress and DNA damage, can ultimately cause cell death.^[370] DHE (dihydroethidium) is the most frequently used fluorogenic probe for monitoring intracellular producing of superoxide anion radical. DHE is characterized by blue fluorescence ($\lambda_{\text{ex}} = 355 \text{ nm}$, $\lambda_{\text{em}} = 430 \text{ nm}$). As a result of the reaction between DHE and superoxide anion radical 2-hydroxyethylidine is produced.^[371] This compound shows strong red fluorescence ($\lambda_{\text{ex}} = 460 \text{ nm}$, $\lambda_{\text{em}} = 640 \text{ nm}$) after intercalation to DNA.

H₂DCF-DA (diacetate dihydrodichlorofluorescein) is a reduced form of fluorescein. The method is based on the oxidation of this fluorescent probe by intracellular reactive oxygen species (ROS).^[372] H₂DCF-DA is able to freely cross the cell membrane. In the cell interior esterases hydrolyze it to non-fluorinating H₂DCF. Intracellular ROS carry out the oxidation, which is the next stage of chemical transformations and results in receiving the final product 2',7'-dichlorofluorescein (DCF) characterized by a strong fluorescence. This compound remains

in the cytosol and shows maximum excitation at $\lambda_{em} = 529$ nm and maximum emission at $\lambda_{ex} = 495$ nm. The fluorescence intensity is directly proportional to the amount of ROS reacting with the probe.

3.9.3 Changes in mitochondrial transmembrane potential

Mitochondria membrane potential (MMP) is a key indicator of cellular activity and is required for ATP generation. A decrease in MMP leads to lowering ATP along with changes in the pH of mitochondrial intermembrane space and matrix.^[370] This change in pH allows certain fluorescent dyes to accumulate and produce fluorescent signal, which in turn represents the health of the mitochondria.

JC-1 is a cationic dye widely used as fluorescent probe for detecting depolarization of the mitochondrial membrane. The selective accumulation of JC-1 in the mitochondria is dependent on the mitochondrial transmembrane potential. Sharp decline in ATP production is often connected with pathology states, which causes depletion of energy and depolarization of mitochondrial membrane.^[370] Changes in mitochondrial potential are characteristic for the initial stages of programmed cell death. The application of the JC-1 fluorescent probe allows for spectrofluorimetric analysis of changes in the mitochondrial membrane potential. JC-1 tends to accumulate in large quantities in hyperpolarized mitochondrial membrane, where it forms aggregates that emit red fluorescence ($\lambda_{ex} = 485$ nm, $\lambda_{em} = 538$ nm). When the depolarization of the mitochondrial membrane occurs and the membrane permeability increases, the aggregates breakdown to monomers emitting green fluorescence ($\lambda_{ex} = 530$ nm, $\lambda_{em} = 590$ nm). Ratio of aggregates ($\lambda_{em} = 590$ nm) and monomers fluorescence ($\lambda_{em} = 540$ nm) reflects the damage of mitochondrial membranes.

3.9.4 Flow cytometric detection of phosphatidyl serine exposure

Flow cytometry (FC) is a laser-based technique, which depends on how different particles or cells suspended in liquid interact with light. This leads to the light being refracted or emitted differently and is measured by an electronic detection apparatus. This detection apparatus can detect forward scattered, side scattered light and also fluorescence emission. It is a popular method in cell biology to count, sort and profile cells in a heterogenous fluid mixture. In this work dual staining of cells with annexin V and propidium iodide (PI) was used to assess apoptosis (cell death). This helps in distinguishing viable cells (unstained with either fluorochrome) from apoptotic cells (stained with Annexin V) and necrotic cells (stained with PI).^[373]

4 Experimental Details and Methodology

4.1 Details of chemicals/components used

Table 4.1: Details of chemicals and components used.

Chemical	Purity	Manufacturer/remark
Acetone	A.G.	Acros Organics, Belgien
Amberlite IR120 H		Sigma-Aldrich GmbH
Ammonia solution, saturated	A.G.	Acros Organics, Belgien
3-Azido-1-Propanol	≈ 90 % (¹ H-NMR)	IPF DD, Abt. bioakt. resp. P.
2,2 Bis(hydroxymethyl)propionic acid	98 %	Sigma-Aldrich GmbH
Borontrifluoride-Dietherate (in Diethylether)	≥ 46 %	Sigma-Aldrich GmbH
Deuteriochloroform (99,8 % D)	99.9 %	Euriso-Top GmbH
Dialysis membrane MWCO 5kDa		Carl Roth GmbH
4-Diaminopyridine	≥ 99 %	Sigma-Aldrich GmbH
Dichloromethane (DCM)	99.6 %	Acros Organics, Belgien
Dicyclohexylcarbodiimide (DCC)	≥ 99 %	Fluka GmbH, Deutschland
Diethylether, stabilised (BHT)	≥ 99 %	Acros Organics, Belgien
2,2-Dimethoxypropane	98 %	Sigma-Aldrich GmbH
Dimethylacetamide (DMAC)	99.5 %	Sigma-Aldrich GmbH
Dimethylsulfoxide-d ₆ (99,9 % D)	99.8 %	Euriso-Top GmbH
Dowex 50W-X2 H ⁺ , 100-200 mesh		Sigma-Aldrich GmbH
Ethanol absolute	99.8%	VWR International GmbH
Ethyl acetate	99.5 %	Sigma-Aldrich GmbH
Silica gel 60 Å		Carl Roth GmbH
Copper sulfate pentahydrate	≥ 99.5%	Carl Roth GmbH
Lithium chloride	≥ 99 %	Merck Schuchardt OHG
α-D-Mannose-Pentaacetate	96 %	Iris Biotech GmbH
Methanol	A.G.	Acros Organics, Belgien
Molecular sieve 4 Å		Merck KGaA
Sodium chloride	99.8 %	Carl Roth GmbH
Sodium hydrogen carbonate	99.5 %	Acros Organics, Belgien
Sodium hydrogen sulfate	99.0 %	Merck KGaA
Sodium hydrogen sulfate	99,0 %	Merck KGaA
Sodium -L-Ascorbate	≥ 98 %	Sigma-Aldrich GmbH
Sodium methoxide (25 wt. % in Methanol)	≈ 25 %	Sigma-Aldrich GmbH
Sodium sulfate	≥ 99 %	Sigma-Aldrich GmbH
n-Hexane	98.5 %	Merck KGaA

Para-Toluene sulfonic acid	A.G.	Fluka GmbH
4-Pentynoic acid	95 %	Sigma-Aldrich GmbH
Pyridine	99.0 %	Sigma-Aldrich GmbH
Distilled water	99.9 %	Merck Millipore KGaA
Tetrahydrofuran, stabilised (BHT)	A.G.	Acros Organics, Belgium
Toluene	A.G.	Acros Organics, Belgium
Bovine serum albumin	≥ 98%	Sigma
MTT (3-(4,5-Dimethylthiazol-2-yl)-2,5-diphenyltetrazolium bromide)	A.G.	Sigma
Thioflavin T	A.G.	Sigma
Phosphate buffered saline (PBS)		
Dulbecco modified Eagle's medium	A.G.	Sigma
96 well plates		
(3-aminopropyl) triethoxysilane (APTES)	≥ 98%	Sigma-Aldrich
Mica	NA	NA

A.G. – Analytical Grade; NA – Not Available

4.1.1 Other materials

- A β 40 [DAEFRHDSGYEVHHQKLVFFAEDVGSNKGAIIGLMVGGVV] (JPT, Germany and Novopeptide, China)
- Bis-MPA hydroxyl dendrimer, generation 3, TMP core (Polymer Factory, Sweden)

4.1.2 Peptide preparation

Freshly prepared A β 40 solutions were used in each experiment in PBS/phosphate buffer at pH 7.4 and used immediately.

4.1.3 Buffer preparation

Sometimes the techniques used in this work have some influence on the choice of buffer used. In case of CD spectroscopy and AF4 studies, 1 mM buffer was used while 10 mM PBS buffer was used in the rest. In case, of ThT assay phosphate buffer at 10 mM was used. The pH of most experiments was 7.4 to recreate physiological conditions as much as possible.

4.1.4 Fibril growth conditions

In this study, A β 40 peptide concentration of 50 μ M was used on the basis of our literature studies and was kept constant for all the experiments. The peptide was incubated at 37 °C in respective buffers. This temperature, concentration, gentle agitation and buffer concentration allowed reproducible fibril growth curves, with a lag phase and high concentration of fibrils at the end of the process as shown by ThT assay.

4.2 Synthesis and characterization of polymers

First to third generation glyco-pseudodendrimers (GI-P) on 2-bis(hydroxymethyl)propionic acid (bis-MPA) core modified with a dense mannose shell (P-G1-Man, P-G2-Man and P-G3-Man) were prepared as described previously.^[336] Fourth to sixth generation glyco-dendrimers (GI-D) were synthesized according to the same method starting with hydroxyl dendrimers of third generation with trimethylol propane core (G3-TMP) (D-G4-Man, D-G5-Man and D-G6-Man) from Polymer Factory, Sweden. Moreover, mannose units were introduced to the surface of dendrimers and pseudodendrimers on CuAAC “click” chemistry.^[18]

4.2.1 Synthesis and characterization of pseudodendrimers and dendrimers

For the synthesis of pseudodendrimers, firstly hyperbranched polymer (hb) of bis-MPA was synthesized. In the next step, the anhydride of protected monomer based on bis-MPA (AB*₂) was synthesized. And In the third step, pseudodendrimer of the first generation was synthesized using the hb polymer and protected monomer AB*₂. Next two generations were synthesized using the previous generations and the protected monomer.

Dendrimers were synthesized starting with hydroxyl dendrimers of third generation with trimethylol propane core (PFD-G3-TMP) with the AB*₂. Next two generations of the dendrimers were synthesized using the previous generations and AB*₂.

4.2.1.1 Synthesis of hyperbranched polymer (1)

In a two-necked flask bis-MPA (20 g, 0.150 mol) and para-toluene sulfonic acid (p-TSA; 30.4 mg, 0.12 mol%) were heated to the reaction temperature of 185 °C with a magnetic stirrer, a gas inlet and an outlet tube. A constant flow of N₂ was maintained for first 2 h for removing the water formed during the reaction, followed by vacuum (5-6 mbar) for the next 5 h. The product was cooled down and dissolved in Tetrahydrofuran (THF). For purification, the polymer was precipitated two times from cold diethyl ether (-78 °C) and the white solid was dried at 40 °C in vacuum for 24 h.

Yield: 95%

¹H NMR (DMSO-d₆, ppm): 1.03 (CH₃, t); 1.08 (CH₃, l); 1.18 (CH₃, d); 3.47-3.49 (m, CH₂OH); 4.12 (m, CH₂OCO); 4.60 (OH, t); 4.91 (OH, l); 12.84 (COOH) (Figure 5.5)

4.2.1.2 Synthesis of protected monomer

The synthesis of protected monomer (AB₂*) was carried out in 2 steps:

4.2.1.2.1 bis-MPA acetonide (2)

For the synthesis of bis-MPA acetonide (2), protocol was followed as established by Hult et al.^[374] 25 g (186 mmol) of 2,2-bis-(hydroxymethyl) propionic acid(bis-MPA) and 0.6 eq of dimethoxypropane (DMP) was dissolved in 90 ml acetone, with stirring, 0.022 eq of the catalyst (p-toluenesulfonic acid) p-TSA was added and left for 12 h with stirring. 2 ml of ethanol/ammonia solution (1:1) added dropwise and solvent was removed by rotary evaporator. The residue is diluted to 100 ml CH₂Cl₂, extracted with water (2x150 mL) and the organic phase

was dried over Na₂SO₄, filtered and the solvent was removed by rotary evaporator. The product is dried at under vacuum to give 1 as white solid.

Yield: 22 g (86%)

¹H NMR (CDCl₃, ppm): 1.15 (s, CH₃); 1.34 (s, CH₃); 1.38 (s, CH₃); 3.62 (d, -CH₂O-); 4.10 (d, -CH₂O-). (Figure 1, Appendix)

¹³C NMR (CDCl₃, ppm): 18.4 (CH₃); 21.9 (CH₃); 25.3 (CH₃); 41.7 (-C); 65.9 (-CH₂O-); 98.4 (COO); 179.7 (COOH). (Figure 2, Appendix)

4.2.1.2.2 bis-MPA-acetonide anhydride (3)

Synthesis was based on the method developed by Malkoch et al.^[339] 1 eq of 1 was dissolved in 10 eq of anhydrous CH₂Cl₂. 0.5 eq of DCC was added and the solution stirred for 2 days at room temperature. The solution was cooled to about -40 °C, the solid was filtered off and the solvent removed in rotary evaporator, to give 2 as a colorless viscous oil as product.

Yield: 9.7 g (100%)

¹H NMR (CDCl₃, ppm): 1.18 (s, CH₃); 1.33 (s, CH₃); 1.37 (s, CH₃); 3.63 (d, -COCH₂-); 4.15 (d, -COCH₂-). (Figure 5.7)

¹³C NMR (CDCl₃, ppm): 17.73 (CH₃); 21.80 (CH₃); 25.34 (CH₃); 43.67(-CH₂O-); 65.69 (CH₂); 98.43(COO); 169.51 (OC-O-CO). (Figure 5.8)

4.2.1.3 Synthesis of protected pseudodendrimers (4, 6 and 8) and protected dendrimers (10, 12, and 14)

Synthesis was undertaken according to the procedure in literature.^[339] Respective amounts of starting material and 0.15 eq of DMAP dissolved in 5 eq of anhydrous pyridine. 1.3 eq of 2 was dissolved in 15 eq of anhydrous CH₂Cl₂ and added to the corresponding dendrimer solution and stirred for 18 hours at room temperature. Subsequently, washed two times each with a 10% (m/m) NaHSO₄ (2x50 ml), 10% (m/m) NaHCO₃ (2x50 ml) solution and a saturated NaCl (2x50 ml) solution. The organic phase was dried over Na₂SO₄, filtered, and residual solvent was removed by distillation on rotary evaporator. 50 ml of toluene was added to the remaining solution, to remove residual pyridine followed by distillation at 50 °C in vacuum, to give brownish viscous oil.

Pseudodendrimers 4, 6, and 8: ¹H NMR (CDCl₃, ppm): 1.15 (s, CH₃, t); 1.33 (s, CH₃, l); 1.40 (s, CH₃, d); 3.55 (m, -COCH₂-); 4.06 (m, -COCH₂-); 4.22 (m, -COCH₂-) (Figure 5.10, Figure 3 and 4 Appendix)

Dendrimers 10, 12 and 14: ¹H NMR (CDCl₃, ppm): 0.88 (t, CH₃ TMP); 1.07 (s, CH₃, t); 1.13 (s, CH₃, l); 1.20 (s, CH₃, d); 1.26 (s, CH₃, Acetonide); 1.33 (s, CH₃, Acetonide); 3.55 (m, -COCH₂-); 4.05 (m, -COCH₂-); 4.25 (m, -COCH₂-) (Figure 5.20, Figure 5 and 6 Appendix)

Table 4.2: Quantities used in the synthesis of protected pseudodendrimers and dendrimers.

Sample number	Starting material (g)	AB* ₂ (protected monomer)	Product (g)	Yield (100 %)
4	3	11.78	5.29	61
6	2.5	7.4	5.04	98
8	1.5	1.87	2.1	47
10	3	12.02	8.86	100
12	3	11.62	8.51	100
14	3	11.33	8.46	100

4.2.1.4 Deprotection of pseudodendrimers (5,7, and 9) and dendrimers (11,13 and 15)

Respective mass of protected dendrimers and pseudodendrimers (Table 4.3) was dissolved in ~30 eq of methanol. 3-4 g of the cation exchange resin Dowex 50Wx2 was added and the solution stirred for 5 h. The solvent was removed on rotary evaporator and dried at 40 °C under vacuum for 24 h, to give 8, 9, 10 and 11 as slightly orange solid.

Table 4.3: Quantities used in the deprotection of protected pseudodendrimers and dendrimers.

Sample number	Protected polymers (g)	Methanol (ml)	Product (g)	Yield (100 %)
5	4.5	100	5.54	100
7	4.6	100	3.92	76
9	4.6	100	1.77	38
11	8.862	71	1.96	100
13	8.508	67	1.98	100
15	8.5	66	1.93	100

Pseudodendrimers 10, 11 and 12: ¹H NMR (CDCl₃, ppm): 1.02 (s, CH₃, t); 1.09 (s, CH₃, l); 1.18 (s, CH₃, d); 3.46 (m, CH₂, -CH₂OH); 4.12 (m, CH₂, -CH₂OH), 4.56 (t, OH), 4.85 (l, OH) (Figure 5.11, 5.14 and 5.16)

Dendrimers 11, 13 and 15: ¹H NMR (DMSO-d₆, ppm): 0.96 (F, CH₃); 1.02 (s, CH₃, t); 1.02 (CH₃, l); 1.18 (s, CH₃, l); 1.33 (s, CH₃ D); 3.44 (m, CH₂, -CH₂OH); 4.12 (m, CH₂, -CH₂OH) (Figure 5.21, Figure 7 and 9 Appendix)

4.2.2 Synthesis of glyco-pseudodendrimers and glyco-dendrimers

The synthesis of glycopolymers GI-P and GI-D were carried out after synthesizing the intermediate compounds that were required for “click” chemistry.

4.2.2.1 Pentynoic anhydride (16)

Synthesis was done according to the literature protocol.^[375] 7.13 g (73 mmol) of 4-pentynoic acid was dissolved in 46 ml (10 eq) pre-dried CH₂Cl₂ and cooled in an ice bath. 7.5 g (36 mmol, 0.5 eq) DCC was dissolved in 20 ml of pre-dried CH₂Cl₂ was added slowly. The ice bath was removed and the reaction mixture was continuously stirred at room temperature for 6 hours. The reaction was cooled to about -40 °C, the DCU was removed as white solid by repeated filtration with a glass frit (pore size 4) and the solvent was evaporated and the product was dried at 40 °C under vacuum to give 3 as yellowish viscous oil.

Yield: 7 g (100%)

¹H NMR (CDCl₃, ppm): 1.93 (t, CH₂); 2.45 (m, CH₂); 2.55 (s, CH) (Figure 5.24a)

¹³C NMR (CDCl₃, ppm): 13.83 (CH₂); 34.39 (CH₂); 69.68 (CH); 81.42; 167.18 (OC-O-CO) (Figure 5.24b)

4.2.2.2 Synthesis of pentinate modified pseudodendrimers (17, 18 and 19) and dendrimers (20, 21 and 22)

Respective amounts of 10, 11, 12, 13, 14 and 15 were dissolved in 15 eq of CH₂Cl₂. To this 0.15 eq of DMAP and 5 eq pyridine was added. The reaction solution was kept under constant stirring for about 18 h at room temperature. Excess anhydride was quenched by adding 1-2 ml Ultrapure® water under vigorous stirring. The reaction solution is made up to 500 ml with CH₂Cl₂ and washed two times each with a 10% (m/m) NaHSO₄ (2x50 ml), 10% (m/m) NaHCO₃ (2x50 ml) solution and a saturated brine (2x50 ml) solution. The organic phase was dried over Na₂SO₄ and filtered off. The solvent was removed by distillation. The remaining solution was mixed with 10 ml of toluene and pyridine was removed by azeotropic distillation. The residue was dried under vacuum at 50 °C to give 17, 18, 19, 20, 21 and 22 as slightly brownish, highly viscous oil.

Table 4.4: Quantities used in the post-modification of pseudodendrimers and dendrimers.

Sample number	Pseudodendrimers/dendrimers (g)	Pentynoic anhydride (g)	DMAP (g)	Pyridine (ml)	Product (g)	Yield (%)
17	1.2	2.28	0.72	5	1.72	82
18	0.65	1.3	0.405	5	1.78	100
19	0.65	1.3	0.4	5	1.27	93
20	1	2.089	0.165	4	1.96	100
21	1	2.036	0.161	4	1.98	100
22	1	2.017	0.160	4	1.93	100

Pseudodendrimers 17, 18 and 19: ¹H NMR (CDCl₃, ppm): 1.19 (s, CH₃); 1.93 (s, CH); 2.31 (t, CH₂); 2.50 (t, CH₂); 4.19 (m, CH₂OCO). (Figure 5.26, Figure 10 and 11 Appendix)

Dendrimers 20, 21 and 22: ¹H NMR (CDCl₃, ppm): 1.19 (s, CH₃); 1.95 (s, CH); 2.40 (t, CH₂); 2.49 (t, CH₂); 4.19 (m, CH₂OCO). (Figure 12, 13 and 14 Appendix)

4.2.2.3 3-Azido-1-propanol (23)

Azidopropanol was synthesized according to the literature.^[376] 3-bromo-1-propanol (20g, 144 mmol) and NaN₃ (15.32 g, 1.64 eq) was dissolved in a mixture of acetone (240 ml) and water (40 ml) and the resulting solution was refluxed overnight at 60 °C. Acetone removed on rotary evaporator, 100 ml water added and the mixture was extracted with diethyl ether (3 x 50 ml). The organic layers collected were dried over Na₂SO₄ and, after removal of the solvent under reduced pressure; 16 was isolated as colorless oil.

Yield: 12.12 g (83%)

¹H NMR (CDCl₃, ppm): 1.77 (q, 2H, CH₂); 3.38 (t, CH₂); 3.68(t, CH₂). (Figure 17 Appendix)

¹³C NMR (CDCl₃, ppm): 31.3 (CH₂); 48.5 (CH₂-N); 59.7 (CH₂). (Figure 18 Appendix)

4.2.2.4 Mannose propyl azide tetracetate (24).

Synthesis was performed according to the literature protocol.^[18] 16.8 g (43 mmol) of α -D-mannose pentaacetate and 5.2 g (1.2 eq) of 3-azido-1-propanol is dissolved in 150 ml of anhydrous CH₂Cl₂, cooled to 0 °C on ice bath and few beads of 4A molecular sieves were added. 24.43 g (4 eq) of BF₃-Et₂O were added dropwise to the flask. The flask was sealed airtight, the ice bath removed and the solution stirred for 48 hours. The molecular sieve filtered off and the solution was dropped into 150 ml of ice water. The organic phase was washed with ice water, each twice with a 10% (m / m) NaHCO₃ (2 X 50 mL) and a saturated NaCl (2 X 50 mL) solution. The organic phase is dried over Na₂SO₄ and later filtered off, the solvent removed by distillation. The remaining residue was purified by column chromatography on silica gel with an ethyl acetate / n-hexane mixture (50:50) as an eluent, the solvent of the fractions removed by distillation and, after drying at 40 °C under vacuum, the product 17 as pale yellow highly viscous oil was obtained.

Yield 3.02 g (60-80%)

¹H NMR (CDCl₃, ppm): 1.8 (m, 2H, CH₂); 1.93 (s, 3H, CH₃); 1.98 (s, 3H, CH₃); 2.04 (s, 3H, CH₃); 2.09 (s, 3H, CH₃); 3.36 (t, 2H, CH₂); 3.48 (m, 1H, CH); 3.74 (m, 1H, CH); 3.91 (m, 1H, CH); 4.07 (m, 1H, CH); 4.20 (m, 1H, CH); 4.75 (s, 1H, CH); 5.21 (m, 3H, CH). (Figure 5.31)

¹³C NMR (CDCl₃, ppm): 20.64 (CH₃); 28.66 (CH₂); 48.12 (CH₂); 62.53 (CH); 66.19 (CH₂); 68.70 (CH); 69.04 (CH); 69.53 (CH); 97.65 (CH); 169.7 (COO). (Figure 5.32)

4.2.2.5 Mannosepropylazide (25)

5.78 g (13 mmol) of 18 was dissolved in 100 ml of methanol, after which 1 ml of a 25% Na-O-CH₃ solution was added and stirred for 2 hours at room temperature. 2 g of the cation exchange resin Amberlite IR120 H was added and the solution was further stirred for 30 minutes until the pH was adjusted to approx. 7 was reached. The exchange resin was filtered off and the solvent was removed to give 18 as dark yellow viscous oil as product.

Yield: 3.3 g (94%)

^1H NMR (DMSO- d_6 , ppm): 1.78 (t, 2H, CH₂); 3.39-3.45 (m 7H, 2xCH₂, 2xCH); 3.60 (s, CH); 3.66 (t, CH₂); 4.39 (t, CH-O); 4.50-4.67 (2xs, 4H 4xOH). (Figure 5.34)

4.2.2.6 Glyco-pseudodendrimers (26, 27 and 28) and glyco-dendrimers (29, 30 and 31)

Synthesis was done according to the synthetic protocol in literature.^[18] Respective amounts of pseudodendrimers and dendrimers pentinate 20, 21, 22, 23, 24 and 25 was dissolved in 30 ml of THF. 1.2 eq of 19, 0.06 eq of CuSO₄.5H₂O and 0.12 eq of sodium L-ascorbate was dissolved in 30 ml of water and added to the dendrimer solution and the solution was continuously stirred for 2 days at 45 °C. The solvent was removed by distillation to a THF content of about 5% (m/m) and remaining solution was dialyzed (membrane: reg. Cell., MWCO 5 kDa) for 2 days in a solution of distilled water and 5% (m/m) THF (redistilled, unstabilized) and 2 more days purified in pure water. The purified polymer solution was filtered through glass frit, insoluble residue in filter is washed with some water and the solvent of the filtered solution was removed by distillation. After freeze drying, a white to slightly greenish solids are obtained as product.

Table 4.5: Quantities used in the synthesis of mannose functionalized glyco-pseudodendrimers and glyco-dendrimers.

Sample number	Pseudodendrimer/ Dendrimer pentinate (g)	19 (g)	CuSO ₄ . 5H ₂ O (g)	Sodium L-ascorbate (ml)	Product (g)	Yield (%)
26	0.4	0.58	0.027	0.044	0.362	20
27	0.3	0.49	0.021	0.034	0.382	21
28	0.4	0.34	0.016	0.025	0.579	18
29	0.5	0.661	0.031	0.050	0.269	21
30	0.6	0.886	0.041	0.050	0.275	19
31	0.6	0.882	0.042	0.050	0.294	18

Glyco-pseudodendrimers 26, 27 and 28: ^1H NMR (DMSO- d_6 , ppm): 1.10 (CH₃); 2.04 (CH₂); 2.65 (CH₂); 2.84 (CH₂); 3.38 (CH); 3.48 (CH₂); 3.62 (CH₂); 4.11 (CH₂); 4.34 (CH₂); 4.39 (CH) 4.52-4.68 (4x OH); 7.83 (CHN₃C) (Figure 5.36, Figure 19 and 20 Appendix)

Glyco-dendrimers 29, 30 and 31: ^1H NMR (DMSO- d_6 , ppm): 1.10-1.25 (CH₃); 2.02 (CH₂); 2.62 (CH₂); 2.82 (CH₂); 3.39 (CH₂); 3.48 (CH₂); 3.62 (CH₂); 4.09 (CH₂OCO); 4.33 (CH₂); 4.39 (CH); 4.52-4.67 (4xOH); 7.80 (CHN₃C). (Figure 21, 22 and 23 Appendix)

4.3 Analytical techniques and their general details

4.3.1 SEC-MALS – Instrumentation, software and analysis

Size Exclusion Chromatography - Multi Angle Light Scattering (SEC-MALS) comprised of the SEC column coupled with MALS and refractive index (RI) detectors. After injection of the sample to the inlet system, the separation in the SEC column leads to elution of polymers with large polymer eluting first. Thereafter, slices of polymers with ideally uniform hydrodynamic volume pass the MALS detector and then finally to the dRI detector.

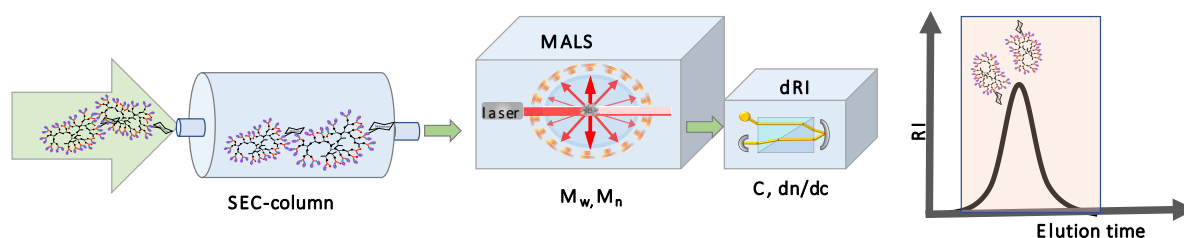


Figure 4.1: Scheme of SEC-MALS-dRI used in this work, comprising of the SEC column coupled to 2 detectors i.e. MALS and dRI. Important quantities obtained are assigned below the respective detectors.

SEC-MALS measurements were done on HPLC-pump 1200 isocratic pump, Agilent Technologies Inc. (US). A 3-angle light scattering detector Mini DAWN (TREOS) ($\lambda = 690$ nm) from Wyatt Technologies Corp (US) with Polar gel-M separation column (300 x 7.5 mm) from PL and the Knauer RI detector (K-2301) are used. The flow rate was 1.0 ml / min. As eluent DMAC was used with 3 g/l LiCl. The measurements were made at room temperature. Astra (version 6.1.7; Wyatt Technology Corporation) was used for measurement, data collection and analysis.

4.3.2 AF4 - Instrumentation, software and analysis

In this work AF4 setup comprises of the channel coupled to MALS, dRI and online Dynamic Light Scattering (DLS). After injection of the samples by the inlet system, the fractionation according to hydrodynamic volume of the polymers leads to elution of small sized polymer first. Subsequently, hydrodynamic uniform fractions of polymers pass through MALS detector which integrates online DLS and then to the dRI detector. Astra 7.3.2 (Wyatt Technology, USA) was used for controlling experimental parameters, data collection and analysis.

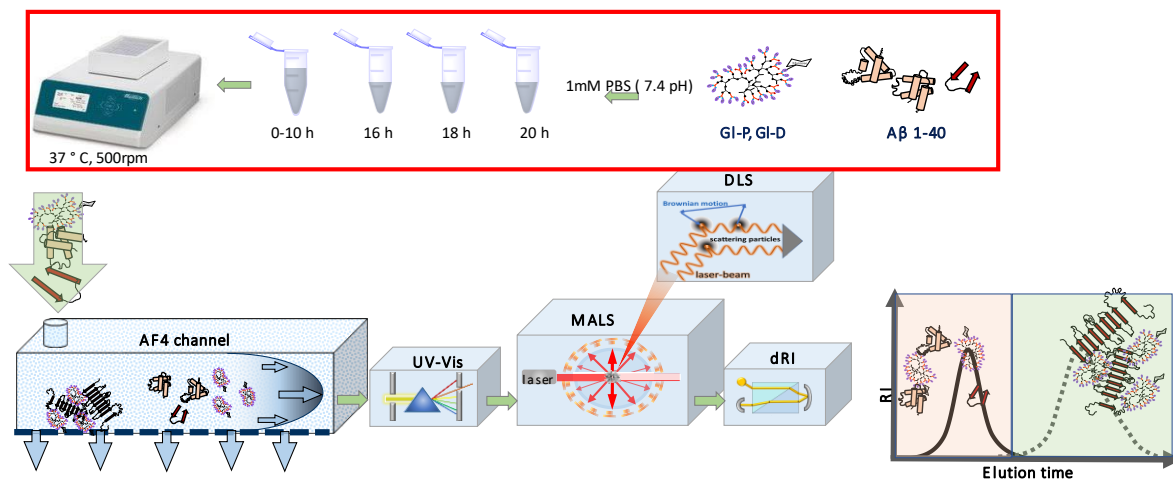


Figure 4.2: Scheme of AF4 setup used in this work coupled to MALS and dRI with online DLS detector. Red box shows the sample preparation involved in this experiment, thermoshaker was used to incubate samples.

4.3.2.1 Sample preparation

20 μM of each glyco-pseudodendrimer and glyco-dendrimer was dissolved in 1mM PBS (pH 7.4) buffer and filtered through 0.2 μm PTFE syringe filter.

4.3.2.2 Method development for analysis of GI-P and GI-D

The development of AF4 separation method requires optimization of several parameters, especially the cross-flow and channel flow rates. The cross-flow force determines the elution properties of the probe, and is normally chosen based on the size of the analytes. A high cross flow is useful to fractionate smaller components, whereas lower cross flow rates work well for the separation of larger components. In case of narrowly distributed samples, a constant cross flow with relatively higher strength is suitable to separate each fraction as in case of BSA (monomer, dimer and trimers) (Section 2.4). The fractionation of broadly distributed samples requires the application of cross flow gradients in order to reduce the analysis time over the entire size distribution. To achieve a high recovery of the sample, the channel flow should be adapted to the cross-flow strength. The use of relatively low flow rates can be advantageous for the online DLS of very large particles, which require more time (i.e., higher acquisition times) to be accurately analyzed.

The following discussion focuses on the method developed for both GI-P and GI-D to compare their molecular characteristics with each other. In this experiment since the knowledge of polymers at lower concentration was required, the concentration of the samples used were 20 μM in 1Mm PBS buffer at pH 7.4 used as model system for AF4 method development.

AF4 is carried out in a LC equipped with PES membrane (MWCO of 5kDa) and PTFE spacer having a thickness of 490 μm . The injection volume is 100 μL . The eluent buffer with 0.01% (w/v) SDS was used to limit the interactions between the sample and channel membrane.^[173] After each run, 10 μL of the buffer is injected into the channel to have stable RI baseline. The molar mass is calculated using refractive index increment dn/dc . The dn/dc of 0.150 mL/g was used, which was determined by manual injection into the RI detector of P-G3-Man with varied

concentrations and was assumed the same for all samples. The channel outlet detector flow was set to 0.80 mL/min. The focusing step was performed for 3 min with a focus flow rate of 3 mL/min. For the separation step, an initial cross flow rate of 3.5 ml/min was set and maintained for 20 min using isocratic step. In the second elution step the cross flow was lowered to 0.15ml/min using linear gradient. In the third elution step cross flow was maintained at 0.15 ml/min for 10 mins. Then the cross-flow rate was maintained at 0 ml/min for 10 mins to ensure complete elution of the very large aggregates.

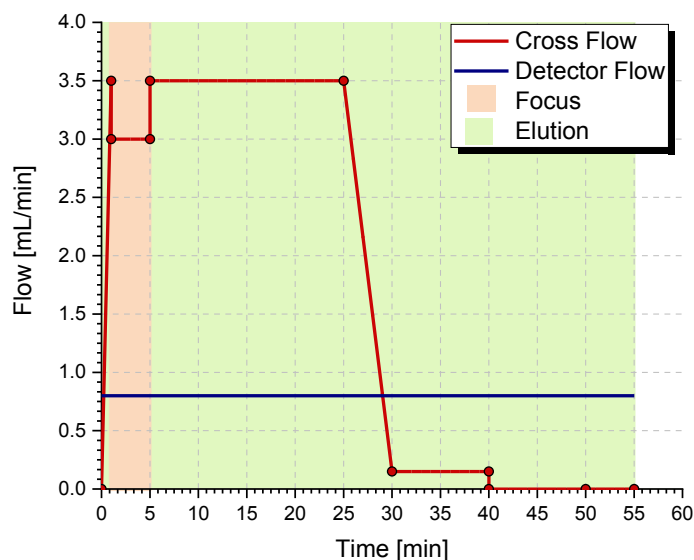


Figure 4.3: Graphical representation of the optimized flow profile for GI-Ps and GI-Ds.

4.3.2.3 Method development for analysis of A β 40 and its interaction with GI-P and GI-D

As the sample preparation method is crucial for the aggregation, the sample preparation was kept as similar as possible to that of ThT assay except the dye. Before mixing all the stock solutions were kept inside the refrigerator. 50 μ M stock solution of A β 40 was freshly prepared. 50 μ l of 0.041 mg/ml (pH 5.6) Heparin and 25 μ l dendrimer of particular concentration (concentration which showed maximum inhibition of aggregation in ThT assay) was added to 1000 μ l of A β 40 solution. The solution was passed through a PTFE syringe filter (0.2 μ m) and placed inside the thermoshaker at 37 $^{\circ}$ C at 500 rpm short mix program, to give gentle mixing to the sample. Samples were taken from the cuvettes at different time intervals 0 h, 2 h, 5 h, 7 h and 10 h. Samples for 16 h, 18 h and 24 h were prepared from the same stock solution and placed in autosampler right before the sample injection. 250 μ l A β 40 and respective amounts of Heparin and dendrimers so that their final concentration remains the same and were measured on the next day. Only single injections were made to avoid delay with repeats of the same sample. Figure 4.4 shows the flow profile for A β 40 amyloids. The flow profile was optimized so that it suits all the different components of the samples (amyloid, heparin, and GI-P/GI-D).

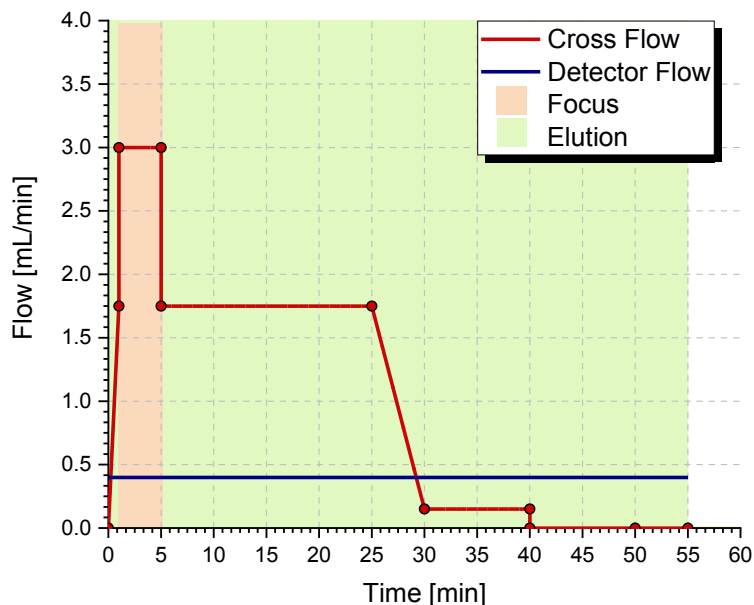


Figure 4.4. Graphical representation of the optimized flow profile for A β 40 amyloid and its interaction with GI-P/GI-D.

4.3.3 Batch DLS - Instrumentation, software and analysis

The batch DLS device comprises of laser (660 nm), sample compartments and detector. The light beam passes through the sample and is scattered. This dynamic light scattering is measured by fluctuations in scattered light intensity.

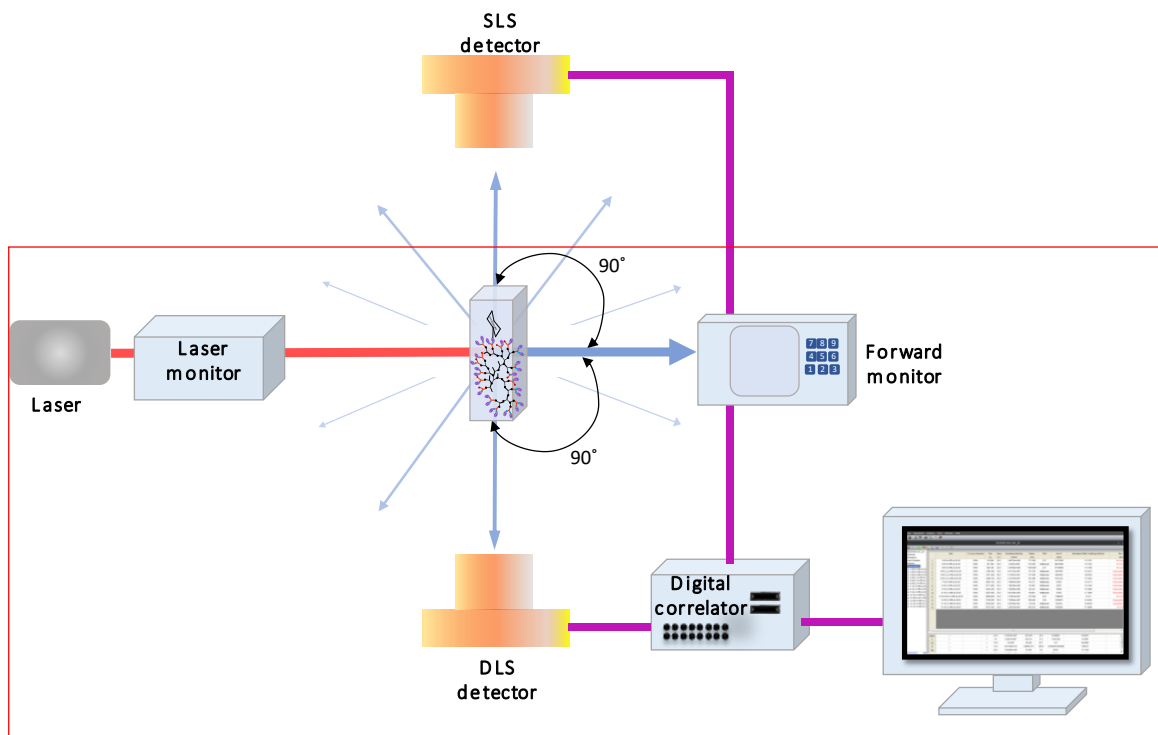


Figure 4.5: Scheme of batch DLS setup.

DLS studies were performed at 25 °C, using a Wyatt DynaPro® Nanostar (Wyatt Technology, US) with 10 acquisitions of each 5 seconds were measured for each sample with auto adjustment of attenuator and laser power. The samples were filtered prior to the measurements with PTFE 13 mm diameter with 0.45 µm pore size. Dynamics (Wyatt Technology, USA) software used for controlling experimental parameters, data collection and analysis.

4.3.3.1 Sample preparation

The samples were dissolved in different solvents at 3 mg/ml concentration and were measured after 1 h of sample dissolution at room temperature.

4.3.4. Theoretical calculations and molecular dynamics simulations

4.3.4.1 Ab-initio calculations

Ab initio calculations were performed in order to optimize the geometry and determine the atomic charges of bis-MPA, mannose carrying end group 3(1-N(mannosetetrahydroxylpropyl)-triazolyl) propionic acid (Man), tris(hydroxymethyl) propane (THP) as a dendritic kernel with three attachment opportunities and the solvent tetrahydrofuran (THF) by minimizing the corresponding Hartree-Fock energy and in order to determine the atomic charges^[377] applying the software package GAMESS^[378] using the basis set 6-31G.

4.3.4.2 Modelling of the polymer structures

The building up of polymers in general was performed applying an own written unpublished software.^[379]

4.3.4.2.1 Pseudodendrimers

The monomer unit bis-MPA was applied to build up the G0 hyperbranched core with 1 unit as a starting monomer and attaching 28 further monomer units in a random manner saturated by hydroxide groups. It is also to be noted that this hyperbranched core G0 is one probable configuration (configurational distribution) of one given monomer mass in a polymerization degree distribution (mass distribution).

The hb-G0-OH hyperbranched core was modified by removing the saturating OH groups and attaching further 30 monomer units of bis-MPA (this is as much as it was possible by the steric opportunities). The further open attachment opportunities were saturated by hydroxide groups because of steric hindrance. This results in formation of first generation pseudodendrimer, P-G1-OH. This P-G1-OH has to be optimized by applying the GROMACS^[380] package as a single molecule without solvent molecules and no periodic boundary conditions with the aim of removing the steric hindrances applying the force field G43a1 with the conjugate gradient algorithm. As will be seen below, this turns out to be very useful for the further construction of the higher generations.

P-G1-OH pseudodendrimer with removed steric hindrances was treated in the same manner in order to attach a second shell of 60 bis-MPA units building up the P-G2-OH pseudodendrimer with afterwards optimization by GROMACS applying the same conditions as described above.

Applying the same method, P-G3-OH pseudodendrimer could be build up by starting with the P-G2-OH polymer attaching additional 240 bis-MPA units and further saturating by OH groups with a following optimization.

4.3.4.2.2 Dendrimers

The monomer unit THP as a 3-fold kernel structure was applied to build up the D-G0-OH dendritic polymer as the zeroth generation by attaching three bis-MPA molecules including the corresponding saturation by OH groups with a following single molecule optimization by GROMACS (see also above).

This optimized D-G0-OH structure could be used to build up the D-G1-OH dendritic polymer by attaching further six bis-MPA molecule models. This procedure could be continued up to the D-G6-OH structure (D-G0-OH + 6 bis-MPA → D-G1-OH + 12 bis-MPA → D-G2-OH + 24 bis-MPA → D-G3-OH + 48 bis-MPA → D-G4-OH + 96 → D-G5-OH + 192 bis-MPA → D-G6-OH).

4.3.4.2.3 Modification of the polymers with special end groups

Each of the pseudodendrimers P-G_x-OH (x=1-3) and dendrimers D-G_x-OH (x = 0-6) was modified by exchanging the saturating hydroxyl groups by the Man group as much as it was possible because of steric hindrances. The P-G1-OH could be modified with 60 Man groups. The P-G2-OH could be modified with 62 Man groups, where the rest of the free valences were saturated with OH groups. At the P-G3-OH pseudo dendrimer 110 Man groups could be attached what means a saturating of the 130 free valences by OH groups. In case of dendrimers D-G_x-OH each of the OH group could be exchanged by the Man group, so e.g., the D-G6-Man has 11687 atoms and a molar mass of 88003 g/mol.

4.3.4.2.4 Preparing of the THF solvent box

The solvent THF is not a part of any forcefield. Therefore, the following procedure was used to build up a THF solvent box. The single molecule THF was multiplied 8 times in the x, y and z direction including a corresponding shifting and three randomly given rotation angles. This box was optimized and equilibrated by the GROMACS package as an NpT ensemble with a constant pressure of 101.3 kPa and a constant temperature of 298 K as the thermodynamic standard state applying the Berendsen thermostatic bath coupling method.^[380,381] The resulting THF solvent box could be used as a group file for preparing a solvated polymer by the program genbox of the GROMACS package in the same manner like SPC or TIP3P water boxes.

4.3.4.2.5 Solvation of the polymer structures

Additionally, each of the P-G_x-O_y (x = 1-3, y = OH, Man) polymers and also the D-G_x-O_y (x = 0-6, y = OH, Man) were packed separately into a cubic simulation box with starting box lengths of 15 nm in every direction filled up with explicit THF, SPC or TIP3P (water molecules) as the corresponding solvents applying periodic boundary conditions in every direction.

4.3.4.3 Molecular dynamics simulations

The MD procedure included three different types of steps. The first step was the optimization of the solvated polymer with periodic boundary conditions. The applied force field was the G43a1 of the GROMACS package. The cut-off procedure was chosen for the van der Waals and the Coulomb interactions. The corresponding energetically minimized structures could be applied for the equilibration run, which was separated in a step for preparation up to 100 ps and second step up to 1000 ps with a time step of 0.5 fs as an NpT ensemble with a constant pressure of 101.3 kPa and a constant temperature of 298 K as the thermodynamic standard state applying the Berendsen thermostatic bath coupling method.^[380] At every 5000 steps, an ensemble output was written.

4.3.4.3.1 Evaluation of the simulation trajectories

The evaluation tools `g_gyrate`, `g_density` and `g_rdf` of the GROMACS package were used to derive the ensemble averages of the polymers. Because the ensemble approximates exponentially up to the set pressure and temperature the last 500 ps (i.e., from 500 to 1000 ps) were used for the evaluation.

4.4 Investigation of interaction of GI-P and GI-D with Amyloid beta (A β 1- 40)

4.4.1 ThT Assay - Instrumentation and software

The experiment was performed on Tecan Infinite 200 PRO, using multifunctional plate reader (MTP) in 96-well microplates. Fluorescence intensity measurement technique was used. The optical system of the fluorescence top and bottom system of the device consists of the following system:

1. Light source system
2. Fluorescence Optics, and
3. Fluorescence detection system

The Infinite 200 PRO system utilizes a high energy Xenon arc discharge lamp with a condenser made to focus the flash light on the entrance slit of the fluorescence system. The fluorescence system consists of Emission filter and Excitation filter. The fluorescence emission spectrum does not depend on the excitation wavelength. Therefore, to get a maximum of total fluorescence signal, relatively broad excitation band pass filters (2-40 nm) can be used. The diameter is about 2 nm for both top and bottom optic system. In top optics system, emission is measured from above the well and in bottom optics system from the bottom, passing through a fiber. The filter discriminates unspecific scattering and fluorescence. Such low levels of light in fluorescence is measured by a photomultiplier tube (PMT).

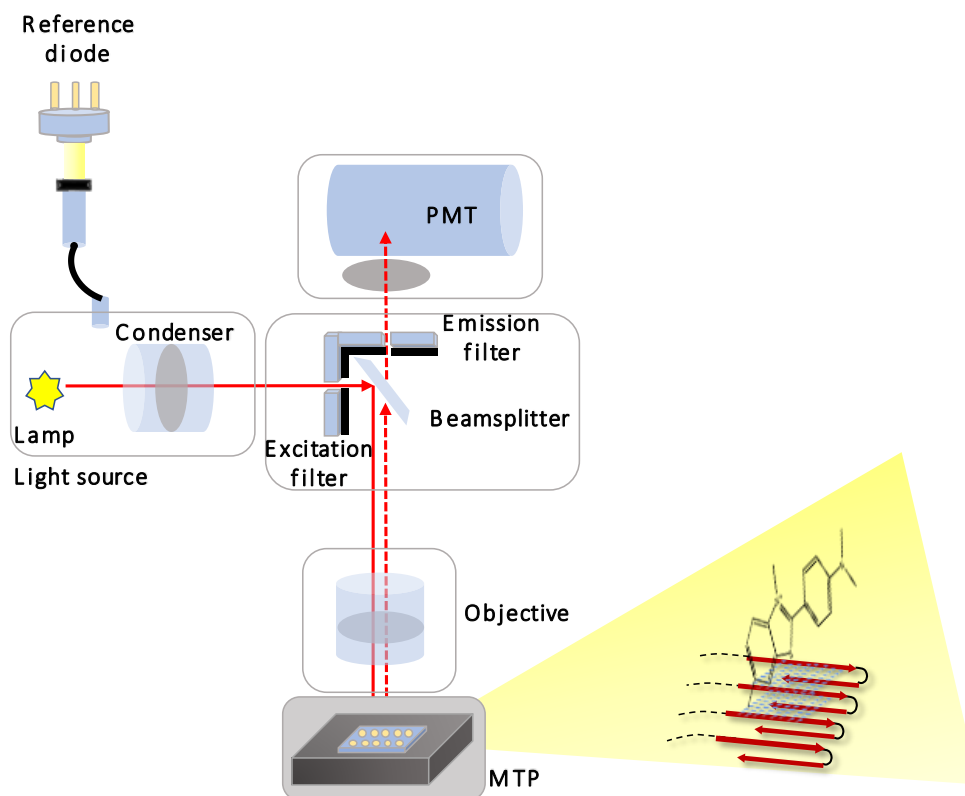


Figure 4.6: Scheme of the ThT fluorescence setup: the solid arrows indicate the excitation light path; the dashed arrows determine the emission light path.

The Infinite 200 PRO is operated using a personal computer-based software control i-control or Magellan software may be used as the user interface.

4.4.1.1 Sample preparation

Thioflavin T (ThT) stock solutions, 350 μM , were prepared in 10 mM phosphate buffer (pH 7.4 with 2% NaN_3). ThT final concentration in the fluorescence cuvette was 35 μM . Stock solutions of 0.41 mg/ml of heparin were prepared and added so that the final concentration in each cuvette is 0.041 mg/ml. Aliquots of HCL was added to make the final pH 5.6. Stock solution of glycopseudodendrimers and glyco-dendrimers, and added to the cuvettes right before the fluorescence measurements so that the final concentration in each well was 0.1 μM , 1 μM , 2 μM , 5 μM and 10 μM . These experiments were performed at 37 $^\circ\text{C}$ under continuous but gentle agitation of the plate for 21 h. The excitation and emission wavelengths of 450 and 490 nm, respectively were used. Samples were made in triplicates and repeated three times. The band width was 2.5 nm.

4.4.1.2 Kinetics based on ThT assay- software and data analysis

Following the referred protocol the kinetics of the aggregation was monitored by the changes in the fluorescence intensity during the course of the experiments using the online fitting software AmyloFit.^[355] After discussing the results with Dr. Meisl the model ‘secondary nucleation dominated’ was used, with the reaction orders set to 2 as typical for $\text{A}\beta$ 42/ $\text{A}\beta$ 40 and under the constraint of allowing deviations from the kinetics in only one parameter at a time. This allowed to investigate which microscopic step or which species of the aggregation

mixture was most likely affected by the glyco-pseudodendrimers and glyco-dendrimers. Repeats of the experiment were analyzed separately and combined at the end to estimate uncertainty. Only the lower concentrations (0.1 μM , 1 μM and 2 μM) were used to perform this analysis.

4.4.2 CD spectroscopy - Instrumentation and software

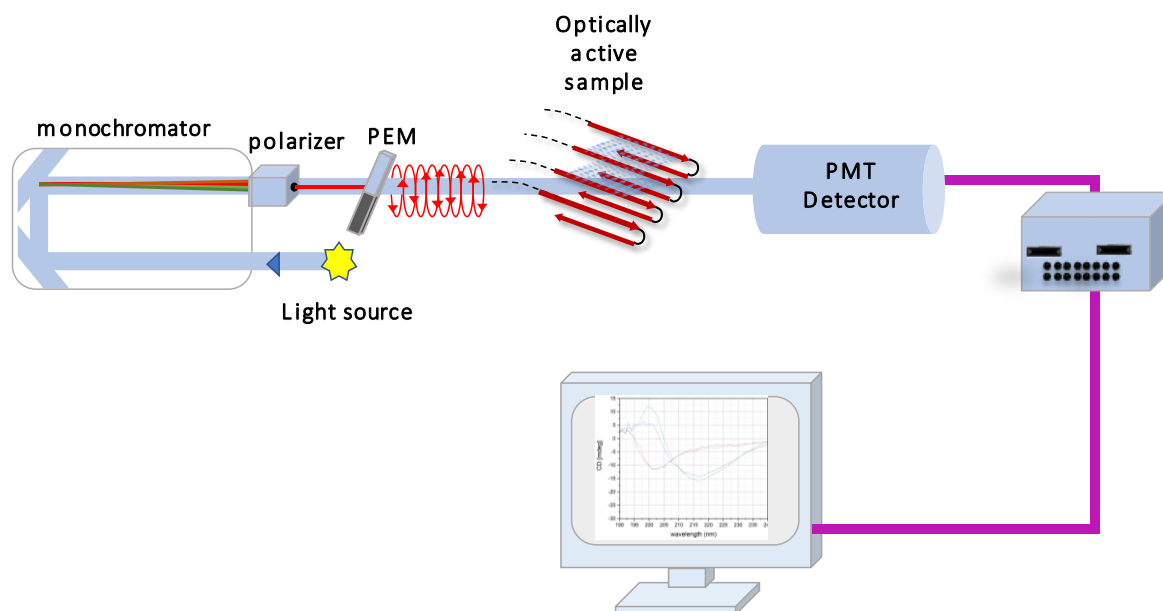


Figure 4.7: A schematic representation of CD spectropolarimeter.

A CD instrumentation consists of Lamp (Xe or Xe/Hg), monochromator, polarizer, sample compartment and a photomultiplier as a detector. The monochromator uses two synthetic single-crystal quartz prisms. The light beam passes through the polarizer and is transformed into linearly polarized light. The photo elastic modulator (PEM) then converts the linearly polarized light beam into left and right circularly polarized light which then passes through the sample in the sample compartment which is temperature controlled. The light beam is then going to the detector system which consists of a PMT and an amplifier.

The experiments were performed on J-815 CD Spectropolarimeter from JASCO, Japan with a Peltier temperature controller and single cuvette holder; and CDPro software was used for data collection and analysis. The CD spectra (195–260 nm) were recorded for A β 40 in the presence/absence of synthesized glyco-pseudodendrimers and glyco-dendrimers on the spectropolarimeter, in 1 mm, 0.2 cm path length quartz cuvettes, a response time of 1 s, 2 nm bandwidth and a scan rate of 50 nm/min, thermostated at 37 °C. Each spectrum was the average of three repetitions.

4.4.2.1 Sample preparation

These experiments were carried out only for samples which showed maximum effect of inhibition on the aggregation of A β 40. In these experiments, we used P-G1-Man, P-G2-Man, P-G3-Man, D-G4-Man, D-G5-Man and D-G6-Man at final concentrations of 1, 10, 2, 1, 5 and 5 μM , respectively. The conditions were made similar to the ThT sample preparation, as much

as possible. The final concentration of A β 40 was 50 μ M, with heparin (0.041mg/ml, pH 5.6) and with respective amounts of glyco-pseudodendrimers and glyco-dendrimers. The changes in the secondary structure of A β 40 in the presence and absence of dendrimers were tested immediately 0 and after 1, 5 and 24 h of incubation at 37 $^{\circ}$ C. the. Each spectrum was analyzed for the content of α -helix and β -sheet using the BeStSel software.

4.4.3 AFM - Instrumentation and software

AFM is a very-high-resolution type of scanning probe microscopy (SPM), with a resolution on the order of Angstrom (\AA). As mentioned earlier, the high resolution in XY and Z direction is ensured by the coupling of piezoelectric elements with the probe on the end of the cantilever.

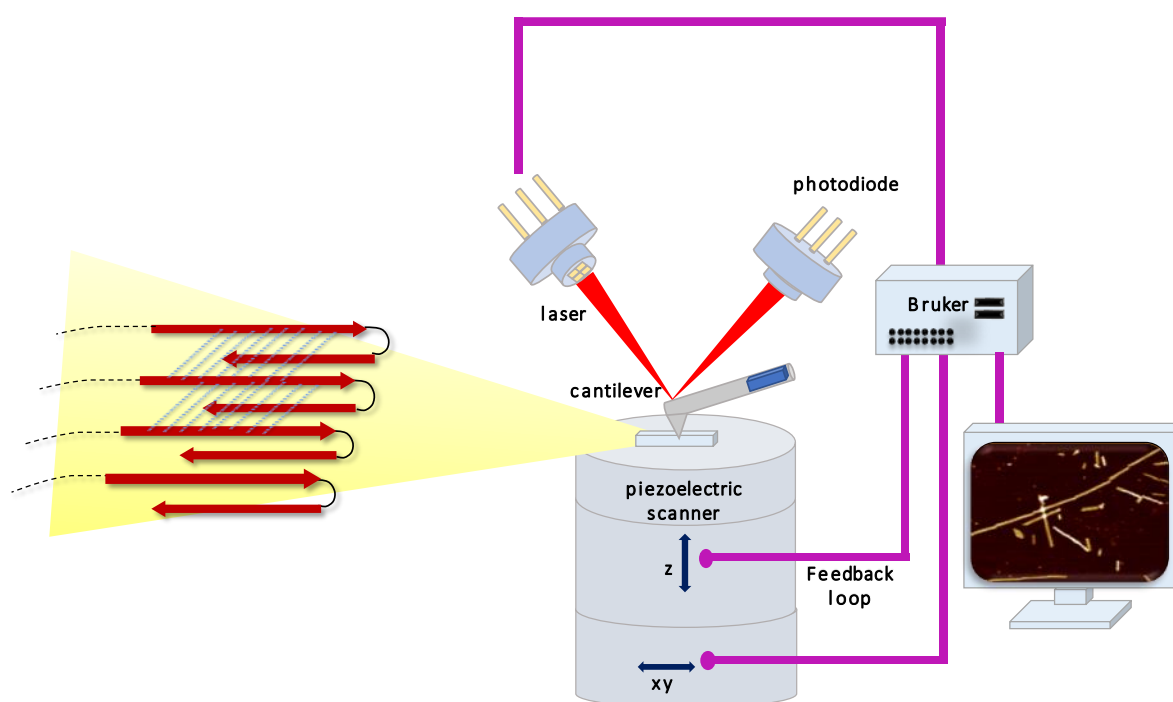


Figure 4.8: A schematic representation of AFM instrumentation.

In this study the tapping mode is used for scanning samples in air. The AFM measurements are carried out on Dimension FASTSCAN with SCANASYST (Bruker-Nano, USA) equipped with the software NanoScope for setting experimental parameters, data collection and analysis. Silicon nitride sensors with a nominal spring constant of 0.7 N/m and tip radius of 2 nm are used. The set point was 0.02 V.

4.4.3.1 Substrate and sample preparation

After a fresh cleavage of mica with an adhesive tape, 10 μ l of 1%-solution of 3-aminopropyldimethoxysilane (APTES) in water was dropped on the surface of mica to positively functionalize it and incubated for 5 min. The surface is then rinsed with deionized water and gently dried with N₂ gas. The samples are dropped on the mica substrate, allowed to incubate for 10 min and rinse with water and gently dried with N₂ gas.

These experiments were also carried out for sample which showed maximum effect of inhibition on the aggregation of A β 40 i.e., in absence and presence of P-G2-Man at 10 μ M concentration in phosphate buffer (10 mM, pH 7.4). 0.041 mg/ml heparin (pH 5.6) and ThT (35 μ M).

4.4.3.2 Height determination and counting procedures

Height was determined using the "Particle Analysis" tool of Bruker NanoScope Analysis software. The threshold height was determined by visual inspection of the complete coverage of all nanostructures. It is possible that 2 or more fibrils could be placed close enough that the program is unable to differentiate between individual fibrils which would lead to several "clumped" nanostructures to be counted as a single structure; taking this into account, it is possible that the total nanostructure counts reported in this work were lower than the actual number of nanostructures in the image. However, the average height calculations were not affected by this. All the images were flattened to first order to remove any bends and tilts.

For the quantitative analysis of all AFM images, we calculated the heights single fibrils at 6 different positions on the same fibril along the white line using the "section" tool of the NanoScope analysis

To study this further, we calculated the cross-sectional heights and roughness of different fibrils. The height measurements were made from scan sizes of 1 x 1 μ m or less by measuring cross sectional height across the white dotted line. The heights for different fibrils species were taken corresponding to the peaks (~5).

AFM images were visually inspected to randomly select fibrils and measure the lengths for >150 fibrils. Also; AFM images were visually inspected to see aggregates (amorphous aggregates or clumped fibrils)

4.4.3.3 Topography and diameter

AFM images were visually inspected for twist and patterns. The negative peak force error image showed twisted pattern very clearly. The fibrils are assessed by measuring the height in cross section of >100 individual fibrils. Fibril diameters are estimated from the height of fibril in cross section.

4.5 Cytotoxicity

4.5.1 Zeta potential

The particle size and zeta potential were measured by dynamic light scattering using Zetasizer (Nano ZS, Malvern Instruments, Malvern, UK). All measurements were performed following established protocol.^[268] In short, 1mM stock solution in 10 mM phosphate buffer of each sample was diluted to 10 μ M with MilliQ water. Firstly, all samples were measured for size in quartz cuvettes at 25 °C (6 runs, 6 measurements). Special cuvettes DTS1070 were used for zeta potential measurements, by activating the cuvettes with ethanol (twice) and then washing it with distilled water (twice).

4.5.2 Cell culturing

Two cell lines were used in this study-HMEC-1 (immortalized human microvascular endothelial cell) and HeLa (human epithelial) derived from human cervical cancer cells. HMEC-1 cells were grown in MCDB131 medium supplemented with 10% (v/v) fetal bovine serum, 200 mM L-glutamine, 10 mg/ml hydrocortisone and 1 mg/ml EGF (Epidermal Growth Factor). HeLa cells were grown in DMEM medium supplemented with 10% (v/v) fetal bovine serum. Cells were cultured at 37 °C in humidified air containing 5% CO₂ and sub-cultured every 2-3 days. After reaching 80-90% confluence, cells were used in experiments.

Both cell lines were seeded in a 96-well plate at an initial density of ca. 2×10^4 cells per well in 100 μ l of complete cell suspension in respective media and incubated for 24 h.

4.5.3 Sample preparation

The desired concentration of each glyco-pseudodendrimers (P-G1-Man, P-G2-Man and P-G3-Man) from 1mM Stock in PBS buffer was prepared, so that the final concentration in each well is 0.1 μ M, 1 μ M, 10 μ M and 100 μ M. 10 μ l of each sample in each well and incubated for 24 h at 37 °C.

4.5.4 MTT method

After the 24 h treatment with glyco-pseudodendrimer, the contents were removed gently, blotting on paper towel and washed with PBS. MTT solution (0.5 mg/ml in PBS, pH 7.4) were added to all wells and incubated for another 3 h at 37 °C. After 3 h, the contents were removed and 100 μ l of DMSO was added in each well. Plates were shaken for 1 min and the absorbance was measured at $\lambda = 580$ nm and $\lambda = 720$ nm by means of Biotek Synergy HTX Multi-Mode reader (USA).

$$\text{Cell viability (\%)} = \left(\frac{X}{X_c} \right) \cdot 100$$

whereas, X is the absorbance of cells treated with different glyco-pseudodendrimer each with different concentration and X_c is the absorbance of control cells (cells without glyco-pseudodendrimers)

Cytotoxicity of drugs was expressed as their IC₅₀ and IC₇₀ concentrations that reduce cell viability by 50% and 70% relative to the control (untreated cells), which viability was assumed as 100%.^[382]

4.5.5 Changes in mitochondrial transmembrane potential (JC-1 method)

Again, both the cell lines were used for this experiment. The cells were seeded in 96-well black plates at a density of 2×10^4 cell per well and incubated overnight in a humidified atmosphere containing 5% CO₂ at 37 °C. Then, cells were treated with 37 μM concentration of each GI-Ps. Fluorescent probe JC-1 (5,5',6,6'-tetrachloro - 1,1', 3,3'- tetraethylbenzimidazolcarbo- cyanine iodide) was applied to study mitochondrial transmembrane potential changes. In this method the cells were treated with glyco-pseudodendrimers for 3 h and 24 h. 5 μM JC-1 solution in HBBS buffer was prepared. After the treatment, the contents were removed and cells were washed with PBS and later on removed. JC-1 solution 50 μl in each well was added and incubated for 30 mins at 37 °C. Fluorescence measurement was measured at $\lambda_{ex}= 485$ nm and $\lambda_{em}= 535$ nm and $\lambda_{ex}= 535$ nm and $\lambda_{em}= 595$ nm by means of Biotek Synergy HTX multi mode reader (USA)

4.5.6 Flow cytometric detection of phosphatidyl serine exposure (Annexin V and PI method)

Briefly, 5×10^5 cells in culture medium were seeded into 12-well microplates 24 h before GI-Ps treatment. The IC₅₀ concentration of GI-Ps was added to appropriate wells and the microplates were incubated in a CO₂ incubator for 3 h and 24 h. Then, control and GI-P treated cells were washed with cold PBS and resuspended in 500 μL buffer that contained 5 μL of Annexin V fluorescein isothiocyanate (FITC) and 5 μL of PI and stained for 15 minutes at room temperature. Finally, 10,000 cells were analyzed for FITC and PI fluorescence on a flow cytometer (LSR II, Becton Dickinson). Gates were set for FSC and SSC to exclude debris was adjusted to avoid overlapping of the different spectra. The percentage of apoptotic cells was calculated as the sum of those stained with annexin V alone (early apoptosis) and stained with both Annexin V and PI (late apoptosis).

5 Results and Discussion

The main focus of this work has been the synthesis of functionalized highly branched polymer scaffolds along with their investigation towards Alzheimer's disease (AD). Herein, hyperbranched glyco-pseudodendrimers (GI-P) and comparative glyco-dendrimers (GI-D) with ordered branching were explored as anti-Alzheimer's agents. Although a detailed discussion on the motivations, general strategy and experimental methodology has been done in Section 2.6, a brief recap is warranted.

For the study, the monomer, the specific functional unit and the way of its incorporation, were specifically chosen. Anti-Alzheimer's agents are aimed at suppressing the agglomeration of amyloidogenic peptides ($A\beta$) and proteins, which are understood to be the underlying cause of neuronal degradation in AD. In principle, several aliphatic and aromatic monomers could be selected for the preparation of hyperbranched and dendritic structures. Correspondingly, with regards to polymer synthesis, various possibilities exist, ranging from polycondensation to ATRP. As discussed earlier in the Section 2.4.2.2.4, the choice for the monomer and the templates in this work were dictated not only by their availability and methods for production, but, more importantly, also based on the biomedical viewpoint of the selected moiety and their implementation.

2,2-Bis(hydroxymethyl)propionic acid (bis-MPA) was chosen as the monomer for the hyperbranched GI-P because of several reasons: ease of availability, facile pre-established methods with high-yields, and straightforward conditions for synthesis.^[15,296,327,383,384] For a comparative study, multifunctional GI-D based on trimethyl propane (TMP) core of third generation (PFD-G3-TMP-OH) was bought from Polymer Factory, Sweden in order to synthesize next three generations.

As for the functional units, it should possess an affinity for the $A\beta$ protein, because this is the driving force for their interactions with proteins. Saccharides are good candidates for such studies. Mannose in particular interferes with the metabolic pathway of glucose, inhibit growth of cancer cells. These characteristics are essential to develop drugs for different diseases. In this work, it is mannose because of preliminary investigations described in the literature which shows the varied potential of mannose in clinical applications.^[341,385-389] Also, the method of functional unit incorporation into the polymer backbone is highly important as directly affects the protein interaction. Generally, this modification could be performed in two ways: in the focal point/usage of core moiety and the end groups.^[305,310] Through these two methods either monofunctional or multifunctional polymer templates can be prepared. For this work, the latter modification pathway has been applied in order to have better interaction properties with the specific protein chosen for the study.

In Alzheimer's Disease (AD), a progressive deposition of β amyloid ($A\beta$), a 39-43 amino acid residue peptide derived from amyloid precursor protein, takes place.^[390] Searching for

substances inhibiting A β aggregation has been the focus of many research groups working on the same topic. Studies have shown that A β 42 proliferates more rapidly than A β 40.^[391] This makes A β 40 a strong candidate to do *in vitro* studies.^[268,392] For the same reasons, in this work A β 40 was chosen as protein to study its behavior with the synthesized glycopolymers.

5.1 Synthesis and characterization of glyco-pseudodendrimers and glyco-dendrimers

Figure 5.1 depicts the synthesis summary of three generations of mannose functionalized GI-P based on bis-MPA hyperbranched (hb) polyester along with the synthesis of three generations of mannose functionalized GI-D based on TMP core. The GI-D were synthesized starting with third generation and forming next three generations in order to have a comparable molar mass with similar number of functional end groups.

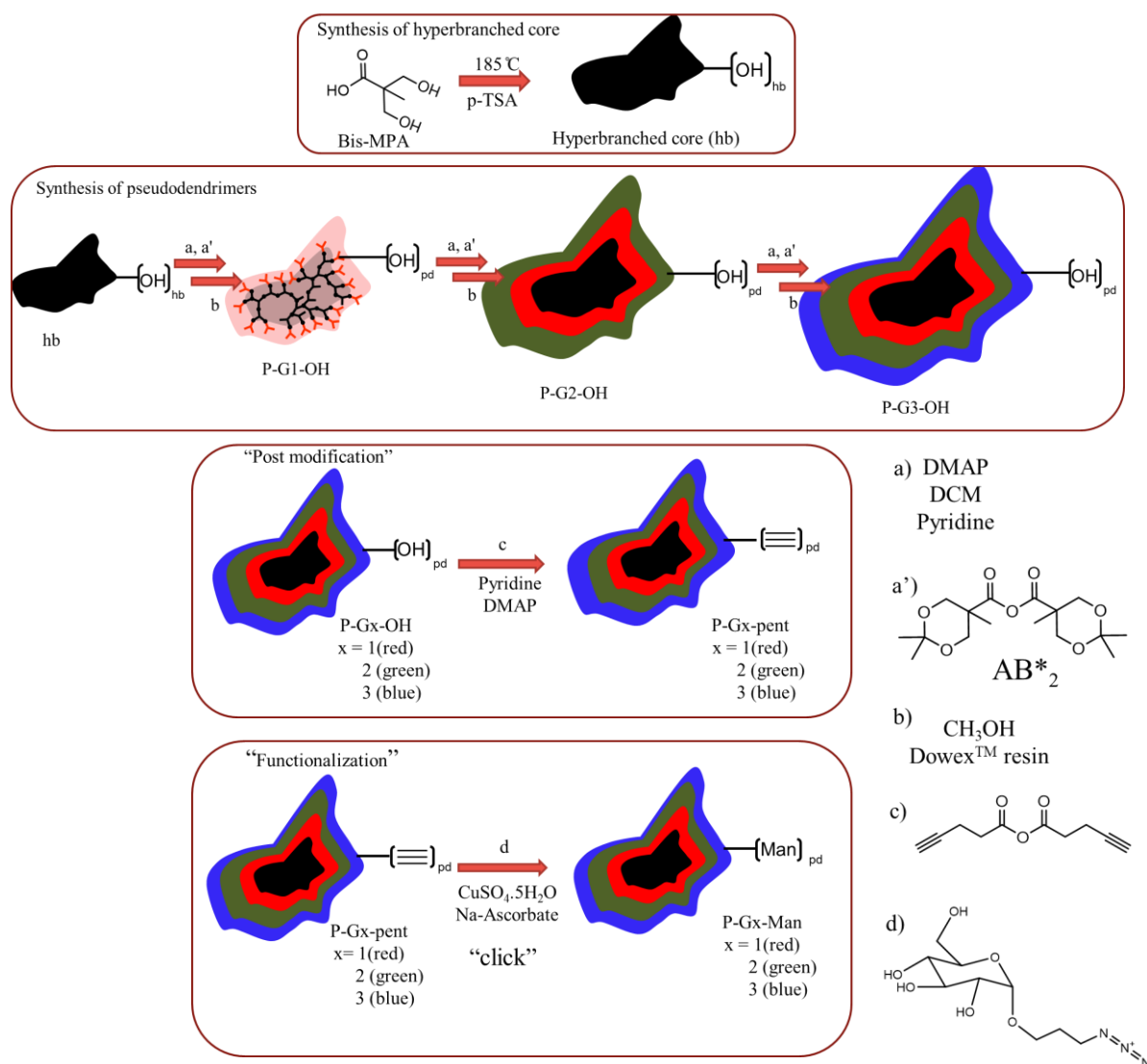


Figure 5.1: Outline of the synthesis strategy for glyco-pseudodendrimers used in this work.

Figure 5.1 shows the synthesis of GI-P. The scheme is subdivided into four parts:

1. Synthesis of hyperbranched polymer
2. Synthesis of pseudodendrimers
3. Post-modification
4. Functionalization

In the first part, hb polymer was synthesized (hb-G0-OH) using melt polycondensation using bis-MPA as AB₂ monomer type. It is an esterification reaction performed in bulk using an acid catalyst and involves no purification. The first part also involved the synthesis of protected monomer based on bis-MPA (AB*₂). The second part involved the repeated protection and deprotection using acetonide protected anhydride AB*₂ monomer type forming three generations of pseudodendrimers. Furthermore, in the third part, for all three generations of pseudodendrimers, the OH groups were modified with 4-pentynoic acid anhydride leading to the formation of alkyne terminated pseudodendrimers. The fourth part involves modification of the alkyne terminated pseudodendrimers with mannose using Cu catalyzed “click” chemistry.

In the case of synthesis of dendrimers, Polymer Factory's bis-MPA hydroxyl dendrimer of third generation was used as starting polymer and all of the above steps (except first step) were used, as is shown in Figure 5.2. All the three-post-modified pseudodendrimers were modified with mannose, forming three generations of GI-D: D-G4-Man, D-G5-Man and D-G6-Man.

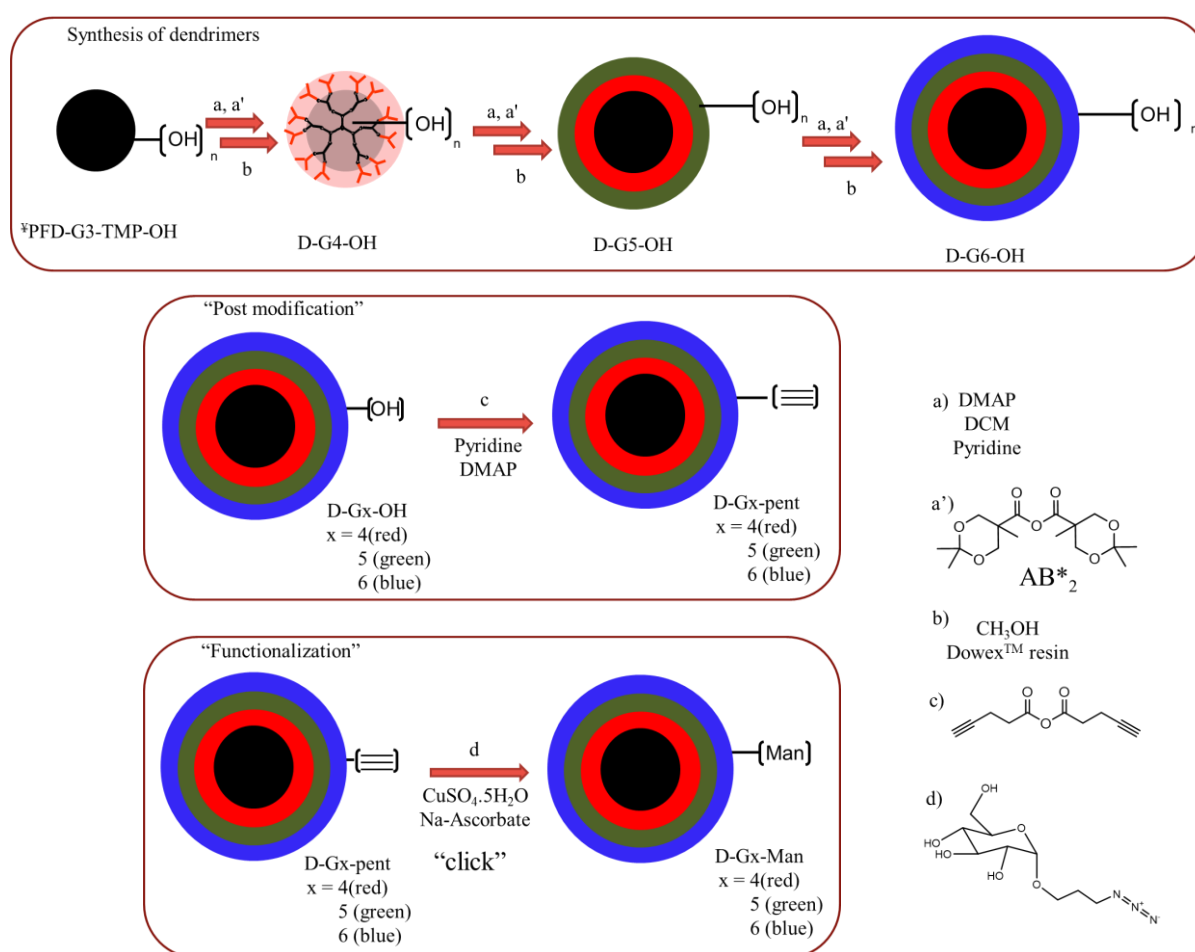


Figure 5.2. Outline of the synthesis strategy for glyco-dendrimers used in this work, performed in the same way as glyco-pseudodendrimers. [‡] Polymer Factory, Sweden.

5.1.1 Synthesis and characterization of hyperbranched polyester (hb-G0-OH)

In 1990s, Hult et al. brought dendrimers based on bis-MPA into focus of research.^[14,15,393] In the present work hb polymers based on bis-MPA as AB₂ monomer type were prepared by acid catalyzed polymerization in melt in a one-pot synthesis at 185 °C h over a period of 8 hours in the presence of para-toluene sulfonic acid (p-TSA; 0.001 eq) (Figure 5.3). This esterification was carried out in bulk and driven toward high conversion as the water formed was continuously removed. This removal of water is important to obtain high molar mass and was executed with nitrogen at early stages of polymerization, for initial 2 hours and then under reduced pressure of 5-6 mbar for next 5 hours as the condensation reached completion. hb-G0-OH was dissolved in THF and precipitated in cold diethyl ether (-78 °C). The ratio of THF and diethyl ether was 1:3. The advantage of this esterification in bulk is that it involves no purification step. This hb polymer was synthesized during a preliminary work and is used as the starting material for the synthesis of pseudodendrimers.^[336]

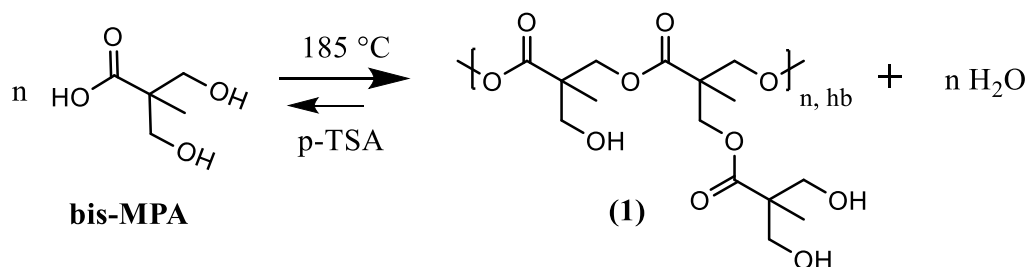


Figure 5.3: Synthesis of hyperbranched polyester hb-G0-OH (1) which serves as a core for next steps.

The chemical structure of hb-G0-OH has typical terminal (T), linear (L) and dendritic (D) repeat units similar to which is generally found in AB₂ hb polymers which was proven by ¹H NMR. The different units of the hb polyester molecule is shown in Figure 5.4.

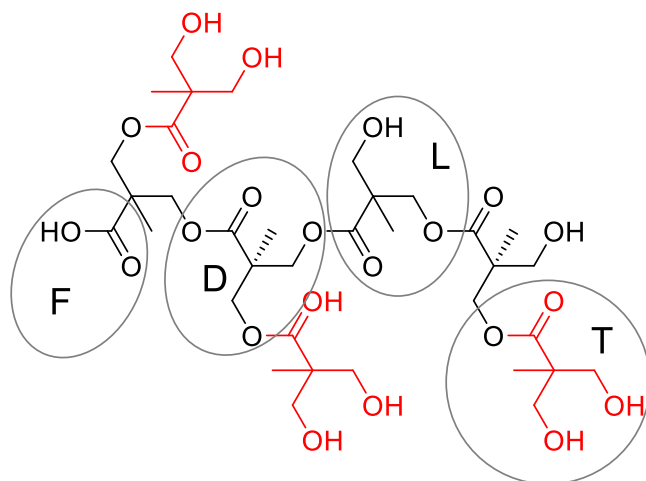


Figure 5.4. The molecular structure of the hb-G0-OH with terminal (T), linear (L) and dendritic (D) repeating units and the focal group (F).

The ¹H NMR spectrum of hb-G0-OH (Figure 5.5) it is clear that in the molecular structure three types of methyl groups are available. The signal 1.02 ppm in this case shows the methyl groups of the terminal units, the signal 1.08 ppm is of the linear units and the signal 1.18 ppm of the

dendritic units. The signals 3.49 ppm and 4.12 ppm are the protons of the backbone of the polymer. The solvent DMSO-d₆ used is able to do rapid chemical exchange of protons and as a result OH peaks appear anywhere in the spectrum. The signals 4.60 ppm and 4.91 ppm are the protons of the terminal and linear hydroxyl groups, respectively.

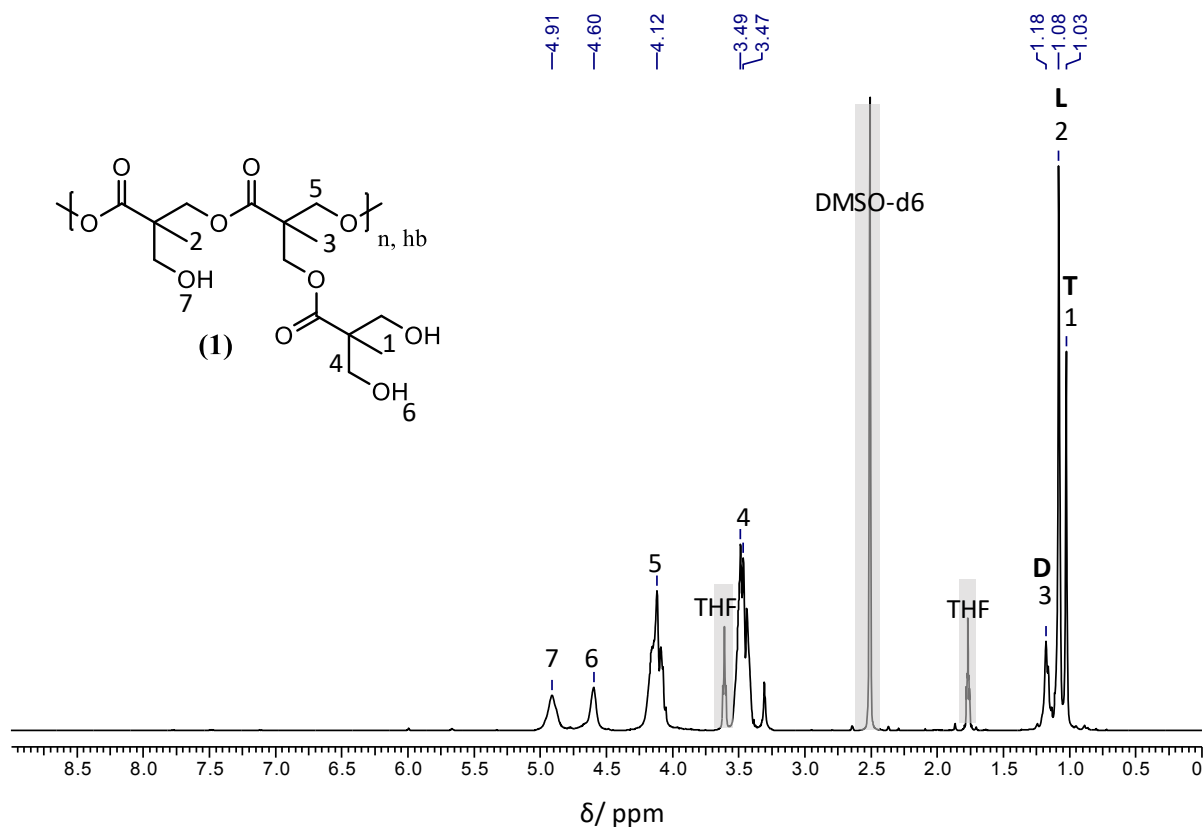


Figure 5.5: ¹H NMR structure of hb-G0-OH displaying terminal (T), linear (L) and dendritic (D) methyl groups. Solvent signals have been greyed out.

On the basis of the signals at 1.03 ppm (terminal), 1.08 ppm (linear) and 1.18 ppm (dendritic) DB can be calculated. The OH signals were also visible at 4.60 ppm and 4.91 ppm for terminal and linear OH groups respectively. The DB of the polymer can be calculated according to Equations 8 and 9 (Section 2.7.2). Since the peaks of the methyl groups are slightly overestimated, as shown in Figure 5.5, semi quantitative evaluation of each signal areas was made by normalizing the signal and then taking the integral values for the calculation of DB. This gives rise to a DB of ~ 0.5.

After determining the DB, number of each –OH units were simulated correlating to the same DB, a method of calculation was developed using the masses of each unit (Figure 5.4), in ACD/ChemSketch (freeware) software (Canada) and then multiplying the mass of each units with the number of –OH groups. After adding all the units, the theoretical number average molar mass of the polymer was obtained. This method of calculation was applied in each case of pseudodendrimers to estimate the number of T, L and D units and hence the total number of OH groups.

Table 5.1: Results of the model calculation of hb-G0-OH.

Structure units	T	L	D	Focal (D)	Σ	DB _{Frechét}	DB _{Frey}
Number of units	8	16	6	1	31	0.51	0.42
M (g/mol) per unit	117	116	115	133			
Σ M(g/mol)	936	1856	690	133		M _n =3,615	
OH groups	16	16		1		Σ OH groups = 33	

This shows that the values of DB from this simulation calculation gives a fairly good agreement to ¹H NMR spectrum (~0.5) except for DB using Frey.

5.1.2 Synthesis and characterization of pseudodendrimers P-G1-OH, P-G2-OH and P-G3-OH

Synthesis of the first generation pseudodendrimer (P-G1-OH) based on the hb polymer is carried out by the reaction of hb polymer (hb-G0-OH) with AB*₂ (protected monomer). The objective of this reaction was the coupling of both L and T hydroxyl group further with the monomer unit of bis-MPA. This, on one hand, would lead to an increase in molar mass and on the other hand would maximize the DB by increasing the T- methyl units and eliminating the L units. The strategy is to attach acetonide protecting groups to protect the two hydroxyl groups of bis-MPA as both the hydroxyl groups of the diol part and the carboxyl group exhibit the same reactivity, so for further reaction only the carboxyl group is available. This is the first step of the formation of AB*₂. The protection of the monomer was carried out by reaction (Figure 5.6) with dimethoxypropane (DMP) in presence of p-TSA as catalyst forming bis-MPA acetonide (2).

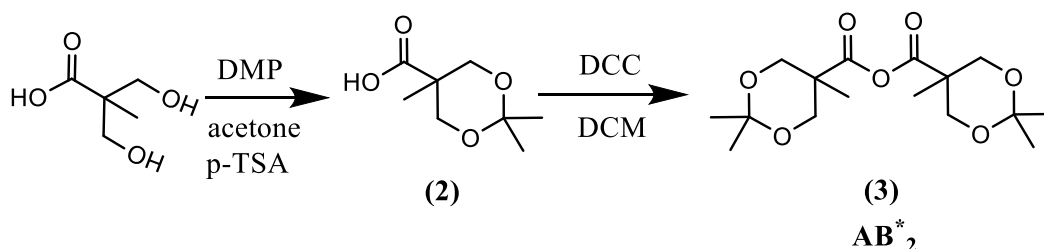


Figure 5.6: Reaction scheme for the formation of protected monomer from bis-MPA first forming bis-MPA acetonide (2) and then forming bis-MPA acetonide anhydride (3) (AB*₂).

In order to assess the results of this reaction, ¹H NMR and ¹³C NMR spectra were recorded. The ¹H NMR (Figure 1, Appendix) shows that an acetonide protecting group has formed, represented by the signal 2 of the CH₃ groups. The splitting between the two signals is due the spatial position and their different proximity to the carboxyl group. In addition, signal 1 shows the methyl group of bis-MPA part in the spectrum. The protons of -CH₂ units would show a slight difference in the spectrum, as each unit due to the spatial structure of the molecule couple differently with the groups on the other side of the quaternary carbon atom, resulting in further splitting. However, prominent signals of each CH₂ units are clearly seen as signals 3 and 4.

In ¹³C NMR spectrum (Figure 2, Appendix) the formation of acetonide protecting group is shown by the signals 2 and 3. As in ¹H NMR, the carbon atoms of the acetonide protecting

group also show a splitting due to their spatial position in the molecule. A splitting of the signal 5 for the $-\text{CH}_2$ of bis-MPA part, however, does not take place.

Preliminary tests showed that the direct reaction of the basic polymer with the protected bis-MPA acetonide monomer in dichloromethane (DCM) in the presence of di(2-pyridyl)trisulphide (DPTS) was carried out with the catalyst to give less than 40% yield, as the reactivity of this monomer is not particularly high.^[394] For this reason, the synthesis of the pseudodendrimer with the acetonide-protected bis-MPA anhydride (AB^*_2) was sought. The efficient use of this anhydride chemistry was introduced by Malkoch et al. in 2002 who in turn was inspired by the benzylidene-protected anhydride esterification strategy reported by Fréché et al.^[19,297] This acetonide-protected anhydride synthesis route allows synthesis of large orthogonally protected dendritic building blocks.

The synthesis of acetonide-protected bis-MPA anhydride (3) was carried as shown in Figure 5.6, in DCM in the presence of N,N' -dicyclohexylcarbodiimide (DCC). The DCC serves as a catalyst as it reacts with bis-MPA-acetonide to split off dicyclohexylurea (DCU), also it removes the water from the reaction solution thereby preventing the hydrolysis of already formed anhydride.^[297] The result of the reaction was determined by ^1H NMR and ^{13}C NMR measurements. The ^1H -NMR spectrum (Figure 5.7) shows almost the same spectrum as it has already been recorded for the bis-MPA acetonide except smaller shifts of some signals. Thus, it does not seem well suited to detect the formation of the anhydride.

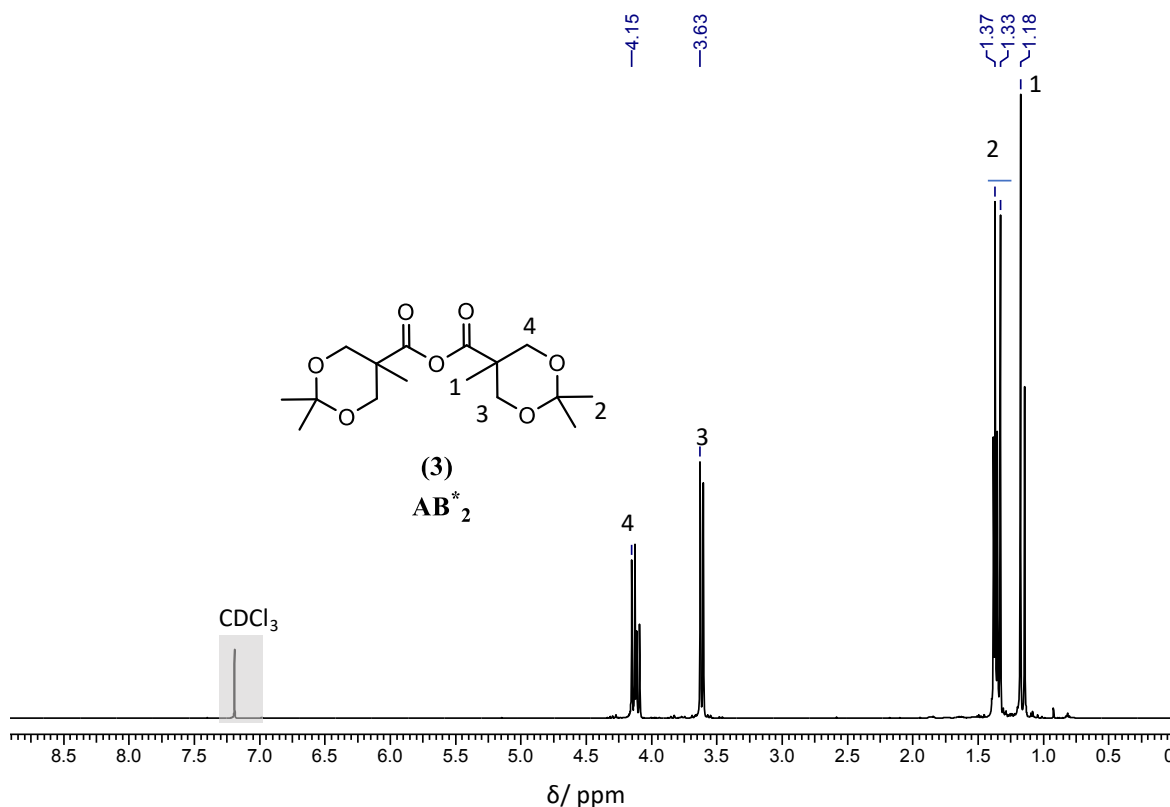


Figure 5.7: ^1H NMR spectrum of the acetonide-protected bis-MPA anhydride (AB^*_2).

^{13}C NMR spectrum shows a significant difference from the acetonide (Figure 5.8). The formation of the anhydride has been clearly demonstrated by the complete disappearance of the

signal of the carboxyl group of the bis-acetonide MPA at 179.85 ppm and the appearance of the signal 7 of the mutually coupled carboxyl groups of the anhydride at 169.52 ppm. The further direct signals correspond essentially to those of the acetonide and show minor deviations in comparison to ^1H NMR.

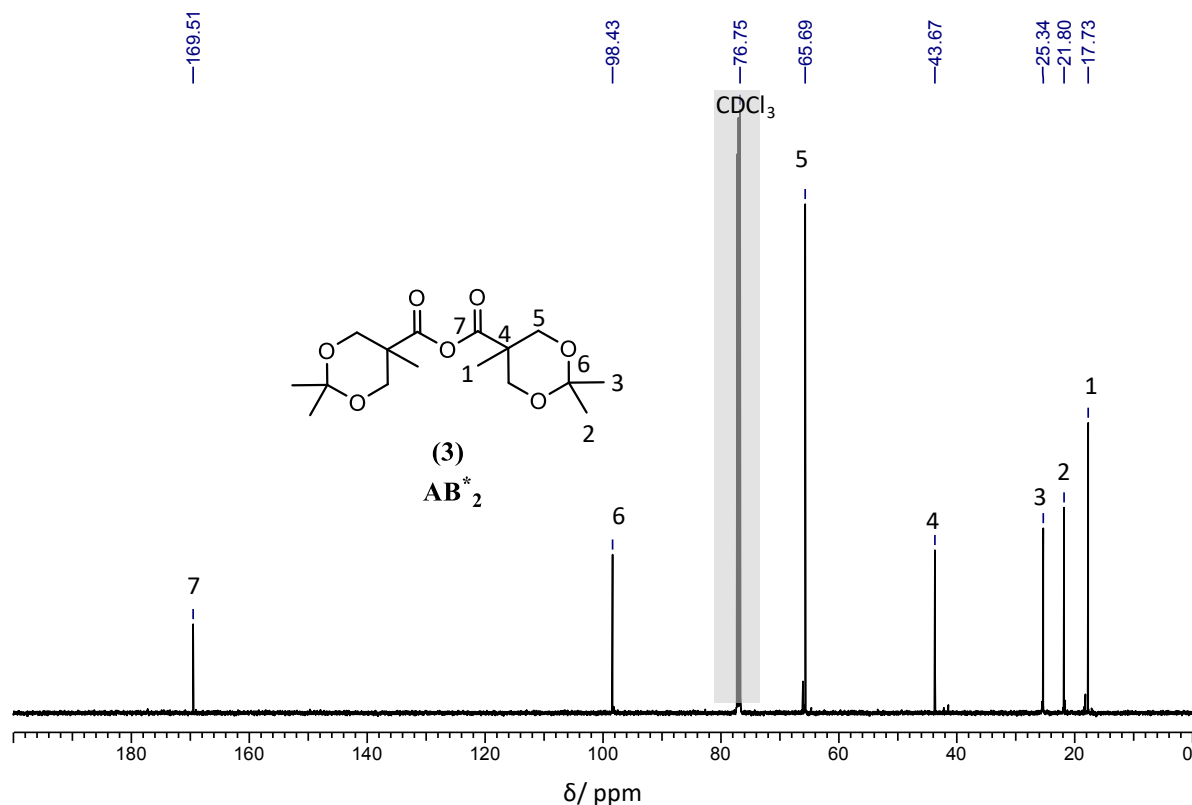


Figure 5.8: ^{13}C NMR spectrum of the acetonide-protected bis-MPA anhydride (AB^*_2).

After synthesis, the anhydride was stored under vacuum and either it was processed quickly because it is highly hygroscopic and can be easily hydrolyzed, or it can be stored at 0 °C but not more than 30 days.

With the help of the acetonide-protected bis-MPA anhydride, three generations of pseudodendrimers were manufactured using the divergent synthesis approach. The esterification was carried out as a classic Steglich esterification with the DMAP catalyst in a mixture of pyridine and dichloromethane. In relation to the total number of OH groups, the 1.3-fold excess of bis-MPA acetonide anhydride was used in order to ensure a complete reaction of the OH groups and to counteract the inactivation of the anhydride by water. The molar equivalent based on the number of OH groups was 0.15 for DMAP, 5 for pyridine and 15 for dichloromethane. It first forms the protected pseudodendrimers (P-G1-pro, P-G2-pro and P-G3-pro) which is later deprotected forming three generations of OH terminated pseudodendrimers having a hyperbranched core P-G1-OH, P-G2-OH and P-G3-OH (Figure 5.9). Since pyridine could not be completely removed by washing the product, toluene was added in the last work-up step to remove the resulting azeotrope more easily by distillation.

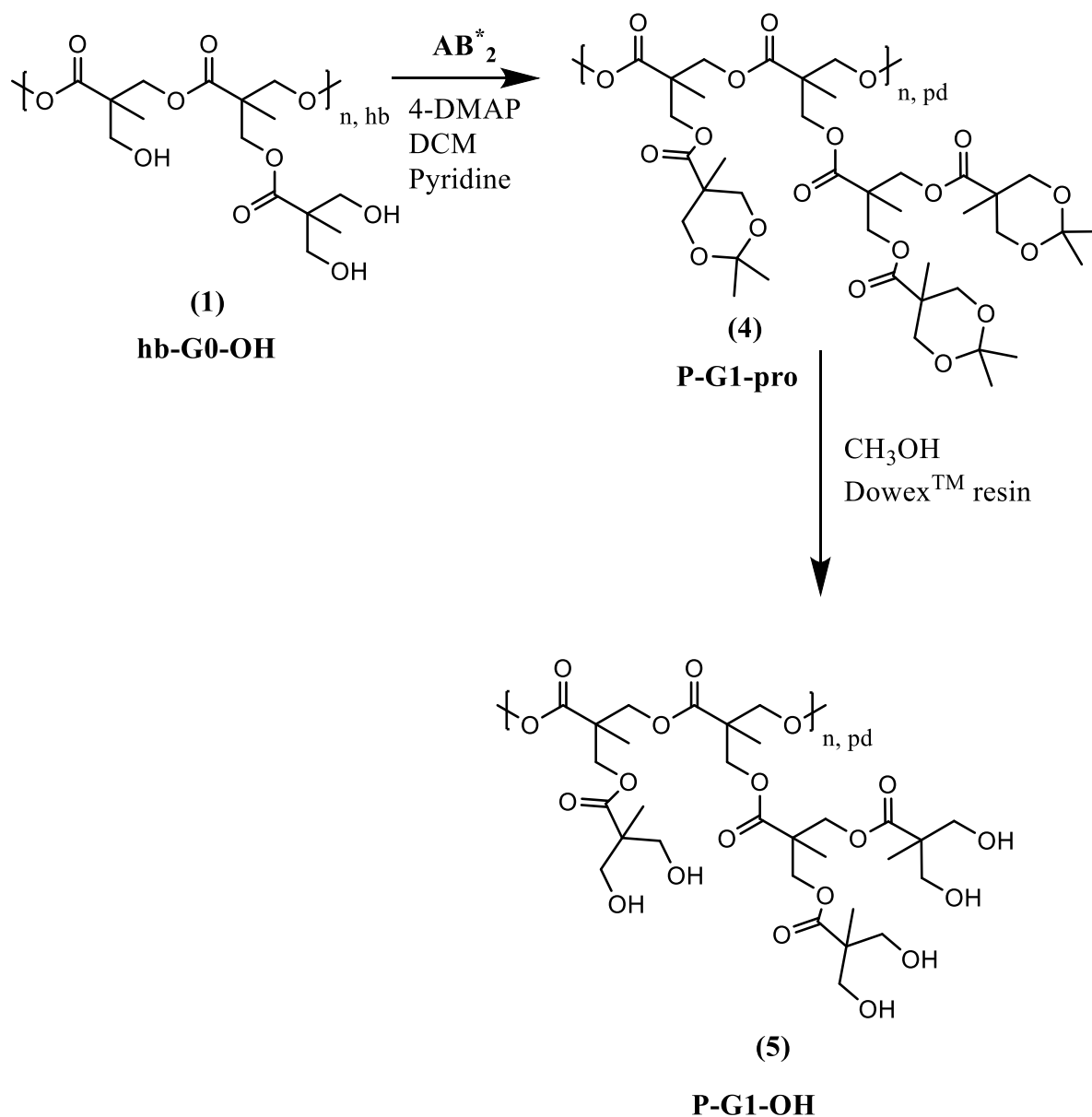


Figure 5.9: Reaction scheme for the formation of first-generation pseudodendrimer (P-G1-OH) forming bis-MPA acetonide (2) and then forming bis-MPA acetonide anhydride (3) (AB^*_2).

After the distillation, the product was obtained as a highly viscous oil, which made further removal of the remaining solvents difficult. The contamination of the product with toluene and pyridine resulted in higher yields (>100%) which means that it can be assumed that the residual solvent content is around 10% and the product yield is almost complete. Synthesis of the fourth generation was also tried but it did not yield any good results probably owing to high increase in number of linear groups with high steric hindrance. The results of this reaction were analyzed with 1H NMR spectroscopy (Figure 5.10), which shows a rather complex picture. The spectra for other protected pseudodendrimers are present in the Appendix. The protons of methyl groups of the backbone were shown by signals 3 and 4. The pendant group was represented by 2, 5, 6, 7, 8 and 9.

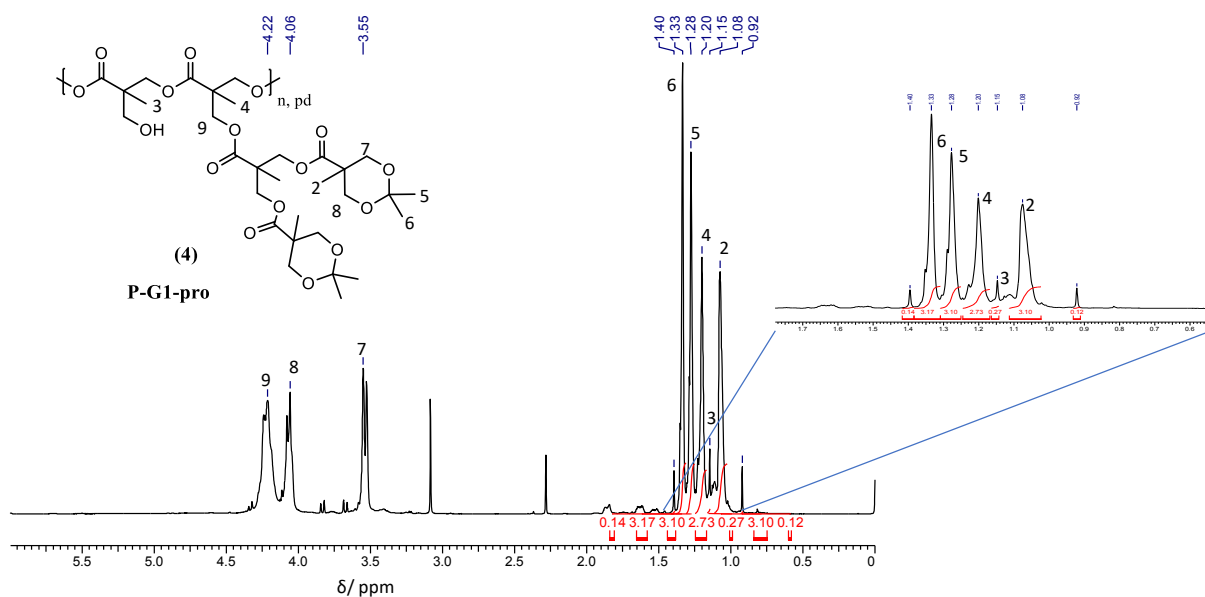


Figure 5.10: ^1H NMR spectrum showing methyl regions for P-G1-pro in CDCl_3 .

Deprotection of the modified polyester was made as shown in Figure 5.9, by reaction with methanol which acts as a solvent under the influence of cation exchange resin Dowex. After the synthesis and purification, first generation of pseudodendrimer P-G1-OH was analyzed by ^1H NMR spectroscopy. The ^1H NMR (Figure 5.11) shows the same signals as already present in the starting polymer hb-G0-OH, although significant differences were obtained.

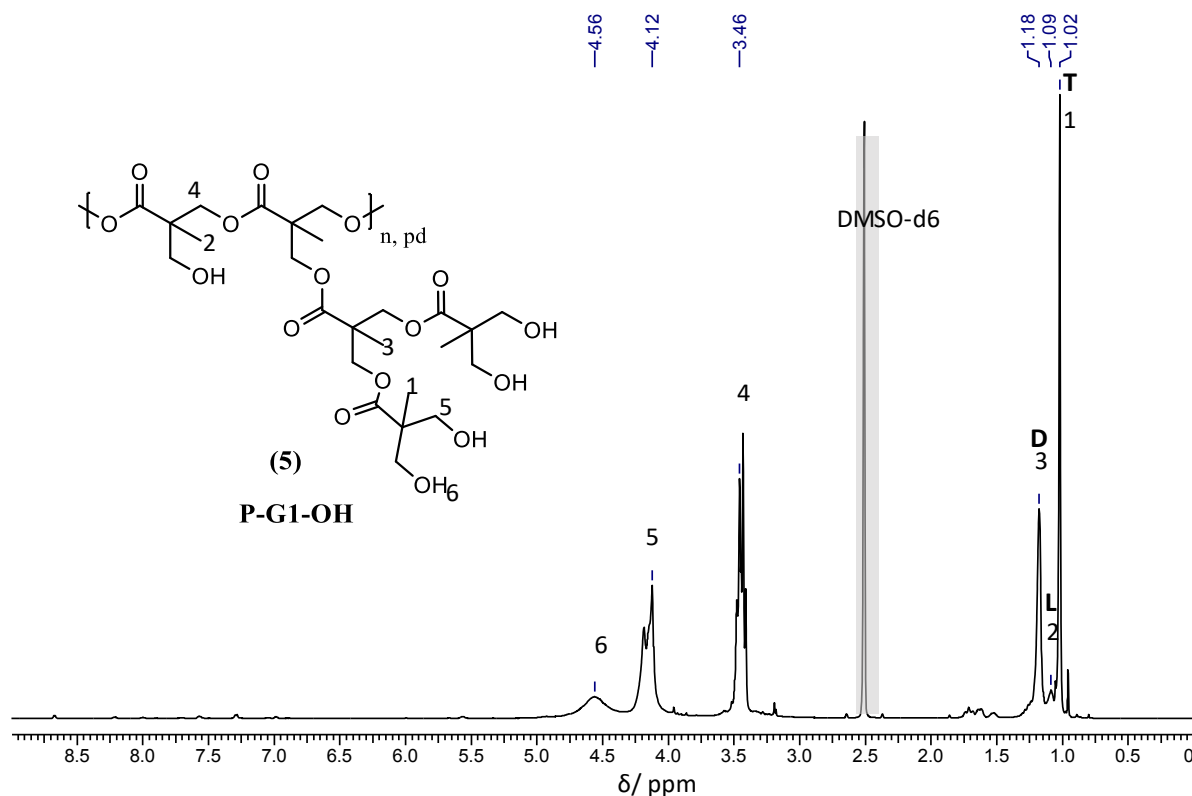


Figure 5.11: ^1H NMR spectrum of the first-generation pseudodendrimer (P-G1-OH). The solvent signal is greyed out.

In the area of the methyl groups, as illustrated in figures 11 and 12, signals at 1.02 ppm, 1.09 ppm and 1.18 ppm, determines that position of terminal, linear and dendritic units, respectively. The amount of terminal and dendritic methyl units shows an increase while those of linear methyl units show a major decrease in comparison to G0-OH. This shows that all the linear methyl units were successfully converted. If the signals from terminal, linear and dendritic groups are integrated, the theoretical molecular structure can be derived and from this the degree of branching, the molar mass and the number of end groups can be determined. The interpretation of the NMR spectra with the use of integral values of the methyl groups indicates the ratio of the frequency of the respective groups, so that through multiplying by the correct factor, the mean number of groups per molecule can be calculated directly. The DB calculated using these integral values is mentioned in Table 5.2. The signal for hydroxyl group at 4.59 ppm belongs to terminal hydroxyl group. In principle, linear hydroxyl group should be completely eliminated but a very minor peak appears at 4.96 ppm. As the linear methyl units are considerably lowered to about 5%, this further increases the DB.

With the specific degree of branching of at least 0.9, it can now be assumed that, virtually the entire outer shell of the polymer is filled with terminal units and thus a high density of functional groups was created on the surface of the polymer. The polymer thus represents the first generation of pseudodendrimer system in this synthesis work of aliphatic-polyester-based pseudodendrimers.

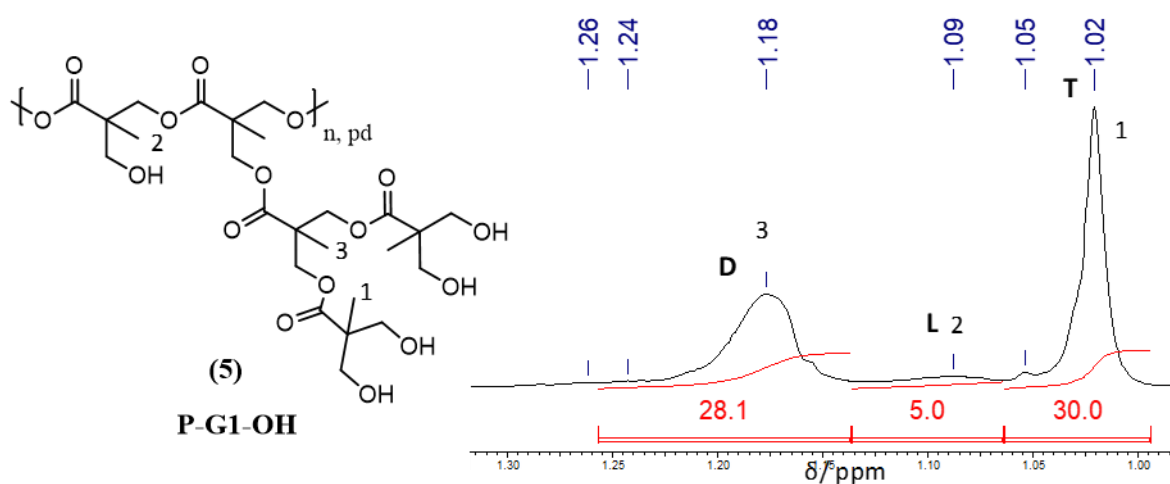


Figure 5.12: A section of ¹H NMR spectrum of the first-generation pseudodendrimer (P-G1-OH); peak due to linear units has decreased.

The next step was the synthesis of second generation of pseudodendrimers (P-G2-OH), which was performed by taking a part of P-G1-OH and proceeding in the same way as done previously in the case of P-G1-pro to form P-G1-pro, which again was deprotected leading to the formation of P-G2-OH (Figure 5.13).

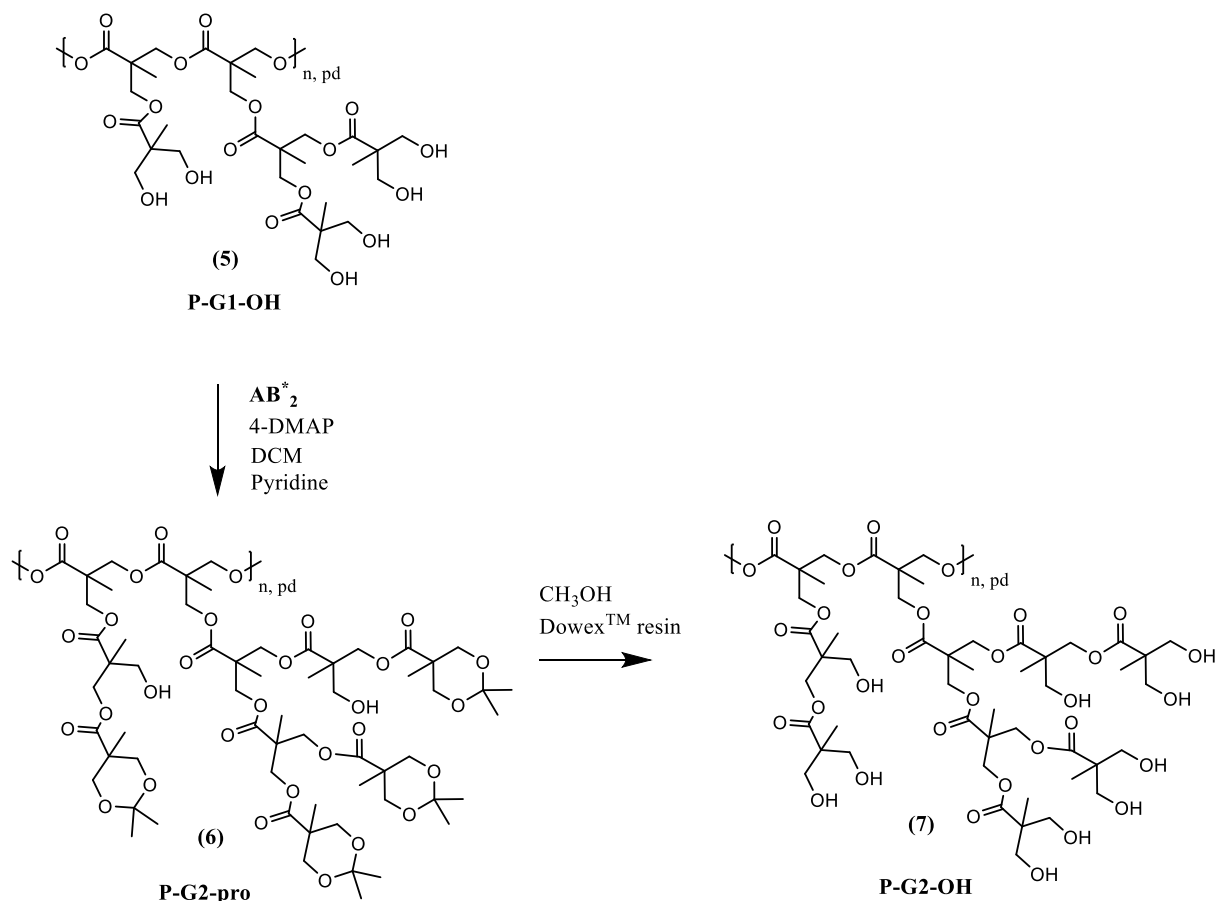


Figure 5.13: Reaction scheme for the formation of second-generation pseudodendrimer (P-G2-OH) involving two steps: first the protection of OH groups of P-G1-OH forming a protected pseudodendrimer P-G2-pro followed by a deprotection step resulting in the formation of pseudodendrimer (P-G2-OH).

The 1H NMR spectrum of P-G2-pro (Figure 3, Appendix) shows that the modification was performed successfully. Signals at 3.59 ppm and 3.98 ppm show the presence of acetonide group. Also, this 1H NMR spectrum of P-G2-pro agrees with P-G1-pro. The 1H NMR spectrum of the second generation pseudodendrimer (P-G2-OH) is shown in Figure 14 which is similar to that of P-G1-OH.

However, a reappearance of linear methyl groups was observed, though very infrequently. This could have been due to the imperfection in the protection steps. 1H NMR spectrum of second generation pseudodendrimer shows terminal methyl groups at 1.02 ppm, dendritic groups at 1.17 ppm and reappearance of linear methyl groups can be observed at 1.07 ppm. The reappearance of methyl groups could possibly be due to steric reasons which lead to a decrease in degree of branching.^[327]

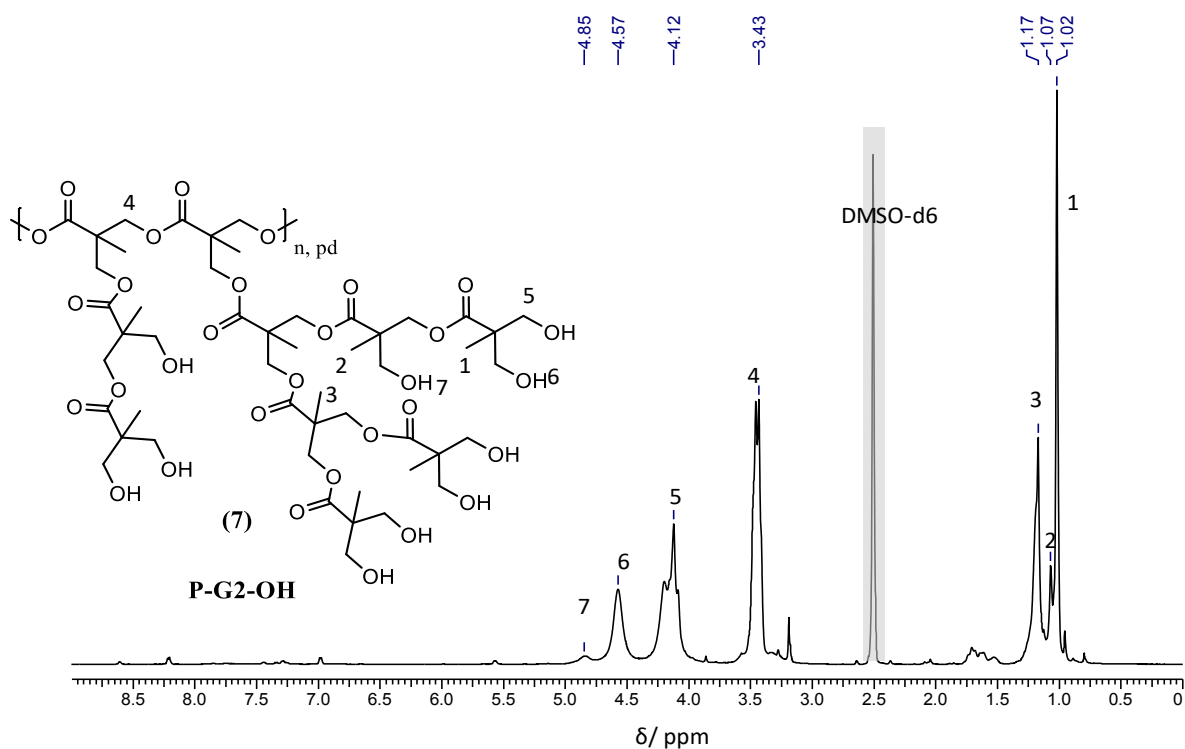


Figure 5.14: ^1H NMR spectrum of the second-generation pseudodendrimer (P-G2-OH).

Due to steric reasons, it is almost impossible to remove the linear groups completely, and since linear OH groups were seen in the protected version of the polymer, so the re-occurrence of linear methyl groups was found.

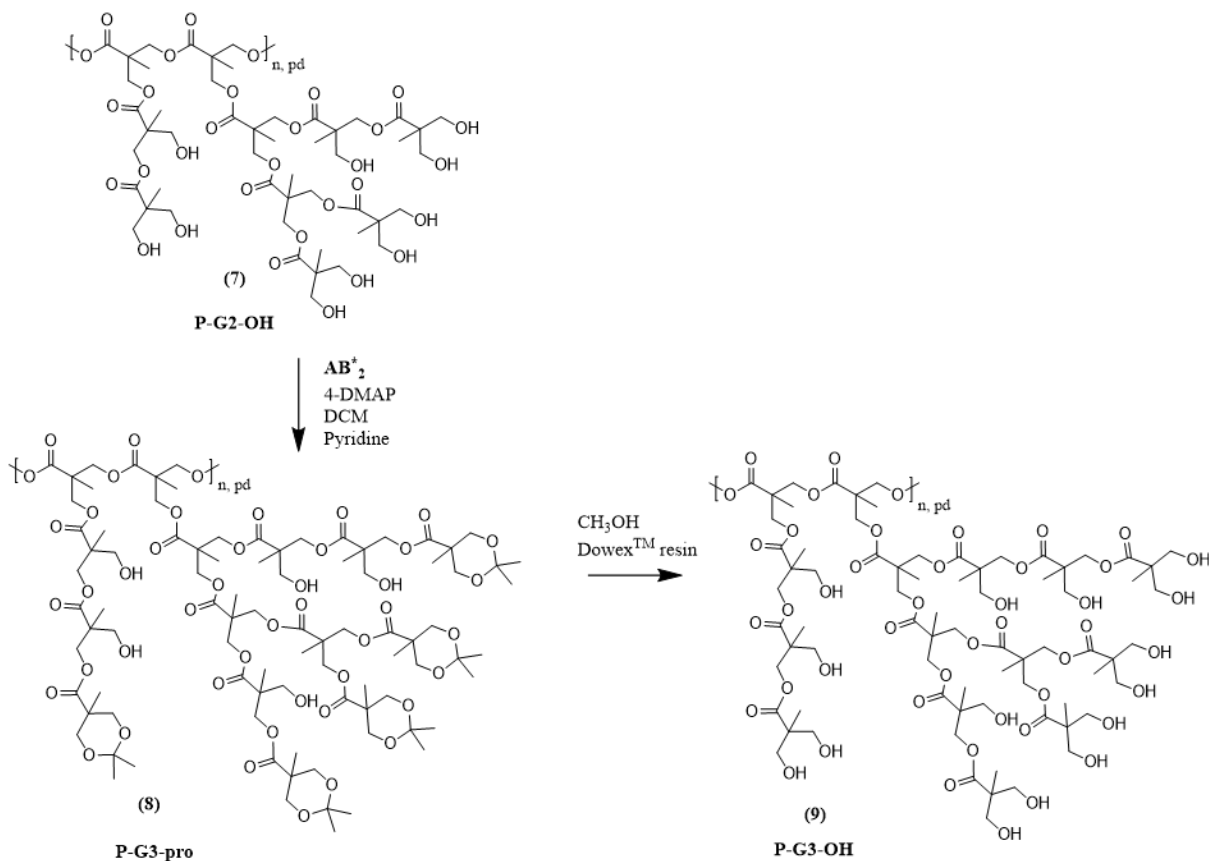


Figure 5.15: Reaction scheme for the formation of third-generation pseudodendrimer (P-G3-OH).

The synthesis of third generation pseudodendrimer was carried out using the second generation pseudodendrimer (P-G2-OH), following the same procedure as is the case of the first and second generation. This gives the protected third generation pseudodendrimer (P-G3-pro) (Figure 5.15).

The P-G3-pro was studied by ^1H NMR spectroscopy (Figure 4, Appendix). The ^1H NMR spectrum show signals of acetonide protecting groups, along with several signals which were overcrowded owing to the complicated structures. The signal of terminal OH groups was also observed. Unfortunately, the signal of linear OH groups appears again, likely due to the same reasons as for the second generation.

The deprotection of P-G3-pro was carried out following the same procedure as for previous generations, considering the number of linear groups which appeared in P-G2-OH. The ^1H NMR spectrum (Figure 5.16) did not show clear signals of linear and terminal OH groups due to overlaying signals of the $-\text{CH}_2$ groups (signals 4 and 5) from bis-MPA.

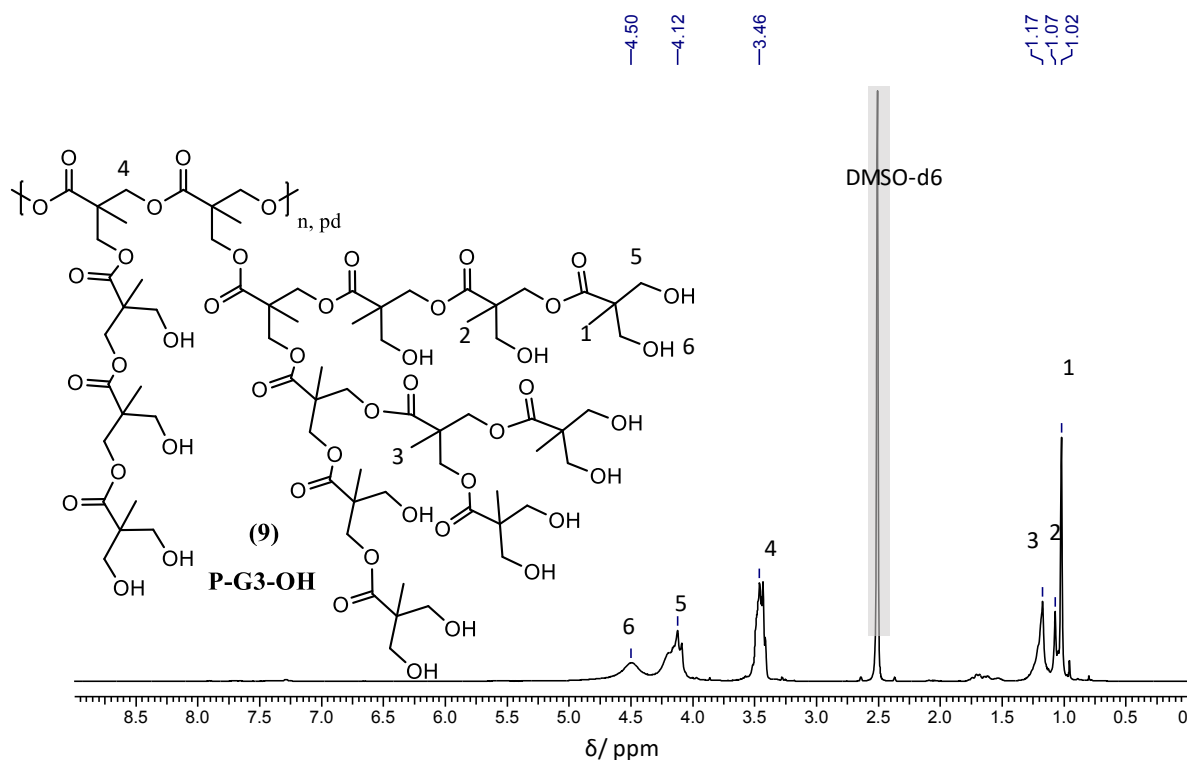


Figure 5.16: ^1H NMR spectrum of the third generation pseudodendrimer (P-G3-OH).

In the region of methyl groups, there was an evident signal of terminal methyl group at 1.02 ppm, dendritic methyl groups at 1.17 ppm and linear methyl groups at 1.07 ppm which has increased as compared to the second generation, which lead to the decrease in degree of branching. Linear $-\text{OH}$ groups could be seen in the region 4.64 ppm. The degree of branching obtained from ^1H -NMR spectra is given in Table 5.2.

The lower degree of branching is because the linear units have increased much more as compared to the first and second generations. Similar observations were made in previously investigated pseudodendritic system, in which the degree of branching decreases with every generation despite the fact that it was a significantly more open dendritic structure (aliphatic-aromatic polyester) than the one synthesized in this work.^[327]

All the four polymers synthesized were also analyzed with SEC-MALS to investigate the course of structural changes with increase in molar masses and the increase in number of generations. The results are summarized in Table 5.2.

Table 5.2: Molecular characteristics of pseudodendrimers G0-G3.

Polymers	M_n (kDa) a	M_n (kDa) b	M_w (kDa) b	D^b	dn/dc b	DB_{Frechet} a	DB_{Frey} a	CH_3 groups ^a	OH groups ^a
hb-G0-OH	3.5	3.5	5	1.4	-0.077	0.5	0.42	31	33
P-G1-OH	6.9	7.1	9.7	1.4	-0.103	0.93	0.92	59	61
P-G2-OH	13.7	12	26	2	0.126	0.89	0.89	118	120
P-G3-OH	15.7	10.1	19.5	2	0.115	0.85	0.85	135	137

^(a)Calculated by the functionality of terminal, linear and dendritic units from ¹H NMR ^(b) Results from SEC-MALS.

The molar mass determination of hb polymers is difficult due to their complicated structure, globular shape and large number of polar end groups, which can interact with the column material in column chromatography. These interactions cause a shift from the expected size exclusion mode into the adsorption mode, as has been repeatedly observed for polar OH-functionalized hb polymers.^[395,396]

Figure 5.17 shows the RI and LS chromatograms of the OH functionalized hb polymer and the next three generations of OH functionalized pseudodendrimers (P-G1-OH, P-G2-OH and P-G3-OH). From these measurements, the molar mass and dispersity were determined mentioned in Table 5.2. The chromatograms when compared to each other, showed a decrease in elution time with increase in generation from hb to P-G1-OH, and to P-G2-OH but only a marginal change on going from P-G2-OH to P-G3-OH. The molar mass curve of hb-G0-OH shows an interesting behavior, i.e., the elution of high molar masses at high elution volume. This effect is caused by the reversible adsorption of the OH groups on the column material. The molar mass dependence on the elution volume shows only marginal increase in molar mass with the generation number, which means structurally there is only a small increase in the dimensions with every succeeding generation.

The signal from the LS detector did not show an exceptionally large signal due to low intensity probably as a result of low concentration or low molar mass in case of hb polyester hb-G0-OH and P-G1-OH. In P-G1-OH, P-G2-OH and P-G3-OH with high number of terminal –OH groups, there is also the probability to interact with the column material.

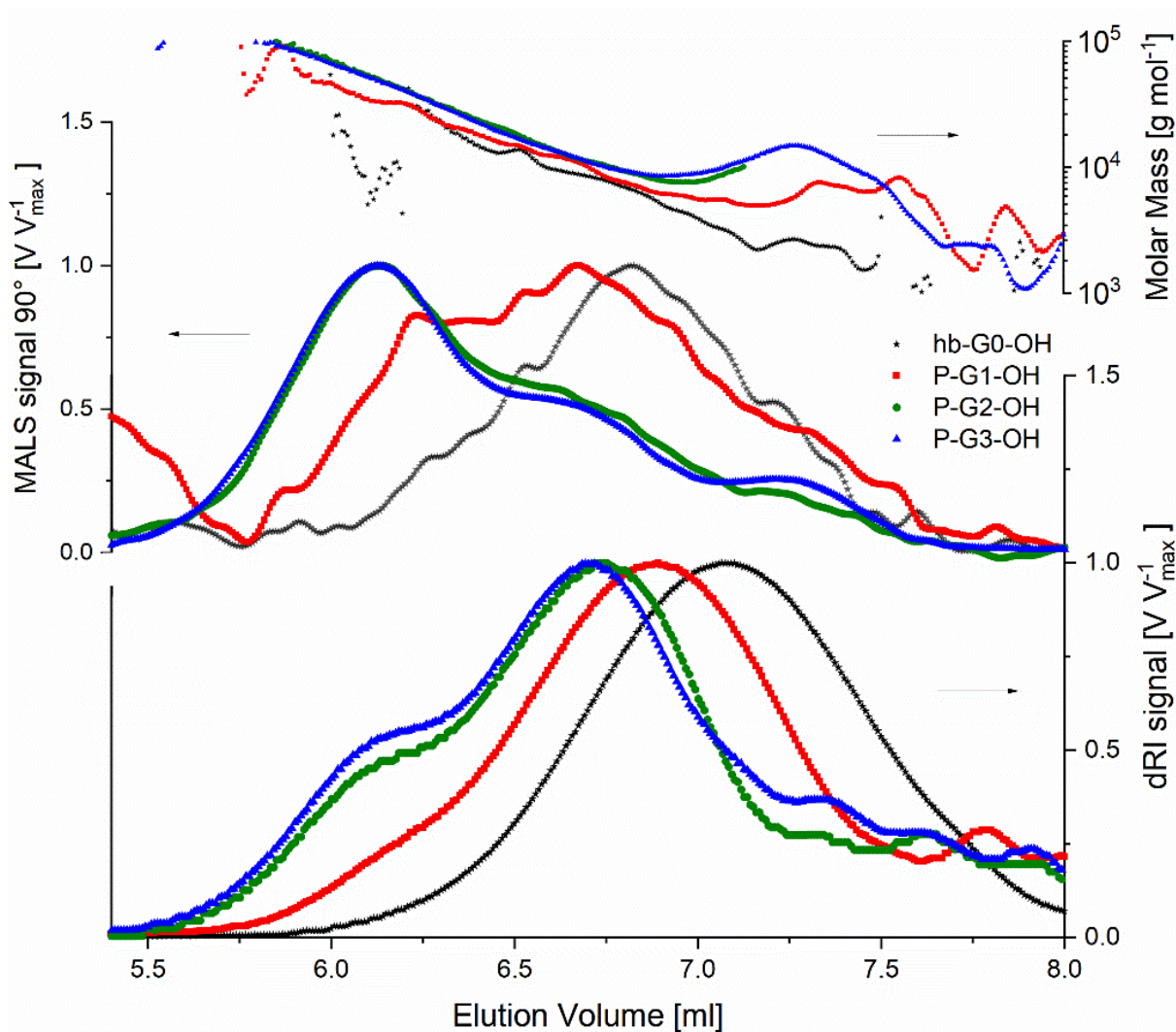


Figure 5.17: Chromatograms of OH functionalized hb-G0-OH to P-G3-OH, measured with SEC coupled to MALS and dRI detector in DMAC for determination of molar mass (MALS signal at 90°).

From Table 5.2, it can be seen that in the case of P-G2-OH and P-G3-OH, the theoretical (or calculated) molar masses do not agree with the measured values from the SEC-MALS. It can only be concluded that once the linear groups start appearing in a substantial amount, it can only lead to more defects. Especially in this kind of work when half of the previous generations has to be preserved for further synthesis, it can be tricky to start over. So to proceed further, the pseudodendrimers which were synthesized in our previous work are used.^[336]

5.1.3 Synthesis and characterization of dendrimers D-G4-OH, D-G5-OH and D-G6-OH

The starting point for all the three generations of dendrimers D-G4-OH, D-G5-OH and D-G6-OH is the third generation bis-MPA dendrimer with a TMP core (PFD-G5-TMP-OH), which was purchased commercially from Polymer factory, Sweden. The third generation was chosen specifically because the molar mass was close to the molar of the hb-G0-OH. So, we have almost similar molar masses of both (pseudodendrimers and dendrimers) the starting material.

The synthesis was carried out as described in the above section, with the acetonide-protected bis-MPA anhydride and deprotected in methanol in presence of Dowex (Figure 5.19).

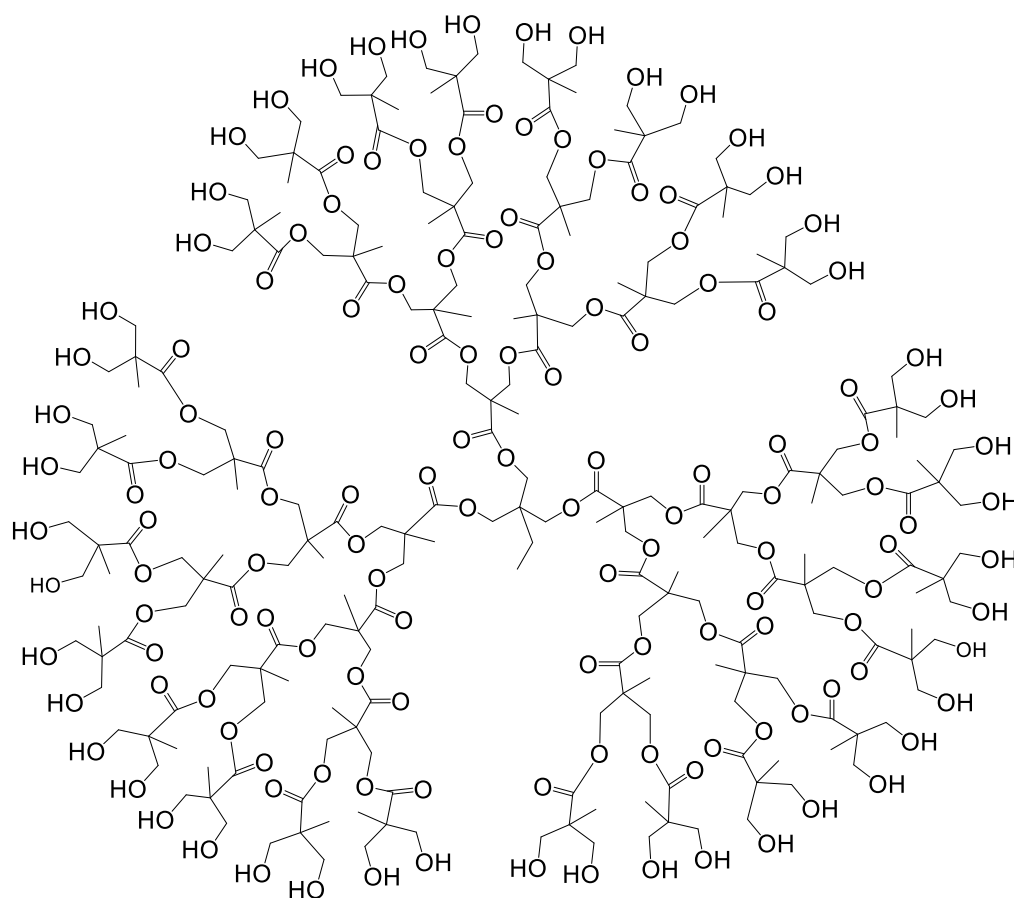


Figure 5.18. Fourth generation dendrimer D-G4-OH displaying 48 OH functional units.

^1H NMR of D-G4-pro (Figure 5.20), D-G5-pro (Figure 5, Appendix) and D-G6-pro (Figure 6, Appendix) showed that the peaks of the protecting acetonide groups overlap the peak of dendritic methyl groups, the calculation based on ^1H NMR was performed only after the deprotection reaction.

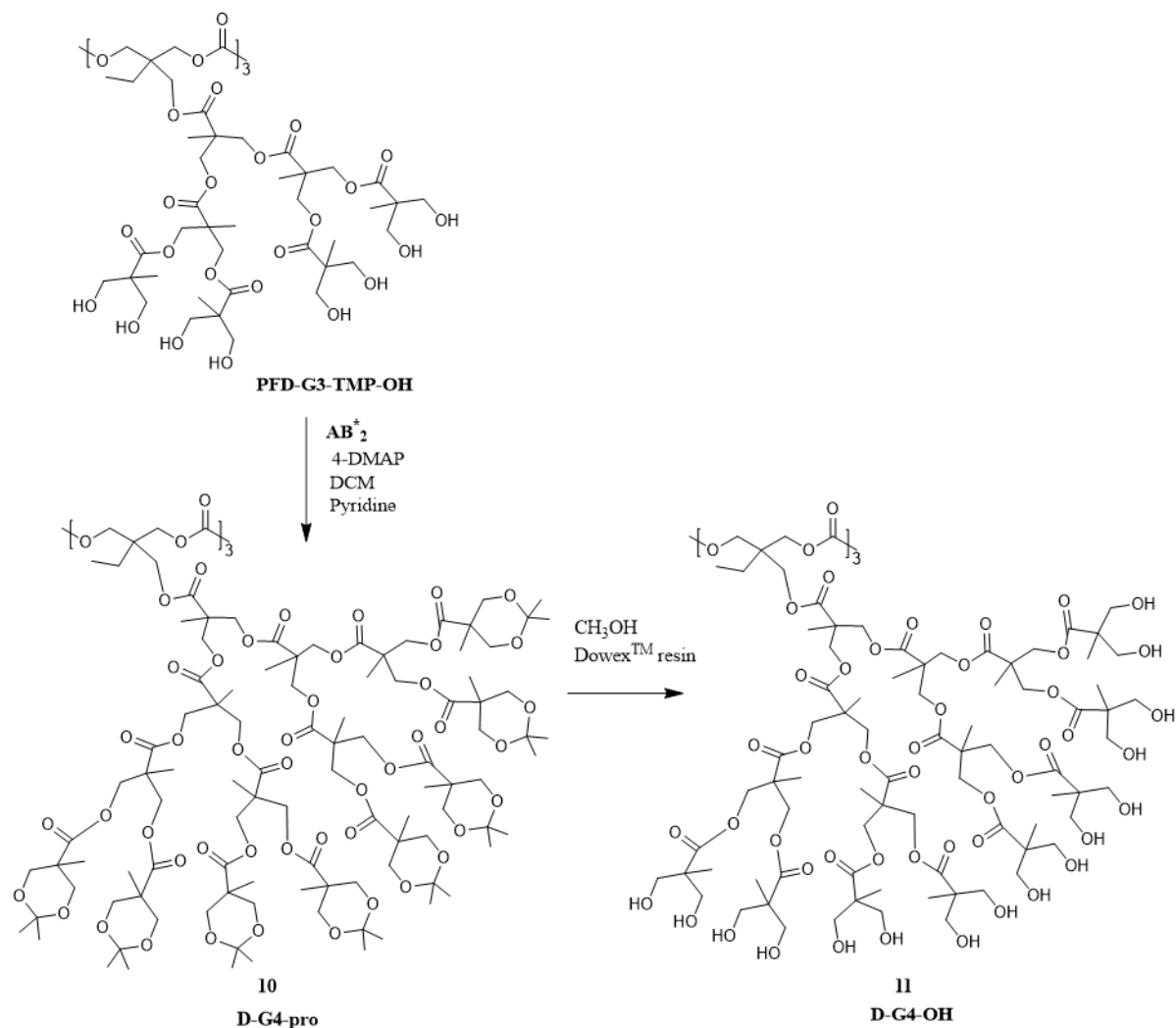


Figure 5.19: Reaction scheme for the formation of fourth-generation dendrimer (D-G4-OH), involving two steps: first the protection of OH groups of PFD-G3-TMP-OH (starting polymer) forming a protected dendrimer D-G4-pro and a deprotection step resulting in the dendrimer formation (D-G4-OH).

Almost complete yields were also achieved in this reaction. Complete deprotection took place in all generations of D-G4-pro, D-G5-pro and D-G6-pro. The respective generations of the product D-G4-OH, D-G5-OH and D-G6-OH could almost be completely isolated by this simple work-up. Here the yields of 104-108% were also above the theoretical value, which is due to the presence of residual toluene and pyridine. Figure 5.21 shows the ^1H NMR spectrum of the deprotected dendrimer of the fourth generation (D-G4-OH).

In Figure 5.21, a section of the spectrum of D-G4-OH is shown. The difference from pseudodendrimers was seen in ^1H NMR spectra of dendrimers, which was a signal at 0.88 ppm arising from the methyl group of the TMP, at 1.07 ppm a signal of terminal methyl group and at 1.20 ppm a signal of dendritic methyl groups are seen similar to pseudodendrimers. Many overlaying signals of methylene groups were present due to which the CH_2 group of TMP could not be seen clearly. Slight shift from pseudodendrimers in NMR signals is attributed to the presence of signal (triplet, due to neighboring $-\text{CH}_2$ group) due to methyl group of TMP. But,

surprisingly a small signal of linear methyl groups appears at 1.13 ppm, which indicates a certain incompleteness of the reaction. The signals at 1.26 ppm and 1.33 ppm are assigned to the methyl groups of the acetonide protective group.

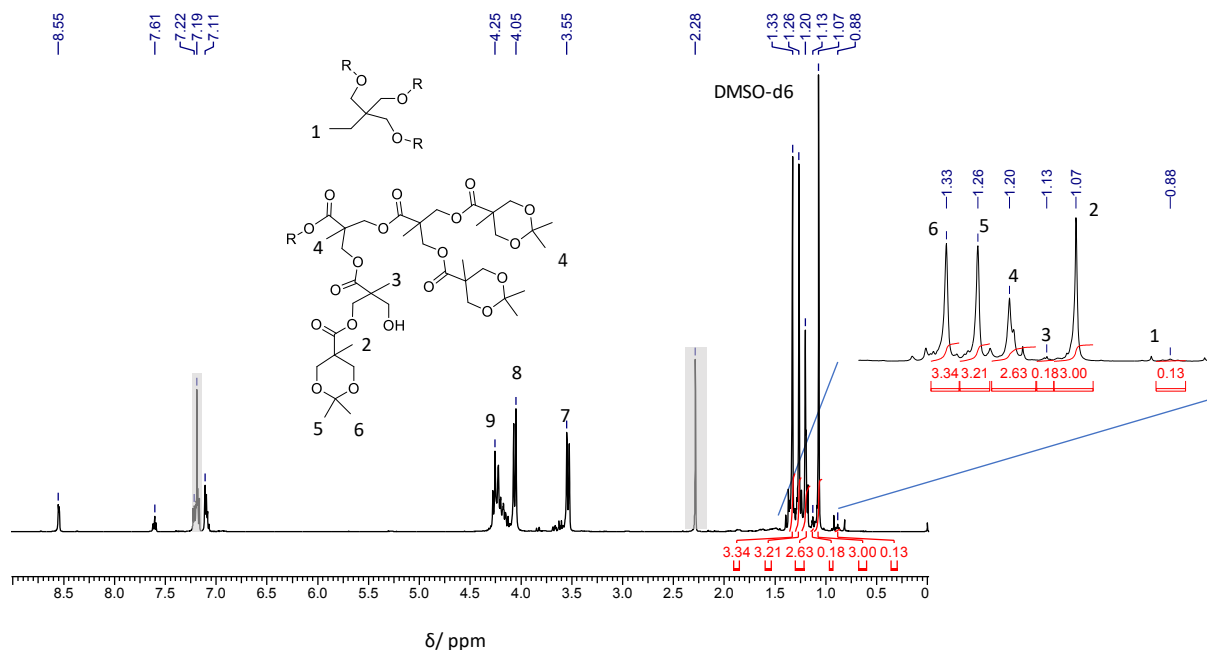


Figure 5.20. ^1H NMR of D-G4-pro displaying concerned signals.

The integral of the terminal methyl groups was set to 3 as a reference. Since the peaks of the acetonide protective group also occur with an integral of about 3, this indicates that the reaction has taken place completely and that the end groups of the dendrimers are completely protected. Based on the ratios of the terminal, linear and dendritic methyl group integrals, the degree of branching can be calculated, as described in Section 2.7.2.

The mean molar mass and the number of end groups could also be calculated. Since the peaks of the protective groups partly overlap the peak of the dendritic methyl group, the calculation based on the ^1H NMR integrals is only carried out after the deprotection reaction. The deprotection was carried out with Dowex in the same way as in the case of pseudodendrimers.

The dendritic groups from the terminal groups are also split up in ^1H NMR (Figure 5.21), so that the dendritic methylene group is found at 4.12 ppm, the methylene group of the terminal bis-MPA unit appearing at 3.44 ppm. In addition to the dendritic methyl group at 1.18 ppm and the terminal methyl group at 1.02 ppm, one finds the signal of methyl groups of linear units, as in the ^1H NMR spectrum of D-G4-pro (Figure 5.20). Thus, it was confirmed from the ^1H NMR spectrum that the reaction did not take place at all of the end groups of the dendrimer. Since the peaks of the methyl groups in the spectrum are not superimposed by the peaks of the methyl groups of the protective groups, an evaluation can be carried out using the integrals of the terminal, dendritic and linear methyl groups, as described in Section 2.1.1. The ^1H NMR spectra for D-G5-OH and D-G6-OH are given in the Appendix (Figure 7 and 8).

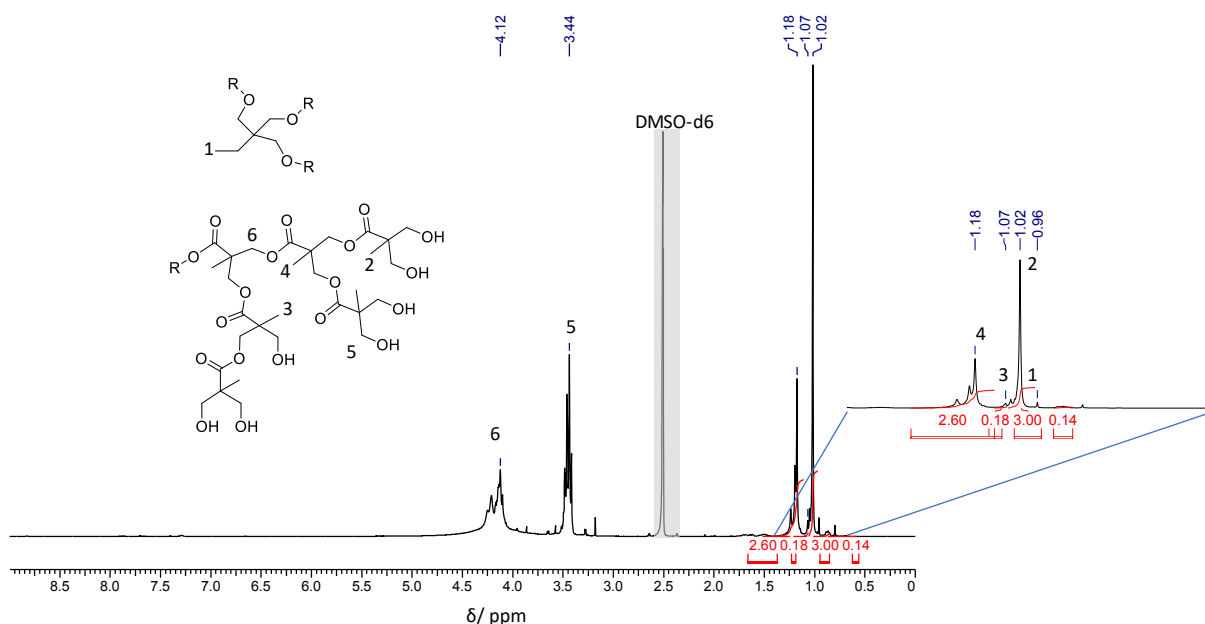


Figure 5.21. ^1H NMR of D-G4-OH showing focal (1), terminal (2), linear (3) and dendritic (4) groups.

In general, the evaluation of ^1H NMR spectra is easier in case of dendrimers in comparison to the pseudodendrimers, because of the well-defined, pre-established structures - known values of OH groups of the dendrimers unlike the pseudodendrimers. Based on the assumption that on an average, one OH group has not reacted (1 defect), then in the case of the fourth generation there would be one linear group and 23 terminal groups. Dividing the theoretical value of the terminal groups of 23 by the practical value of the integral of 3, the factor by which the integrals of the linear and dendritic groups have to be multiplied is obtained. Accordingly, the value of the defects is adjusted so that it agrees with the practical value from the integral for the linear groups. This can be continued for the next generations, while considering the propagation of the defects, whereby the assumption that internal OH groups also do not react in the synthesis of the next generation applies, i.e., the defects cannot be repaired. In reality, this assumption should also largely apply, since steric reasons often prevent the end groups from reacting completely. In addition, it is unlikely that these sterically hindered groups will react during the synthesis, especially since these are also enclosed by bis-MPA groups, which react more likely and additionally shield the internal OH groups. The results of the evaluation of the ^1H NMR spectra are given in Table 5.3. As expected, the number of newly formed defects increases with each generation due to the greater steric hindrance. The number of end groups and the number average molar mass almost double with each generation and are close to the theoretical values of the perfect dendrimer structures, which are also listed in the Table 5.3 for comparison.

Table 5.3: Molecular characteristics of dendrimers G4-G6.

Polymers	M_n (kDa) ^a	OH groups ^a	M_n (kDa) ^b	M_n (kDa) ^c	M_w (kDa) ^c	\bar{D}^c	dn /dc ^c	DB Frechet ^b	DB Frey ^b	OH groups ^b	New defects	Total defects
D-G4-OH	5.4	48	5.2	6	8	1.3	0.1	0.97	0.97	46.6	1.4	1.4
D-G5-OH	11	96	10	10	12	1.2	0.1	0.95	0.94	88.5	3.3	7.5
D-G6-OH	22	192	19	18	21	1.2	0.1	0.94	0.93	168.1	4	23.7

(^a) Theoretical data (^b) calculated by the functionality of terminal, linear and dendritic units from ^1H NMR (^c) Results from SEC-MALS.

The dendrimers were also analyzed by SEC-MALS and Figure 5.22 shows the chromatograms.

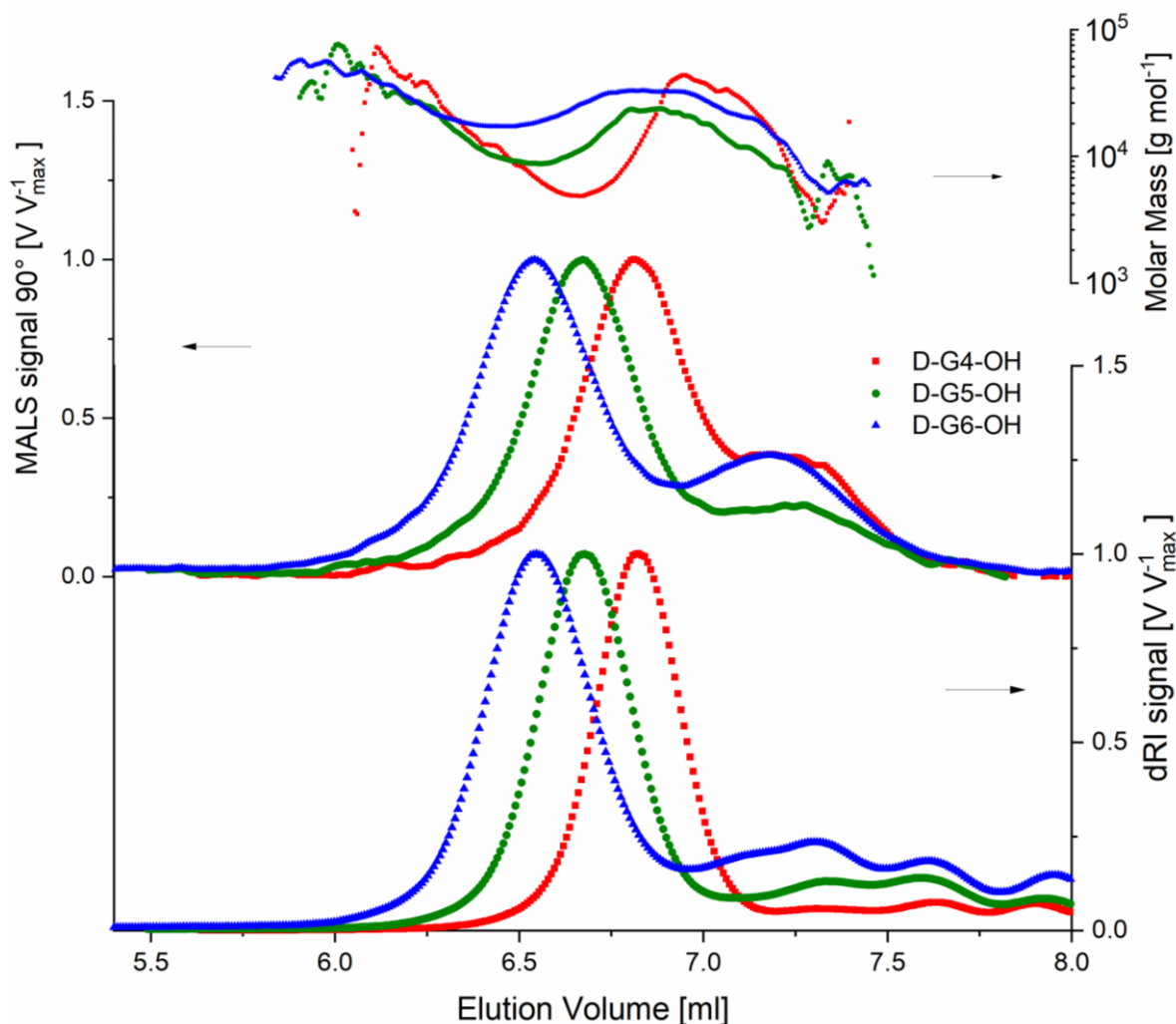


Figure 5.22: Chromatograms of the three generations of OH functionalized dendrimers D-G4-OH, D-G5-OH and D-G6-OH measured with SEC coupled to MALS and dRI detector in DMAC.

The concentration signal of the RI detector, the molar mass-sensitive signal of the LS detector and the absolute molar mass obtained are shown over the retention volume. It can be seen that the molar mass increases from generation to generation as the signals shift to earlier retention times. In addition to the main peak, the RI signals of the chromatograms show a smaller peak in the late elution area. This occurs for all generations in the range of 7 to 7.5 minutes. In addition to the main peak, several peaks appear in the light scattering signal at later elution times, their intensity increasing with each generation.

As can be seen in the absolute molar masses determined by the LS detector, these decrease approximately linearly in the front part of the chromatogram, reach a minimum and then increase again at later elution times. This phenomenon indicates an interaction of the sample with the column material. As described in Section 3.1, the interaction of the sample with the column results in a combination of the elution curves of an entropic SEC separation and that of an enthalpic LAC separation. In the latter, larger molecules are retained by the stronger adsorptive forces and elute later. This also explains the shoulder peak in the concentration signal

and the smaller peaks in the light scattering signal at late elution times. Since larger molecules have a stronger adsorptive interaction with the column, the phenomenon should be more pronounced for the higher generations of dendrimers. This is exactly the case, as observed from the molar mass curves. The separation curves flatten out more and more for the higher generations according to the molar mass. The higher retention of the higher generations brought about by the stronger interaction is also reflected in the higher intensity of the LS signal in the late elution area. The higher concentration of the higher generations in this area is not shown in the RI signal, since the detector is more sensitive to small molecules, which means that high-generation dendrimers generate the same signal as smaller dendrimers with lower concentrations. Table 5.3 summarizes the mean values of the molar mass distributions. In spite of the interaction with the column material, similar number average molar masses were obtained for generations four to six compared to the NMR results. As described in Section 3.1, the interaction with the column results in broader distributions and thus greater dispersities. Therefore, it can be assumed that the true dispersity is below the values given in the Table 5.3. Since the measurement for generations four to six showed a dispersity of 1.2 to 1.3, it can be assumed that the dendrimers possess very narrow distribution.

5.1.4 Synthesis and characterization of glycopolymers GI-P and GI-D

Glycopolymers possess the ability to interact with proteins and hence are very sought after in clinical therapeutics. In order to synthesize glycopolymers, it is necessary to modify the –OH groups of the synthesized pseudodendrimers and dendrimers into suitable functional groups so that they react with the sugar molecules. In this work, “click” reaction is used as the connecting link between GI-P/GI-D and sugars. The prerequisite for the “Click” reaction is the presence of a terminal triple bond on one molecule and a terminal azide group on the other molecule. For the modification of –OH terminated pseudodendrimers and dendrimers, 4-pentynoic acid was chosen which would provide the flexibility to the polymer and also the alkyne group for further modification. The azide group was attached to the mannose molecules in the form of a propyl azide ether. Pentyl and propyl chains were selected in order to counteract the steric hindrance of the groups with one another. Thus, the mannose molecules are not linked directly to the functional groups of the polymers, but are separated by the pentyl group, the triazole ring and the propyl group so that they have enough space on the surface of the dendrimer to allow the most complete possible modification.

As for the modification of basic polymer (G0), the anhydride was used, in the same way 4-pentynoic anhydride is required. This synthesis of 4-pentynoic anhydride was carried out according to the following reaction scheme (Figure 5.23), in DCM as solvent in presence of DCC which acts as a catalyst and also helps in the removal of water formed during the reaction. Anhydride being unstable, pentynoic anhydride was synthesized when required and used immediately.

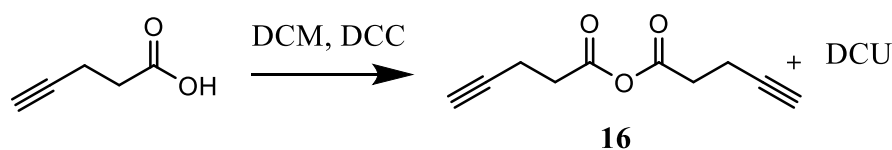


Figure 5.23: Reaction scheme for the synthesis of pentynoic anhydride.

The product of this synthesis was measured by ^1H NMR and ^{13}C NMR measurements.

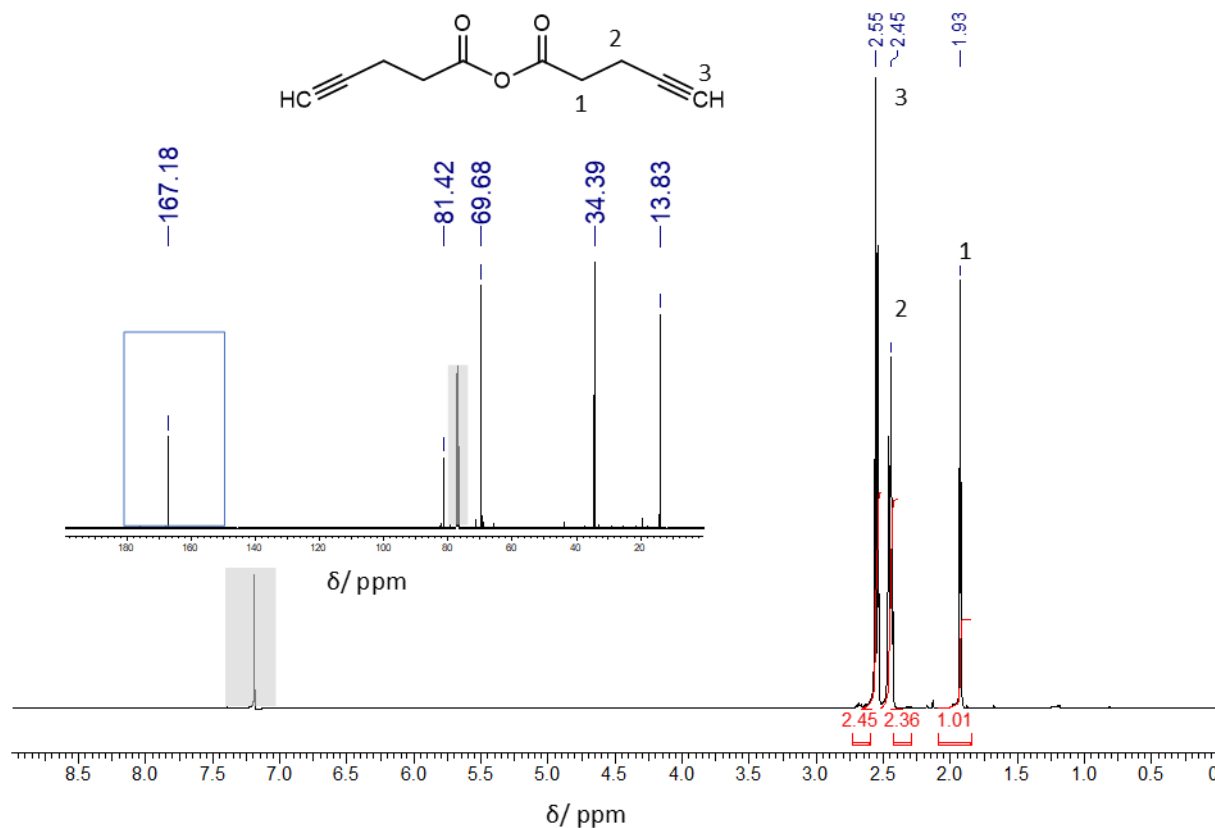


Figure 5.24: ^1H NMR spectrum of 4-pentynoic anhydride along with ^{13}C NMR spectrum in the inset. Solvent signal is greyed out.

As with bis-MPA-acetonide anhydride, the ^1H NMR spectrum of the anhydride (Figure 5.24 b) shows hardly any differences compared to the spectrum of the pentynoic acid, apart from the slight shift in the peaks. Only when looking at the ^{13}C NMR (Figure 5.17 a) spectrum it becomes clear that the occurrence of the peak at 167 ppm provides evidence of the formation of the anhydride. In contrast, the peak of the carboxyl group of the free pentynoic acid has completely disappeared, so that it can be assumed that there is no residual pentynoic acid and that the anhydride was formed completely.

The synthesis of pseudodendrimers with alkyne end groups was carried out according to the reaction in Figure 5.25. The esterification reaction was carried out in the same manner as the modification of the base polymer (hb-G0-OH) with the pentynoic anhydride forming corresponding pseudodendrimers in DCM/pyridine. A brown viscous oil was obtained as a product for all three generations 17, 18 and 19 (P-G1-pent, P-G2-pent and P-G3-pent, respectively).

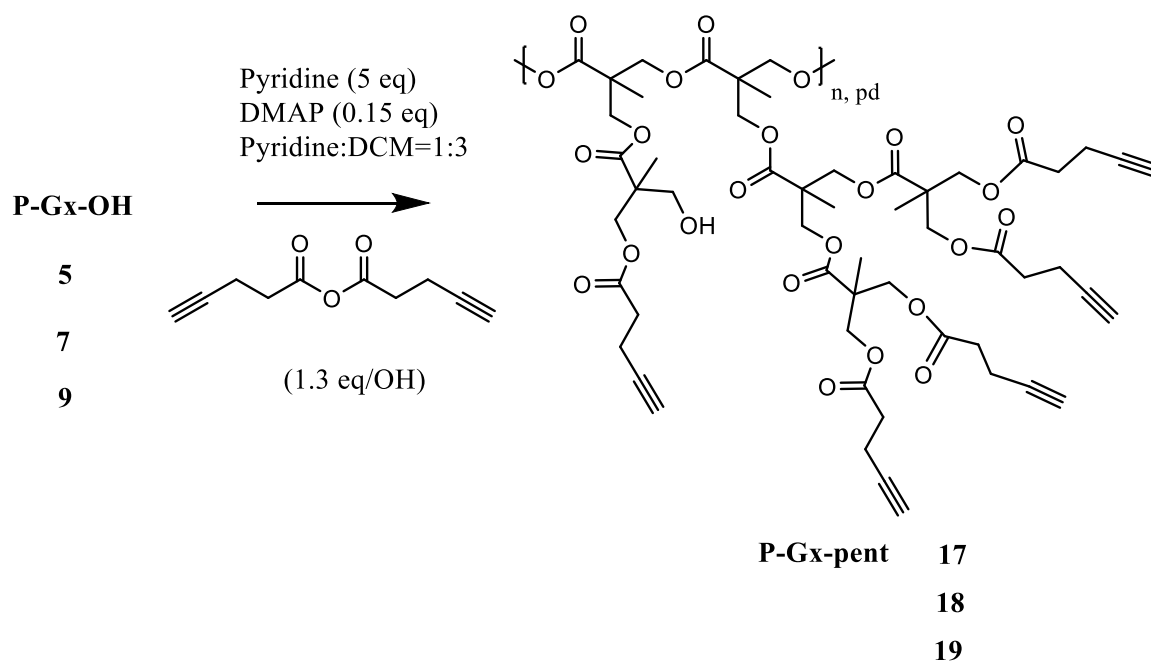


Figure 5.25: Reaction of pseudodendrimers (P-Gx; x=1 to 3) with 4-pentynoic anhydride forming corresponding generations of pentinate modified pseudodendrimers (P-Gx-pent).

The product obtained was investigated by ^1H NMR to have a better view of alkyne end groups. In Figure 5.26, there is no clear distinction between the terminal methyl groups and dendritic methyl groups due to their similar chemical environment as these are now surrounded by ester linkages, unlike in the case of the pseudodendritic polymer, so only one signal at 1.19 ppm is seen.

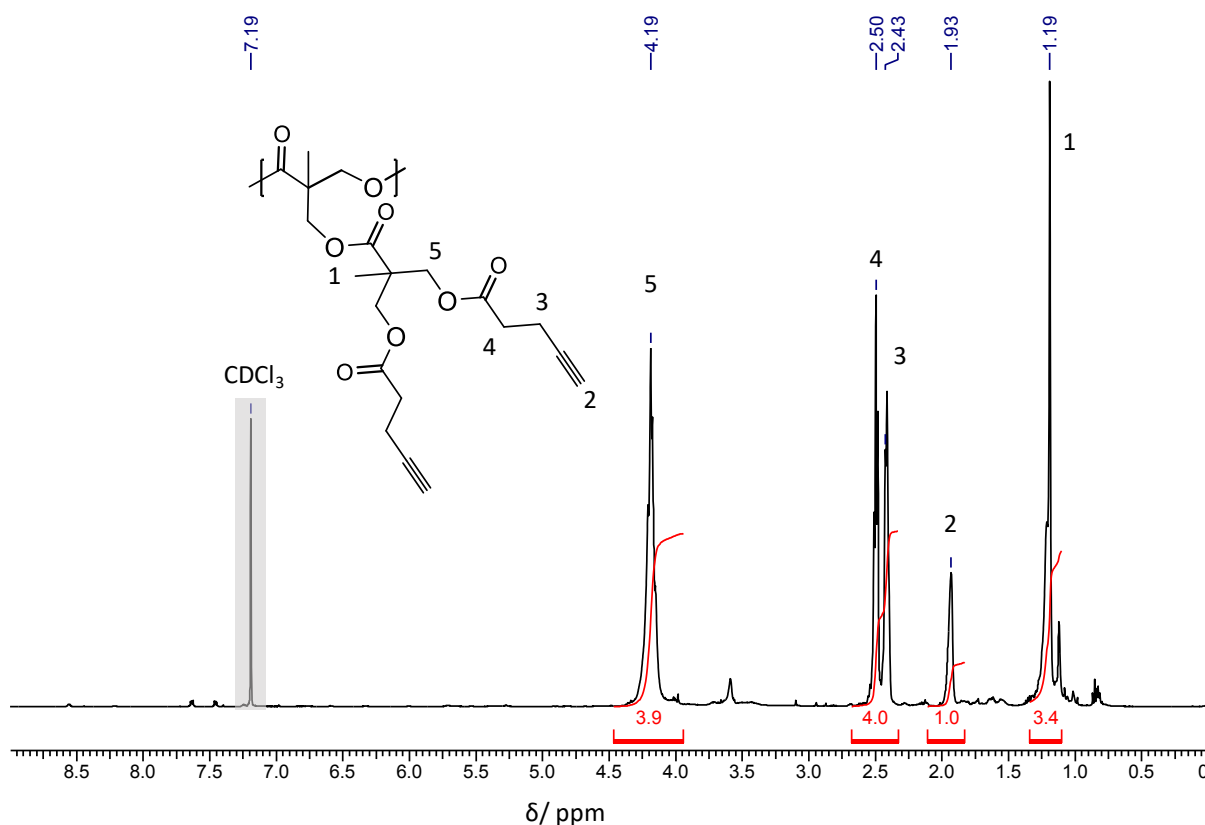


Figure 5.26: ^1H NMR spectrum of the first generation pentinate (P-G1-pent).

Furthermore, the signal at 1.93 ppm stands for the alkyne end group, the signals at 2.14 ppm and 2.49 ppm stand for the CH₂ group of the pentynoic acid groups. The signal at 4.19 ppm shows CH₂ groups as the connecting links to ester bonds. Here as well, no distinction can be made as to which groups belongs to the backbone and the branches. The mean number of methyl groups per molecule is known from the structure determination of the unmodified pseudodendrimers.

Theoretically, the number of pentynoic end groups corresponds to the number of hydroxyl groups in the polymer. Figure 15 (Appendix) illustrates the calculation of degree of modification of all three generation of pseudodendrimers which was published earlier.^[336]

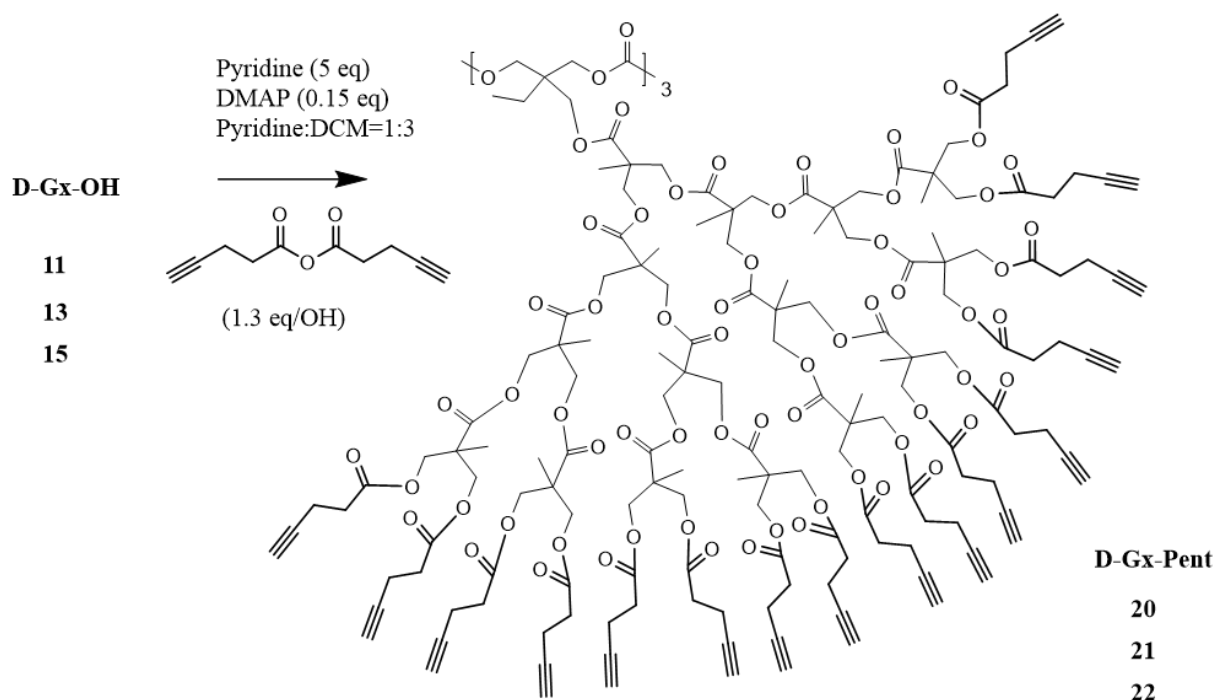


Figure 5.27: Reaction of dendrimers (D-Gx; x=4 to 6, for succeeding generations) with 4-pentynoic anhydride forming corresponding generations of pentinate modified dendrimers (D-Gx-pent).

Figure 5.27 shows the reaction for post-modification of the dendrimer with terminal pentinate groups resulting into three generations (20, 21 and 22) of alkyne end group modified dendrimers namely, D-G4-pent, D-G5-pent and D-G6-pent. Again, the esterification of the dendrimers to the corresponding dendrimer pentinate was then carried out with pentynoic anhydride, analogously to the esterification with pseudodendrimers. Here also, 1.3-fold excess of anhydride was used and the other ratios of the reactants were also identical. A brown viscous oil was obtained as a product for all generations. The yields of the reactions ranged from 82-104%, the yields over 100% being explained by the contamination of the product with residual toluene and pyridine. Figure 5.28 shows the ¹H NMR spectrum of D-G4-pent.

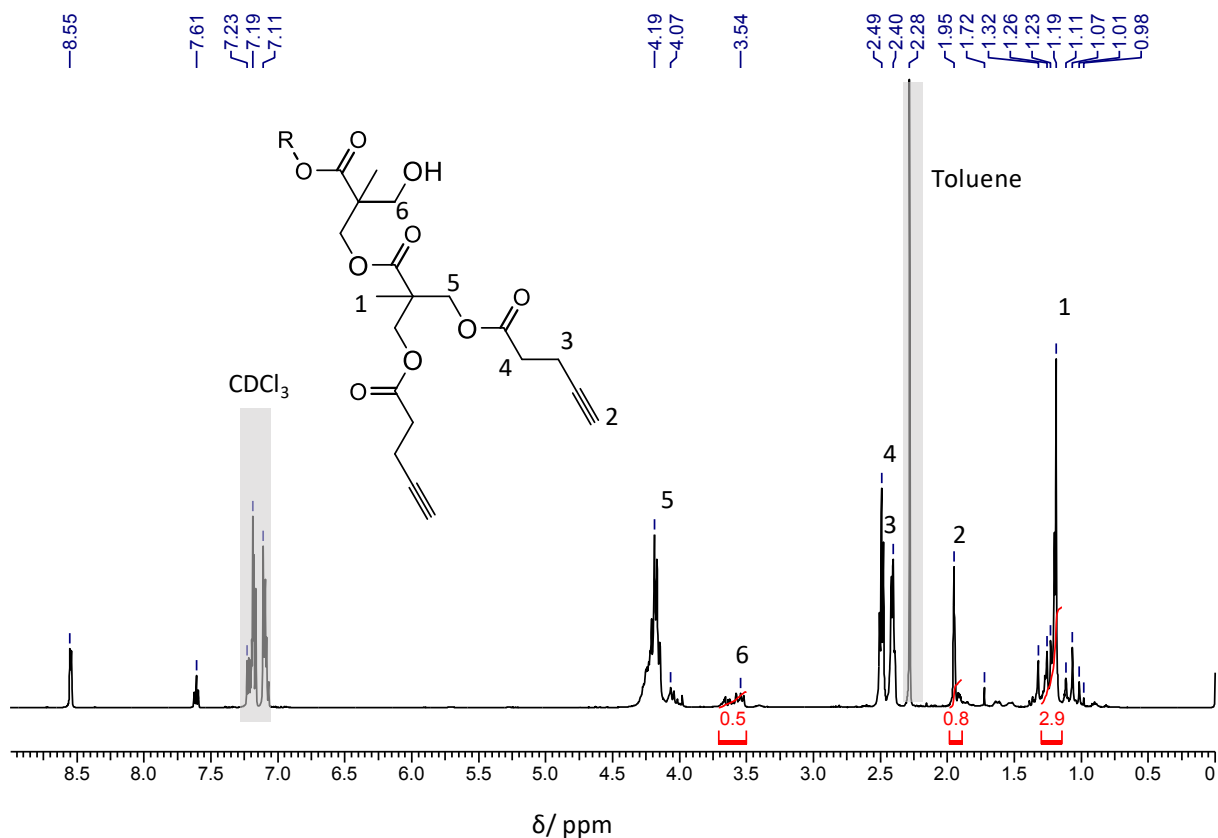


Figure 5.28: ^1H NMR spectrum for D-G4-pent.

Due to the pentinate residue, the terminal methyl groups are chemically so similar to the dendritic methyl groups that the peaks of the methyl groups no longer appear separately and only one peak can be seen at 1.19 ppm. In the case of D-G4-pent, the integral of pentinate proton signal at 1.95 ppm is 0.8, which corresponds to a conversion of 80%. Upon dividing the integral of the signal at 3.58 ppm, which is the signal for residual pentinate, by the two protons of the methylene group, a value of approx. 20% is obtained, which indicates the number of unreacted groups and confirms the result. After the synthesis of D-G4-pent, freshly synthesized pentynoic anhydride was used exclusively, which resulted in complete conversions for the fifth and sixth generations (D-G5-pent and D-G6-pent), as could be demonstrated by ^1H NMR (Figure 12 and 13 in Appendix, respectively). The integral of the pentinate peak at 1.95 ppm was about 1, with the methylene peak at 3.58 ppm no longer being detectable.

Subsequently, next step of “functionalization” was undertaken for all 6 polymers post-modified with terminal alkyne end groups.

For the production of mannose propylazide, azidopropanol was required, which first was produced from bromopropanol according to the following reaction:

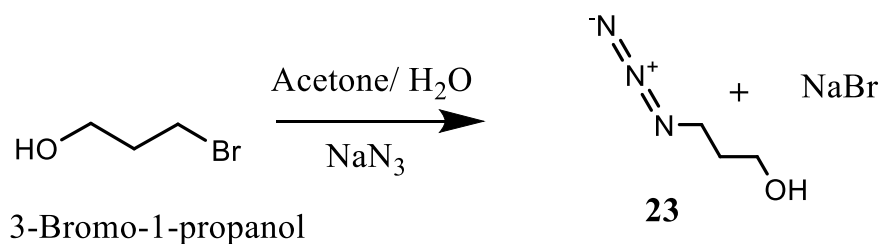


Figure 5.29: Reaction for the synthesis of azidopropanol (23) from 3-bromo-1-propanol and sodium azide.

The product was analyzed by ^1H NMR spectroscopy (Figure 17 Appendix). The middle CH_2 group at 1.77 ppm was set as the reference with an integral value of 2. The two outer methyl groups at 3.68 and 3.38 ppm, with an integral value of 1.8 ppm to 1.9 ppm, almost correspond to the reference integral value and suggest that the desired product is obtained. The peaks of residual 3-bromo-1-propanol are expected to be found at 2.19 ppm, 3.52 ppm and 3.74 ppm.^[397] Since these peaks do not appear in the spectrum and the ratios of the integrals agree well, the presence of the desired product in good purity is confirmed. The ^{13}C NMR spectrum (Figure 18, Appendix) also clearly shows the presence of the three CH_2 groups of 3-azido-1-propanol.

The next step in the synthesis of glycopolymers is the synthesis α -D-mannose propylazide tetraacetate from α -D-mannose pentaacetate and 3-azido-1-propanol (Figure 5.30).

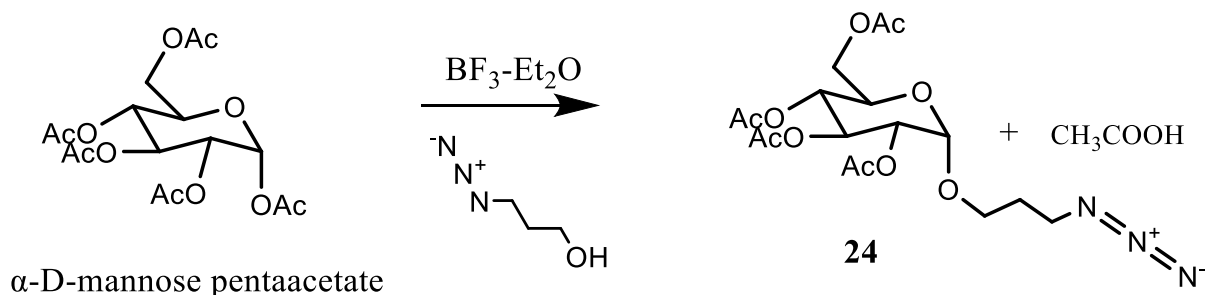


Figure 5.30: Reaction of α -D-mannose pentaacetate with 3-azido-1-propanol forming mannose propylazide tetraacetate (24).

The reaction was carried out in pre-dried DCM with the addition of molecular sieves and under a nitrogen atmosphere, since the boron trifluoride-dietherate ($\text{BF}_3\text{-Et}_2\text{O}$) catalyst used is sensitive to air and moisture, leading to decomposition on contact with oxygen and water. For this reason, a large excess of catalyst was used in order to account for decomposition and to provide a sufficient amount of catalyst for the entire reaction time. In several approaches, only between 50% and 60% conversion could be achieved with a yield of 60% to 80%. An excess of azidopropanol could not be used to increase the yield since the residual azidopropanol is difficult to separate from the product. In addition, residual azidopropanol would react with the pentinate groups of the dendrimer in the “click” reaction. Unreacted mannose molecules would not interfere with the click reaction and would be separated off in the last step of the dialysis, which is why the α -D-mannose propylazide pentaacetate produced did not have to be of absolute purity in terms of unreacted mannose.

Figure 5.31 shows the ^1H NMR spectrum of the pure product fraction. The signals at 1.84 ppm, 3.36 ppm and 3.48-3.74 ppm are the signals arising from the protons of propyl chain of the azidopropanol part attached to mannose tetraacetate. The signals at 1.83-2.09 ppm represent the signals from acetate part and signals at 3.90 ppm, 4.04-4.23 ppm, 4.75 ppm and 5.17-5.21 ppm represent the mannose part. Due to the steric effects and cyclic structure of the mannose splitting of signals are seen, which is common for such sugar structures. The successful connection of azidopropyl group to the mannose ring is shown by the signal at 4.75 ppm.

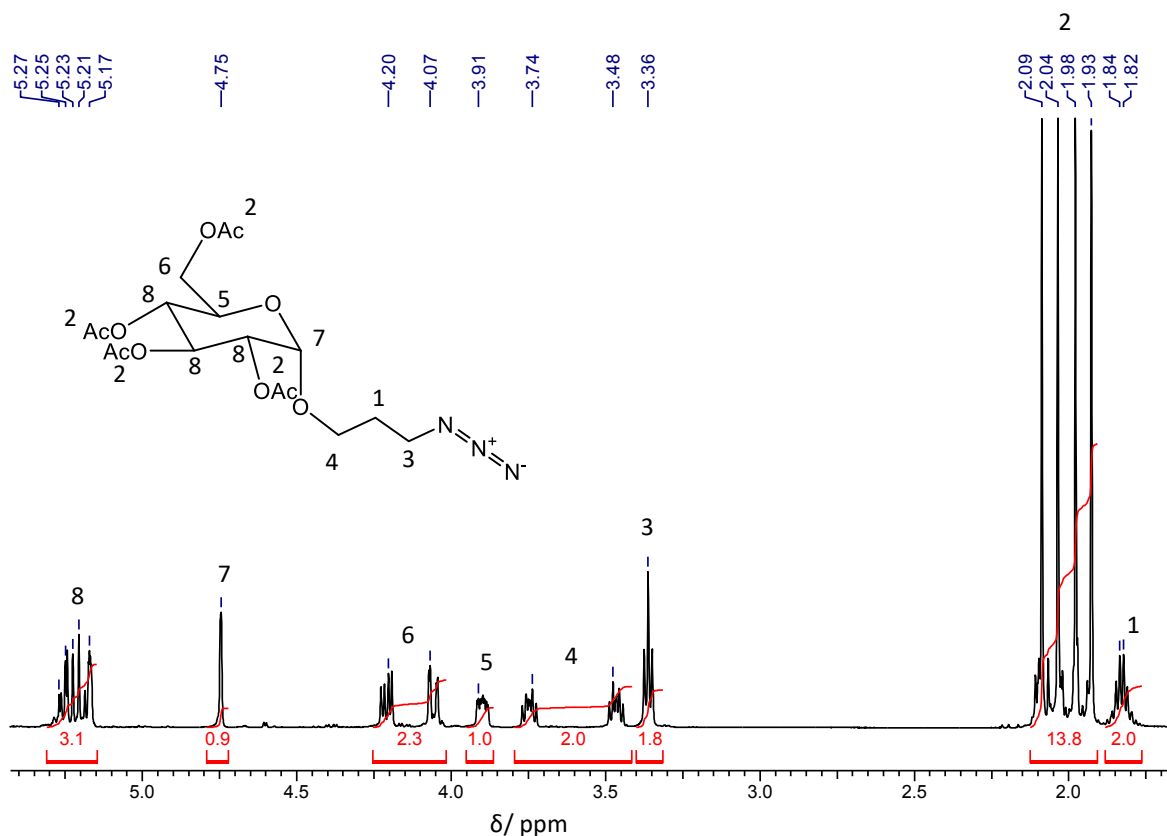


Figure 5.31: ^1H NMR spectrum of mannose propylazide tetraacetate (24).

In the ^{13}C NMR spectrum (Figure 5.32), signals at 28.67 ppm, 48.12 ppm and 62.54-69.54 ppm represent the CH_2 groups of azidopropanol attached to the mannose ring. The signal at 20.66 ppm represents the methyl groups of the acetate units and signals 4, 6-10 and 11 represent the signals of the mannose ring. Here, based on signal 10 it can be concluded that azidopropanol group is attached to the mannose ring. This reaction was carried out separately for pseudodendrimers and dendrimers to have sufficient and fresh materials in the final stage of the synthesis of glycopolymers.

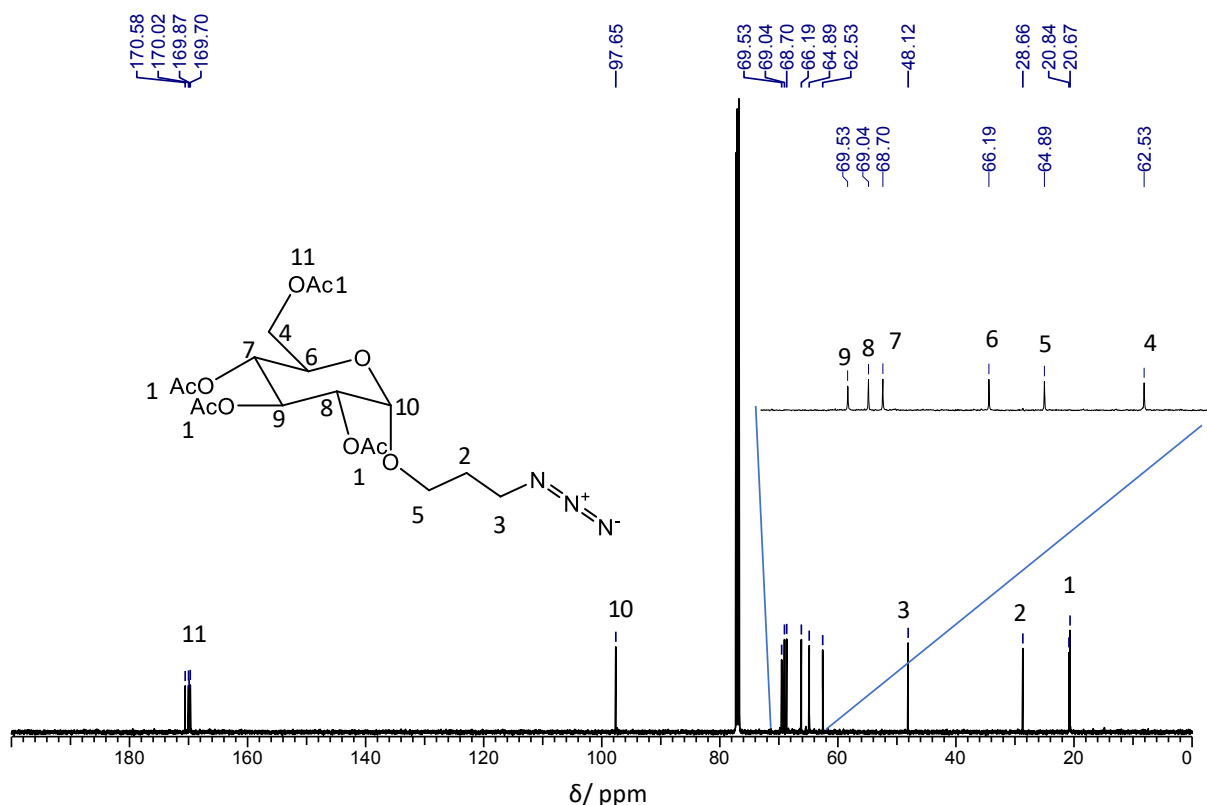


Figure 5.32: ^{13}C NMR spectrum of mannosyl propylazide tetraacetate (**24**).

To remove the unreacted azidopropanol and excess catalyst completely, the product was purified by column chromatography in normal phase mode with silica gel as stationary phase and ethyl acetate/n-hexane mixtures as eluent. As there was a very small difference in the retention factors of the product and unreacted azidopropanol, also as the amount of sample to be purified was quite large, the purification step was performed several times. This led to a decrease of the total yield.

The next step was the deprotection of the acetate groups of mannosyl propylazide tetraacetate. This was a simple Zemplen deacetylation transesterification reaction, which was done using methanol and sodium methoxide (Figure 5.33).

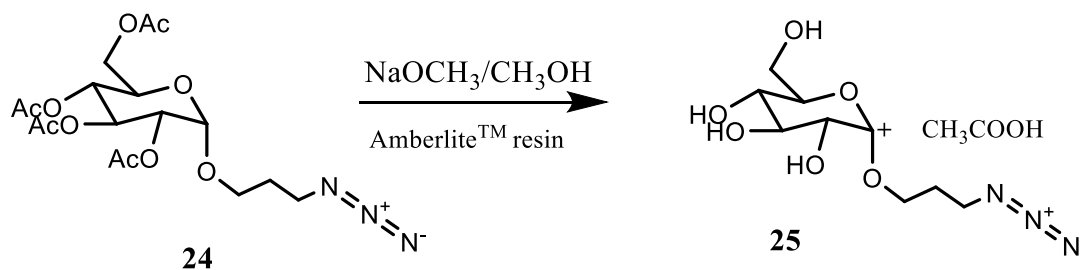


Figure 5.33: Deprotection of α -D-mannosyl propylazide tetraacetate (**24**) to form α -D-mannosyl tetrahydroxyl propylazide (**25**) in presence of Amberlite resin.

By using sodium methoxide, the acetate groups were split off as methyl esters. By using the proton form of the cation exchange resin Amberlite IR120H, the sodium ions were exchanged for hydrogen ions, where the hydroxyl groups could be formed. The protons of the hydroxyl groups formed can be seen in the ^1H NMR spectrum in Figure 5.34 in the range from 4.50–4.67 ppm, which confirms the complete removal of the acetate groups. The integrals also show that it must be almost pure mannose propylazide. No unreacted mannose peaks could be identified either.

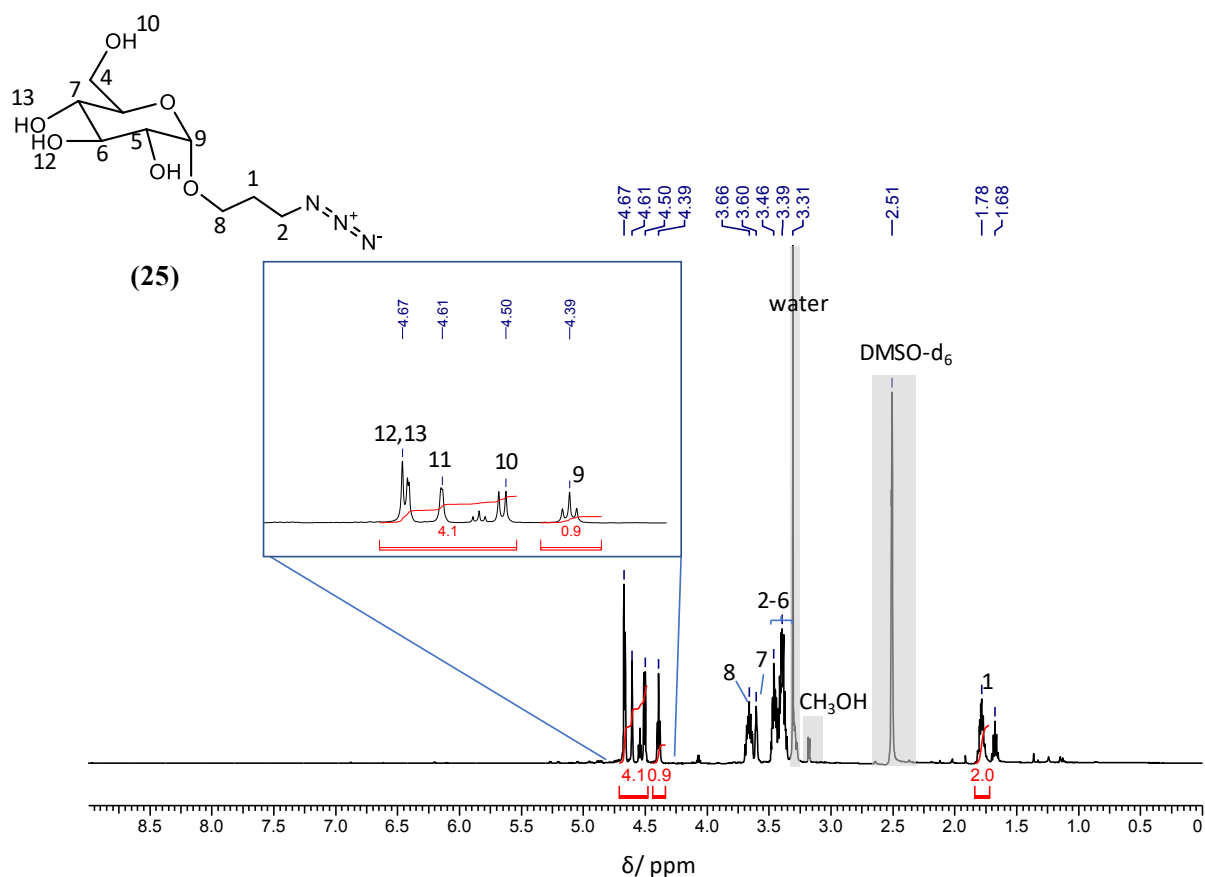


Figure 5.34: ^1H NMR spectrum for mannose tetrahydroxyl propylazide (25).

In the final step of the functionalization-synthesis of glycopolymers, copper catalyzed click reaction was carried out with the P-Gx-pent ($x = 1, 2, 3$)/D-Gx-pent ($x = 4, 5, 6$) and mannose tetrahydroxyl propylazide. The reaction of the click chemistry used with all three P-Gx-pent (Figure 5.35). The reagents were adapted based on the number of terminal alkyne end groups. 1.2 eq of mannose tetrahydroxyl propylazide per alkyne end groups, and 0.06 eq CuSO_4 with 0.12 eq sodium ascorbate as reducing agents were used.

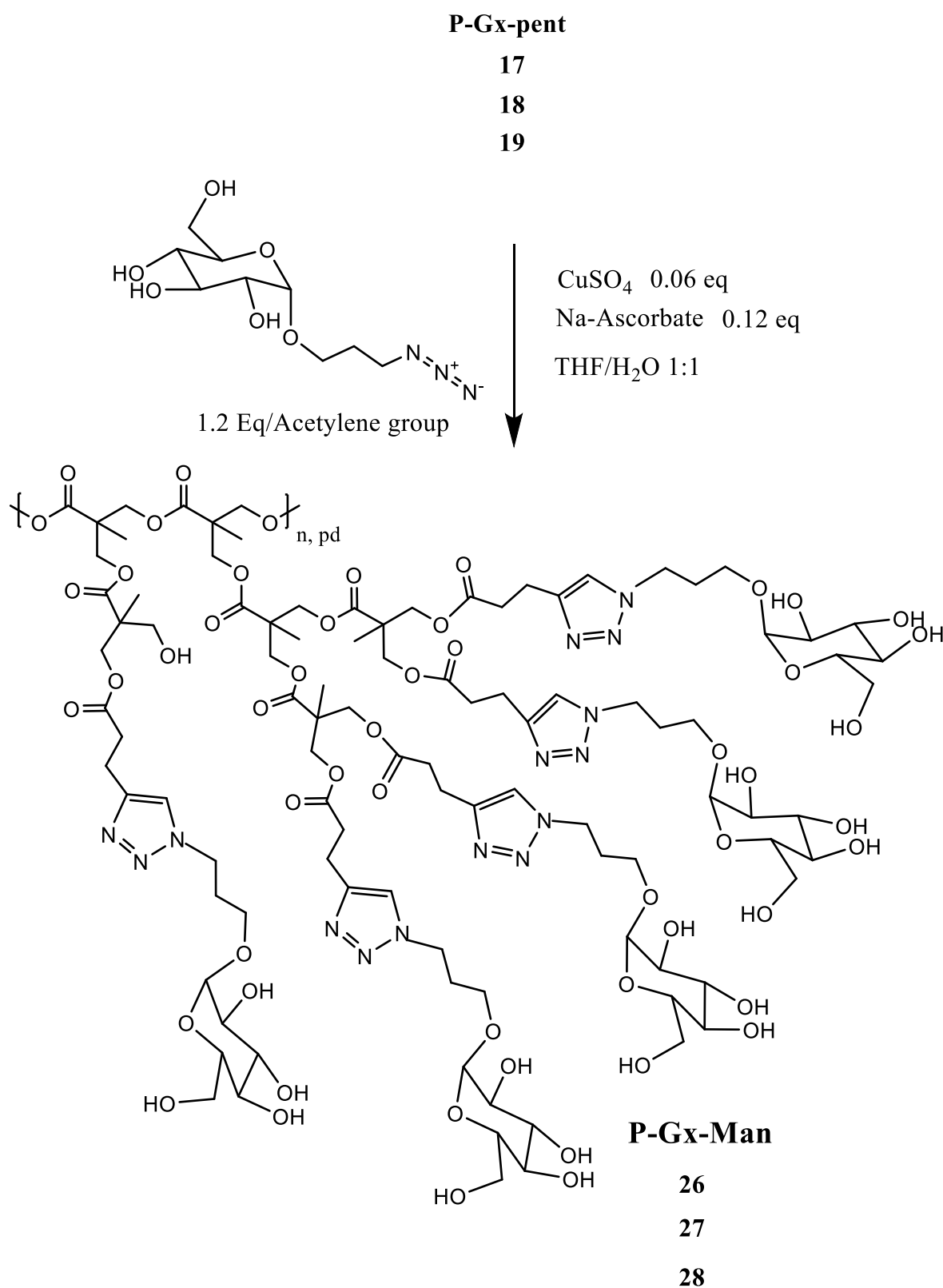


Figure 5.35: Copper catalyzed click reaction for pseudodendrimers. All post-modified pseudodendrimers (P-Gx-pent) were used with mannose propylazide in THF:water (1:1) in the presence of CuSO₄·5H₂O and sodium ascorbate forming three generations of glyco-pseudodendrimers (P-Gx-Man; x=1, 2, 3).

Since the pseudodendrimers and dendrimers with terminal alkyne end groups do not dissolve in water, a mixture of THF and water in 1:1 ratio was used as the solvent. After the reaction, the THF was removed by starting with 5% THF by volume, and gradually decreasing it to zero, over 5 days. The final product obtained was free of any impurities and contained only residues of water which was difficult to remove but did not interfere with further studies.

The ^1H NMR spectra for all three generation of mannose functionalized pseudodendrimers P-G1-Man, P-G2-Man and P-G3-Man showed a complex picture due to their pseudodendritic structure in addition to the complexity shown by ring structure of mannose. Figure 5.36 shows the ^1H NMR spectrum of P-G1-Man. The signals present at 1.10-1.18 ppm represent the signals arising from protons of methyl groups of the pseudodendrimers backbone, signals at 2.64, 2.84, 4.17 ppm also belong to the same. The mannose part, however, is represented by 3.39, 3.48, 3.62, 4.38 and 4.38 ppm. The hydroxyl groups of the mannose part are represented by 4.52, 4.59, 4.67 ppm. The most important signal arising from the proton of the triazole ring is shown at 7.83 ppm. Similarly, D-G1-Man, D-G2-Man and D-G3-Man were also synthesized. The degree of modification was calculated from ^1H NMR spectra using the integral of signal of triazole proton at 7.83 ppm. Spectra of the samples are shown in Appendix (Figure 19-23). The degree of modification is shown in the Table 5.4.

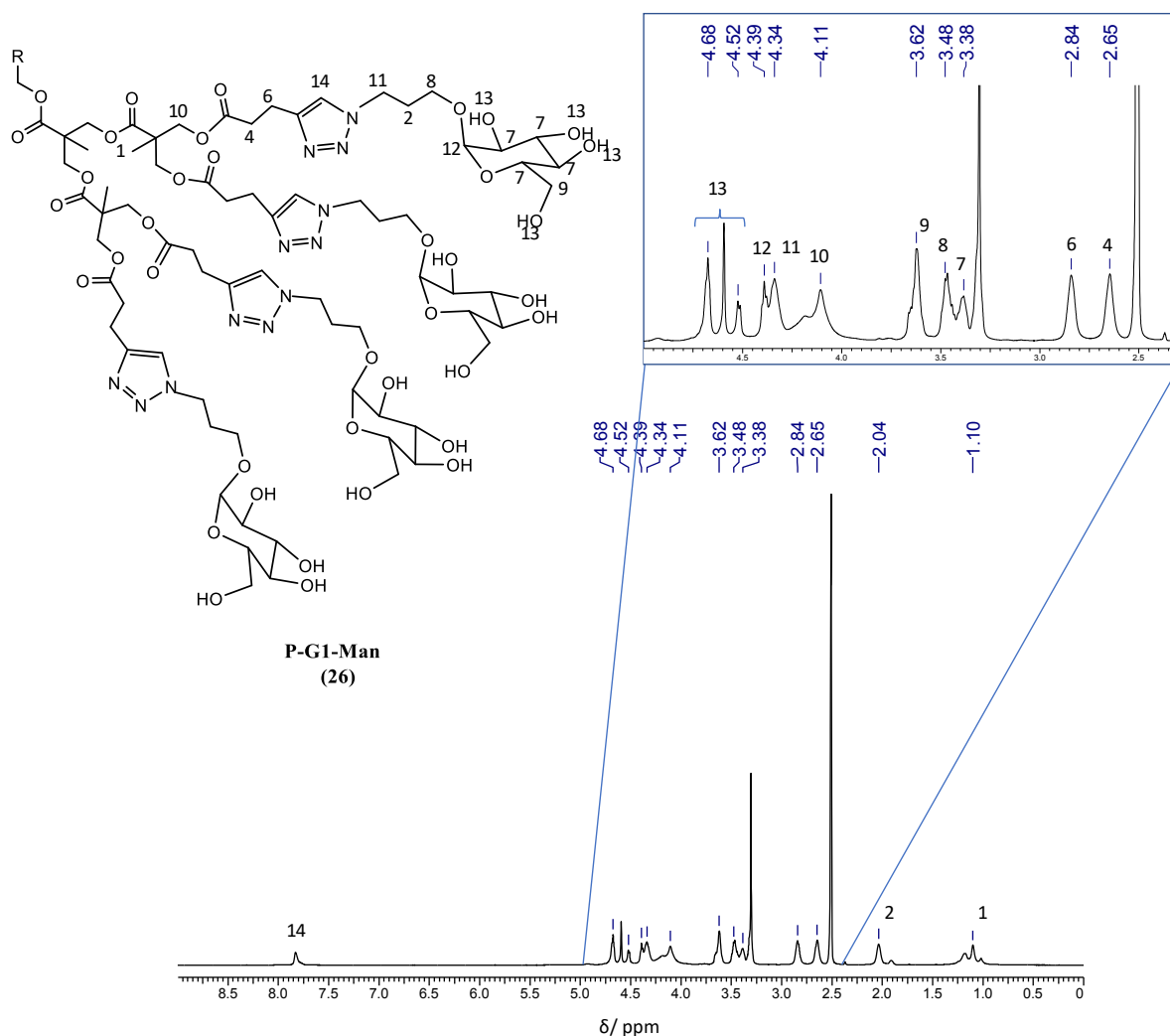


Figure 5.36: ^1H NMR spectrum of P-G1-Man.

5.1.4.1 Molecular size determination of GI-P and GI-D using SEC

All the six polymer samples were also characterized with SEC-MALS to evaluate the molar masses and dispersity. Figure 5.37 shows the SEC chromatograms of GI-P.

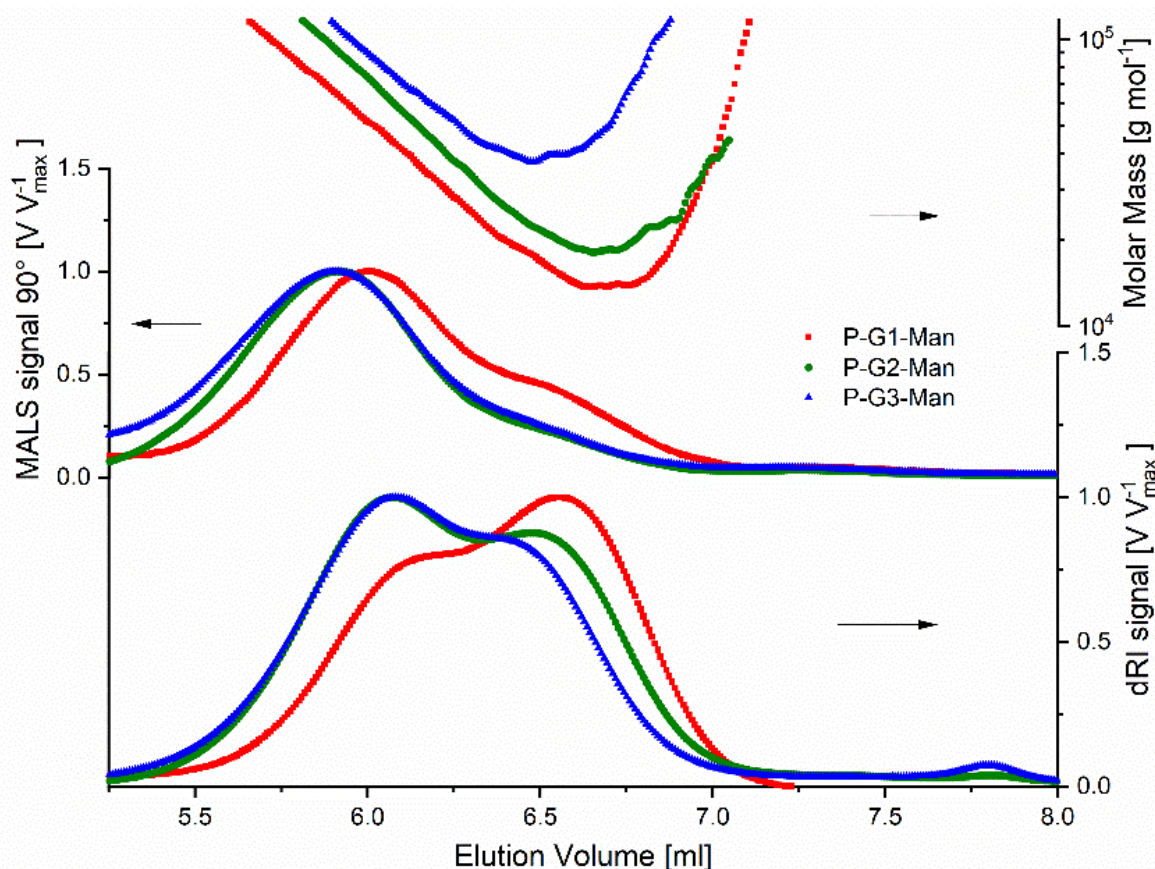


Figure 5.37: Chromatograms of mannose functionalized P-G1-Man, P-G2-Man and P-G3-Man in DMAC with SEC coupled to a LS and RI detectors.

The molar masses of P-G1-Man, P-G2-Man and P-G3-Man are found to be 25, 41 and 69 kDa, respectively with a somewhat bimodal distribution, along with a slightly broad dispersity of 1.7-1.8. This multimodal behavior tells us about the heterogeneity or perhaps the presence of different structural moieties. The RI signals show that there is a noticeable decrease in the elution time from P-G1-man to P-G2-Man but only a marginal change in the elution time is observed between P-G2-Man and P-G3-Man. This is because the degree of modification was 100% in both the cases, so despite being low in molar mass in comparison to P-G3-Man, P-G2-Man elutes at a similar time. The LS signal shows a small shoulder between 6.5-7.0 min, which is more pronounced in case of P-G1-Man. A shoulder is seen in the RI signal between 6.5-7.0 min in P-G1-Man suggesting some unreacted groups. In the molar mass curves, a regular increase is observed going from P-G1-Man to P-G3-Man. In the case of P-G2-Man and P-G3-Man, the reduced shoulders in LS and the corresponding RI signal suggest lower amounts of unreacted groups. The dn/dc is between 0.12-0.11, so a relative error of 12-15% in molar mass measurement can be considered.

Figure 5.38 illustrates the RI and LS chromatograms of the three generations of GI-D; D-G4Man, D-G5-Man and D-G6-Man. Unlike GI-Ps, a clear trend of the increasing molar mass

with each generation is seen in the RI and LS signals. The molar masses of D-G1-Man, D-G2-Man and D-G3-Man are 21, 38 and 65 kDa, respectively having an almost monomodal distribution with a very low dispersity of 1.1. A decrease in the elution time from D-G1-Man to D-G3-Man is seen in the RI signal. In D-G6-Man, a small shoulder is observed between 6.5-7.5 which is likely due to small number of defects, resulting in a small number of unreacted OH groups to be still present in the structure as mentioned earlier in Section 5.1.3. The degree of modification summarized in Table 5.4 is based on the conversion from terminal alkyne end groups to mannose groups.

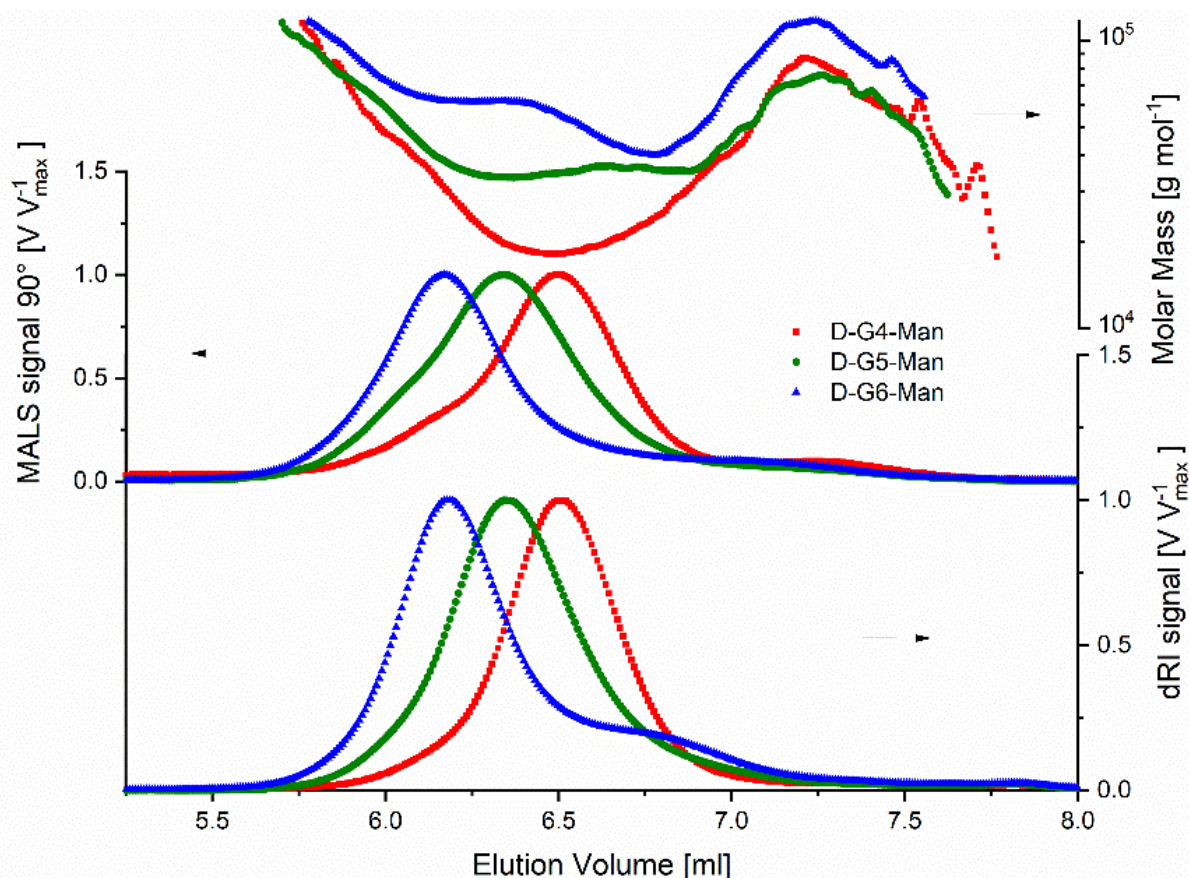


Figure 5.38: Chromatograms of mannose functionalized D-G4-Man, D-G5-Man and D-G6-Man in DMAC with SEC coupled to a LS and RI detectors.

Table 5.4: Molecular characteristics of glyco-pseudodendrimers and glyco-dendrimers.

Polymer	M_n^a (kDa)	M_n^b (kDa)	M_w^b (kDa)	\bar{D}^b	dn/dc (ml/g)	Mannose units ^c	Degree of modification ^c
P-G1-Man	23	25	46	1.7	0.121	44	77
P-G2-Man	57	41	93	1.8	0.112	90	88
P-G3-Man	78	69	118	1.8	0.113	168	84
D-G4-Man	22	21	24	1.1	0.124	37	78
D-G5-Man	46	38	41	1.1	0.117	87	98
D-G6-Man	92	65	69	1.1	0.118	165	98

(a) Theoretical molar masses (b) SEC-LS (c) 1H NMR. The degree of modification is based on the conversion terminal alkyne end groups to mannose groups

5.1.4.2 Particle size determination using batch DLS

The general principle of DLS has been explained in Section 3.3. DLS determines the hydrodynamic size (R_h) of a molecule in solution by irradiating it with a laser and analyzing the scattered light. Batch measurements of DLS determine semi quantitative aspects of the hydrodynamic radius distribution. In general, DLS works well for particles with low dispersity, thus providing effective average radius, but it is strongly influenced when analyzing broadly distributed samples. Therefore, the conclusions drawn from DLS are of a rather qualitative nature.

Concerning the glyco-dendrimers, as these have many surface functional groups, their hydrodynamic radius distribution cannot be obtained by chromatography mode. In this work, DLS was utilized in order to have a better view on the structural size of the synthesized glycopolymers and the results are shown in Figure 5.39.

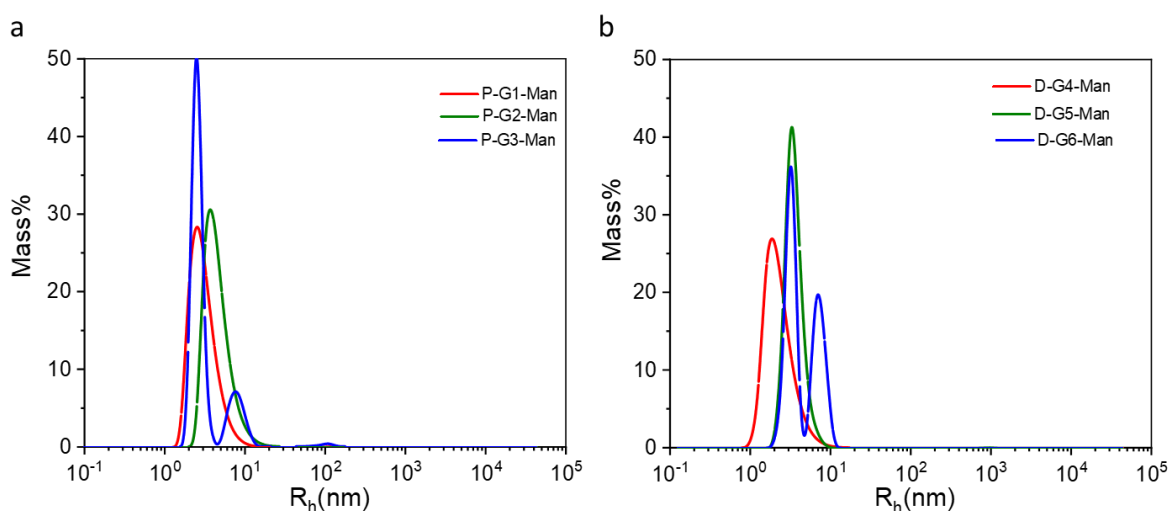


Figure 5.39: DLS in DMAC using 0.2 μm filter for a) GI-Ps b) GI-Ds.

For the GI-Ps, an increase in R_h value is seen going from P-G1-Man to P-G2-Man but the R_h value decreases for P-G3-Man. In case of P-G3-Man and D-G6-Man we see bimodal distribution. This is due to a high number of defects in these two. No big aggregates were seen but this was evident as the samples were filtered.

The average R_h values obtained are listed in Table 5.5. An interesting observation in case of GI-P is that the average R_h value was highest in case of P-G2-Man. Whereas, GI-Ds showed a regular increase in R_h values with generation number as expected. The apparent density is calculated using these values and is discussed in the following Section 5.1.4.3.

As the aim is to evaluate the physiological conditions, the R_h values in PBS (10 mM, pH 7.4) were additionally measured and are shown in Figure 5.40. The average R_h values obtained are listed in Table 5.5. A similar behavior in PBS as in the case of DMAC is seen in both set of samples with R_h values of 3-4 nm.

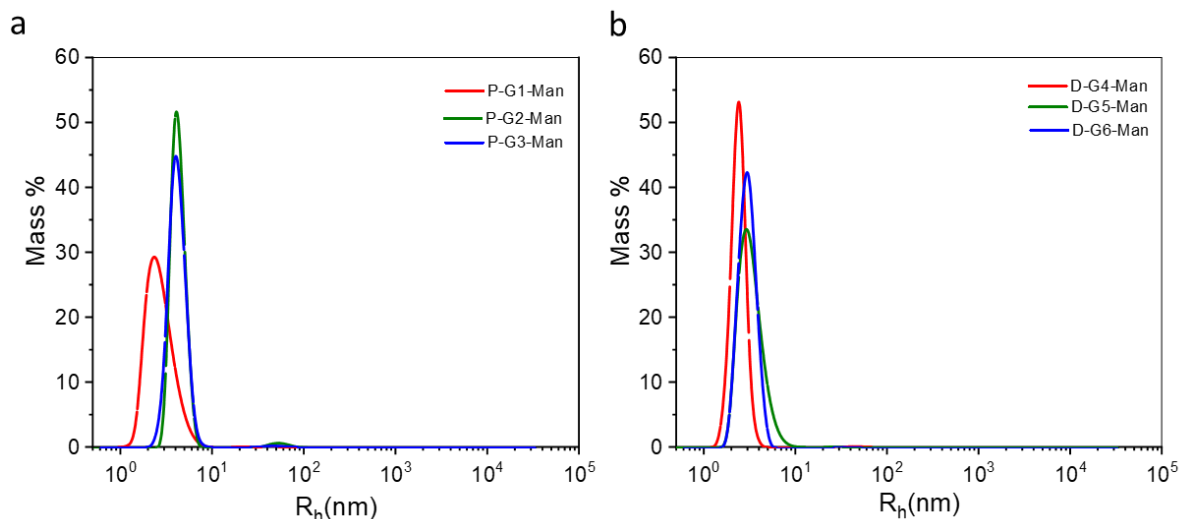


Figure 5.40: DLS in PBS using 0.2 μm filter for a) GI-Ps b) GI-Ds.

Table 5.5: R_h values for glyco-pseudodendrimers and glyco-dendrimers determined from Batch DLS in DMAC and PBS.

Polymers	R_h (nm) _{DMAC}	R_h (nm) _{PBS}
P-G1-Man	2.9	2.4
P-G2-Man	4.2	4.2
P-G3-Man	3.8	4.0
D-G4-Man	2.7	2.4
D-G5-Man	4.0	3.0
D-G6-Man	4.4	4.3

5.1.4.3 Apparent densities

The presence of many functional groups along with a hyperbranched core and low molar masses make it difficult to assess the topology of synthesized samples.

So, the apparent densities were calculated using the R_h values determined from the batch DLS measurements. Figure 5.41 shows the corresponding data obtained. These results reveal interesting details about the structures of GI-P and GI-D. The apparent density curve for GI-P shows a decrease until P-G2-Man and then a nearly exponential increase in case of P-G3-Man.

The corresponding dendrimers GI-D shows a lower apparent density. There is still an increase on going from D-G5-Man to D-G6-Man, however it is not as much as it was in case of P-G3-Man. So far, following points can be concluded:

1. For nearly the same number of mannose groups, GI-P has higher densities in comparison to GI-D.
2. The topology of P-G3-Man despite being the one with highest number of functional groups does not have the largest volume in solution. Instead, P-G2-Man has the lowest density and highest volume in solution.

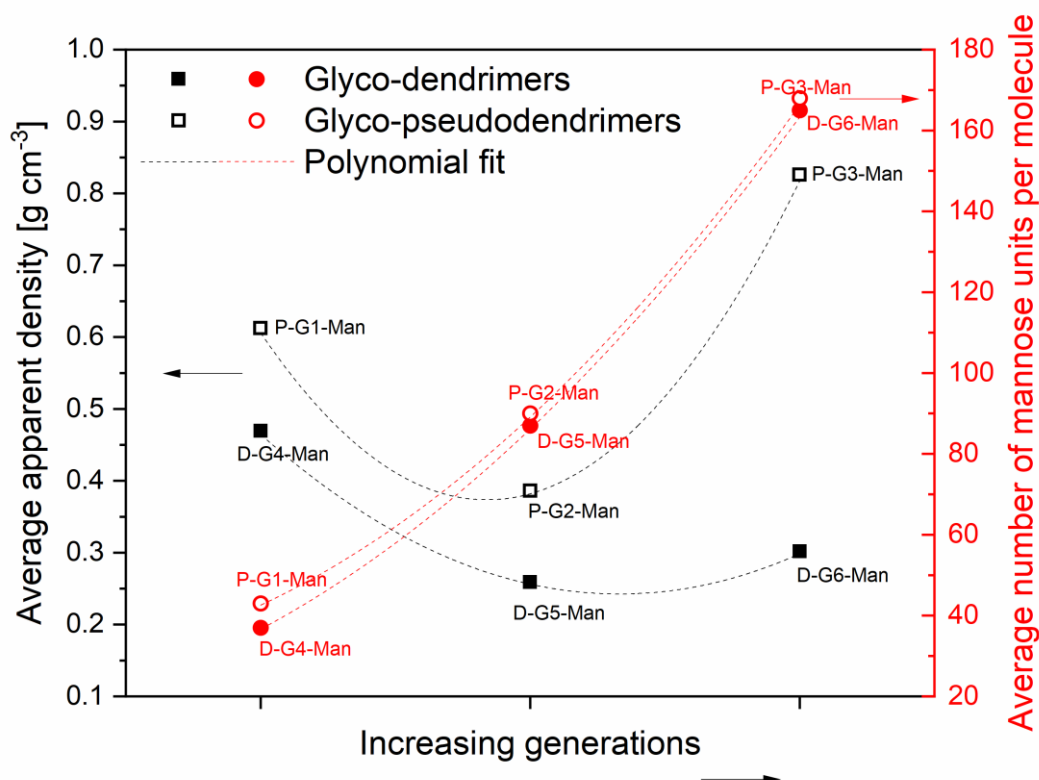


Figure 5.41: Comparison of apparent densities of GI-Ps and GI-Ds, showing that GI-Ds have lower densities than GI-Ps for almost similar number of mannose groups on the surface.

The structure of GI-P is different from GI-D in a way that the mannose modification has taken place also in the cavities of the GI-P but in case of GI-D the dendritic structure has an open core but does not allow for such modifications in the cavities. This perhaps, makes GI-Ps core along the modifications in cavities lying close to the core, bulkier, which is why they have higher apparent densities. This could be better verified by viewing the molecular shape in 3D and hence, molecular dynamics simulations were performed which is discussed in Section 5.1.5.

5.1.4.4 Molecular size determination of GI-Ps and GI-Ds using AF4

The theoretical background as well as the separation mechanism of AF4 has been described in detail in Chapter 3. The use of the channel instead of the column in SEC offers a gentle separation mechanism with marginal pressures and no shear forces. AF4 is an extremely powerful technique for analyzing small molecules as well as aggregates. Until now, AF4 has been applied to study amyloids only once.^[173] This study showed how AF4-MALS can be applied to a complex mixtures of A β 42 aggregates. A deeper insight into the physiological conditions and aggregates involved with amyloids through the application of AF4 was very attractive within the framework of the present research work and therefore undertaken. To apply AF4 to investigate the inhibition of aggregates with the GI-P and GI-D, it was necessary to first characterize them with AF4 in aqueous system. The method development of GI-P, GI-D and A β 40 are described in Section 4.2.3. Normally, with the coupling of AF4 to MALS-UV-Vis-

RI detectors, a wide array of information can be collected. In this work, since the synthesized polymers lie on the lower M_w range and small sizes, information based on conformation was not possible to achieve. But a general overview of the characterization of the polymer like molar mass and R_h could be determined.

Figure 5.42 illustrates the RI signals of AF4-MALS. The determined absolute M_n of each generation of GI-P and GI-D increased with increasing generation number. Also, the fractograms showed multimodal behavior, which indicates that the samples had well defined architectures and few larger aggregates in very low concentration. The fraction of aggregates was excluded in the analysis of molar mass. Dispersity of these samples can be also found in Table 5.6. The R_g determination was not possible because of the smaller size of the samples (3-5 nm), whereas to determine R_g the nominal value of roughly 15 nm radius for the start of quantifiable angular dependence is required. This has been explained in detail in Chapter 3. The molar masses are mentioned in Table 5.6. In case of GI-P a nice elution behavior is seen going from P-G1-Man to P-G3-Man, despite the fact that the difference in molar masses from each succeeding generation was not much. The signal intensity of LS detector was too low because of the small size of the polymers. The absolute molar masses were determined after determining the dn/dc value of P-G2-Man offline and values are given in Table 5.6.

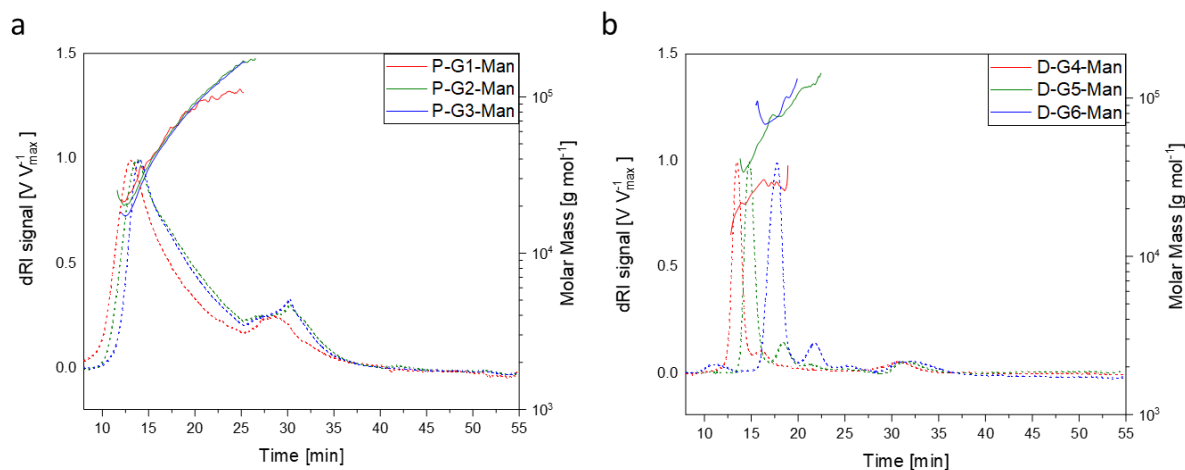


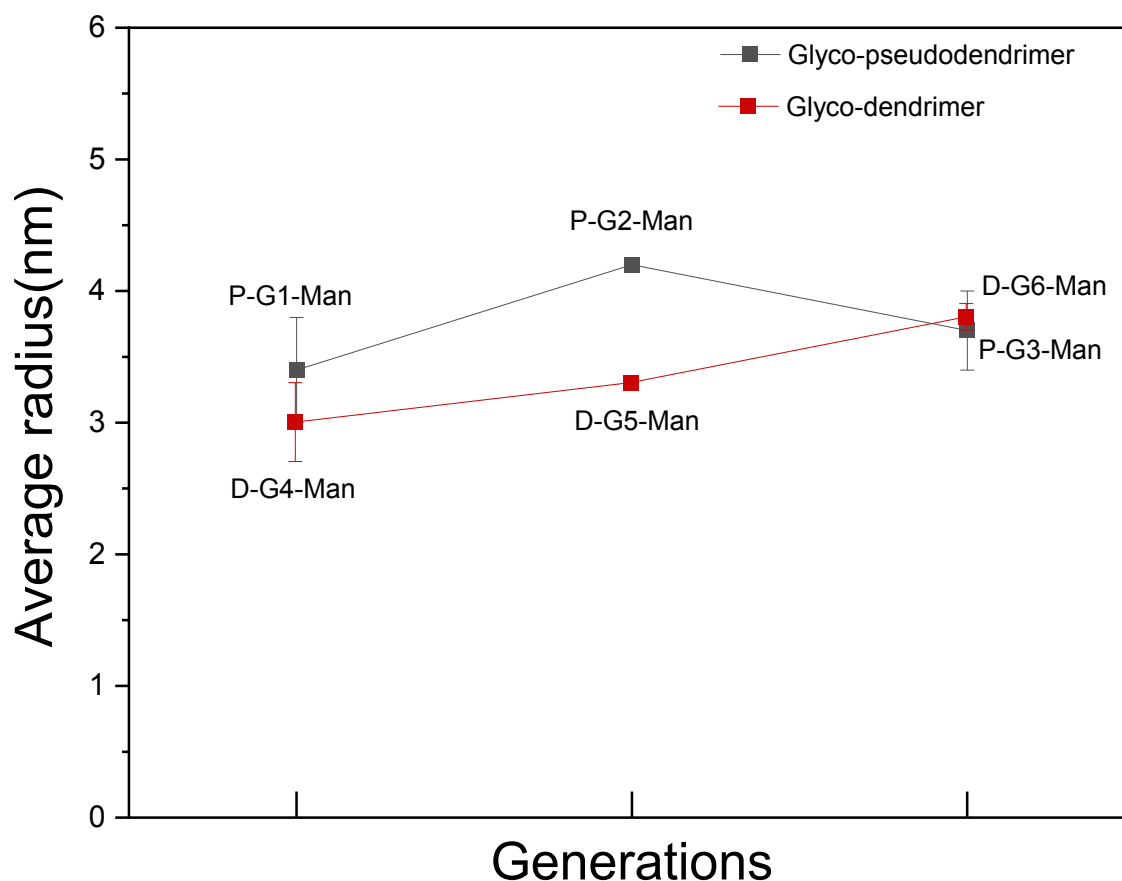
Figure 5.42: AF4 fractograms of a) GI-Ps and b) GI-Ds in PBS buffer showing detector signals (dashed line-RI) and molar masses (symbols) depending on elution time.

To further explore the molecular structure, hydrodynamic radius (R_h) was calculated by online DLS coupled to AF4. Table 5.6 and Figure 5.43 shows the R_h values obtained for the polymers. R_h values were calculated using Debye method and polynomial fit of order 2. The results show R_h of GI-P was higher as compared to GI-D which confirms the behavior with the results from previously measured batch DLS. Determination of R_h was not possible in case of SEC-MALS as was there was not enough signal response.

Table 5.6: Molar masses of the glyco-pseudodendrimers and glyco-dendrimers determined from AF4 and SEC.

Polymers	M_n^a (kDa)	M_w^a (kDa)	\bar{D}^a	R_h (nm) ^a	M_n^b (kDa)	M_w^b (kDa)
P-G1-Man	31	48.4	1.6	3.4±0.4	25	46
P-G2-Man	39	64	1.6	4.2±0.03	41	93
P-G3-Man	43	69.2	1.6	3.7±0.3	69	118
D-G4-Man	20	21	1.1	3±0.3	21	24
D-G5-Man	40	42	1.1	3.3±0.05	38	41
D-G6-Man	85	92	1.1	3.8±0.1	65	69

^a) AF4-MALS and ^b) SEC-MALS. The samples were measured in PBS buffer in AF4 whereas DMAC was used in SEC.

**Figure 5.43:** A comparison of R_h values obtained from online DLS (AF4) between G1-P and G1-D obtained with AF4 in PBS buffer.

After successfully characterizing the synthesized polymers, their interaction with amyloid protein was investigated. However, more information was required regarding the shape of the polymers which would shed some light on their behavior with amyloid protein.

5.1.5 Molecular dynamics simulation

To understand the physical behavior of synthesized polymers it is important to study their structural properties. The experimental techniques suffer limitation when it comes to studying the structural properties at molecular level. Simulation techniques e.g. molecular dynamics (MD) and Monte Carlo (MC), provides an alternative route.^[398–400] Several MD simulations of PAMAM and PPI dendrimers have been carried out.^[401,402] This gave information based on size, shape and density distributions. Different forcefields such as Dreiding, CVFF, AMBER, GAFF, CHARMM, and sometimes, a combination of different forcefields, can be used.^[403–407] In this work GROMOSS G43b1 forcefield has been employed. This would help us understand the thermodynamic properties of the synthesized polymers. So, in the future we would like to use synthesized GI-P/GI-D for drug delivery system, this should be able to give more accurate predictions of free energies of dendrimer-drug complex. So, both unmodified pseudodendrimers and dendrimers as well as mannose functionalized GI-Ps and GI-Ds were simulated, and the radius of gyration, partial monomer density and radial distribution functions were monitored in THF as performed by Boye et al.^[408] and in water because mannose coated samples were soluble in water. The following experiments were performed by Dr. Peter Fiedel at IPF, Dresden.

Table 5.7: Theoretical molecular characteristics of the systems in this work, from molecular dynamics simulations. Both unmodified and mannose-modified pseudodendrimers and dendrimers are simulated with generation number, number of end groups in THF and water.

Sample	Number of OH groups	Number of Mannose groups	Molar mass _t (g/mol)	M _n SEC-MALS (g/mol)
hb-G0-OH	30	-	3385	3500
P-G1-OH	60	-	6868	6900
P-G2-OH	120	-	13835	13700
P-G3-OH	240	-	27770	15700
P-G1-Man	-	60	27469	25000
P-G2-Man	-	62	35123	41000
P-G3-Man	-	110	65538	69000
D-G4-OH	48	-	5359	5200
D-G5-OH	96	-	10933	10000
D-G6-OH	192	-	22080	19000
D-G4-Man	-	45	20810	21000
D-G5-Man	-	96	43894	38000
D-G6-Man	-	192	88003	65000

(t =theoretical)

The initial structures and topologies have been discussed in experimental methods in Chapter 4. Table 5.7 shows the molecular size data from MD simulations and SEC-MALS. We can see that there is reasonably good agreement among molar masses determined from SEC-MALS except in case of P-G2-Man and P-G3-Man. In case of P-G2-Man only 62 mannose groups could be saturated theoretically due to steric hindrance; so it has 58 residual OH groups and P-

G3-Man has 110 mannose groups and 130 residual OH groups. Figure 5.44 and 5.45 show the models for pseudodendrimers series and dendrimers series respectively.

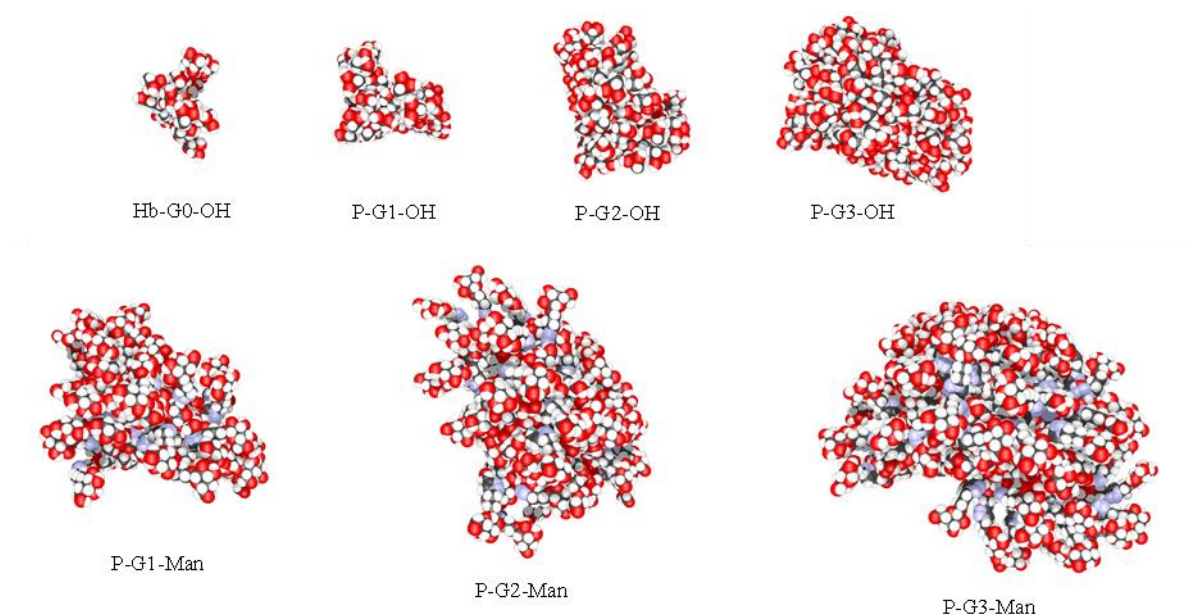


Figure 5.44: Molecular dynamics simulations for different generations of pseudodendrimers (with OH groups) and glyco-pseudodendrimers (with mannose groups).

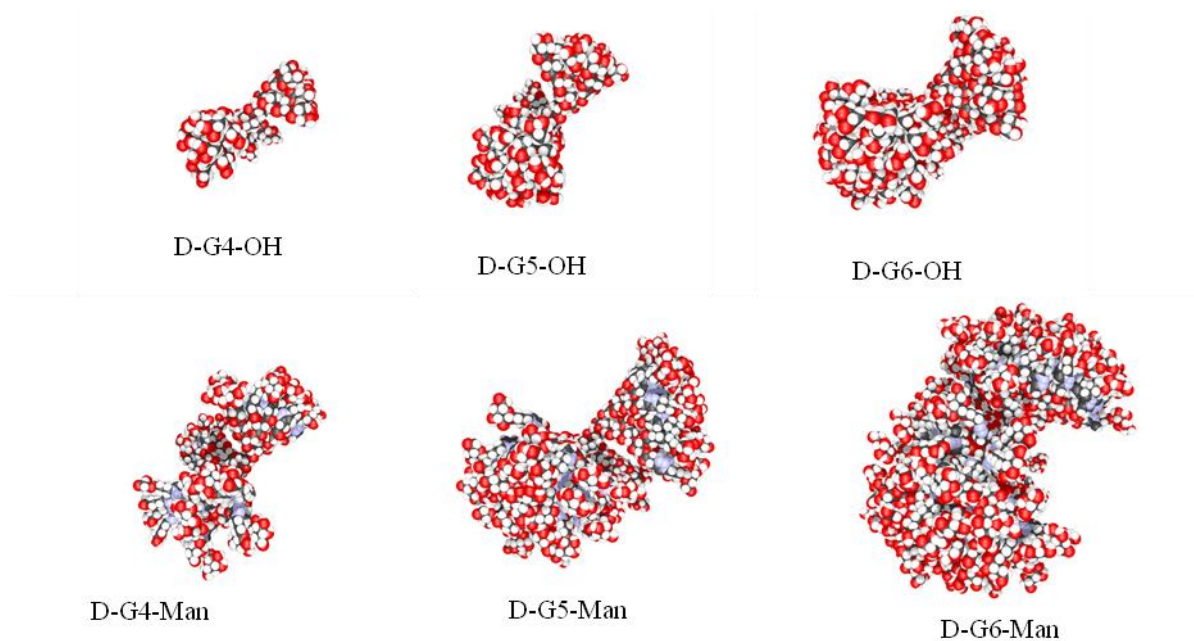


Figure 5.45: Molecular dynamics simulations for different generations of dendrimers (with OH groups) and glyco-dendrimers (with mannose groups).

On comparing the models of pseudodendrimer and dendrimer series it can be seen that in the mannose functionalized pseudodendrimers, the core is more compact and mannose units are more or less uniformly distributed. Whereas in the dendrimers series, it can be seen that the dendrimers have a “propeller” shape, where the core is not so dense. However, mannose units are uniformly distributed at each “blade” of the propeller shaped dendrimers leaving voids in between. This was clearer with 3D view on Rasmol software.

Radius of gyration (R_g) can be quantitatively estimated by the mean-square radius of gyration from center of mass of the polymer. R_g was calculated for each system and plotted as a function of simulation trajectories time (ps). As no experimental data was achievable due to their small size, there is no comparison of the simulated data. However, the data in each series can be compared, e.g., in Figure 5.46a,b, a clear increase in R_g values is seen before modification with mannose (thin lines) and after modification with mannose (thick lines). One point to note here is that R_g is relatively smaller on comparison to experimental R_h values determined (batch DLS and AF4). Firstly, of course, there is a mass distribution of the synthesized polymers. These R_g calculations include one polymer mass, and molar mass distribution is not considered. The experimental measurements of the R_h show the overall radius of polymer molecule including some solvent spheres at the outside, because the scattering beam may see this solvent molecule plus the polymer as a whole.

The Brownian motion allows separation of two solutes dissolved in water by different distances r at different times. The radial distribution function, $g(r)$, gives the probability of finding a particle in the distance r from another particle; here reference is made to the segments of the molecule relative to the center of mass of the polymer. Figure 5.46c,d shows the radial distribution function of unmodified pseudodendrimers and dendrimers, respectively based on the number of atoms. The most immediate observation is that, the dendrimers have 1.5 times denser inner core and a longer tail of this distribution at large distances r from the center. The P-Gx-OH have a greater number of atoms than their counterparts, D-Gx-OH, because of which radial distribution function related to number of atoms becomes higher in D-Gx-OH. This causes the D-Gx-OH to become denser in comparison to the P-Gx-OH. Going from unmodified to mannose modified pseudodendrimers or dendrimers (Figure 5.46 b-f) it is observed that the maximum distribution is reduced and becomes broad. This indicates that the P/D-Gx-Man become less compact on addition of mannose units on the surface. This is because of the additional number of atoms given to the structure because of the addition of mannose propylazide groups and hence the number of atoms related radial distribution function is lower relative to P/D-Gx-OH. Another factor which is worth considering here, is the interaction with solvent molecules. Probably, surface mannose groups react differently to THF in comparison to the surface OH groups. However, when comparing modified G1-P to G1-D (Figure 5.46 e and f), the situation is only marginally different, i.e., the distribution function is high in case of P-Gx-Man relative to D-Gx-Man as the total number of atoms is lower in the former case except P-G1-Man. This implies that the core of pseudodendrimers is denser as compared to corresponding dendrimers. In the case of P-G2-Man, it has denser core in comparison to D-G5-Man, but of course less dense than P-G1-Man but more than P-G3-Man. This could also be an artefact of the sample, as these are results from one simulation of one structure. At the same time, the overall structure is less compact due to an optimum ratio of theoretical mannose groups and remaining OH groups. Of course, P-G3-Man has maximum number of mannose groups and maximum number of residuals OH groups because of which it suffers from considerable steric hindrance, which can probably lead to some “backfolding”.

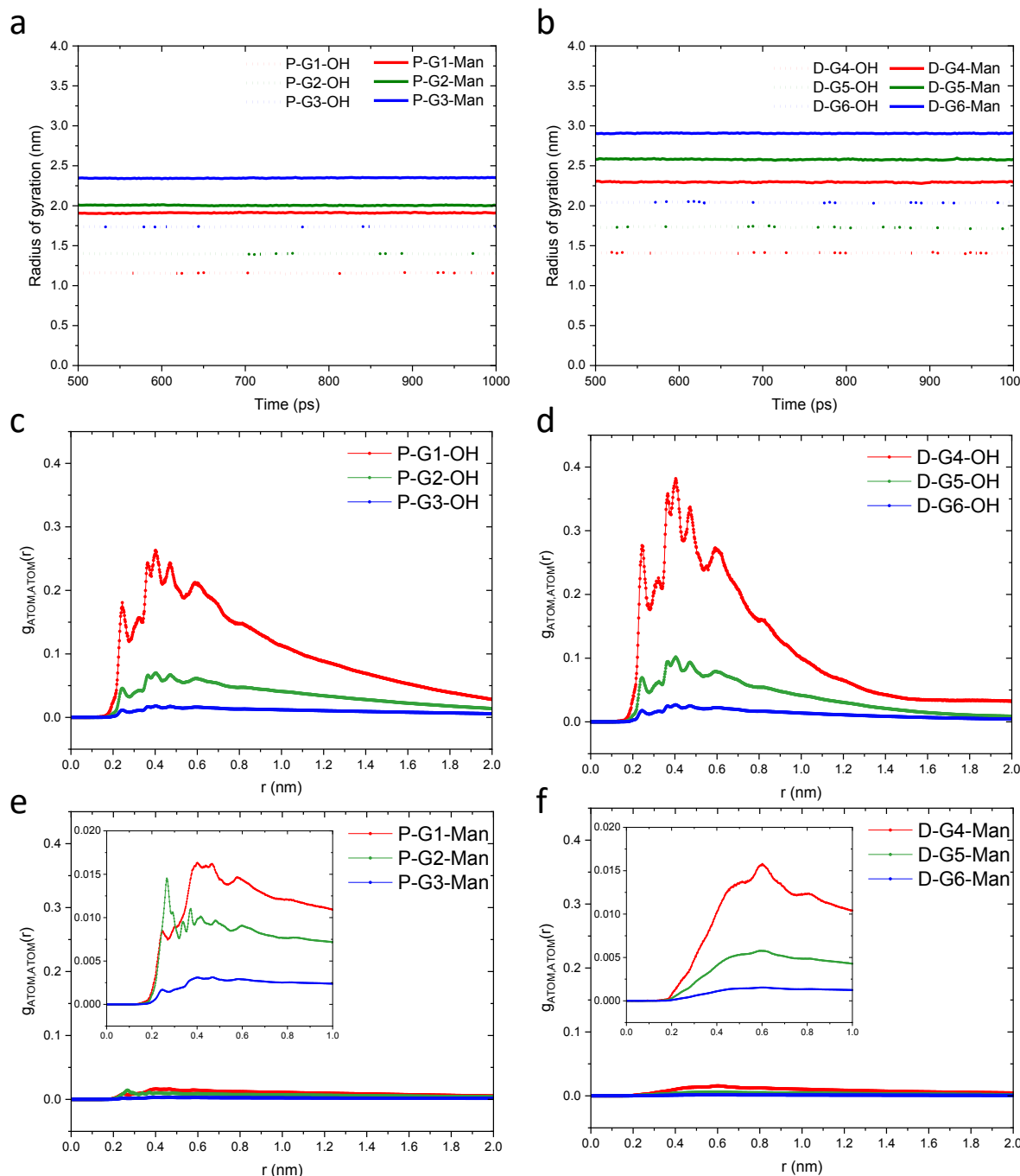


Figure 5.46: R_g values for a) unmodified pseudodendrimers and glyco-pseudodendrimers b) unmodified dendrimers and glyco-dendrimers; radial distribution function of c) unmodified pseudodendrimers d) unmodified dendrimers e) glyco-pseudodendrimers and f) glyco-dendrimers, as determined from simulation studies in THF.

The following conclusions can be drawn from the MD simulations:

1. On comparing the polymer series, the core is more compact in the mannose functionalized pseudodendrimers and also the mannose units are more or less uniformly distributed.
2. The R_g data suggests that dendrimers are bigger in size in THF, but only slightly. Solvent molecules can have an effect on the overall radius of the molecule.

5.2 Investigation of the interaction of GI-P and GI-D with amyloid beta (A β 40)

This subchapter is devoted to the study of investigation of synthesized mannose functionalized GI-Ps and GI-Ds as anti-Alzheimer's agents. The theoretical background of A β amyloid and its progression as one of the several culprits of not only AD but a number of diseases has been discussed in Chapter 2. As outlined before, AD is a neurodegenerative disease associated with protein misfolding and misprocessing, resulting in aggregation and accumulation of plaques. These plaques can be made of amyloid proteins or tau protein. Both kinds of plaques have an amyloid structure.^[390,409,410] There are several therapeutic strategies to stop progression of amyloid fibrils. One of such strategy to modulate the formation of aggregates.^[411] The formation of aggregates of amyloids is monitored by changes in the fluorescence intensity of thioflavin T (ThT), which is sensitive to the presence of amyloid fibrils.^[412,413] It is also possible to use Circular dichroism (CD) or Fourier transformed infrared spectroscopy (FTIR) to follow transformation of secondary structure into β -forms which is the characteristic for aggregates. These spectroscopic techniques allow the monitoring of aggregation process revealing additional information with regard to the kinetics. These approaches had already been exploited multiple times for such studies.^[4,211,414]

In this work, different techniques have been utilized to evaluate the protein-polymer interaction. ThT Assay was used to understand which generation of GI-P or GI-D acts in the best way to inhibit the aggregation of A β 40 amyloid and at which concentration. Additional investigations with regards to understanding the kinetics of inhibition of aggregation were also carried out. CD spectroscopy was also employed which makes it possible to quantify the changes in secondary structures of amyloid. Moreover, AF4 was employed for the first time to study the inhibition of aggregation behavior of A β 40 amyloid. Additionally, detailed AFM analysis was performed to get a viewpoint on structure and morphology. Lastly, cytotoxicity experiments have been performed on the polymers.

5.2.1 ThT Assay

In the last decade many different dendrimers have been tested against the aggregation behavior of amyloid protein.^[4,9,269] Since A β 40 has a long lag phase, addition of heparin can considerable shorten it by accelerating the aggregation profile. Thereby, making the experiment in a reasonable time window.^[189] This advantage of heparin is used when studying the aggregation kinetics of slow aggregating proteins.^[4] To identify the right concentration, it is important to test the different concentrations of amyloid for their aggregation behavior. The 3 different concentration of A β 40 amyloid (20, 50, 60 μ M) was tested, to identify the right concentration for optimum growth profile with saturated "plateau". In this work, the fluorescence intensity at 50 μ M concentration allowed us to obtain reliable results in presence and in absence of synthesized glycopolymers and was in accordance with earlier work.^[268,414] ThT of 35 μ M concentration was used. Further, five different concentration of synthesized GI-P and GI-D (0.1 μ M, 1 μ M, 2 μ M, 5 μ M, 10 μ M) were tested with A β 40. The results of ThT assay of each generation of GI-P were compared with their corresponding generation of GI-D, as they were nearly of the same molar mass and same radii and also similar number of monomer units. Figure 5.47a,b shows the results of ThT assay of P-G1-Man (30 kDa) and D-G4-Man (20 kDa), respectively.

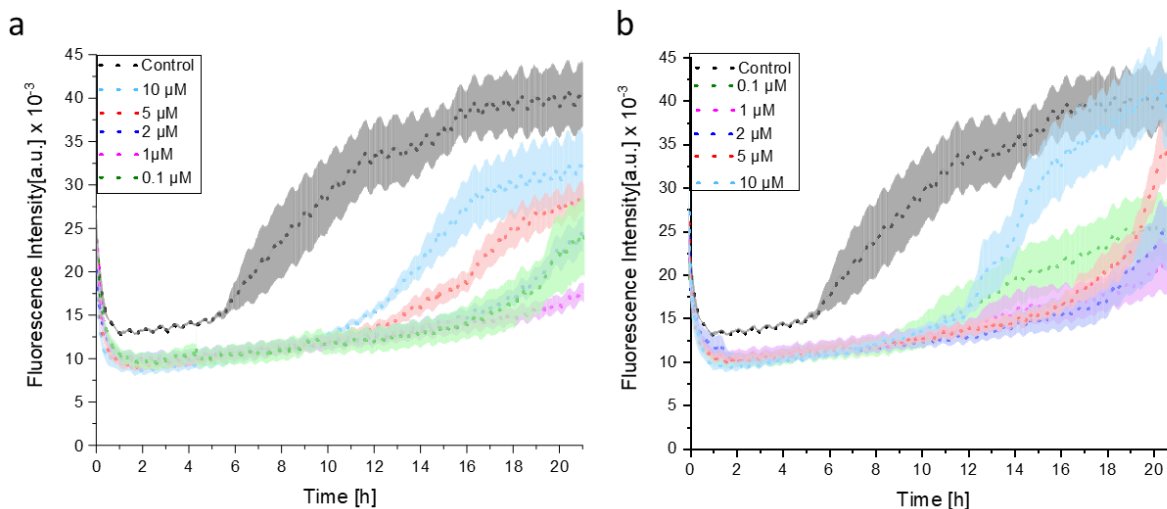


Figure 5.47: ThT assay of A β 40 (50 μ M) with different concentrations of a) P-G1-Man b) D-G4-Man. Control data refers to zero concentration of glycopolymer.

The results of these two sets of experiments were quite surprising unlike the rest two. In these the effect of inhibition of aggregation was not concentration dependent, it was actually quite the opposite. In case of P-G1-Man, the higher concentrations (5-10 μ M) did not show a drastic decrease in aggregate content, but the lower concentrations (0.1, 1 and 2 μ M) showed the higher ability to inhibit the aggregation, with 1 μ M being the best among these. This shows a considerable increase in the lag phase, quite close to the baseline, where the elongation phase is close to being completely absent. Therefore, it is clear that these synthesized dendrimers are interacting with amyloid peptide. D-G4-Man also shows concentration dependent behavior, except for the fact that at 5 μ M concentration an exponential increase in the fluorescence intensity at later time intervals was observed.

Figure 5.48a,b shows the next two set of samples, P-G2-Man (39 kDa) and D-G5 Man (40 kDa) compared to each other. In case of P-G2-Man a very strong dependency on concentration is seen. The lower concentration (0.1 μ M and 1 μ M) shows similar fluorescence intensity signal as the control. The higher concentration (2-10 μ M) shows gradual decrease in the fluorescence intensity, with 10 μ M showing the most shift towards the baseline, indicating a nearly complete halt in elongation phase. In case of D-G5-Man, no concentration dependency was seen. 5 μ M concentration showed the maximum shortening of the elongation phase but not the complete halt as it was seen in case of P-G2-Man. On studying the kinetic analysis of P-G2-Man, interesting results were obtained which are explained in the next subsection.

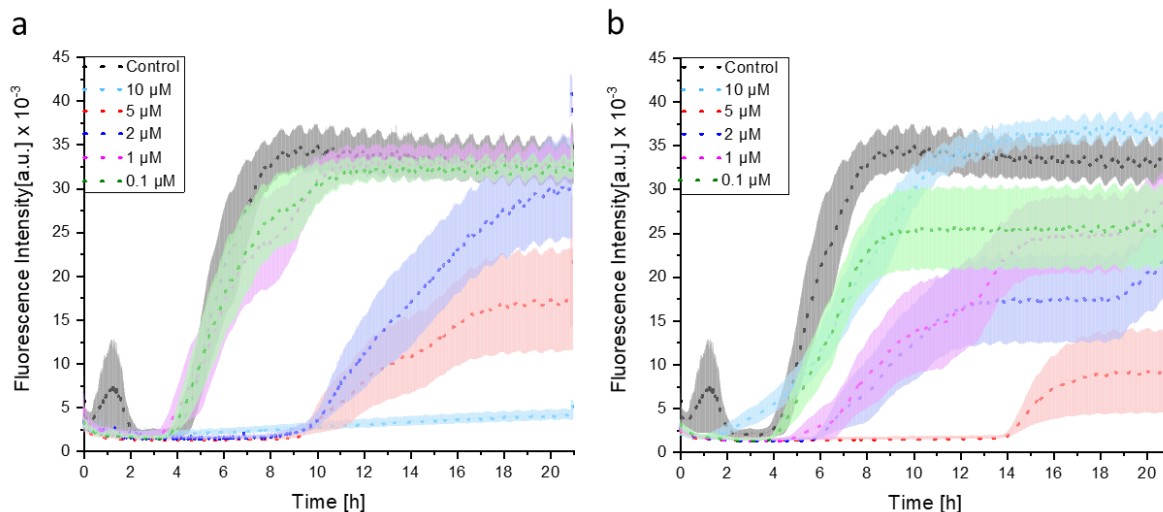


Figure 5.48: ThT assay of A β 40 (50 μ M) with different concentrations of a) P-G2-Man b) D-G5-Man. Control data refers to zero concentration of glycopolymer.

Figure 5.49a,b shows ThT assay of P-G3-Man and D-G6-Man. In case of P-G3-Man and D-G6-Man, 2 μ M and 5 μ M showed the maximum shortening of the elongation phase respectively.

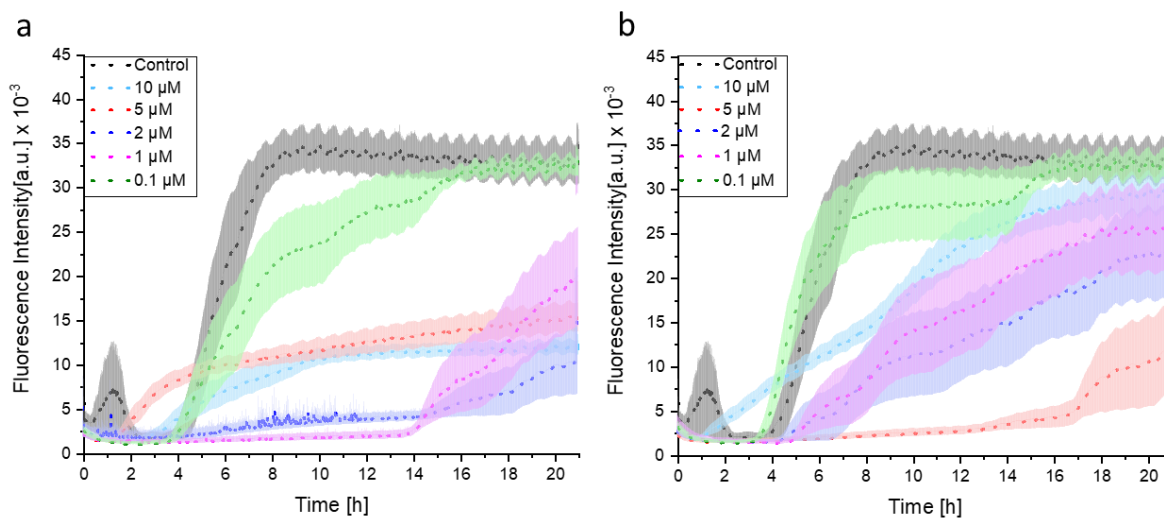


Figure 5.49: ThT assay of A β 40 (50 μ M) with different concentrations of a) P-G3-Man b) D-G6-Man. Control data refers to zero concentration of glycopolymer.

The results from ThT Assay enables to identify which sample and which concentration works best in inhibiting the aggregation of A β 40. In this work, when A β 40 at 50 μ M concentration was used, P-G2-Man at 10 μ M showed the maximum capacity to inhibiting its aggregation by displaying only the lag phase and no elongation was observed in ThT curve (Figure 5.48a). A quantitative study of the aggregation kinetics of P-G2-Man shall give a better view as to which microscopic steps of the A β 40 amyloid aggregation are being affected. This is discussed in the following text.

5.2.1.1 Kinetics based on ThT Assay

The most important understanding from previous studies that came through after studying the kinetics of protein misfolding disorders is a realization that for many proteins the mature, fibrillar state is thermodynamically more stable than the native state.^[415] Native protein species are small, intrinsically disordered and their transition to stable fibrillar form strongly depends on the rate of transition. However, it is not as simple, several complex mechanisms are involved.

Recent developments in this field have established that the microscopic process of amyloid fibril formation involves a variety of distinct microscopic steps.^[113,416] The first step is the primary nucleation event in which two or more monomeric species interact with each other. In the next step resulting oligomeric species can grow through sequestration of different species, and, additionally, proliferation can result from secondary processes including fragmentation and surface induced nucleation.^[167] The last step is formation fibrillar aggregates such as amyloid fibrils. During this, fragmentation increases the number of sites from which fibrils can elongate, and additionally, further nucleation can occur on the surfaces of the growing aggregates (plaques). So there is a feedback loop in which accumulation of aggregates catalyzes the formation of more aggregates, leading to faster proliferation and spread.^[417] Since, amyloid has always been challenging to study either due to variations in sample-to-sample investigations or because of experiments based on hypothesis driven mechanisms. Recent developments suggest that the kinetic analysis of these mechanisms can provide strong evidence about the process of amyloid aggregation and, when an inhibitor is introduced, certain microscopic steps are affected.

In this work the chemical kinetics approach based on Amylofit software was applied.^[355] This method was developed keeping in mind the aggregation behavior of A β 42; however, it is suitable for data from any similar aggregation kinetic experiments. This is a very good platform to deal with such plethora of data without the need knowledge of programming or mathematics background. The data from ThT assay for P-G2-Man were analyzed using this software as it showed maximum inhibitory effect at 10 μ M concentration. This particular generation of glyco-pseudodendrimer showed a concentration-dependent effect, and at a 5:1 molar ratio of A β 40, using 50 μ M of A β 40, amyloid assembly was completely suppressed, as seen by the reduction in the level of ThT fluorescence observed (Figure 5.48a). The rate constants agreed well with similar experiments in terms of rate constants for primary nucleation, however not so much in case of rate constant for elongation.^[414] Klajnert et al. used the A β 40 with heparin against phosphorus dendrimers, but used nucleation dependent polymerization mechanism using a different model.^[414] In this work we have used secondary nucleation dominated mechanism using global fitting model by Meisl et al., which is a recent development concerning the kinetics of amyloids.^[418] Using a different approach is bound to lead to differences in the values obtained after fitting of ThT data. Upon examination of rate constant data, it is observed that the rate constants at 0.1 and 1 μ M concentrations of P-G2-Man increases for primary nucleation (K_n) and elongation (K_+) but decreases for secondary nucleation (K_2). This indicates a low energy barrier for first two microscopic processes but high energy barrier for the latter (K_2). This reaction occurs faster in case of primary nucleation and elongation but slower in case of secondary nucleation. However, a change in this trend is seen when P-G2-Man at 2-5 μ M

concentrations is used, where all microscopic processes rate constants are decreasing relative to the control (0 μM). This indicates a high energy barrier in all the three microscopic processes which perhaps makes it very slow. In particular, primary nucleation (K_n) increases slowly when the P-G2-Man concentration is 0-1 μM , but decreases drastically at higher concentrations by 10 and 13 orders of magnitude relative to the control. This value is way beyond the error limits, which accounts for the bad fitting (Figure 5.42 a, first column). K_2 also decreases and same pattern is shown by the K_+ . Meisl et al. reported K_n , K_+ and K_2 for $\text{A}\beta$ 40 at 30 μM concentration in quiescent condition to be 2×10^{-6} , 3×10^5 and 3×10^3 , respectively.^[419] Due to the lack of data availability for rate constants for $\text{A}\beta$ 40 using this software, the values of $\text{A}\beta$ 40 at 50 μM under perturbed conditions are reported as given in Table 5.8. Also, in this work heparin was used to start the aggregation process faster, based on an earlier work.^[4,268,269,414]

To further probe the mechanism of action of P-G2-Man, one rate constant in the rate law was systematically varied.^[355] Based on the global fits to the normalized kinetic data alone, mechanisms based on inhibition of secondary nucleation and inhibition of elongation were similarly likely possible as the main modes of action of the P-G2-Man. By comparing how well these modified rate laws can describe the data, a mechanism that involves inhibition of primary nucleation could be ruled out as shown in Figure 5.50a.

Table 5.8: Rate constant values from Amylofit software^[418] obtained for $\text{A}\beta$ 40 at five different concentrations of P-G2-Man.

P-G2-Man (μM)	P-G2-Man/peptide ratio	K_n ($\text{M}^{-2}\text{s}^{-1}$)	K_2 ($\text{M}^{-2}\text{s}^{-1}$)	K_+ ($\text{M}^{-1}\text{s}^{-1}$)
0	0	1.37×10^{-8}	1.01×10^6	4.9
0.1	0.002	3.59×10^{-8}	5.7×10^5	4.9
1	0.02	5.77×10^{-8}	8.4×10^5	6
2	0.04	1.18×10^{-18}	2.1×10^5	0.9
5	0.1	7.72×10^{-21}	1.6×10^5	0.75

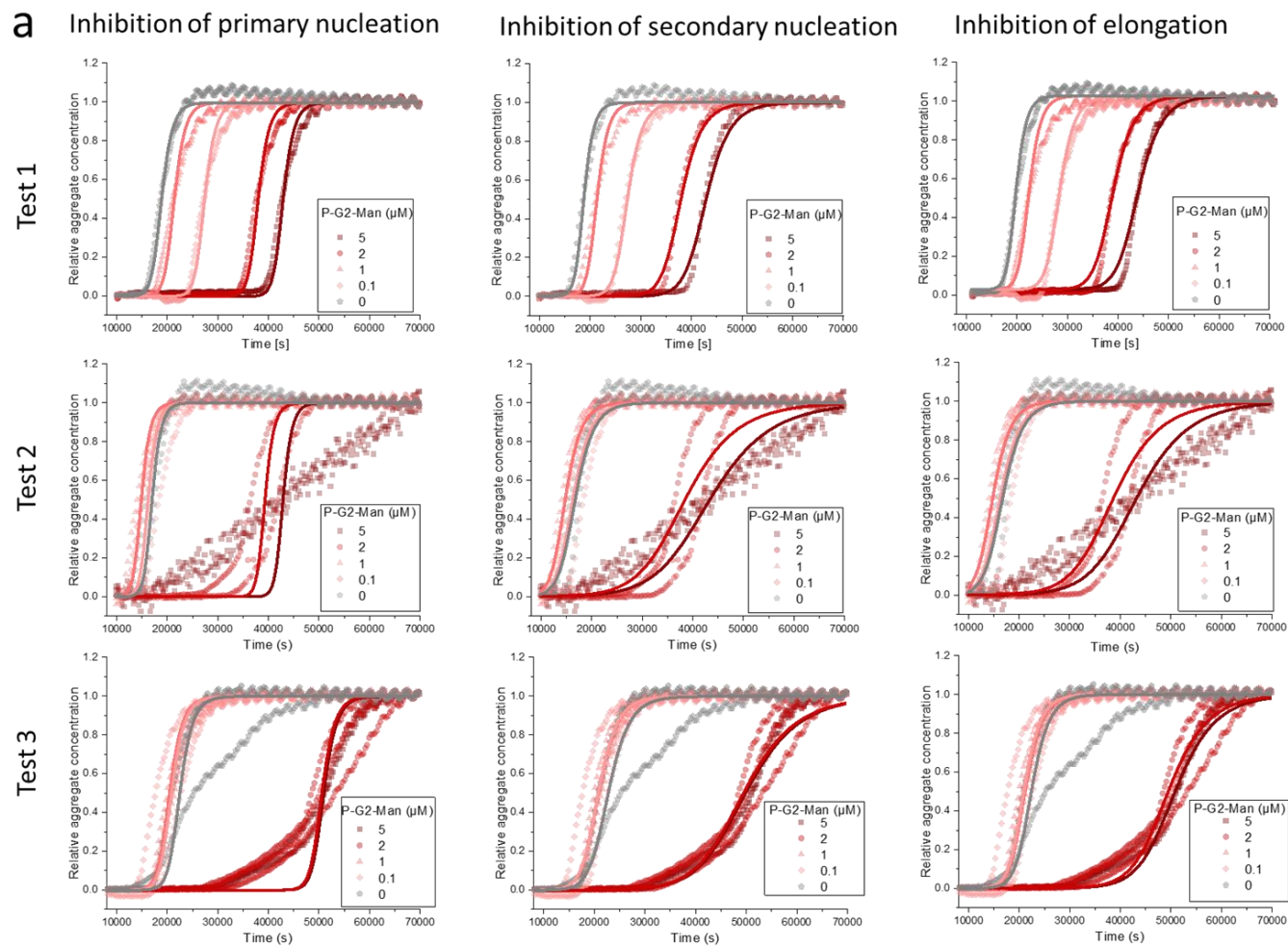


Figure 5.50: a) Global fitting by chemical kinetics analysis reveals inhibition through secondary nucleation and elongation. In a perturbed system, to show the main mechanism of inhibition, the results from ThT assay were normalized and fitted under the constraint that deviation was allowed in only one microscopic step. Each column represents one mode of kinetic step and each row represents the repeats of experiments. b) Proposed behavior based on the results of global fitting of kinetic analysis as the fits are better in case of two microscopic processes i.e., inhibition of secondary nucleation and inhibition of elongation at 50 μM A β 40. (representation of amyloids and pseudodendrimers are not to scale).

5.2.2 CD spectroscopy

Circular Dichroism (CD) is an important tool for rapid determination of the secondary structure as well as the folding properties of proteins. By estimation of the secondary structural components of a protein with time one can study the effects of its interaction with different agents.^[357] The details of CD spectroscopy are described in Section 3.7 and experimental details in Section 4.4.2. In order to have further information on the secondary structure development upon addition of G1-P and G1-D, CD spectroscopy was performed. A β 40 at 50 μ M (0.002 M, repeated unit) was mixed with respective solutions of synthesized G1-P and G1-D which showed maximum inhibitory effect in ThT assay. Based on the shapes of signals from CD it can be said that for control (Figure 5.51b) most of the changes start happening after 5 h of incubation. The bands observed at 0 h and 1 h are similar with a negative ellipticity at 222 nm and signals observed after 5 h shows two interesting features. A negative band is seen at 215 nm along with a positive band at 200 nm. This resembles well-defined antiparallel β -sheets. Here, it should be mentioned that proteins which are prone to form aggregates of different sizes like amyloids, synuclein, prion, etc., have distinct physiological effects depending on the environmental conditions. Prediction of these β -sheet rich proteins content has been challenging and controversial because of their intrinsic structural and spectral diversity.^[358]

In Figure 5.51c (P-G1-Man) the changes in the signal appear only at 24 h. In Figure 5.51d (P-G2-Man) only a mild change is observed even at 24 h where no positive band is seen. In Figure 5.50e (P-G3-Man), f (D-G4-Man) and g (D-G5-Man) the same trend is displayed as in the case of P-G1-Man. However, in 5.50h (D-G6-Man) again there was no positive band. Based on the observation of these changes over time, it can be said that minimal changes were seen in case of samples with P-G2-Man and D-G6-Man. Thus, with the addition of P-G2-Man and D-G6-Man, the aggregation behavior of A β 40 under these conditions has undergone the much sought-after mitigation.

As outlined earlier, CD spectroscopy also enables us to calculate the secondary structural components. An analysis of the changes in secondary structure upon addition of synthesized G1-P and G1-D over time would be quite valuable, for which different softwares are available. But it is known that amyloids are β -sheet rich proteins which are predicted as helix by most of the previously available methods^[358] (See Section 3.8 for details). In this study BeStSel software^[361] was employed for this specific purpose and results are summarized in Figure 5.52. In Figure 5.52c, for the β -sheet content, a decrease is seen only for P-G2-Man, along with an increase of α helix, unlike P-G3-Man and D-G6-Man. With the exception of P-G3-Man, there was a sudden increase of 9% in α -helix content. The total content of only α and β secondary structures (Figure 5.52h) decreases in the order of D-G6-Man>P-G2-Man>P-G3-Man relative to the control. It should be mentioned that the negative curve in D-G6-Man could be due to an error. It can be inferred that the protein folding behavior of A β 40 to secondary structures, in presence of synthesized polymers acting as inhibitors, were limited to minimum values in these three samples only. Multiple repeats could not be performed, and discrepancies due to sample preparation could be one of the possible reasons for such results. However, the results from all other samples were in good agreement with ThT data.

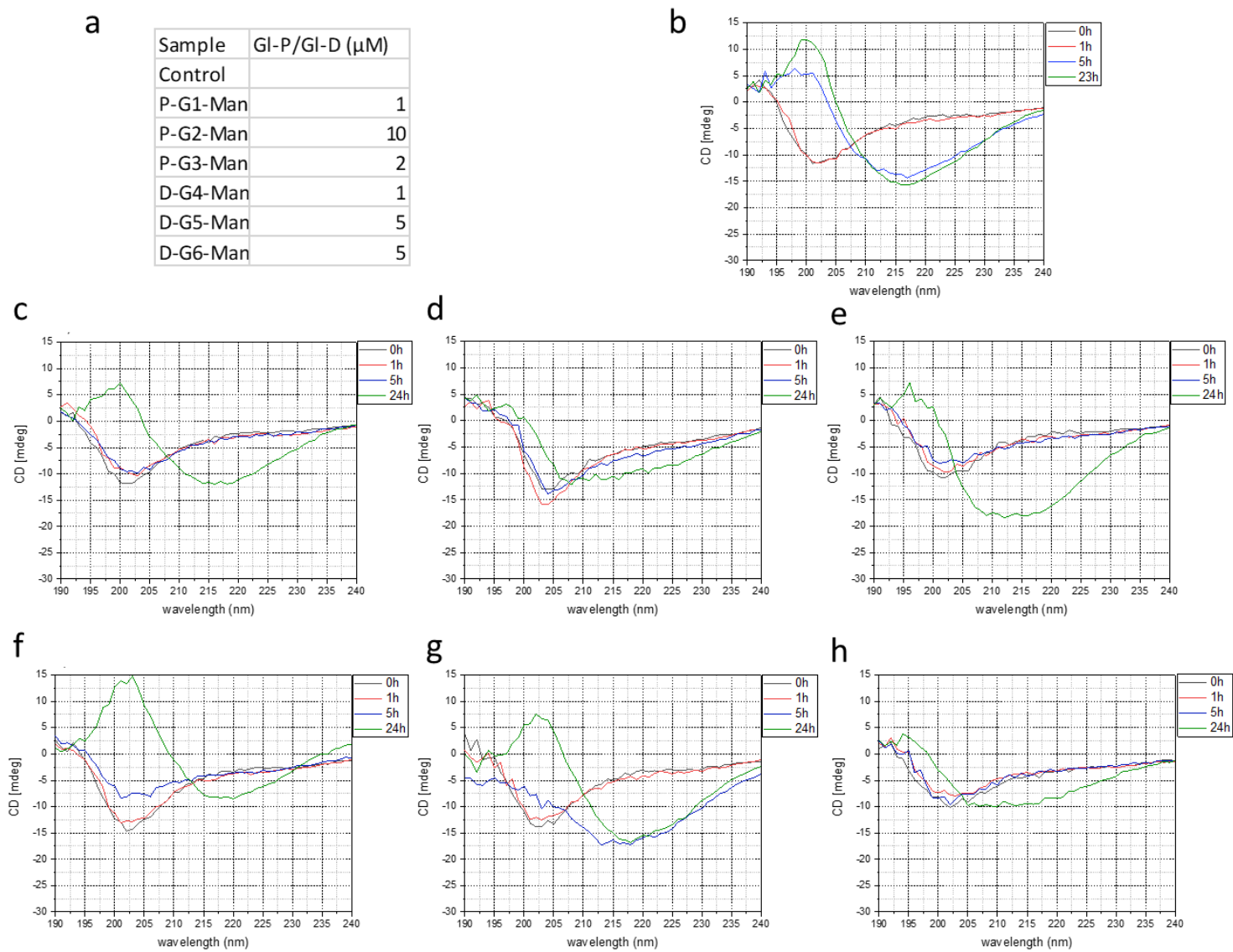


Figure 5.51: CD spectroscopy a) Summary of samples; spectra over different time intervals with heparin in 1 mM PBS buffer b) control ($\text{A}\beta$ 40 at $50 \mu\text{M}$) c) P-G1-Man d) P-G2-Man e) P-G3-Man f) D-G4-Man g) D-G5-Man and h) D-G6-Man.

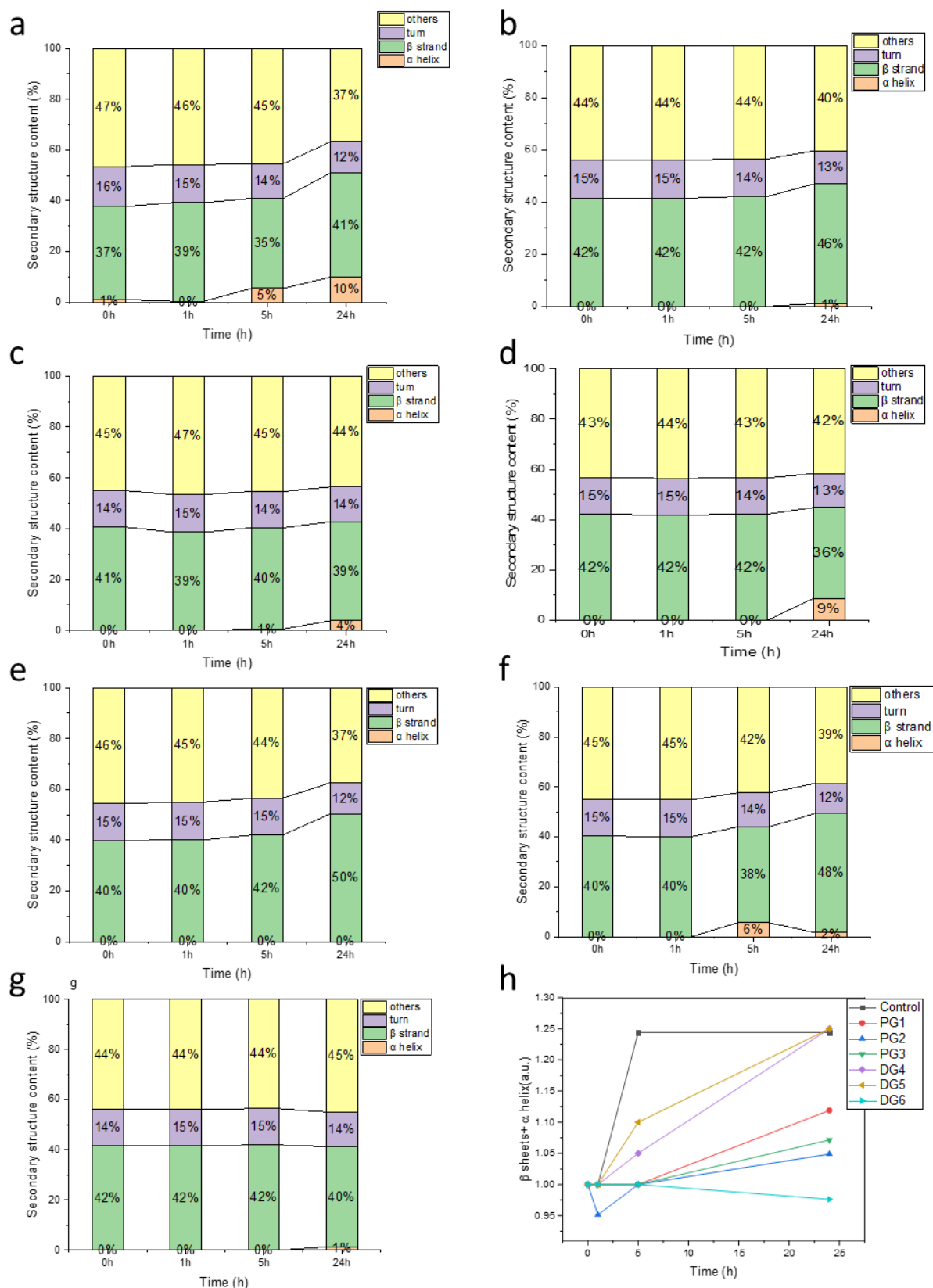


Figure 5.52: Summary of the secondary structure distributions for A β 40 in presence and absence of GlPs and Gl-Ds, obtained by BeStSel^[361] software at 0h, 1 h, 5 h and 24 h (a) A β 40 (50 μ M) with heparin (0.041 mg/ml) (Control), A β 40 (50 μ M) with heparin after addition of (b) P-G1-Man (1 μ M), (c) P-G2-Man (10 μ M), (d) P-G3-Man (2 μ M), (e) D-G4-Man (1 μ M), (f) D-G5-Man (5 μ M) and (g) D-G6-Man (5 μ M) and h) content of β sheets and α helix together.

5.2.3 Time dependent AF4-MALS

The fibrillation behavior of amyloids is a complex process through different transient and metastable intermediates which are challenging to be precisely monitored and characterized. So far; these have been done by spectroscopic, separation and imaging techniques.^[366,420–422] However, these techniques give only the averaged information and are often difficult to analyze over time. Therefore, a separation technique that gives a time dependent profile of the species present in the sample is advantageous over the above methods. In this work, AF4-MALS detection profile has been applied to study the time dependent aggregation pattern of A β 40 with inhibitors (GI-P and GI-D). So far there has been only one reported study involving AF4 and A β 42 aggregates without any kind of inhibitors.^[173], and this present work is the first known study for A β 40.

5.3.2.1 Separation of A β 40 by AF4

The method development procedure has been discussed in Section 4.3.2.3. Figure 4.4 shows the flow profile for A β 40 amyloids. The flow profile was optimized so that it suits all the different components of the samples (amyloid, heparin, and GI-P/GI-D).

The channel outlet detector flow was set to 0.40 mL/min. A low flow rate would limit the loss of samples during the focusing step. The focusing step was performed for 3 min with a focus flow rate of 3 mL/min. An initial cross flow rate of 1.75 ml/min was set for the separation step and maintained for 20 min using isocratic step. In the second elution step, the cross flow was lowered to 0.15ml/min using linear gradient in 5 mins. In the third elution step, cross flow was maintained at 0.15 ml/min for 10 mins. To ensure complete elution of very large aggregates, in last step, cross-flow rate was maintained at 0 ml/min for 10 mins. The eluent was 1 mM PBS (pH 7.4) with 0.01% (w/v) SDS. SDS was used to limit interactions between sample and channel membrane.^[173] In order to study the kinetic behavior of A β 40 amyloid, measurement without the addition of heparin was also performed. However the process was rather slow as shown in Figure 5.53, similar to what is mentioned in literature.^[423] Figure 5.45 shows the results obtained from A β 40 without heparin. The sample was measured at different elapsed time 0-10 h, 16 h and 24 h. The molar mass of A β 40 was 4.0 kDa with R_h of ~3 nm. The monomeric A β showed a tailed peak at ~11 min. The pathogenic pathway of A β 40 has been extensively studied but with varying conditions (solvent, pH etc.) as summarized in Table 2.1. As a result, there is no consensus either for the early growth phases and on to protofibrils and fibrils, or for the detailed structure of the intermediate and final species. Due to the longest times of the fibrillogenic process and to obtain results in a reasonable time window, heparin was added which has been studied previously by transmission electron microscopy (TEM), atomic force microscopy (AFM), circular dichroism (CD) and ThT assay.^[268,420,423,424] In this work, we have for the first time applied AF4-MALS to study the time-dependent stability of A β 40 as well as inhibition of the aggregation process using synthesized GI-P and GI-D with different molecular sizes.

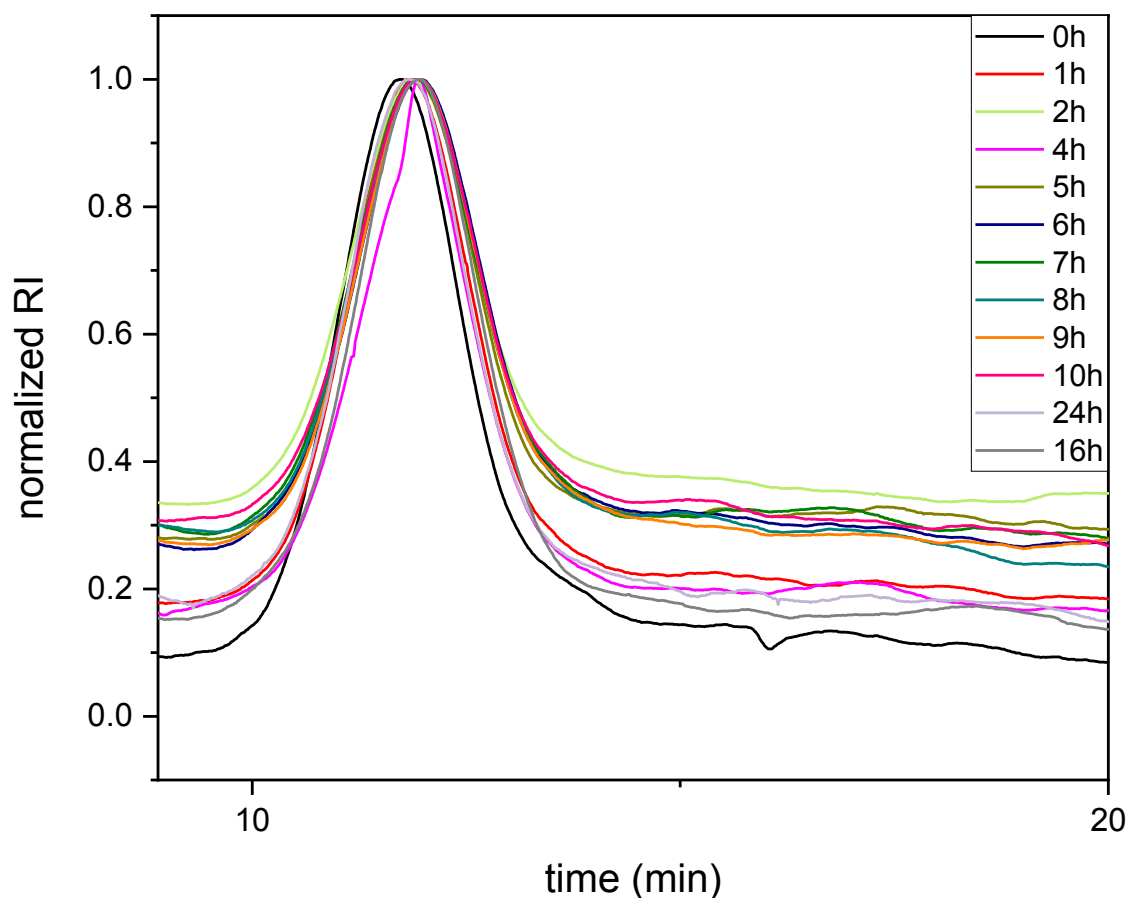


Figure 5.53: Time dependent separation by AF4 of A β 40 without heparin at room temperature in PBS, normalized RI signals of differently incubated samples vs. elution time showing the elution behaviour changes very slow without the presence of heparin in PBS.

5.3.2.2 A β 40 amyloid aggregation in the presence of GI-P and GI-D

To study the aggregation behavior in presence of synthesized GI-P and GI-D, the following points were important:

1. Each sample contains different components
2. An optimum temperature of 37 °C
3. Gentle stirring of the sample
4. Measurement at different time intervals requiring sample preparation starting at different time points

Incorporating all of the above points with a complex system like amyloids which are prone to aggregation made the task at hand even more challenging. Since the samples contained different components, the molar mass determination was not precise. However, quantification of mass distribution was possible based on the signals from RI detector.

Figure 5.54a shows a representative RI signal fractogram A β 40 (50 μ M) with heparin (0.041 mg/ml) (control) at 5h. It shows a multimodal distribution due to the presence of different components. Different smaller species (Fraction 1) eluting at 9 min, 14 min, 17.8 min and 25

min were observed. The large aggregates (Fraction 2) start to elute after 40 min. To quantify the mass distribution, RI-peak integration was applied represented as Fraction 1 within the intervals from 9.3-40 min and Fraction 2 within 40-54 min. The area of Fraction 1 is understood to represent the oligomeric A β 40 and Gl-P/Gl-D whereas Fraction 2 represents only the aggregates. Same assumption was applied for the elution profiles of all the samples at each time point at different times (0, 2, 5, 7, 10, 16, 18 and 20 h).

There have not been any separation studies on amyloids with heparin reported in the literature. Hence the focus of the present study was more on the fraction of aggregates instead of separating the smaller species. During this study, heparin was used to initiate aggregation allowing for a reasonable time window. It should be mentioned that the formation of smaller species (monomer/oligomers) is highly dependent on the purity of the amyloids.

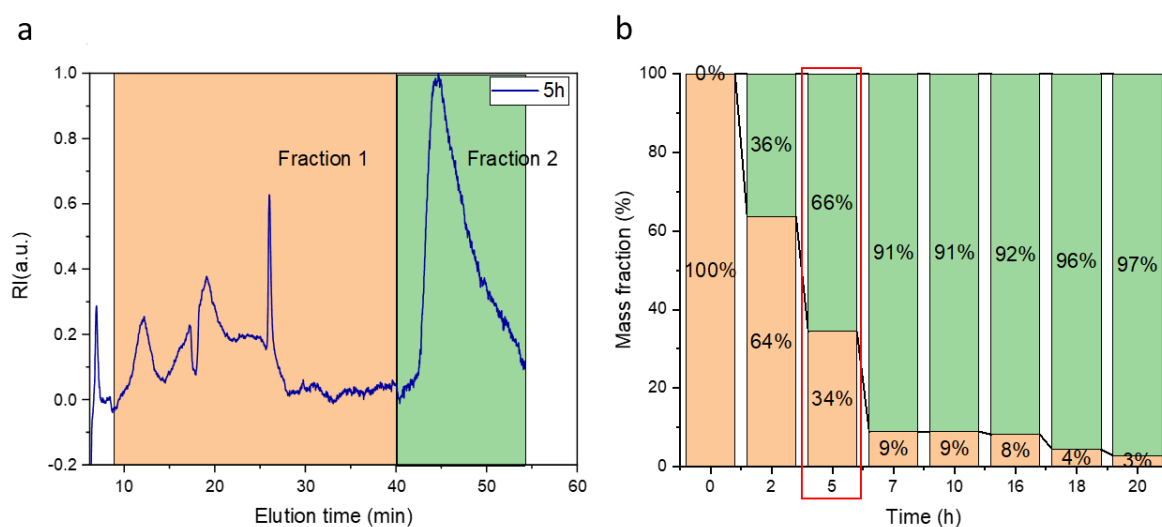


Figure 5.54: a) Fractogram of A β 40 (with heparin) after 5 h of incubation, and b) Mass fraction A β 40 (with heparin) determined at different time interval. The bar encircled with red box highlights the mass fraction of the corresponding fractogram (a).

Figure 5.55 shows the percentage mass fraction of different aggregate fractions for each sample at various time intervals, calculated as described above. The percentage mass fractions of the aggregates are also tabulated in Table 1 (Appendix). Discrepancies could not be excluded due to sample preparation, especially the samples which were prepared at later time points (16 h, 18 h and 20 h) as these were prepared from different stock solution to be measured the next day at exact times.

As can be seen in Figure 5.55a, in the control experiment at 0 h, no A β aggregates were visible. On increasing the incubation time, the percentage of aggregates increases which becomes around 97% after 20 h of incubation. Similar to the control, in P-G1-Man no aggregates are observed at 0 h. However, after 2 h, the percentage of aggregates was only 2% which was markedly less as compared to control at 2 h (36%). As the time of incubation progresses, only a marginal increase is seen in the amount of aggregates. The mass fraction of aggregates as compared to control is lower during the complete kinetic experiment for all studied times starting from 1% and increasing until 22% of aggregates at 20 h. The deviation from the trend for the measured sample after 18 h is possibly due to discrepancies in sample preparation. In

case of P-G2-Man, the formation of aggregates is much slower relative to the control, increasing until only 10% of the aggregates after 20 h incubation time.

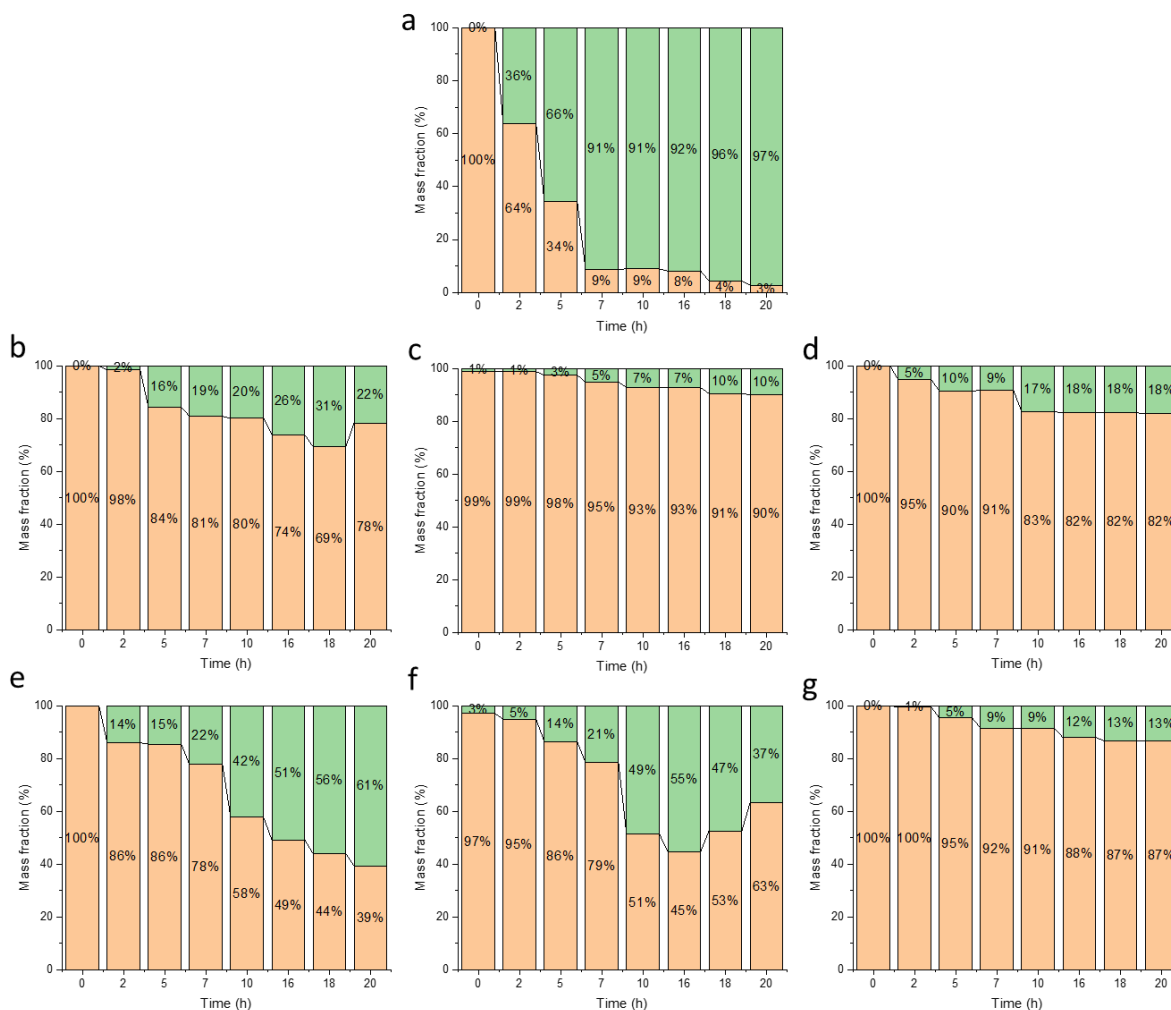


Figure 5.55: Percentage mass fraction of the two aggregate fractions for each sample at different time interval determined from RI signal (a) Aβ 40 (50 μM) (control) (b) Aβ 40+P-G1-Man (1 μM) (c) Aβ 40+P-G2-Man (10 μM) (d) Aβ 40+P-G3-Man (2 μM) (e) Aβ 40+D-G4-Man (1 μM) (f) Aβ 40+D-G5-Man (5 μM) (g) Aβ 40+D-G1-Man (5 μM). All the samples contained final concentration of 50μM Aβ 40, 0.041 mg/ml heparin (pH 5.5) and respective final concentrations of GI-P/GI-D.

In the case of P-G3-Man, the formation of aggregates is also slow contributing to only 18% aggregates at 20 h incubation time. In case of glyco-dendrimers, a different behavior is observed in comparison to glyco-pseudodendrimers. Higher percentages of aggregates were observed at each time interval except for D-G6-Man when compared to their pseudodendrimer counterparts. In D-G6-Man, there is also a very slow aggregation behavior with only 13% aggregates after 20 h incubation. Figure 5.56 shows the comparative trend of aggregates mass fraction in different samples at different time points. The results obtained from calculation of aggregates mass fraction presented here confirm that GI-P of second-generation P-G2-Man at 10μM concentration can decrease the aggregates formation in Aβ 40 to 10% and GI-D of sixth generation (D-G6-Man) at 5μM concentration can inhibit the aggregates formation to 13%.

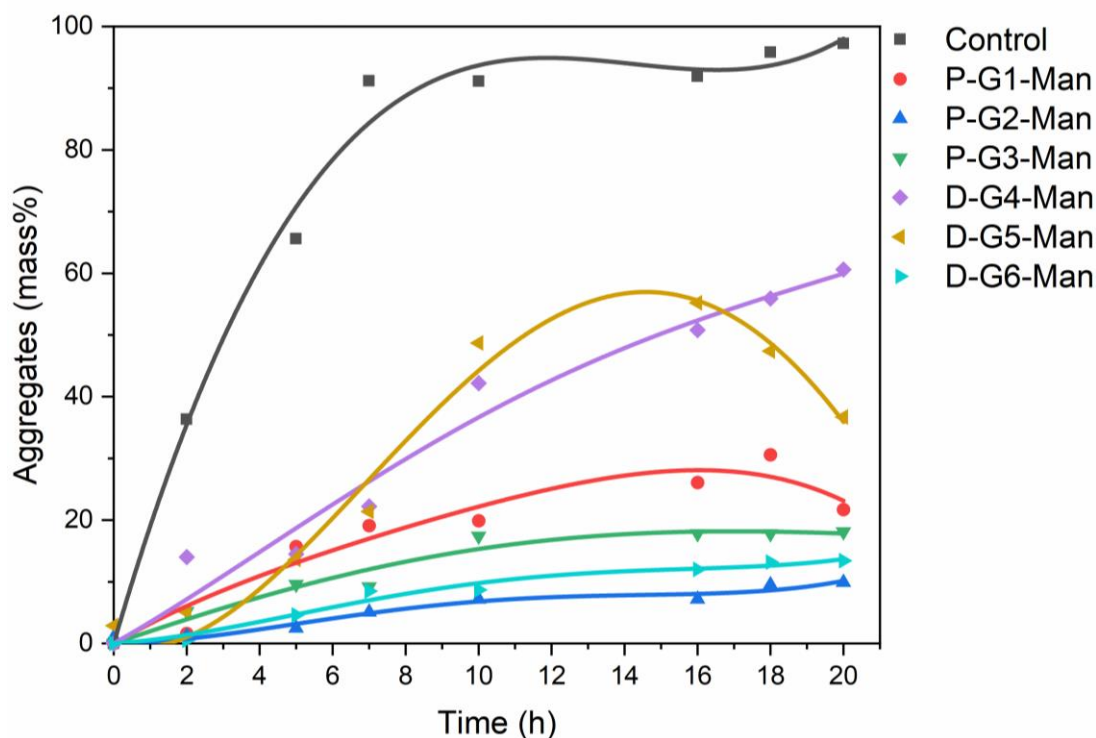


Figure 5.56: Trends of aggregates deduced from AF4 at different elapsed time for GI-Ps and GI-Ds along with control A β 40. Solid lines are polynomial fit (order 4).

The following conclusions can be drawn from our AF4 study:

1. The trends of the aggregates mass fraction are in good agreement with ThT profile of A β 40 amyloid (Figure 5.56, black line).
2. The results are also in good agreement with CD results.
3. First and second generation glyco-pseudodendrimer P-G1-Man and P-G2-Man showed better aggregate inhibition than corresponding glyco-dendrimers fourth and fifth generation D-G4-Man and D-G6-Man, despite being similar in molar masses. Third generation P-G3-Man and sixth D-G6-Man generations showed similar trend.
4. Overall, minimum aggregates were seen in case of P-G2-Man. P-G3-Man and D-G6-Man also had low amount of aggregates. Similar trends were also seen in the case of CD data.
5. Lastly, results from ThT, CD and AF4 experiments are in accordance with each other. P-G2-Man at 10 μ M concentration showed maximum inhibitory effect, followed by D-G6-Man (5 μ M) and P-G3-Man (2 μ M) in that order (see Figure 5.56).

5.2.4 AFM

After having the results from ThT, CD and AF4 experiments, it was worth performing imaging techniques to better understand the effect of P-G2-Man (10 μ M) on aggregation behavior of A β 40 amyloids. To see the inhibitory effect of P-G2-Man on the aggregation behavior of A β amyloid, we had earlier performed a fluorescence assay with Thioflavin T (ThT) which has a typical property to intercalate into the β sheet structure of amyloid fibrils. As mentioned earlier, this technique is commonly used to monitor the fibrillation kinetics.^[213,425–427] Figure 5.57

briefly summarizes, the ThT assay, CD and AF4 results of P-G2-Man with A β 40 with respect to incubation time. In Figure 5.57a, as the incubation time increases in ThT assay, fluorescence intensity of pure A β 40 with heparin shows the typical amyloid aggregation curve with a lag phase (grey), presenting almost no fluorescence intensity in the beginning (lag/nucleation phase). Subsequently, increase in the fluorescence intensity is visible which denotes the elongation of the amyloid fibrils (elongation phase) and is finalized in a plateau-like behaviour over incubation time.

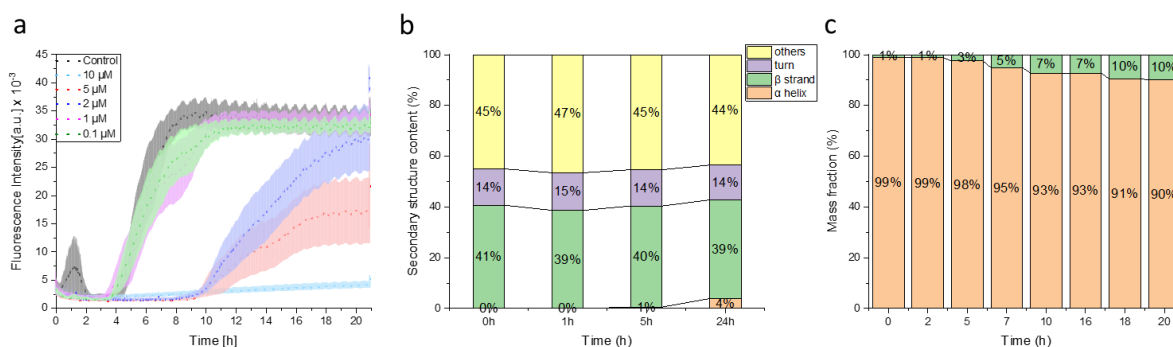


Figure 5.57: Interaction of P-G2-Man with A β 40 a) ThT, b) CD and c) AF4. A nice correlation can be seen for the results with P-G2-Man at 10 μ M concentration in all the three experiments.

However, P-G2-Man at 10 μ M concentration effectively suppressed this increase in fluorescent intensity. As seen from the results in Figure 5.57a, it could be qualitatively confirmed that P-G2-Man effectively inhibits amyloid fibrillation without the assistance of any other reagents. However, amyloid solution could include different amyloidogenic species like monomers, oligomers, protofibrils and mature fibrils, the fluorescence data are inadequate in answering the question regarding the manner in which P-G2-Man affects amyloid fibril formation or fibril growth.^[134] With CD results (Figure 5.57b), the secondary structure showed a decrease in total β sheet and α helix content. As these are β sheet rich proteins, most software do not yield good estimates of secondary sheet content and the reliability of data hugely depends on the algorithm used.^[358,428] For this reason, bulk techniques such as ThT and CD provide average information about this complex fibrillation process. Figure 5.57c gives a quantitative evaluation of the aggregates formed over time with AF4 using RI signals. However, due to the small size of oligomeric species, their morphology is still under debate.^[390]

AFM has been an important tool for understanding the mechanism of amyloid aggregation studies, providing detailed insights into intermolecular and intramolecular forces giving relevant information on large number of molecular mechanisms.^[429–431] To support our above studies, we performed AFM analysis to image the amyloid fibrils. This allows us to investigate the changes in the individual fibril's formation in presence and absence of P-G2-Man with respect to time. The samples were made in the same way as for ThT assay. 10 μ L amyloid solution was placed on a freshly cleaved, positively modified mica surface for 3 min at room temperature, washed with MilliQ water and dried with pure nitrogen gas, and imaged by AFM.

The AFM analysis was carried out for a whole range of samples with many controls to understand the manner in whether different components of samples have any additional effects

or not. Based on the control experiments, it is found that the additional components like the heparin and ThT dye do not participate in the growth of amyloid fibrils as can be seen that height and length of heparin and ThT dye are very small as compared to the amyloid fibrils.

5.2.4.1 Height

Figure 5.58 shows the topographical images of the A β solution control (Figure 5.58 a-d) and with P-G2-Man (Figure 5.58 e-h) in presence of P-G2-Man with respect to different incubation time. For the quantitative analysis of all AFM images, the heights of single fibrils at 6 different positions on the same fibril along the white line were calculated. (Figure 5.58 a-h).

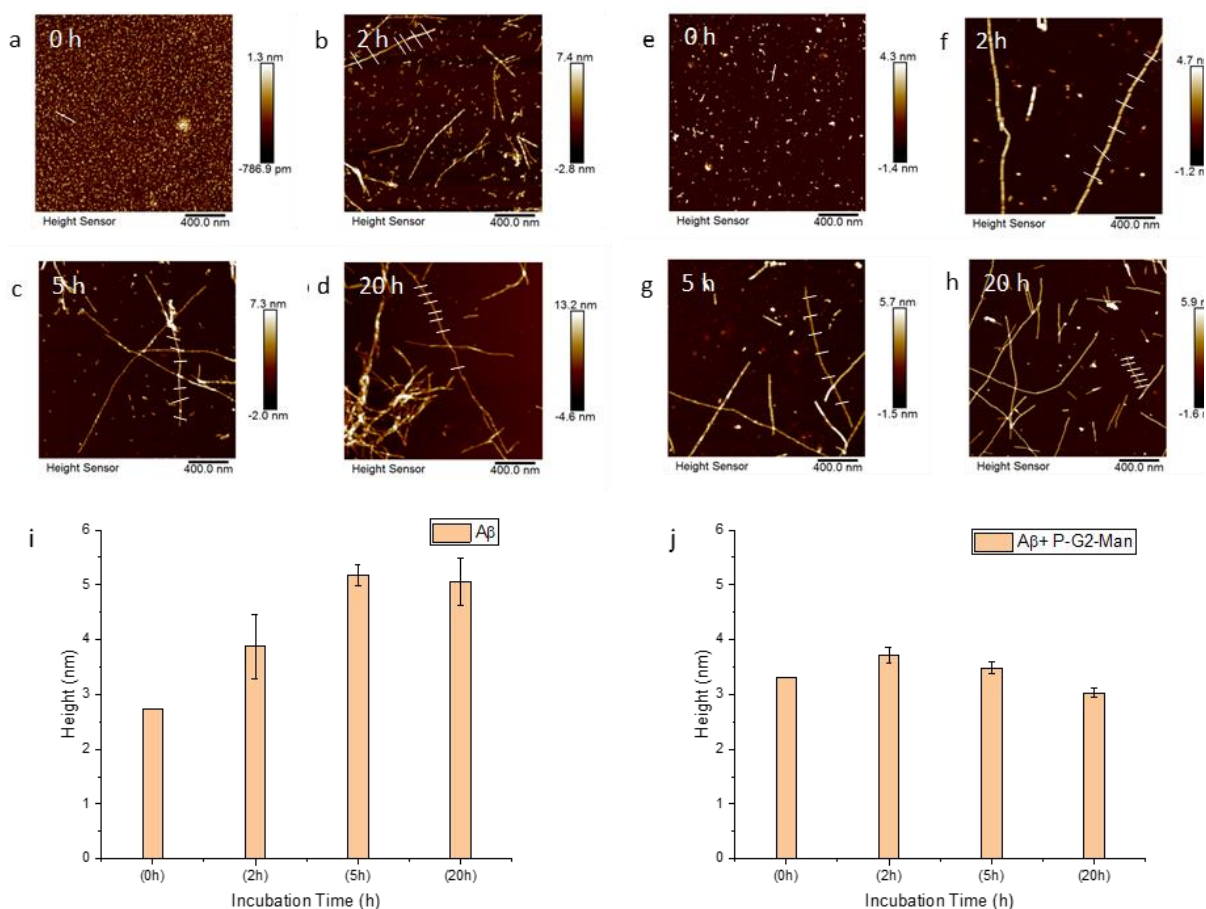


Figure 5.58: AFM images of a-d) Control of A β amyloid (50 μ M). e-h) A β amyloid with P-G2-Man, with increasing incubation time; we sectioned across white line on single fibrils and calculated the mean diameter: i) Mean heights of A β amyloid at different incubation times, j) mean heights of A β amyloid mixed with P-G2-Man.

In the control experiment (Figure 5.58a-d; 5.49i) the heights of the fibrils increased with the incubation time. In presence of P-G2-Man (Figure 5.58e-h; 5.49j), size increased but shorter fibrils or fragmented fibrils were present at 2 h onwards joined to each other in head to tail manner. Similar behaviour was also observed at 5 h (Figure 5.58g), and 20 h (Figure 5.58h).

The heights of single fibrils showed a decrease in comparison to the control. This proves that in the presence of P-G2-Man, with increased incubation time, there is a slower growth in height and size of the fibrils. From the AFM results, it implies that A β fibrillation is indeed suppressed by P-G2-Man. This is consistent with the results of the ThT assay.

To study the heights of different fibrils, the cross sectional heights and roughness of different fibrils were calculated.^[432] The height measurements were made from scan sizes of 1 x 1 μm or less by measuring cross-sectional height across the white dotted line. The heights for different fibrils species were taken corresponding to the peaks (~5). Immediately after the incubation, at 0 h, in control experiment (A β 40), a cross-sectional height range of 0.7-1.3 nm was observed (Figure 5.59). These prefibrillar species with nanometer-size diameters and micrometer-scale lengths, are termed protofilaments. These protofilaments can intertwine and form plaques.

Figure 5.59i shows the cross-section heights of different fibrils along the white dotted line at different time of incubation. After 2 h the average height increases, showing a wide range with cross-sectional height in the range of 1.5-4 nm. After 5 h, it shows 3.1-5.3 nm. Subsequently, these higher order aggregates assemble to form mature amyloid fibrils. Therefore, after 20 h, typical cross-sectional heights of fibrils in the order of 8.2-16 nm (Figure 5.59i) were seen which is consistent with previous studies.^[132,134,422,433-435]

In sample with A β 40 and P-G2-Man, at 0 h the cross-sectional height of 1.0-4 nm (Figure 5.59j). After 2 h of incubation, a cross-sectional height of 2.6-4.9 nm was observed, and after 5 h of incubation, 3.4-4.5 nm cross-sectional heights were seen. Remarkably, after 20 h there was no drastic increase in cross-sectional heights of the fibrils, as fibrils of cross-sectional height in the range 3.1-4.5 nm were seen. Similar behavior was seen with surface roughness analysis. It was found that the surface roughness of A β 40 with P-G2-Man decreased in comparison with the control as shown in the histograms (Figure 5.59k,1), and similar results have been reported by other investigators.^[432,434] This observation suggests that P-G2-Man is interfering with the hierarchical self-assembly amyloid peptide.

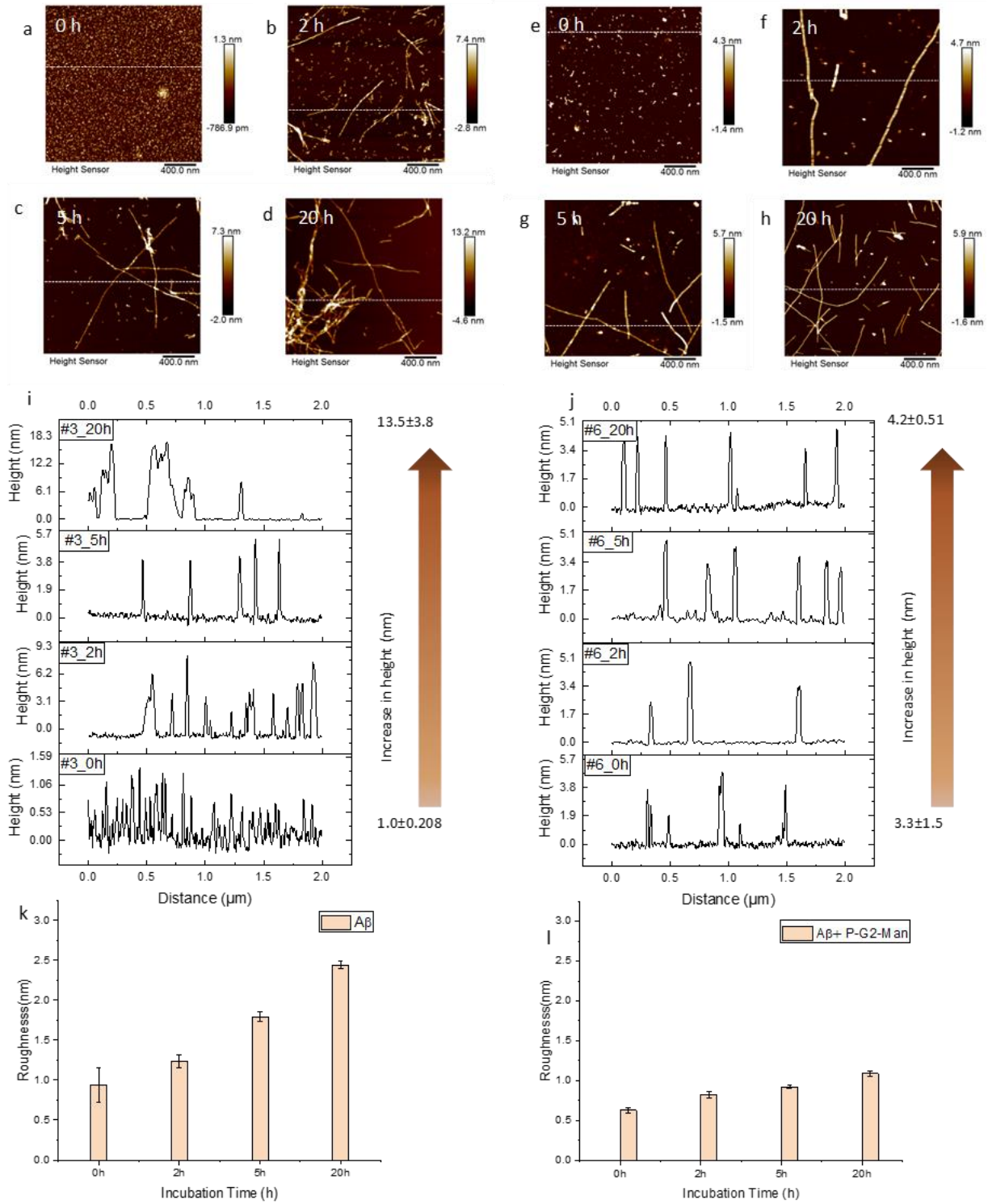


Figure 5.59: AFM analysis of P-G2-Man (10 μ M) treated A β amyloid (50 μ M) with increasing incubation time: a-d) AFM images of control with A β amyloid (50 μ M), e-h) AFM images of A β amyloid with P-G2-Man; i) cross section profiles of A β amyloid aggregate on images a-d) (white dotted lines), j) cross section profiles of A β amyloid aggregate with P-G2-Man on images e-h) (white dotted lines); Roughness was calculated with squares of 1 μ m² at four parts of an AFM image a-h), k) roughness for A β amyloid aggregate, l) roughness for A β amyloid with P-G2-Man.

5.2.4.2 Topography and diameter

On closer view, the AFM images revealed twist patterns in amyloid fibrils. These twist patterns are important, as they can be sites for fragmentation or providing new sites for further aggregation which has been observed before.^[436] These twist patterns are also responsible for a decrease or an increase in the average diameter of the fibril. All the images were flattened to first order to remove any bends and tilts. The fibrils are assessed by measuring the height in cross section of >100 individual fibrils. Figure 5.60 compares fibrils assembled in control and with P-G2-Man at 20 h. Fibril diameters are estimated from the height of fibril in cross section. In case of A β 40 (control), the average diameter of the fibrils imaged is 8.8 ± 4 nm consistent with previous studies.^[105,366,437]

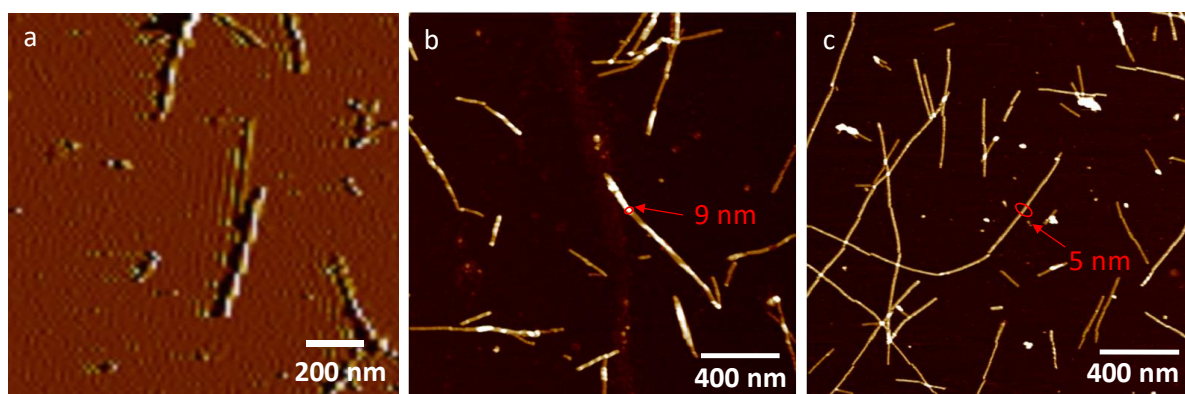


Figure 5.60: AFM images a) Higher magnification peak force error image of amyloid fibrils after 20 h of incubation, showing twists pattern in fibrils, b) A β 40 (control) after 20 h incubation showing diameter of 9 nm and (c) A β 40 with P-G2-Man after 20 h incubation showing a diameter of 5 nm.

Amyloid fibrils have structural heterogeneity which give rise to this broad distribution. In sample A β 40 in the presence of P-G2-man, the average diameter of the fibrils is 3.9 ± 1.3 nm. Also, fragments are seen in this sample which are arranged in head-to-tail manner. The pseudodendrimers are also of a similar dimension of ~ 8 nm; however, their concentration is low in comparison to the amyloid (amyloid:P-G2-Man 5:1). As a result, no globular deposits were observed. This observation suggests that the amyloid fibrils were on their way of becoming mature fibrils, but P-G2-Man likely interferes with the further assembly of protofilaments.

5.2.4.3 Length

To see the effect of P-G2-Man on A β 40, their lengths were also analyzed. For this, the lengths of >100 fibrils were measured, which were incubated for different incubation times. In control (Figure 5.61a-d), at 0 h a proteinaceous film with small species are seen which are < 20 nm in length, at 2 h two types of species are seen, one is ~ 40 nm and large species <100 nm in length. At 5 h and 20 h, a very broad range of species are seen, extending up to several micrometers; these are mature amyloid fibrils. In A β 40 with P-G2-Man, however, no significant difference was observed in terms of length in comparison to control, but a particular type of fragmentation was seen (Figure 5.61f-h). The range of these fragments was 80-600 nm (Figure 5.61f). This

observation suggests that the growth of fibrils has perhaps slowed down but the presence of P-G2-Man does not inhibit it completely.

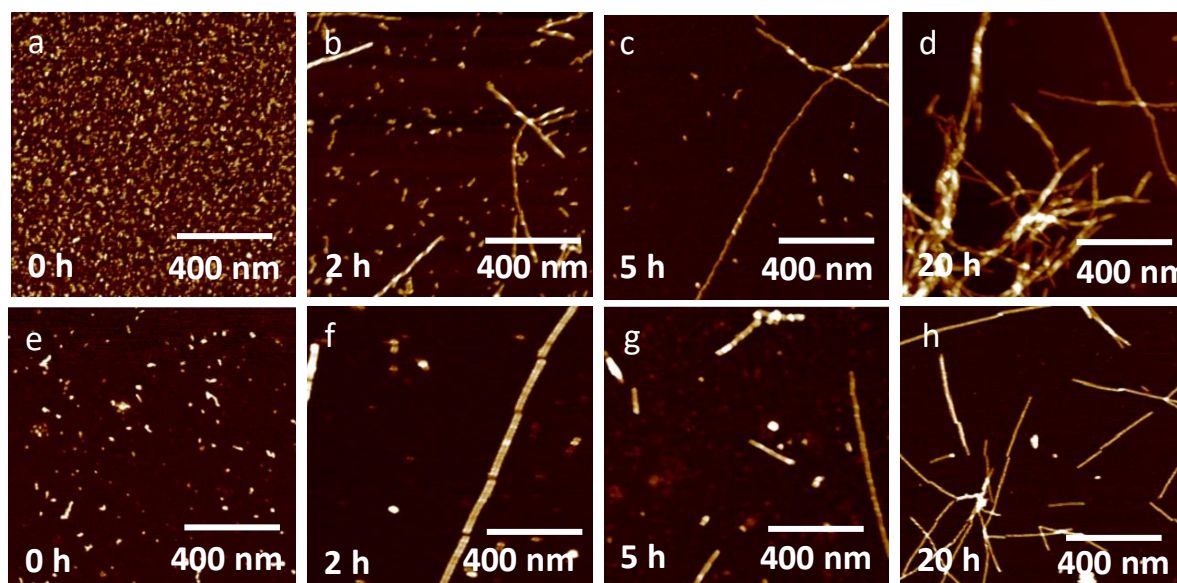


Figure 5.61: AFM images for A β 40 solution a) 0 h, b) 2 h, c) 5 h, d) 20 h, and A β 40 solution with P-G2-Man e) 0 h, f) 2 h, g) 5 h, h) 20 h.

5.2.4.4 Morphology

The AFM images were visually inspected closely to see if there are aggregates, amorphous aggregates or fibrils clumping. A β 40 amyloid fibrils showed few clumped fibrils (Figure 5.62c). However, A β amyloid with P-G2-Man, showed no such clumping but entanglement of longer fibrils was seen in both cases (Figure 5.62a, b). No amorphous aggregates were observed in the present work, in consonance with what has been reported earlier.^[9]

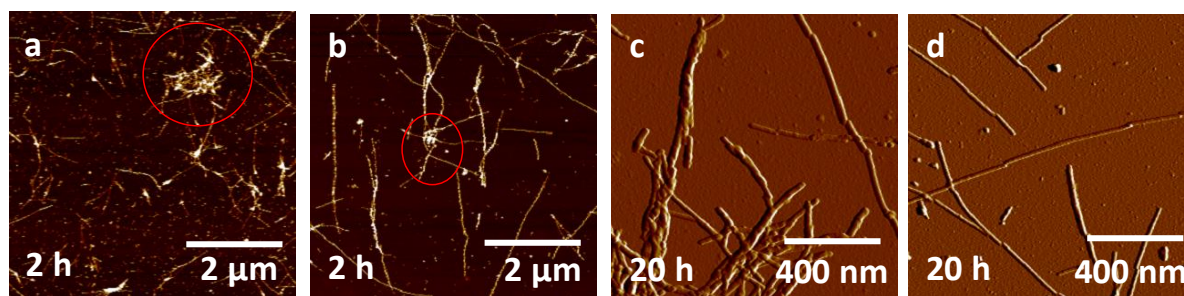


Figure 5.62: AFM images showing morphology at 2 h of a) A β 40 and b) A β 40 with P-G2-Man; a) and b) show entanglement marked with red. c) peak force error image for A β 40 showing clumped fibrils. d) Peak force error image for A β 40 with P-G2-Man.

The following points can be summarized from AFM study:

1. The glyco-pseudodendrimers affects the dimensions of amyloid fibrils by slowing down their diameter and height.
2. Second generation glyco-pseudodendrimer (P-G2-Man) has the potential to inhibit the A β amyloid fibril formation process through interfering the hierarchical assembly of protofilaments.
3. AFM study is in coherence with the ThT, CD and AF4 studies.

5.2.5 Cytotoxicity

The substances to be used in drug delivery systems should be non-toxic in nature unless they are specifically designed for targeted applications. The number and nature of functional groups, mainly determines the cytotoxicity of dendrimers. High toxicity is shown by cationic dendrimers whereas, anionic and neutral dendrimers show slight or no toxic effects.^[8,369,438] This cytotoxicity of dendrimers can be explained based on the interaction between negatively charged cell membranes and the positively charged dendrimer surface. This leads to the formation of nanopores in the cell membrane, causes damage, following the leakage of cytoplasm, ultimately leading to cell death. Zeta potential measurements are a quick method to know the charges on the surface. The following experiments were performed by Dr. Anna Janaszewska at Department of General Biophysics, University of Lodz, Poland.

The zeta potential of three generations of GI-P and GI-D were measured and are summarized in Figure 5.63.

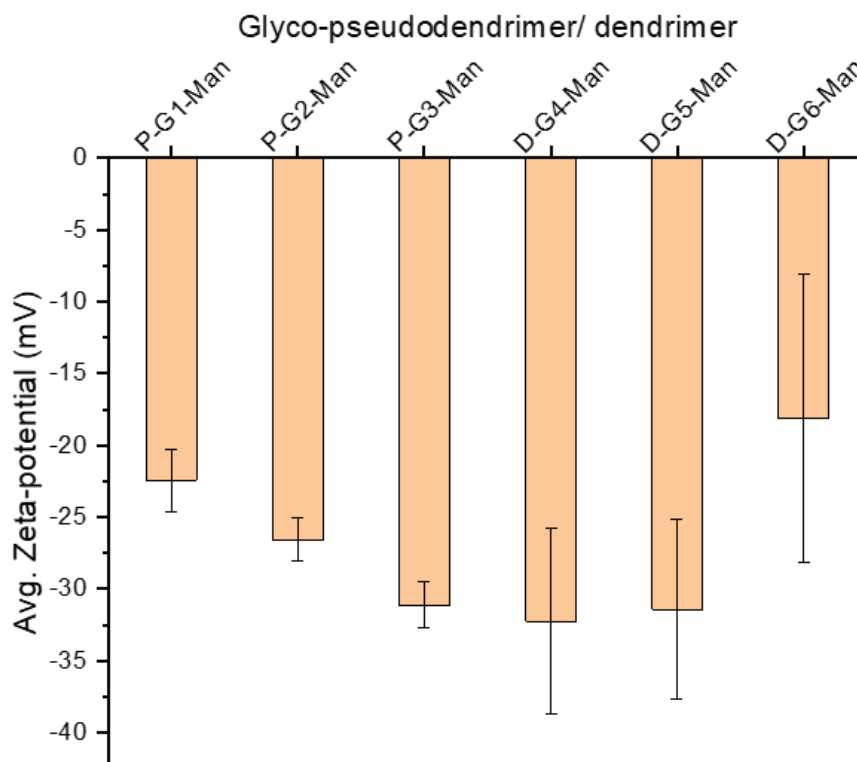


Figure 5.63: Zeta potential measurements of glyco-pseudodendrimers and glyco-dendrimers in 10 mM phosphate buffer (pH 7.4).

Figure 5.63 show the results for zeta potential measurements. This experiment was performed in phosphate buffer and without the use of any filters. The zeta potential values were negative around ~ 20 -30 mV. This overall negative charge could serve as an advantage during cytotoxic studies. As in the previous experiments, GI-P showed better interaction with the aggregates of A β 40, it was decided to proceed with the cytotoxicity experiments of only GI-P.

Unless stated otherwise, two cell lines were used for all cytotoxic studies, HMEC-1 and HeLa, isolated for use in this study and were maintained as explained in Section 4.5.2.

5.2.5.1 MTT Assay

To examine the cytotoxicity of synthesized GI-P/GI-D, MTT assay (3-[4,5-dimethylthiazole-2-yl]-2,5-diphenyltetrazolium bromide) was used.^[368] It is a widely used method to assess cell viability. This occurs by the enzymatic reduction of MTT to MTT formazan with mitochondrial succinate dehydrogenase enzyme which is release during cellular respiration. Hence, the MTT assay serves to assess the cellular energy capacity of a cell.^[368]

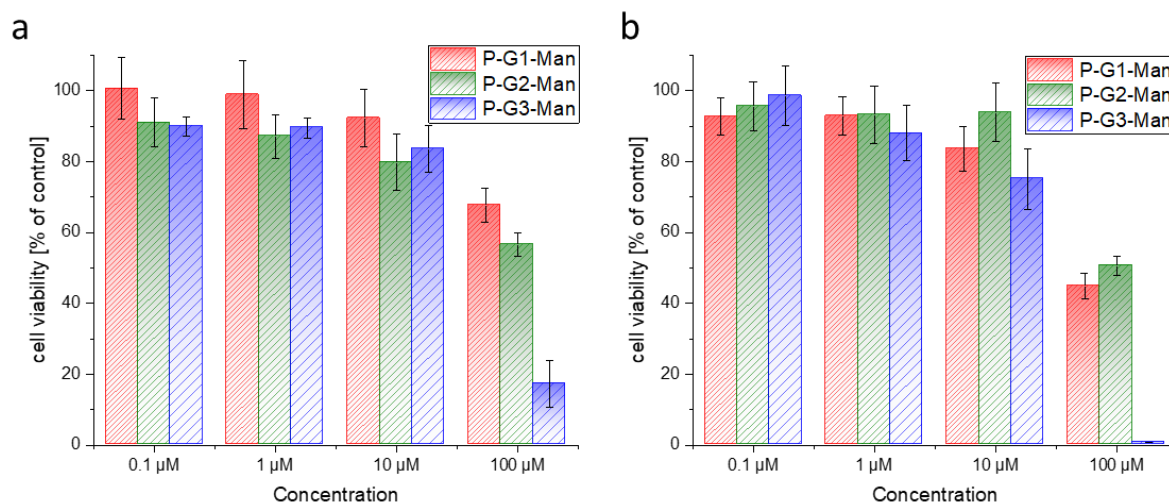


Figure 5.64: Influence of P-G1-Man, P-G2-Man and P-G3-Man glyco-pseudodendrimers on the viability of a) HMEC-1 and b) HeLa cells after 24-hour incubation.

Analysis of the obtained results suggests that all investigated GI-P presented relatively weak cytotoxicity (decrease in cells survival rate not exceeding 20%) towards either endothelial (HMEC-1) as well as carcinoma cells (HeLa) for concentrations up to 10 μM. A significant decrease in the viability of both cell lines was observed after incubation only with the 10-fold higher concentration (100 μM). This is an advantage, as in all our previous experiments we have used concentration only up to 10 μM.

After 24 h incubation, only P-G3-Man showed the strong inhibition of proliferation of the HMEC-1 (about 83% on average) and HeLa (about 99% on average). The obtained results show that interestingly, cancer HeLa cells were more sensitive to the cytotoxicity of the highest 100 μM concentration of analyzed GI-Ps than the non-cancer HMEC-1 cells.

Using results obtained in the MTT test, the IC₅₀ and IC₇₀ values (half maximal inhibitory concentrations) for all analyzed GI-Ps were calculated in GraphPad Prism 6 (Table 5.9).

Table 5.9. IC₅₀ and IC₇₀ values [μM] of glyco-pseudodendrimers in non-cancer HMEC-1 and cancer HeLa human cell lines.

Sample	HMEC-1		HeLa	
	IC ₅₀	IC ₇₀	IC ₅₀	IC ₇₀
P-G1-Man	> 100 μM	= 89 μM	= 85 μM	= 35 μM
P-G2-Man	> 100 μM	= 35 μM	> 100 μM	= 59 μM
P-G3-Man	= 52 μM	= 27 μM	= 37 μM	= 16 μM

Using IC₅₀ values one can determine the quantity of sample required to inhibit a biological processes by 50 per cent. Based on the results of the cytotoxic experiments, for further investigations, one dendrimer concentration was selected. The IC₅₀ value for G1-Ps, which showed the highest cytotoxicity toward to HeLa cells (P-G3-Man) was selected. The next experiments were performed for all compounds for 37 μM concentration.

5.2.5.2 Changes in mitochondrial transmembrane potential

Mitochondria membrane potential (MMP) is a key indicator of cellular activity and is required for energy production inside the cell. If MMP decreases, the cell loses energy which leads to altering the pH of the mitochondrial intermembrane and matrix.^[370]

JC-1 is a cationic dye widely used as fluorescent probe for detecting depolarization of the mitochondrial membrane.^[370] The selective accumulation of JC-1 in the mitochondria is dependent on the mitochondrial transmembrane potential. Sharp decline in ATP production is often connected with pathology states, which causes depletion of energy and depolarization of mitochondrial membrane.^[370] Changes in mitochondrial potential are characteristic for the initial stages of programmed cell death, i.e., apoptosis. The application of the JC-1 fluorescent probe allows for spectrofluorimetric analysis of changes in the mitochondrial membrane potential. JC-1 tends to accumulate in large quantities in hyperpolarized mitochondrial membrane, where it forms aggregates that emit red fluorescence ($\lambda_{\text{ex}} = 485 \text{ nm}$, $\lambda_{\text{em}} = 538 \text{ nm}$). When the depolarization of the mitochondrial membrane occurs and the membrane permeability increases, the aggregates breakdown to monomers emitting green fluorescence ($\lambda_{\text{ex}} = 530 \text{ nm}$, $\lambda_{\text{em}} = 590 \text{ nm}$). Ratio of aggregates ($\lambda_{\text{em}} = 590 \text{ nm}$) and monomers fluorescence ($\lambda_{\text{em}} = 540 \text{ nm}$) reflects the damage of mitochondrial membranes.

Figure 5.65 shows the data obtained from JC-1 experiments. Based on the emission and excitation, the cell viability could be assessed.

The obtained results suggested that all analyzed G1-Ps induce time-independent changes in mitochondrial membrane potential (Figure 5.65 a and b). Moreover, regardless of tested cell lines, the ratio of JC-1 probe fluorescence was decreased by approximately 15-20% after 3 h treatment with P-G1-Man, P-G2-Man and P-G3-Man. At this point, there was no difference between the different generations of G1-Ps. Moreover, such differences did not appear after next hours of incubation, when value of mitochondrial membrane potential return to control level.

This could mean that the observed cytotoxicity of the studied GI-Ps is not associated with changes in mitochondrial potential only, e.g. with oxidative stress and the generation of free radicals. But to check this, a method in which the fluorophore will not interact with the tested compounds is needed, causing fluorescence quenching. Hence, the proposal was to use a new method based on chemiluminescence.

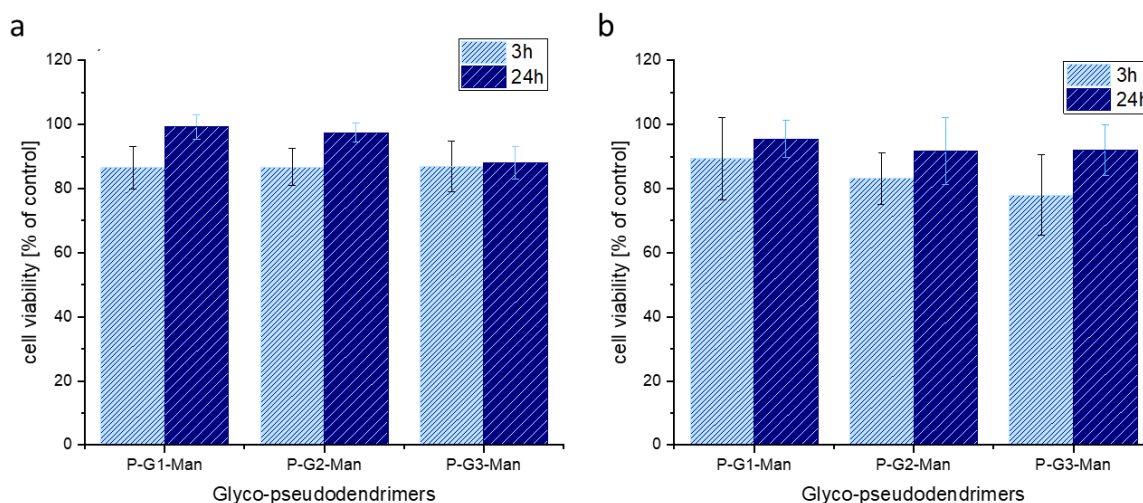


Figure 5.65: Changes in mitochondrial membrane potential based on cell viability using JC-1 assay, after treatment of a) HMEC-1 and b) HeLa cells with glyco-pseudodendrimers.

5.2.5.3 Flow cytometric detection of phosphatidyl serine exposure

Dual staining of cells with annexin V and propidium iodide (PI) was used to assess apoptosis. This technique is often used in biological experiments where sorting and profiling of cells are required. In this the viable cells remain unstained, apoptotic cells are stained with Annexin V and necrotic cells are stained with PI.^[373]

The next step of the study was measurement of phosphatidylserine externalization directly related to apoptotic processes. Figure 5.66 shows the influence of dendrimers on the induction of apoptosis in HMEC-1 and HeLa cell lines, estimated by annexin V/propidium iodide assay.

To evaluate the possible role of necrotic or programmed cell death features on the cytotoxicity of dendrimers, the mode of cell death triggered by these nanoparticles was investigated. The quantitative results obtained from phosphatidylserine externalization assay were consistent with the results of cytotoxicity test, showing that cancer HeLa cells were more sensitive to GI-Ps than non-cancer HMEC-1 cells. In the cancer cells, after 24 h treatment, the maximum level of necrotic cells was observed for P-G3-Man and was 41% while in the non-cancer cells was 24%, respectively. In both investigated cell lines, tested GI-Ps, induced both apoptosis and necrosis, but necrosis was the dominant process. After 24 h treatment, the percentage of the dead cell fraction for all investigated dendrimers increased significantly in comparison to the 3 h incubation time, whereas the changes in apoptotic fraction were inconsiderable.

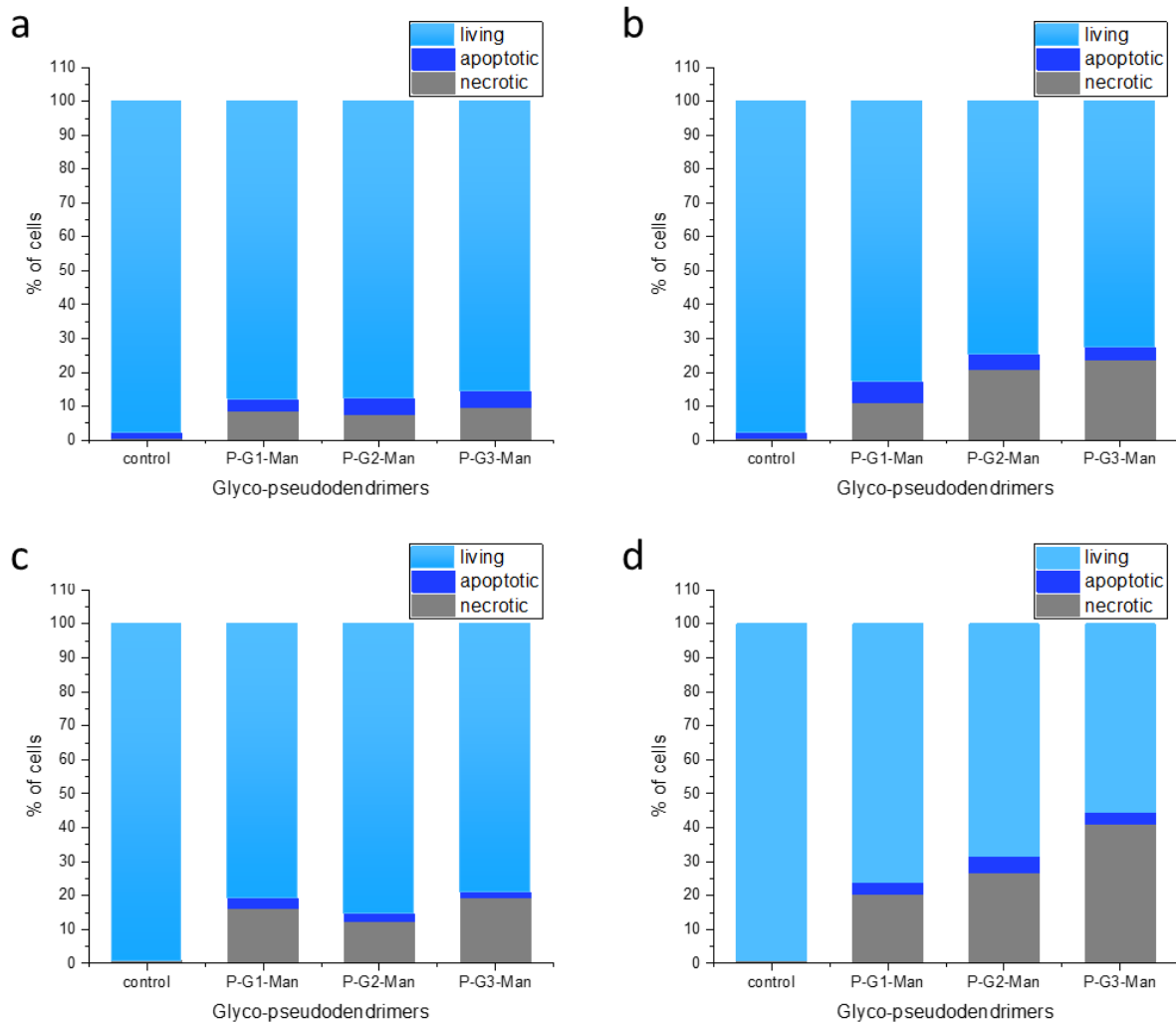


Figure 5.66: Influence of glyco-pseudodendrimers on the apoptosis induction in cell lines, estimated by annexin V/propidium iodide assay for HMEC-1 at a) 3 h, b) 24h and for HeLa at c) 3 h, d) 24 h. Quantitative results of the effect of polymers on the level of live, necrotic and apoptotic cells are represented by the mean \pm standard deviation (S.D.) for three independent experiments.

Observed necrosis confirms the hypothesis that mitochondria, which through the outflow of calcium and cytochrome C activate the caspase pathway and direct cells to the path of programmed death - apoptosis, may not actually participate in the observed cell death. The cell lines used just serve to test the toxicity of synthesized polymers. Since, G1-D could not be tested for their toxicity, but in the future, it would be interesting to study a comparison of the toxicity of these two.

6 Conclusions and Outlook

As the world population ages, we face a looming epidemic of Alzheimer's disease (AD), which induces cognition dysfunctions in elderly persons, varying from difficult-to-diagnose subtle changes to severe incapacitating impairments. Healthcare systems are challenged to meet the needs of these patients which would result in huge costs and man hours, in addition utmost commitment and empathy for adequate and proper patient care. Prevention of AD onset and progression is an ambitious goal that does not seem fully achievable in the near future, although delaying/palliation of the disability may be feasible in the face of current global thrust. Through our present work, we realize that the global burden of the disease can be significantly reduced even through a slight advancement in therapeutics and preventive strategies which can produce a small delay in AD onset and progression. However, newer therapeutic strategies warrant development of thorough understanding of the cellular mechanisms of the AD onset and progression. Amyloid cascade hypothesis is a trove of information concerning these mechanisms in the cerebral neurons. According to which, amyloid peptides play a central role in triggering cell toxicity in brain. However, amyloid plaque formation is a complex mechanism, involving mainly amyloid and tau proteins, which further involve many different species. Of the two, the former is the most abundant forms of protein in AD brain. A β forms fibrillar, extracellular deposits, triggering pathogenic changes leading to neuronal death and synaptic dysfunction. Despite understanding the physiopathology of the disease, the exact process of assembly of A β into highly organized fibrils, is still not fully understood.

To recapitulate the basis of the present work, two of the most commonly studied dendrimers which can modulate the amyloid peptide aggregation are polyamidoamine (PAMAM) and phosphorus dendrimers. Dendritic structure, generation, pH of the medium and dendrimer-peptide ratio are important parameters responsible for their potential anti-amyloidogenic activity. However, the intrinsic toxicity of these dendrimers has prevented their evaluation as anti-amyloidogenic agents. Thereafter, PPI glyco-dendrimers showed a specific interaction capacity with biological molecules governed by hydrogen bonding, and have already proven to be effective antiprion agents in cell cultures. So, several works followed focusing on the development of biocompatible dendritic structures with hydrogen bonding sugar on the surface.

One of the promising approaches to prevent the modulation of aggregates is the use of glycopolymers as anti-amyloidogenic agents. Amyloid plaques interact strongly with the glyco-dendrimers and are thus able to modulate its aggregation behavior, leading to a markedly reduced neurotoxicity, which has been verified *in vivo*. However, the synthesis of glyco-dendrimers is complicated involving multiple steps. Pseudodendrimers are an alternative to dendrimers based on hyperbranched polymers. In contrast to dendrimers, these polymers can be easily synthesized via few steps. In addition, a higher molar mass and a dense shell of functional end groups are possible. Therefore, pseudodendrimers can possibly overcome the drawbacks of dendrimers with regards to synthesis and functionality.

In the present work, three generations of pseudodendrimers based on bis-MPA were synthesized and then decorated with mannose leading to the formation of dense shell glyco-pseudodendrimers. Additionally, three generations of dendrimers based on PFD-G3-TMP-OH were synthesized and then decorated with mannose forming glyco-dendrimers. Here, the number of steps in synthesis of dendrimers are the same as pseudodendrimers, but we started with the third generation of dendrimer which is already expensive compared to the price of bis-MPA, the starting material for pseudodendrimers. Using SEC-MALS, the average molar mass was determined, corresponding to almost 80-100% degree of modification. Pseudodendrimers showed a high dispersity in comparison to dendrimers. Batch DLS, the most widespread LS technique for particle analysis, confirmed the hydrodynamic size (i.e. R_h) to be in the range of 3-4 nm. Average apparent density showed that P-G2-Man has the lowest density in glyco-pseudodendrimers and D-G5-Man has the lowest density in glyco-dendrimers. But P-G2-Man has higher density when compared to its counterpart D-G5-Man. AF4-MALS confirmed these average molar mass values and hydrodynamic size based on online DLS.

The second part of this work involved the study of interaction of these synthesized glyco-pseudodendrimers and glyco-dendrimers with amyloid protein A β 40. ThT fluorescence assay confirmed their interaction with the amyloid, with P-G2-Man at 10 μ M showing maximum effect on the inhibition of aggregation of amyloid. The kinetic analysis of the data revealed that the P-G2-Man at 10 μ M acts on the two microscopic processes involved i.e., secondary nucleation and elongation. CD spectroscopy data confirmed the behavior of chosen concentrations from ThT assay. As per the secondary structure determination from CD data, the total α and β sheet content followed the trend D-G6-Man < P-G2-Man < P-G3-Man relative to the control. The chosen concentrations analyzed with AF4-MALS, at different incubation time intervals revealed that the P-G2-Man at 10 μ M concentration formed minimum amount of aggregates relative to the control. However, D-G6-Man (5 μ M) and P-G3-Man (2 μ M) also showed low amount of aggregates. AFM of P-G2-Man (10 μ M) confirmed that glyco-pseudodendrimers indeed affected the dimensions of amyloid fibrils. Our observations clearly confirm that glyco-pseudodendrimers are affecting the aggregation behavior by interfering in the secondary nucleation and elongation steps. This suggests that glyco-pseudodendrimers indeed have the ability to interact with A β 40 amyloid by affecting two main microscopic steps. All these results suggest that glyco-pseudodendrimers are better at limiting the aggregation behavior of A β 40, with P-G2-Man being the most effective. D-G6-Man also showed better interaction behavior, but the synthesis of D-G6-Man would be challenging, especially if starting from the core. Nevertheless, it is still possible.

In a nutshell, findings of this work suggest that glyco-pseudodendrimers used in this work are a better alternative to their counterparts (glyco-dendrimers) for use as anti-amyloidogenic agents. The reason for glyco-pseudodendrimers being better than glyco-dendrimers probably lies in the structural difference in 3D space, having an optimal number of functional groups in the periphery. A lot more research in molecular dynamics is required, which would probably lead to a better understanding of their behavior. Here, it is worth mentioning that the metastable nature of A β is strongly affected by the ionic environment which rapidly affects aggregate composition. Therefore, focusing on just one polymer and its interaction with A β 40 would lead

to a deeper understanding of dendrimers-aggregate complex, especially with the use of advanced characterization tools, particularly AF4.

The cytotoxic studies of glyco-pseudodendrimers revealed that they have an overall negative zeta potential which is an advantage as it will not interact with the negatively charged cell membranes. MTT assay showed a relatively weak cytotoxicity for glyco-pseudodendrimers. The changes in mitochondrial membrane potential also suggested the weak cytotoxicity and flow cytometric detection method revealed necrosis as the dominant death of cells.

Overall, the findings presented in this thesis serve as a preliminary work on polyester based pseudodendritic structures and build an excellent basis for further investigations of glyco-pseudodendrimers particularly the second generation to understand its structure more deeply. Definitely, modifying its chemical structure with different sugar units, providing new linkage would open a new window of this glyco-pseudodendrimers. Additionally, incorporating new dyes would be important for imaging tools in future. Another future prospect is to use these pseudodendrimers with different aggregating proteins like prion and amyloids, A β 42 in particular. In particular, testing pseudodendrimers with A β 40 at different pH as well as testing the enzymatic and non-enzymatic degradation of these polyester structures should make excellent next steps. It is hereby strongly proposed to extend this research to A β 42 amyloid so that it can be compared with previous studies. Last but not the least, further studies can be made by isolating different monomeric and oligomeric species of amyloid to have further information on which species are particularly involved in interacting with the pseudodendrimers, leading us to deeper understanding of the protein-polymer interaction and shall pave the way for a potential anti-Alzheimer agent.

7 Bibliography

- [1] G. F. Chen, T. H. Xu, Y. Yan, Y. R. Zhou, Y. Jiang, K. Melcher, H. E. Xu, *Acta Pharmacol. Sin.* **2017**, *38*, 1205–1235.
- [2] N. Benseny-Cases, O. Klementieva, J. Cladera, *New J. Chem.* **2012**, *36*, 211–216.
- [3] B. Klajnert, M. Cortijo-Arellano, J. Cladera, M. Bryszewska, *Biochem. Biophys. Res. Commun.* **2006**, *345*, 21–28.
- [4] B. Klajnert, M. Cortijo-Arellano, M. Bryszewska, J. Cladera, *Biochem. Biophys. Res. Commun.* **2006**, *339*, 577–582.
- [5] T. Wasiaik, M. Ionov, K. Nieznanski, H. Nieznanska, O. Klementieva, M. Granell, J. Cladera, J. Majoral, P. A. Caminade, B. Klajnert, *Mol. Pharm.* **2011**.
- [6] A. Janaszewska, K. McZyńska, G. Matuszko, D. Appelhans, B. Voit, B. Klajnert, M. Bryszewska, *New J. Chem.* **2012**, *36*, 428–437.
- [7] H. B. Agashe, A. K. Babbar, S. Jain, R. K. Sharma, A. K. Mishra, A. Asthana, M. Garg, T. Dutta, N. K. Jain, *Nanomed.: Nanotechnol. Biol. Med.* **2007**, *3*, 120–127.
- [8] M. Ciolkowski, J. F. Petersen, M. Ficker, A. Janaszewska, J. B. Christensen, B. Klajnert, M. Bryszewska, *Nanomed.: Nanotechnol. Biol. Med.* **2012**, *8*, 815–817.
- [9] O. Klementieva, N. Benseny-Cases, A. Gella, D. Appelhans, B. Voit, J. Cladera, *Biomacromolecules* **2011**, *12*, 3903–3909.
- [10] A. Janaszewska, B. Ziemba, K. Ciepluch, D. Appelhans, B. Voit, B. Klajnert, M. Bryszewska, *New J. Chem.* **2012**, *36*, 350–353.
- [11] O. Klementieva, E. Aso, D. Filippini, N. Benseny-Cases, M. Carmona, S. Juvés, D. Appelhans, J. Cladera, I. Ferrer, *Biomacromolecules* **2013**, *14*, 3570–3580.
- [12] E. Aso, I. Martinsson, D. Appelhans, C. Effenberg, N. Benseny-Cases, J. Cladera, G. Gouras, I. Ferrer, O. Klementieva, *Nanomed.: Nanotechnol. Biol. Med.* **2019**, *17*, 198–209.
- [13] N. Benseny-Cases, E. Álvarez-Marimon, E. Aso, M. Carmona, O. Klementieva, D. Appelhans, I. Ferrer, J. Cladera, *Sci. Rep.* **2021**, *11*, 1–9.
- [14] E. Malmström, M. Johansson, A. Hult, *Macromolecules* **1995**, *28*, 1698–1703.
- [15] H. Ihre, A. Hult, E. Söderlind, *J. Am. Chem. Soc.* **1996**, *118*, 6388–6395.
- [16] B. N. Vedha Hari, K. Kalaimagal, R. Porkodi, P. K. Gajula, J. Y. Ajay, *Int. J. PharmTech Res.* **2012**, *4*, 432–451.
- [17] A. Córdova, K. D. Janda, *J. Am. Chem. Soc.* **2001**, *123*, 8248–8259.

- [18] P. Wu, M. Malkoch, J. N. Hunt, R. Vestberg, E. Kaltgrad, M. G. Finn, V. V. Fokin, K. B. Sharpless, C. J. Hawker, *Chem. Commun.* **2005**, 5775.
- [19] M. Malkoch, E. Malmström, A. Hult, *Macromolecules* **2002**, *35*, 8307–8314.
- [20] P. Antoni, M. J. Robb, L. Campos, M. Montanez, A. Hult, E. Malmström, M. Malkoch, C. J. Hawker, *Macromolecules* **2010**, *43*, 6625–6631.
- [21] A. D. M. Ghirardello, K. Öberg, S. Staderini, O. Renaudet, N. Berthet, P. Dumy, Y. Hed, A. Marra, M. Malkoch, *J. Polym. Sci. A Polym. Chem.* **2014**, *52*, 2422–2433.
- [22] M. Malkoch, K. Schleicher, E. Drockenmuller, C. J. Hawker, T. P. Russell, P. Wu, V. V. Fokin, *Macromolecules* **2005**, *38*, 3663–3678.
- [23] A. Carlmark, C. Hawker, A. Hult, M. Malkoch, *Chem. Soc. Rev.* **2009**, *38*, 352–362.
- [24] A. Alzheimer, *Neurol. Cent.* **1906**, *25*, 1134.
- [25] R. A. Stelzmann, H. N. Schnitzlein, F. R. Murtagh, *Clin. Anat.* **1995**, *8*, 429–431.
- [26] K. Maurer, S. Volk, H. Gerbaldo, *Lancet* **1997**, *349*, 1546–1549.
- [27] R. Dahm, *Curr. Biol.* **2006**, *16*, 906–910.
- [28] National Institute on Aging, “What causes Alzheimer’s Disease”, updated 24th December **2019**, <https://www.nia.nih.gov/health/what-causes-alzheimers-disease>, accessed on 23rd June 2022.
- [29] L. E. Hebert, J. L. Bienias, N. T. Aggarwal, R. S. Wilson, D. A. Bennett, R. C. Shah, D. A. Evans, *Neurology* **2010**, *75*, 786–791.
- [30] S. Gauthier, P. Rose-Neto, J. A. Morais, C. Webster, *World Alzheimer Report 2021: Journey through the Diagnosis of Dementia*, London, England: Alzheimer’s Disease International, **2021**.
- [31] A. M. Saunders, W. J. Strittmatter, D. Schmechel, P. H. St. George-Hyslop, M. A. Pericak-Vance, S. H. Joo, B. L. Rosi, J. F. Gusella, D. R. Crapper-Mac Lachlan, M. J. Alberts, et al., *Neurology* **1993**, *43*, 1467–1472.
- [32] L. A. Farrer, L. A. Cupples, J. L. Haines, B. Hyman, W. A. Kukull, R. Mayeux, R. H. Myers, M. A. Pericak-Vance, N. Risch, C. M. Van Duijn, *J. Am. Med. Assoc.* **1997**, *278*, 1349–1356.
- [33] C. T. Loy, P. R. Schofield, A. M. Turner, J. B. J. Kwok, *Lancet* **2014**, *383*, 828–840.
- [34] D. M. Holtzman, J. Herz, G. Bu, *Cold Spring Harb. Perspect. Med.* **2012**, *2*, 1–24.
- [35] D. M. Michaelson, *Alzheimer’s Dement.* **2014**, *10*, 861–868.
- [36] K. B. Rajan, L. L. Barnes, R. S. Wilson, E. A. McAninch, J. Weuve, D. Sighoko, D. A. Evans, *J. Am. Geriatr. Soc.* **2017**, *65*, 2425–2430.
- [37] W. J. Jansen, R. Ossenkoppele, D. L. Knol, B. M. Tijms, P. Scheltens, F. R. J. Verhey, P. J. Visser, *J. Am. Med. Assoc.* **2015**, *313*, 1924–1938.

- [38] R. C. Green, L. A. Cupples, R. Go, K. S. Benke, P. A. Griffith, M. Williams, Y. Hipps, D. Bachman, L. A. Farrer, *J. Am. Med. Assoc.* **2002**, *287*, 329–336.
- [39] P. T. Nelson, E. Head, F. A. Schmitt, P. R. Davis, J. H. Neltner, G. A. Jicha, E. L. Abner, C. D. Smith, L. J. Van Eldik, R. J. Kryscio, et al., *Acta Neuropathol.* **2011**, *121*, 571–587.
- [40] B. Reisberg, S. H. Ferris, M. J. de Leon, T. Crook, *Am. J. Psychiatry* **1982**, *139*, 1136–1139.
- [41] National Institute on Aging, “Alzheimer's Disease Fact Sheet”, ”, updated 08th July **2021**, <https://www.nia.nih.gov/health/alzheimers-disease-fact-sheet#causes>, accessed on 23rd July 2022.
- [42] R. S. Wilson, E. Segawa, P. A. Boyle, S. E. Anagnos, L. P. Hizel, D. A. Bennett, *Psychol. Aging* **2012**, *27*, 1008–1017.
- [43] P. A. Boyle, L. Yu, R. S. Wilson, S. E. Leurgans, J. A. Schneider, D. A. Bennett, *Am. Neurol. Assoc.* **2017**, *83*, 74–83.
- [44] M. F. Folstein, S. E. Folstein, P. R. McHugh, *Proc. Int. Offshore Polar Eng. Conf.* **1975**, *12*, 189–198.
- [45] K. A. Johnson, S. Minoshima, N. I. Bohnen, K. J. Donohoe, N. L. Foster, P. Herscovitch, J. H. Karlawish, C. C. Rowe, M. C. Carrillo, D. M. Hartley, et al., *Alzheimer's Dement.* **2013**, *9*, e1–e16.
- [46] L. M. Shaw, J. Arias, K. Blennow, D. Galasko, J. L. Molinuevo, S. Salloway, S. Schindler, M. C. Carrillo, J. A. Hendrix, A. Ross, et al., *Alzheimer's Dement.* **2018**, *14*, 1505–1521.
- [47] M. Bieschowsky, *Neurol. Zentralblatt* **1902**, *21*, 579–84.
- [48] D. M. Walsh, A. Lomakin, G. B. Benedek, M. M. Condron, D. B. Teplow, *J. Biol. Chem.* **1997**, *272*, 22364–22372.
- [49] H. LeVine, *Methods Enzymol.* **1999**, *309*, 274–284.
- [50] K. S. Kosik, C. L. Joachim, D. J. Selkoe, *Proc. Natl. Acad. Sci. U. S. A.* **1986**, *83*, 4044–4048.
- [51] H. Braak, E. Braak, *Acta Neuropathol.* **1991**, *82*, 239–259.
- [52] Z. S. Khachaturian, *Arch. Neurol.* **1985**, *4*, 1097–1105.
- [53] G. G. Fillenbaum, G. van Belle, J. C. Morris, R. C. Mohs, S. S. Mirra, P. C. Davis, P. N. Tariot, J. M. Silverman, C. M. Clark, K. A. Welsh-Bohmer, et al., *Alzheimer's Dement.* **2008**, *4*, 96–109.
- [54] G. G. Glenner, C. W. Wong, *Biochem. Biophys. Res. Commun.* **1984**, *120*, 885–890.
- [55] C. L. Masters, G. Multhaup, G. Simms, J. Pottgiesser, R. N. Martins, K. Beyreuther, *EMBO J.* **1985**, *4*, 2757–2763.
- [56] J. Kang, H.-G. Lemaire, A. Unterbeck, J. M. Salbaum, C. L. Masters, L.-H. Grzeschik, G. Multhaup, K. Beyreuther, B. Müller-Hill, *Nature* **1987**, *325*, 733–736.

- [57] M. S. Brown, J. Ye, R. B. Rawson, J. L. Goldstein, *Cell* **2000**, *100*, 391–398.
- [58] R. Sandbrink, C. L. Masters, K. Beyreuther, *J. Biol. Chem.* **1994**, *269*, 1510–1517.
- [59] S. Lammich, E. Kojro, R. Postina, S. Gilbert, R. Pfeiffer, M. Jasionowski, C. Haass, F. Fahrenholz, *Proc. Natl. Acad. Sci. U. S. A.* **1999**, *96*, 3922–3927.
- [60] A. M. Wertkin, R. S. Turner, S. J. Pleasure, T. E. Golde, S. G. Younkin, J. Q. Trojanowski, V. M. Y. Lee, *Proc. Natl. Acad. Sci. U. S. A.* **1993**, *90*, 9513–9517.
- [61] T. D. Stein, N. J. Anders, C. DeCarli, S. L. Chan, M. P. Mattson, J. A. Johnson, *J. Neurosci.* **2004**, *24*, 7707–7717.
- [62] H. W. Querfurth, F. M. LaFerla, *N. Engl. J. Med.* **2010**, *362*, 329–344.
- [63] F. M. LaFerla, K. N. Green, S. Oddo, *Nat. Rev. Neurosci.* **2007**, *8*, 499–509.
- [64] R. Postina, *Curr. Alzheimer Res.* **2008**, *5*, 179–186.
- [65] G. Joshi, Y. Wang, *Bioessays* **2015**, *37*, 240–247.
- [66] M. Takami, Y. Nagashima, Y. Sano, S. Ishihara, M. Morishima-Kawashima, S. Funamoto, Y. Ihara, *J. Neurosci.* **2009**, *29*, 13042–13052.
- [67] F. Olsson, S. Schmidt, V. Althoff, L. M. Muntter, S. Jin, S. Rosqvist, U. Lendahl, G. Multhaup, J. Lundkvist, *J. Biol. Chem.* **2014**, *289*, 1540–1550.
- [68] C. M. Carroll, Y. M. Li, *Brain Res. Bull.* **2016**, *126*, 199–206.
- [69] C. L. Masters, G. Simms, N. A. Weinman, G. Multhaup, B. L. McDonald, K. Beyreuther, *Proc. Natl. Acad. Sci. U. S. A.* **1985**, *82*, 4245–4249.
- [70] R. Riek, P. Güntert, H. Döbeli, B. Wipf, K. Wüthrich, *Eur. J. Biochem.* **2001**, *268*, 5930–5936.
- [71] M. A. Findeis, *Pharmacol. Ther.* **2007**, *116*, 266–286.
- [72] E. M. Castaño, J. Ghiso, F. Prelli, P. D. Gorevic, A. Migheli, B. Frangione, *Biochem. Biophys. Res. Commun.* **1986**, *141*, 782–789.
- [73] M. W. Kirschner, T. Mitchison, *Nature* **1986**, *324*, 621.
- [74] D. A. Kirschner, H. Inouye, L. K. Duffy, A. Sinclair, M. Lind, D. J. Selkoe, *Proc. Natl. Acad. Sci. U. S. A.* **1987**, *84*, 6953–6957.
- [75] D. Burdick, B. Soreghan, M. Kwon, J. Kosmoski, M. Knauer, A. Henschen, J. Yates, C. Cotman, C. Glabe, *J. Biol. Chem.* **1992**, *267*, 546–554.
- [76] C. Haass, M. G. Schlossmacher, A. Y. Hung, C. Vigo-Pelfry, A. Mellon, B. L. Ostaszewski, D. Schenk, D. B. Teplow, D. J. Selkoe, *Nature* **1992**, *359*, 322–325.
- [77] S. Oddo, A. Caccamo, J. D. Shepherd, M. P. Murphy, T. E. Golde, R. Kaye, R. Metherate, M. P. Mattson, Y. Akbari, F. M. LaFerla, *Neuron* **2003**, *39*, 409–421.
- [78] S. Oddo, A. Caccamo, L. Tran, M. P. Lambert, C. G. Glabe, W. L. Klein, F. M. LaFerla, *J. Biol. Chem.* **2006**, *281*, 1599–1604.

- [79] J. Wegiel, I. Kuchna, K. Nowicki, J. Frackowiak, B. Mazur-Kolecka, H. Imaki, J. Wegiel, P. D. Mehta, W. P. Silverman, B. Reisberg, et al., *Acta Neuropathol.* **2007**, *113*, 389–402.
- [80] D. J. Selkoe, *Neuron* **1991**, *6*, 487–498.
- [81] D. J. Selkoe, *Physiol. Rev.* **2001**, *81*, 741–760.
- [82] M. I. Olson, C. Shaw, *Brain* **1969**, *92*, 147–156.
- [83] A. Rovelet-Lecrux, D. Hannequin, G. Raux, N. Le Meur, A. Laquerrière, A. Vital, C. Dumanchin, S. Feuillette, A. Brice, M. Vercelletto, et al., *Nat. Genet.* **2006**, *38*, 24–26.
- [84] T. Tomiyama, T. Nagata, H. Shimada, R. Teraoka, A. Fukushima, H. Kanemitsu, H. Takuma, R. Kuwano, M. Imagawa, S. Ataka, et al., *Ann. Neurol.* **2008**, *63*, 377–387.
- [85] J. A. Hardy, G. A. Higgins, *Science* **1992**, *256*, 184–185.
- [86] R. Katzman, M. Zhang, Ouang-Ya-Qu, Z. Wang, W. T. Liu, E. Yu, S. C. Wong, D. P. Salmon, I. Grant, *J. Clin. Epidemiol.* **1988**, *41*, 971–978.
- [87] W. G. Rosen, R. C. Mohs, K. L. Davis, *Am. J. Psychiatry* **1984**, *141*, 1356–1364.
- [88] R. D. Terry, E. Masliah, D. P. Salmon, N. Butters, R. Deteresa, R. Hill, L. A. Hansen, R. Katzman, *Ann. Neurol.* **1991**, *30*, 572–580.
- [89] M. R. D’Andrea, G. M. Cole, M. D. Ard, *Neurobiol. Aging* **2004**, *25*, 675–683.
- [90] Y. Kuo, M. R. Emmerling, C. Vigo-pelfrey, T. C. Kasunic, J. B. Kirkpatrick, G. H. Murdoch, M. J. Ball, A. E. Roher, *J. Biol. Chem.* **1996**, *271*, 4077–4081.
- [91] D. M. Walsh, D. J. Selkoe, *J. Neurochem.* **2007**, *101*, 1172–1184.
- [92] R. Roychaudhuri, M. Yang, M. M. Hoshi, D. B. Teplow, *J. Biol. Chem.* **2009**, *284*, 4749–4753.
- [93] F. Rahimi, A. Shanmugam, G. Bitan, *Curr. Alzheimer Res.* **2008**, *5*, 319–341.
- [94] D. J. Selkoe, J. Hardy, *EMBO Mol. Med.* **2016**, *8*, 595–608.
- [95] J. T. Jarrett, P. T. Lansbury, *Cell* **1993**, *73*, 1055–8.
- [96] M. P. Lambert, A. K. Barlo, B. A. Chromy, C. Edwards, R. Freed, M. Liosatos, T. E. Morgan, I. Rozovsky, B. Trommer, K.L.Viola, et al., *Neurobiology* **21998**, *95*, 6448–6453.
- [97] B. A. Chromy, R. J. Nowak, M. P. Lambert, K. L. Viola, L. Chang, P. T. Velasco, B. W. Jones, S. J. Fernandez, P. N. Lacor, P. Horowitz, et al., *Biochemistry* **2003**, *42*, 12749–12760.
- [98] D. M. Walsh, D. M. Hartley, Y. Kusumoto, Y. Fezoui, M. M. Condron, A. Lomakin, G. B. Benedek, D. J. Selkoe, D. B. Teplow, *J. Biol. Chem.* **1999**, *274*, 25945–25952.
- [99] J. D. Harper, P. T. Lansbury, *Annu. Rev. Biochem.* **1997**, *66*, 385–407.
- [100] J. D. Harper, S. S. Wong, C. M. Lieber, P. T. Lansbury, *Biochemistry* **1999**, *38*, 8972–8980.

- [101] H. Yamaguchi, M. L. C. Maat-Schieman, S. G. Van Duinen, F. A. Prins, P. Neeskens, R. Natté, R. A. C. Roos, *J. Neuropathol. Exp. Neurol.* **2000**, *59*, 723–732.
- [102] T. Kowalewski, D. M. Holtzman, *Proc. Natl. Acad. Sci. U. S. A.* **1999**, *96*, 3688–3693.
- [103] I. Kheterpal, A. Williams, C. Murphy, B. Bledsoe, R. Wetzel, *Biochemistry* **2001**, *40*, 11757–11767.
- [104] M. Arimon, I. Díez-Pérez, M. J. Kogan, N. Durany, E. Giralt, F. Sanz, X. Fernández-Busquets, *FASEB J.* **2005**, *19*, 1344–1346.
- [105] J. Greenwald, R. Riek, *Structure* **2010**, *18*, 1244–1260.
- [106] F. Chiti, C. M. Dobson, *Annu. Rev. Biochem.* **2006**, *75*, 333–366.
- [107] F. Chiti, C. M. Dobson, *Nat. Chem. Biol.* **2009**, *5*, 15–22.
- [108] I. A. Mastrangelo, M. Ahmed, T. Sato, W. Liu, C. Wang, P. Hough, S. O. Smith, *J. Mol. Biol.* **2006**, *358*, 106–119.
- [109] A. Lomakin, D. B. Teplow, D. A. Kirschner, G. B. Benedeki, *Proc. Natl. Acad. Sci. U. S. A.* **1997**, *94*, 7942–7947.
- [110] T. Ban, M. Hoshino, S. Takahashi, D. Hamada, K. Hasegawa, H. Naiki, Y. Goto, *J. Mol. Biol.* **2004**, *344*, 757–767.
- [111] J. Zheng, H. Jang, R. Nussinov, *Biochemistry* **2008**, *47*, 2497–2509.
- [112] M. Necula, R. Kaye, S. Milton, C. G. Glabe, *J. Biol. Chem.* **2007**, *282*, 10311–10324.
- [113] S. I. A. Cohen, M. Vendruscolo, C. M. Dobson, T. P. J. Knowles, *J. Mol. Biol.* **2012**, *421*, 160–171.
- [114] S. Tomaselli, V. Esposito, P. Vangone, N. A. J. Van Nuland, A. M. J. J. Bonvin, R. Guerrini, T. Tancredi, P. A. Temussi, D. Picone, *ChemBioChem* **2006**, *7*, 257–267.
- [115] S. Yun, B. Urbanc, L. Cruz, G. Bitan, D. B. Teplow, H. E. Stanley, *Biophys. J.* **2007**, *92*, 4064–4077.
- [116] T. Lührs, C. Ritter, M. Adrian, D. Riek-loher, B. Bohrmann, H. Do, D. Schubert, R. Riek, *Proc. Natl. Acad. Sci. U. S. A.* **2005**, *102*, 17342–17347.
- [117] Y. Yan, C. Wang, *J. Mol. Biol.* **2006**, *364*, 853–862.
- [118] M. S. Z. Kellermayer, Á. Karsai, M. Benke, K. Soós, B. Penke, *Proc. Natl. Acad. Sci. U. S. A.* **2008**, *105*, 141–144.
- [119] S. Chimon, M. A. Shaibat, C. R. Jones, D. C. Calero, B. Aizezi, Y. Ishii, *Nat. Struct. Mol. Biol.* **2007**, *14*, 1157–1164.
- [120] W. Kim, M. H. Hecht, *Proc. Natl. Acad. Sci. U. S. A.* **2006**, *103*, 15824–15829.
- [121] W. E. Van Nostrand, J. P. Melchor, H. S. Cho, S. M. Greenberg, G. W. Rebeck, *J. Biol. Chem.* **2001**, *276*, 32860–32866.

- [122] C. Nilsberth, C. B. Westlind-Danielsson, A. Eckman, M. M. Condrón, K. Axelman, C. Forsell, C. Stenh, J. Luthman, D. B. Teplow, S. G. Younkin, J. Näslund, et al., *Nat. Neurosci.* **2001**, *4*, 887–893.
- [123] K. Murakami, K. Irie, A. Morimoto, H. Ohigashi, M. Shindo, M. Nagao, T. Shimizu, T. Shirasawa, *Biochem. Biophys. Res. Commun.* **2002**, *294*, 5–10.
- [124] M. A. Leissring, *J. Biol. Chem.* **2008**, *283*, 29645–29649.
- [125] H. Cynis, E. Scheel, T. C. Saido, S. Schilling, H. U. Demuth, *Biochemistry* **2008**, *47*, 7405–7413.
- [126] S. Schilling, U. Zeitschel, T. Hoffmann, U. Heiser, M. Francke, A. Kehlen, M. Holzer, B. Hutter-Paier, M. Prokesch, M. Windisch, et al., *Nat. Med.* **2008**, *14*, 1106–1111.
- [127] S. Schilling, T. Lauber, M. Schaupp, S. Manhart, E. Scheel, G. Böhm, H. U. Demuth, *Biochemistry* **2006**, *45*, 12393–12399.
- [128] J. Näslund, A. Schierhorn, U. Hellman, L. Lannfelt, A. D. Roses, L. O. Tjernberg, J. Silberring, S. E. Gandy, B. Winblad, P. Greengard, et al., *Proc. Natl. Acad. Sci. U. S. A.* **1994**, *91*, 8378–8382.
- [129] T. C. Saido, T. Iwatsubo, D. M. A. Mann, H. Shimada, Y. Ihara, S. Kawashima, *Neuron* **1995**, *14*, 457–466.
- [130] L. Miravalle, M. Calero, M. Takao, A. E. Roher, B. Ghetti, R. Vidal, *Biochemistry* **2005**, *44*, 10810–10821.
- [131] E. D. Eanes, G. G. Glenner, *J. Histochem. Cytochem.* **1968**, *16*, 673–677.
- [132] M. Sunde, L. C. Serpell, M. Bartlam, P. E. Fraser, M. B. Pepys, C. C. F. Blake, *J. Mol. Biol.* **1997**, *273*, 729–739.
- [133] M. W. Schmidt, K. K. Baldridge, J. A. Boatz, S. T. Elbert, M. S. Gordon, J. H. Jensen, S. Koseki, N. Matsunaga, K. A. Nguyen, S. Su, et al., *J. Comput. Chem.* **1993**, *14*, 1347–1363.
- [134] M. S. Z. Kellermayer, L. Grama, A. Karsai, A. Nagy, A. Kahn, Z. L. Datki, B. Penke, *J. Biol. Chem.* **2005**, *280*, 8464–8470.
- [135] A. T. Petkova, Y. Ishii, J. J. Balbach, O. N. Antzutkin, R. D. Leapman, F. Delaglio, R. Tycko, *Proc. Natl. Acad. Sci. U. S. A.* **2002**, *99*, 16742–16747.
- [136] L. C. Serpell, *Biochim. Biophys. Acta* **2000**, *1502*, 16–30.
- [137] C. C. Lee, A. Nayak, A. Sethuraman, G. Belfort, G. J. McRae, *Biophys. J.* **2007**, *92*, 3448–3458.
- [138] H. D. Nguyen, C. K. Hall, *Proc. Natl. Acad. Sci. U. S. A.* **2004**, *101*, 16180–16185.
- [139] G. Bhak, Y. J. Choe, S. R. Paik, *BMB Rep.* **2009**, *42*, 541–551.
- [140] F. Chiti, M. Stefani, N. Taddei, G. Ramponi, C. M. Dobson, *Nature* **2003**, *424*, 805–808.
- [141] E. Gazit, *FASEB J.* **2002**, *16*, 77–83.

- [142] T. R. Jahn, S. E. Radford, *FEBS J.* **2005**, *272*, 5962–5970.
- [143] M. Diociaiuti, R. Bonanni, I. Cariati, C. Frank, G. D'arcangelo, *Int. J. Mol. Sci.* **2021**, *22*, 6435.
- [144] Y. Fezoui, D. M. Hartley, J. D. Harper, R. Khurana, D. M. Walsh, M. M. Condron, D. J. Selkoe, J. Lansbury, A. L. Fink, D. B. Teplow, *Amyloid* **2000**, *7*, 166–178.
- [145] Y. Singh, P. C. Sharpe, H. N. Hoang, A. J. Lucke, A. W. McDowall, S. P. Bottomley, D. P. Fairlie, *Chem. Eur. J.* **2011**, *17*, 151–160.
- [146] N. D. Lazo, M. A. Grant, M. C. Condron, A. C. Rigby, D. B. Teplow, *Protein Sci.* **2009**, *14*, 1581–1596.
- [147] A. T. Petkova, R. D. Leapman, Z. Guo, W. M. Yau, M. P. Mattson, R. Tycko, *Science* **2005**, *307*, 262–265.
- [148] U. Sengupta, A. N. Nilson, R. Kaye, *EBioMedicine* **2016**, *6*, 42–49.
- [149] N. Benseny-Cases, O. Klementieva, J. Maly, J. Cladera, *Curr. Alzheimer Res.* **2012**, *9*, 962–971.
- [150] A. N. Santos, S. Torkler, D. Nowak, C. Schlittig, M. Goerdes, T. Lauber, L. Trischmann, M. Schaupp, M. Penz, F. W. Tiller, et al., *J. Alzheimer's Dis.* **2007**, *11*, 117–125.
- [151] G. M. Shankar, S. Li, T. H. Mehta, A. Garcia-Munoz, N. E. Shepardson, I. Smith, F. M. Brett, M. A. Farrell, M. J. Rowan, C. A. Lemere, et al., *Nat. Med.* **2008**, *14*, 837–842.
- [152] M. B. Podlisny, B. L. Ostaszewski, S. L. Squazzo, E. H. Koo, R. E. Rydell, D. B. Teplow, D. J. Selkoe, *J. Biol. Chem.* **1995**, *270*, 9564–9570.
- [153] S. Lesné, T. K. Ming, L. Kotilinek, R. Kaye, C. G. Glabe, A. Yang, M. Gallagher, K. H. Ashe, *Nature* **2006**, *440*, 352–357.
- [154] G. Bitan, M. D. Kirkitadze, A. Lomakin, S. S. Vollers, G. B. Benedek, D. B. Teplow, *Proc. Natl. Acad. Sci. U. S. A.* **2003**, *100*, 330–335.
- [155] S. Barghorn, V. Nimmrich, A. Striebinger, G. Krantz, P. Keller, B. Janson, M. Bahr, M. Schmidt, R. S. Bitner, J. Harlan, et al., *J. Neurochem.* **2005**, *95*, 834–847.
- [156] Y. Harigaya, M. Shoji, T. Kawarabayashi, M. Kanai, T. Nakamura, T. Lizuka, Y. Igeta, T. C. Saido, N. Sahara, H. Mori, et al., *Biochem. Biophys. Res. Commun.* **1995**, *211*, 1015–1022.
- [157] A. E. Roher, J. D. Lowenson, S. Clarke, A. S. Woods, R. J. Cotter, E. Gowing, M. J. Ball, *Proc. Natl. Acad. Sci. U. S. A.* **1993**, *90*, 10836–10840.
- [158] I. Kuperstein, K. Broersen, I. Benilova, J. Rozenski, W. Jonckheere, M. Debulpaep, A. Vandersteen, I. Segers-Nolten, K. Van Der Werf, V. Subramaniam, et al., *EMBO J.* **2010**, *29*, 3408–3420.
- [159] G. M. Shankar, B. L. Bloodgood, M. Townsend, D. M. Walsh, D. J. Selkoe, B. L. Sabatini, *J. Neurosci.* **2007**, *27*, 2866–2875.
- [160] D. M. Walsh, I. Klyubin, J. V. Fadeeva, W. K. Cullen, R. Anwyl, M. S. Wolfe, M. J. Rowan, D. J. Selkoe, *Nature* **2002**, *416*, 535–539.

- [161] J. P. Cleary, D. M. Walsh, J. J. Hofmeister, G. M. Shankar, M. A. Kuskowski, D. J. Selkoe, K. H. Ashe, *Nat. Neurosci.* **2005**, *8*, 79–84.
- [162] K. H. Ashe, K. R. Zahs, *Neuron* **2010**, *66*, 631–645.
- [163] G. Bitan, M. D. Kirkitadze, A. Lomakin, S. S. Vollers, G. B. Benedek, D. B. Teplow, *Proc. Natl. Acad. Sci. U. S. A.* **2003**, *100*, 330–335.
- [164] W. B. Stine, K. N. Dahlgren, G. A. Krafft, M. J. LaDu, *J. Biol. Chem.* **2003**, *278*, 11612–11622.
- [165] M. Ahmed, J. Davis, D. Aucoin, T. Sato, S. Ahuja, S. Aimoto, J. I. Elliott, W. E. Van Nostrand, S. O. Smith, *Nat. Struct. Mol. Biol.* **2010**, *17*, 561–567.
- [166] K. Broersen, F. Rousseau, J. Schymkowitz, *Alzheimer's Res. Ther.* **2010**, *2*, 12.
- [167] S. I. A. Cohen, S. Linse, L. M. Luheshi, E. Hellstrand, D. A. White, L. Rajah, D. E. Otzen, M. Vendruscolo, C. M. Dobson, T. P. J. Knowles, *Proc. Natl. Acad. Sci. U. S. A.* **2013**, *110*, 9758–9763.
- [168] I. C. Martins, I. Kuperstein, H. Wilkinson, E. Maes, M. Vanbrabant, W. Jonckheere, P. Van Gelder, D. Hartmann, R. D'Hooge, B. De Strooper, et al., *EMBO J.* **2008**, *27*, 224–233.
- [169] R. W. Hepler, K. M. Grimm, D. D. Nahas, R. Breese, E. C. Dodson, P. Acton, P. M. Keller, M. Yeager, H. Wang, P. Shughrue, et al., *Biochemistry* **2006**, *45*, 15157–15167.
- [170] I. Randrianjatovo-Gbalou, C. E. Marcato-Romain, E. Girbal-Neuhauser, *Anal. Biochem.* **2015**, *488*, 19–21.
- [171] C. Ricci, F. Spinozzi, P. Mariana, maria grazia Ortore, *Curr. Pharm. Des.* **2016**, *22*, 3937–3949.
- [172] V. Lattanzi, I. André, U. Gasser, M. Dubackic, U. Olsson, S. Linse, *Proc. Natl. Acad. Sci. U. S. A.* **2021**, *118*, 6–11.
- [173] D. C. Rambaldi, A. Zattoni, P. Reschiglian, R. Colombo, E. De Lorenzi, *Anal. Bioanal. Chem.* **2009**, *394*, 2145–2149.
- [174] D. M. Walsh, M. Townsend, M. B. Podlisny, G. M. Shankar, J. V. Fadeeva, O. El Agnaf, D. M. Hartley, D. J. Selkoe, *J. Neurosci.* **2005**, *25*, 2455–2462.
- [175] M. M. Murray, S. L. Bernstein, V. Nyugen, M. M. Condron, D. B. Teplow, M. T. Bowers, *J. Am. Chem. Soc.* **2009**, *131*, 6316–6317.
- [176] G. P. Gellermann, H. Byrnes, A. Striebinger, K. Ullrich, R. Mueller, H. Hillen, S. Barghorn, *Neurobiol. Dis.* **2008**, *30*, 212–220.
- [177] A. Deshpande, E. Mina, C. Glabe, J. Busciglio, *J. Neurosci.* **2006**, *26*, 6011–6018.
- [178] M. Hoshi, M. Sato, S. Matsumoto, A. Noguchi, K. Yasutake, N. Yoshida, K. Sato, *Proc. Natl. Acad. Sci. U. S. A.* **2003**, *100*, 6370–6375.
- [179] A. Noguchi, S. Matsumura, M. Dezawa, M. Tada, M. Yanazawa, A. Ito, M. Akioka, S. Kikuchi, M. Sato, M. Noda, et al., *J. Biol. Chem.* **2009**, *284*, 32895–32905.

- [180] H. A. Lashuel, D. M. Hartley, B. M. Petre, J. S. Wall, M. N. Simon, T. Walz, P. T. Lansbury, *J. Mol. Biol.* **2003**, 332, 795–808.
- [181] B. Caughey, P. T. Lansbury, *Annu. Rev. Neurosci.* **2003**, 26, 267–298.
- [182] D. B. Teplow, *Amyloid* **1998**, 5, 121–142.
- [183] J. T. Jarrett, E. P. Berger, P. T. Lansbury, *Biochemistry* **1993**, 32, 4693–4697.
- [184] C. Bate, A. Williams, *J. Alzheimer's Dis.* **2010**, 21, 985–993.
- [185] K. Pauwels, T. L. Williams, K. L. Morris, W. Jonckheere, A. Vandersteen, G. Kelly, J. Schymkowitz, F. Rousseau, A. Pastore, L. C. Serpell, et al., *J. Biol. Chem.* **2012**, 287, 5650–5660.
- [186] M. Nutu, H. Zetterberg, E. Londos, L. Minthon, K. Nägga, K. Blennow, O. Hansson, A. Öhrfelt, *Dement. Geriatr. Cogn. Disord.* **2013**, 36, 99–110.
- [187] C. C. Chang, J. C. Althaus, C. J. L. Carruthers, M. A. Sutton, D. G. Steel, A. Gafni, *PLoS One* **2013**, 8, 1–11.
- [188] H. Hampel, J. Hardy, K. Blennow, C. Chen, G. Perry, S. H. Kim, V. L. Villemagne, A. Paul, V. Michele, T. Iwatsubo, et al., *Mol. Psychiatry* **2021**, 26, 5481–5503.
- [189] I. A. Ahanger, Z. A. Parray, K. Nasreen, F. Ahmad, M. I. Hassan, A. Islam, A. Sharma, *ACS Omega* **2021**, 6, 2328–2339.
- [190] M. S. Malamas, J. Erdei, I. Gunawan, K. Barnes, Y. Hui, M. Johnson, A. Robichaud, P. Zhou, Y. Yan, W. Solvibile, et al., *Bioorganic Med. Chem. Lett.* **2011**, 21, 5164–5170.
- [191] M. Mandal, Y. Wu, J. Misiaszek, G. Li, A. Buevich, J. P. Caldwell, X. Liu, R. D. Mazzola, P. Orth, C. Strickland, et al., *J. Med. Chem.* **2016**, 59, 3231–3248.
- [192] A. Ortega, Á. Rincón, K. L. Jiménez-Aliaga, P. Bermejo-Bescós, S. Martín-Aragón, M. T. Molina, A. G. Csáky, *Bioorganic Med. Chem. Lett.* **2011**, 21, 2183–2187.
- [193] M. Mehta, A. Adem, M. Sabbagh, *Int. J. Alzheimer's Dis.* **2012**, 2012, 1–7.
- [194] M. Weinstock, L. Luques, T. Poltyrev, C. Bejar, S. Shoham, *Neurobiol. Aging* **2011**, 32, 1069–1078.
- [195] A. Hiremathad, K. Chand, L. Tolayan, Rajeshwari, R. S. Keri, A. R. Esteves, S. M. Cardoso, S. Chaves, M. A. Santos, *J. Inorg. Biochem.* **2018**, 179, 82–96.
- [196] N. De Vera, E. Martínez, C. Sanfeliu, *J. Neurosci. Res.* **2008**, 86, 861–872.
- [197] M. Talantovaa, S. Sanz-Blascoa, X. Zhanga, Peng Xiaa, M. W. Akhtara, S. Okamotoa, T. N. Gustavo Dziewczapolskib, G. Caoa, A. E. Pratta, Y.-J. Kanga, et al., *Proc. Natl. Acad. Sci. U. S. A.* **2013**, 110, 2518–2527.
- [198] A. Horwich, *J. Clin. Invest.* **2002**, 110, 1221–1232.
- [199] T. S. Jarvela, H. A. Lam, M. Helwig, N. Lorenzen, D. E. Otzen, P. J. McLean, N. T. Maidment, I. Lindberg, *Proc. Natl. Acad. Sci. U. S. A.* **2016**, 113, E4708–E4715.

- [200] Y. Porat, A. Abramowitz, E. Gazit, *Chem. Biol. Drug Des.* **2006**, *67*, 27–37.
- [201] E. Takai, K. Uda, T. Yoshida, T. Zako, M. Maeda, K. Shiraki, *Phys. Chem. Chem. Phys.* **2014**, *16*, 3566–3572.
- [202] J. Kumar, V. Sim, *Prion* **2014**, *8*, 37–41.
- [203] B. Neddenriep, A. Calciano, D. Conti, E. Sauve, M. Paterson, E. Bruno, D. A. Moffet, *Open Biotechnol. J.* **2012**, *5*, 39–46.
- [204] T. Kawasaki, S. Kamijo, *Biosci. Biotechnol. Biochem.* **2012**, *76*, 762–766.
- [205] D. Goyal, S. Shuaib, S. Mann, B. Goyal, *ACS Comb. Sci.* **2017**, *19*, 55–80.
- [206] T. Kawasaki, K. Onodera, S. Kamijo, *Biosci. Biotechnol. Biochem.* **2010**, *74*, 2214–2219.
- [207] J. R. Horsley, B. Jovcevski, K. L. Wegener, J. Yu, T. L. Pukala, A. D. Abell, *Biochem. J.* **2020**, *477*, 1541–1564.
- [208] H. Sun, J. Liu, S. Li, L. Zhou, J. Wang, L. Liu, F. Lv, Q. Gu, B. Hu, Y. Ma, et al., *Angew. Chem. Int. Ed.* **2019**, *58*, 5988–5993.
- [209] F. Xia, X. Zuo, R. Yang, Y. Xiao, D. Kang, A. Vallée-Bélisle, X. Gong, J. D. Yuen, B. B. Y. Hsu, A. J. Heeger, et al., *Proc. Natl. Acad. Sci. U. S. A.* **2010**, *107*, 10837–10841.
- [210] C. Cabaleiro-Lago, F. Quinlan-Pluck, I. Lynch, S. Lindman, A. M. Minogue, E. Thulin, D. M. Walsh, K. A. Dawson, S. Linse, *J. Am. Chem. Soc.* **2008**, *130*, 15437–15443.
- [211] P. M. H. Heegaard, H. G. Pedersen, J. Flink, U. Boas, *FEBS Lett.* **2004**, *577*, 127–133.
- [212] C. R. Becer, L. Hartman, Eds. , *Glycopolymer Code: Synthesis of Glycopolymers and Their Applications*, Royal Society Of Chemistry, **2015**.
- [213] B. Klajnert, D. Appelhans, H. Komber, N. Morgner, S. Schwarz, S. Richter, B. Brutschy, M. Ionov, A. K. Tonkikh, M. Bryszewska, et al., *Chem. Eur. J* **2008**, *14*, 7030–7041.
- [214] D. Appelhans, A. Klajnert-Maculewicz, Barbara Janaszewska, L. Joanna, B. Voit, *Chem. Soc. Rev.* **2015**, *44*, 3968–3996.
- [215] L. Zuroff, D. Daley, K. L. Black, M. Koronyo-Hamaoui, *Cell Mol. Life Sci.* **2017**, *74*, 2167–2201.
- [216] U.S. National Library of Medicine, “ClinicalTrials.gov”, <https://www.clinicaltrials.gov/>, accessed on 30th March 2022.
- [217] J. Birks, *Cochrane Database Syst. Rev.* **2012**, 1–91.
- [218] S. A. Areosa, F. Sherriff, R. McShane, *Cochrane Database Syst. Rev.* **2005**, 1–80.
- [219] G. Alva, J. L. Cummings, *Psychiatry (Edgmont)*. **2008**, *5*, 27–36.
- [220] M. R. Farlow, G. Alva, X. Meng, J. T. Olin, *Curr. Med. Res. Opin.* **2010**, *26*, 263–269.
- [221] R. F. Zec, N. R. Burkett, *NeuroRehabilitation* **2008**, *23*, 425–438.
- [222] J. Cummings, G. Lee, K. Zhong, J. Fonseca, K. Taghva, *Alzheimer’s Dement. Transl. Res. Clin. Interv.* **2021**, *7*, 1–24.

- [223] R. S. Doody, R. Raman, M. Farlow, T. Iwatsubo, B. Vellas, S. Joffe, K. Kieburtz, F. He, X. Sun, R. G. Thomas, et al., *N. Engl. J. Med.* **2013**, *369*, 341–350.
- [224] V. Coric, S. Salloway, C. H. Van Dyck, B. Dubois, N. Andreasen, M. Brody, C. Curtis, H. Soininen, S. Thein, T. Shiovitz, et al., *JAMA Neurol.* **2015**, *72*, 1324–1333.
- [225] E. Muntimadugu, R. Dhommatti, A. Jain, V. G. S. Challa, M. Shaheen, W. Khan, *Eur. J. Pharm. Sci.* **2016**, *92*, 224–234.
- [226] J. Cummings, G. Lee, A. Ritter, M. Sabbagh, K. Zhong, *Alzheimer's Dement. Transl. Res. Clin. Interv.* **2019**, *5*, 272–293.
- [227] T. Burki, *Lancet* **2018**, *391*, 2486.
- [228] M. F. Egan, J. Kost, T. Voss, Y. Mukai, P. S. Aisen, J. L. Cummings, P. N. Tariot, B. Vellas, C. H. van Dyck, M. Boada, et al., *N. Engl. J. Med.* **2019**, *380*, 1408–1420.
- [229] D. Henley, N. Raghavan, R. Sperling, P. Aisen, R. Raman, G. Romano, *N. Engl. J. Med.* **2019**, *380*, 1483–1485.
- [230] B. Vellas, O. Sol, P. J. Snyder, P.-J. Ousset, R. Haddad, M. Maurin, J.-C. Lemarie, L. Desire, M. P. Pando, *Curr. Alzheimer Res.* **2011**, *999*, 1–10.
- [231] S. Salloway, R. Sperling, R. Keren, A. P. Porsteinsson, C. H. Van Dyck, P. N. Tariot, S. Gilman, D. Arnold, S. Abushakra, C. Hernandez, et al., *Neurology* **2011**, *77*, 1253–1262.
- [232] T. Stark, T. Lieblein, M. Pohland, E. Kalden, P. Freund, R. Zangl, R. Grewal, M. Heilemann, G. P. Eckert, N. Morgner, et al., *Biochemistry* **2017**, *56*, 4840–4849.
- [233] A. Nimmagadda, Y. Shi, J. Cai, *Curr. Med. Chem.* **2019**, *26*, 2313–2329.
- [234] K. G. Yiannopoulou, S. G. Papageorgiou, *Ther. Adv. Neurol. Disord.* **2013**, *6*, 19–33.
- [235] H. S. Krishnan, V. Bernard-Gauthier, M. S. Placzek, K. Dahl, V. Narayanaswami, E. Livni, Z. Chen, J. Yang, T. L. Collier, C. Ran, et al., *Mol. Pharm.* **2018**, *15*, 695–702.
- [236] V. L. Villemagne, C. C. Rowe, K. J. Barnham, R. Cherny, M. Woodward, S. Bozinosvski, O. Salvado, P. Bourgeat, K. Perez, C. Fowler, et al., *Alzheimer's Dement. Transl. Res. Clin. Interv.* **2017**, *3*, 622–635.
- [237] T. Wisniewski, F. Goñi, *Neuron* **2015**, *85*, 1162–1176.
- [238] J. M. O. S. Gilman, M. Koller, R.S. Black, L. Jenkins, S.G. Griffith, N.C. Fox, L. Eisner, L. Kirby, M. Boada Rovira, F. Forette, *Neurology* **2005**, *64*, 1553–1562.
- [239] C. Lopez Lopez, P. N. Tariot, A. Caputo, J. B. Langbaum, F. Liu, M. E. Riviere, C. Langlois, M. L. Rouzade-Dominguez, M. Zalesak, S. Hendrix, et al., *Alzheimer's Dement. Transl. Res. Clin. Interv.* **2019**, *5*, 216–227.
- [240] A. M. Lacosta, M. Pascual-Lucas, P. Pesini, D. Casabona, V. Pérez-Grijalba, I. Marcos-Campos, L. Sarasa, J. Canudas, H. Badi, I. Monleón, et al., *Alzheimer's Res. Ther.* **2018**, *10*, 1–13.
- [241] H. Kim, E. H. Seo, S. H. Lee, B. J. Kim, *Int. J. Mol. Sci.* **2016**, *17*, 1–8.

- [242] M. Hull, C. Sadowsky, H. Arai, G. L. P. Leterme, A. Holstein, K. Booth, Y. Peng, T. Yoshiyama, H. Suzuki, N. Ketter, et al., *Curr. Alzheimer Res.* **2017**, *14*, 696–708.
- [243] C. Y. Wang, P. N. Wang, M. J. Chiu, C. L. Finstad, F. Lin, S. Lynn, Y. H. Tai, X. De Fang, K. Zhao, C. H. Hung, et al., *Alzheimer's Dement. Transl. Res. Clin. Interv.* **2017**, *3*, 262–272.
- [244] H. Davtyan, A. Ghochikyan, I. Petrushina, A. Hovakimyan, A. Davtyan, A. Poghosyan, A. M. Marleau, N. Movsesyan, A. Kiyatkin, S. Rasool, et al., *J. Neurosci.* **2013**, *33*, 4923–4934.
- [245] T. Wisniewski, U. Konietzko, *Lancet Neurol.* **2008**, *7*, 805–811.
- [246] D. L. Brody, D. M. Holtzman, *Bone* **2008**, *31*, 175–193.
- [247] M. Boada, O. López, L. Núñez, Z. M. Szczepiorkowski, M. Torres, C. Grifols, A. Páez, *Alzheimer's Dement. Transl. Res. Clin. Interv.* **2019**, *5*, 61–69.
- [248] E. R. Gillies, J. M. J. Fréchet, *Drug Discov. Today* **2005**, *10*, 35–43.
- [249] S. Svenson, D. A. Tomalia, *Adv. Drug Deliv. Rev.* **2012**, *64*, 102–115.
- [250] S. Svenson, *Eur. J. Pharm. Biopharm.* **2009**, *71*, 445–462.
- [251] A. K. Patri, I. J. Majoros, J. R. Baker, *Curr. Opin. Chem. Biol.* **2002**, *6*, 466–471.
- [252] B. K. Nanjwade, H. M. Bechra, G. K. Derkar, F. V. Manvi, V. K. Nanjwade, *Eur. J. Pharm. Sci.* **2009**, *38*, 185–196.
- [253] E. Herczenik, M. F. B. G. Gebbink, *FASEB J.* **2008**, *22*, 2115–2133.
- [254] V. Buzón, E. Padrós, J. Cladera, *Biochemistry* **2005**, *44*, 13354–13364.
- [255] B. Klajnert, J. Cladera, M. Bryszewska, *Biomacromolecules* **2006**, *7*, 2186–2191.
- [256] B. Klajnert, M. Cangioti, S. Calici, J. P. Majoral, A. M. Caminade, J. Cladera, M. Bryszewska, M. F. Ottaviani, *Macromol. Biosci.* **2007**, *7*, 1065–1074.
- [257] M. Fischer, D. Appelhans, S. Schwarz, B. Klajnert, M. Bryszewska, B. Voit, M. Rogers, *Biomacromolecules* **2010**, *11*, 1314–1325.
- [258] M. Bucciantini, E. Giannoni, F. Chiti, F. Baroni, N. Taddei, G. Ramponi, C. M. Dobson, M. Stefani, *Nature* **2002**, *416*, 507–511.
- [259] H. Mukai, T. Isagawa, E. Goyama, S. Tanaka, N. F. Bence, A. Tamura, Y. Ono, R. R. Kopito, *Proc. Natl. Acad. Sci. U. S. A.* **2005**, *102*, 10887–10892.
- [260] M. Bucciantini, S. Rigacci, A. Berti, L. Pieri, C. Cecchi, D. Nosi, L. Formigli, F. Chiti, M. Stefani, *FASEB J.* **2005**, *19*, 1–23.
- [261] B. Klajnert, M. Cangioti, S. Calici, M. Ionov, J. P. Majoral, A. M. Caminade, J. Cladera, M. Bryszewska, M. F. Ottaviani, *New J. Chem.* **2009**, *33*, 1087–1093.
- [262] B. Ziemia, A. Janaszewska, K. Ciepluch, M. Krotewicz, W. A. Fogel, D. Appelhans, B. Voit, M. Bryszewska, B. Klajnert, *J. Biomed. Mater. Res. A* **2011**, *99 A*, 261–268.

- [263] A. Felczak, N. Wrońska, A. Janaszewska, B. Klajnert, M. Bryszewska, D. Appelhans, B. Voit, S. Różalska, K. Lisowska, *New J. Chem.* **2012**, *36*, 2215–2222.
- [264] A. Janaszewska, J. Lazniewska, P. Trzepiński, M. Marcinkowska, B. Klajnert-Maculewicz, *Biomolecules* **2019**, *9*, 330.
- [265] O. Klementieva, Influence of Cu (II) and Glycodendrimers on Amyloid-Beta Peptide Aggregation Oxana Klementieva Influence of Cu (II) and Glycodendrimers on Amyloid-Beta Peptide Aggregation, Doctoral dissertation, Universitat Internacional de Catalunya, **2012**.
- [266] B. Ziembra, I. Halets, D. Shcharbin, D. Appelhans, B. Voit, I. Pieszynski, M. Bryszewska, B. Klajnert, *J. Biomed. Mater. Res. A* **2012**, *100*, 2870–2880.
- [267] A. Janaszewska, B. Ziembra, K. Ciepluch, D. Appelhans, B. Voit, B. Klajnert, M. Bryszewska, *New J. Chem. New J. Chem* **2012**, *36*, 350–353.
- [268] A. Janaszewska, B. Klajnert-Maculewicz, M. Marcinkowska, P. Duchnowicz, D. Appelhans, G. Grasso, M. A. Deriu, A. Danani, M. Cangiotti, M. F. Ottaviani, *Nano Res.* **2018**, *11*, 1204–1226.
- [269] E. Aso, I. Martinsson, D. Appelhans, C. Effenberg, N. Benseny-Cases, J. Cladera, G. Gouras, I. Ferrer, O. Klementieva, *Nanomed.: Nanotechnol. Biol. Med.* **2019**, *17*, 198–209.
- [270] E. Buhleier, W. Wehner, F. Völgte, *Synthesis* **1978**, *2*, 155–158.
- [271] D. A. Tomalia, H. Baker, J. Dewald, M. Hall, G. Kallos, S. Martin, J. Roeck, J. Ryder, P. Smith, *Polym. J.* **1985**, *17*, 117–132.
- [272] D. A. Tomalia, J. M. J. Fréchet, *J. Polym. Sci. A Polym. Chem.* **2002**, *40*, 2719–2728.
- [273] G. R. Newkome, Z. Yao, G. R. Baker, V. K. Gupta, *J. Org. Chem.* **1985**, *50*, 2003–2004.
- [274] A. W. Bosman, H. M. Janssen, E. W. Meijer, *Chem. Rev.* **1999**, *99*, 1665–1688.
- [275] Y. Kim, S. C. Zimmerman, *Curr. Opin. Chem. Biol.* **1998**, *2*, 733–742.
- [276] D. K. Smith, F. Diederich, *Chem. Eur. J.* **1998**, *4*, 1353–1361.
- [277] S. E. Stiriba, H. Frey, R. Haag, *Angew. Chem. Int. Ed.* **2002**, *41*, 1329–1334.
- [278] B. I. Voit, A. Lederer, *Chem. Rev.* **2009**, 5924–5973.
- [279] B. Klajnert, M. Bryszewska, *Acta Biochim. Pol.* **2000**, *48*, 199–208.
- [280] F. Zeng, S. C. Zimmerman, *Chem. Rev.* **1997**, *97*, 1681–1712.
- [281] A. Herrmann, G. Mihov, G. W. M. Vandermeulen, H. A. Klok, K. Müllen, *Tetrahedron* **2003**, *59*, 3925–3935.
- [282] A. Sánchez, A. Villalonga, G. Martínez-García, C. Parrado, R. Villalonga, *Nanomaterials* **2019**, *9*, 1–18.
- [283] R. W. J. Scott, O. M. Wilson, R. M. Crooks, *J. Phys. Chem. B* **2005**, *109*, 692–704.

- [284] M. S. Diallo, S. Christie, P. Swaminathan, J. H. Johnson, W. A. Goddard, *Environ. Sci. Technol.* **2005**, *39*, 1366–1377.
- [285] M. B. Wazir, M. Daud, F. Ali, M. A. Al-Harhi, *J. Mol. Liq.* **2020**, *315*, 113775.
- [286] H. Tokuhisa, M. Zhao, L. A. Baker, V. T. Phan, D. L. Dermody, M. E. Garcia, R. F. Peez, R. M. Crooks, T. M. Mayer, *J. Am. Chem. Soc.* **1998**, *120*, 4492–4501.
- [287] D. Astruc, F. Chardac, *Chem. Rev.* **2001**, *101*, 2991–3023.
- [288] J. B. Wolinsky, M. W. Grinstaff, *Adv. Drug Deliv. Rev.* **2008**, *60*, 1037–1055.
- [289] Y. Cheng, Z. Xu, M. Ma, T. Xu, *J. Pharm. Sci.* **2008**, *97*, 123–143.
- [290] M. Wang, H. Liu, L. Li, Y. Cheng, *Nat. Commun.* **2014**, *5*, 1–8.
- [291] J. F. G. A. Jansen, E. M. M. de B. den Berg, E. W. Meijer, *Science* **1994**, *226*, 1226–1229.
- [292] F. Vögtle, *Dendrimers II: Architecture, Nanostructure and Supramolecular Chemistry*, Springer Berlin, Heidelberg, **2000**.
- [293] P. E. Froehling, *Dye. Pigment.* **2001**, *48*, 187–195.
- [294] J. M. J. Fréchet, D. A. Tomalia, Eds., *Dendrimers and Other Dendritic Polymers*, John Wiley & Sons, Ltd., **2001**.
- [295] V. Maraval, R. Laurent, P. Marchand, A. M. Caminade, J. P. Majoral, *J. Organomet. Chem.* **2005**, *690*, 2458–2471.
- [296] H. Ihre, A. Hult, E. Söderlind, *J. Am. Chem. Soc.* **1996**, *118*, 6388–6395.
- [297] H. Ihre, A. Hult, J. M. J. Fréchet, I. Gitsov, *Macromolecules* **1998**, *31*, 4061–4068.
- [298] P. Kolhe, J. Khandare, O. Pillai, S. Kannan, M. Lieh-Lai, R. M. Kannan, *Biomaterials* **2006**, *27*, 660–669.
- [299] J. Dandliker, F. Diederich, A. Zingg, J. Gisselbrecht, M. Gross, A. Louati, E. Sanford, *Helv. Chim. Acta* **1997**, *80*, 1773–1801.
- [300] S. Hecht, J. M. J. Fréchet, *Angew. Chem. Int. Ed.* **2001**, *40*, 74–91.
- [301] S. G. Y. Xiao, H. Hong, A. Javadi, J. W. Engle, W. Xu, Y. Yang, Y. Zhang, T. E. Barnhart, W. Cai, *Biomaterials* **2012**, *33*, 3071–3082.
- [302] D. Appelhans, B. Klajnert-Maculewicz, A. Janaszewska, J. Lazniewska, B. Voit, *Chem. Soc. Rev.* **2015**, *44*, 3968–3996.
- [303] C. R. Becer, L. Hartman, Eds., *Glycopolymer Code: Synthesis of Glycopolymers and Their Applications*, Royal Society Of Chemistry, **2015**.
- [304] S. Svenson, *Chem. Soc. Rev.* **2015**, *44*, 4131–4144.
- [305] B. I. Voit, A. Lederer, *Chem. Rev.* **2009**, *109*, 5924–5973.

- [306] A. Lederer, W. Buchard, *Hyperbranched Polymers: Macromolecules in between Deterministic Linear Chains and Dendrimer Structures*, Royal Society Of Chemistry, **2015**.
- [307] A. Hult, M. Johansson, E. Malmström, in *Branched Polymers II* (Ed.: J. Roovers), **1999**, pp. 1–34.
- [308] P. Froehling, *J. Polym. Sci. A Polym. Chem.* **2004**, *42*, 3110–3115.
- [309] B. Voit, *J. Polym. Sci. A Polym. Chem.* **2005**, *43*, 2679–2699.
- [310] C. Gao, D. Yan, *Prog. Polym. Sci.* **2004**, *29*, 183–275.
- [311] C. R. Yates, W. Hayes, *Eur. Polym. J.* **2004**, *40*, 1257–1281.
- [312] B. Bruchmann, *Macromol. Mater. Eng.* **2007**, *292*, 981–992.
- [313] J. F. Stumbé, B. Bruchmann, *Macromol. Rapid Commun.* **2004**, *25*, 921–924.
- [314] S. Abbina, S. Vappala, P. Kumar, E. M. J. Siren, C. C. La, U. Abbasi, D. E. Brooks, J. N. Kizhakkedathu, *J. Mater. Chem. B* **2017**, *5*, 9249–9277.
- [315] R. Haag, M. Radowski, *M. WIPO Patent Application WO/2006/018295*.
- [316] Malkoch, M., Malmström, E., Hult, A., Wallner, M., Gustafsson, L. “Polymer Factory,” <https://www.polymerfactory.com/>, accessed on 23rd June 2022.
- [317] C. J. Hawker, F. Chu, *Macromolecules* **1996**, *29*, 4370–4380.
- [318] M. Jikei, M. A. Kakimoto, *J. Polym. Sci. A Polym. Chem.* **2004**, *42*, 1293–1309.
- [319] D. Hölder, H. Frey, *Acta Polym.* **1997**, *48*, 298–309.
- [320] D. Hölder, A. Burgath, H. Frey, *Acta Polym.* **1997**, *48*, 30–35.
- [321] R. Hanselmann, D. Hölder, H. Frey, *Macromolecules* **1998**, *31*, 3790–3801.
- [322] J. Wang, D. M. Johnson, *Polym. Int.* **2009**, *58*, 1234–1245.
- [323] W. Huang, L. Su, Z. Bo, *J. Am. Chem. Soc.* **2009**, *131*, 10348–10349.
- [324] C. Lach, H. Frey, *Macromolecules* **1998**, *31*, 2381–2383.
- [325] R. Haag, J. F. Stumbé, A. Sunder, H. Frey, A. Hebel, *Macromolecules* **2000**, *33*, 8158–8166.
- [326] R. Haag, A. Sunder, J. F. Stumbé, *J. Am. Chem. Soc.* **2000**, *122*, 2954–2955.
- [327] A. Lederer, T. Hartmann, H. Komber, *Macromol. Rapid Commun.* **2012**, *33*, 1440–1444.
- [328] A. Lederer, W. Burchard, T. Hartmann, J. S. Haataja, N. Houbenov, A. Janke, P. Friedel, R. Schweins, P. Lindner, *Angew. Chem. Int. Ed.* **2015**, *54*, 12578–12583.
- [329] P. J. Flory, *Principles of Polymer Chemistry*, Cornell University Press, **1953**.
- [330] Y. H. Kim, O. W. Webster, *Macromolecules* **1992**, *25*, 5561–5572.
- [331] C. J. Hawker, R. Lee, J. M. J. Fréchet, *J. Am. Chem. Soc.* **1991**, *113*, 4583–4588.

- [332] D. Yan, A. H. E. Muller, K. Matyjaszewski, *Macromolecules* **1997**, *30*, 7024–7033.
- [333] L. J. Markoski, J. L. Thompson, J. S. Moore, *Macromolecules* **2002**, *35*, 1599–1603.
- [334] W. Daniel, S. E. Stiriba, F. Holger, *Acc. Chem. Res.* **2010**, *43*, 129–141.
- [335] M. Calderón, M. A. Quadir, S. K. Sharma, R. Haag, *Adv. Mater.* **2010**, *22*, 190–218.
- [336] S. Firdaus, M. Geisler, P. Friedel, S. Banerjee, D. Appelhans, B. Voit, A. Lederer, *Macromol. Rapid Commun.* **2018**, *39*, 1800364.
- [337] N. Feliu, M. V. Walter, M. I. Montañez, A. Kunzmann, A. Hult, A. Nyström, M. Malkoch, B. Fadeel, *Biomaterials* **2012**, *33*, 1970–1981.
- [338] M. C. Parrott, S. R. Benhabbour, C. Saab, J. a Lemon, S. Parker, J. F. Valliant, A. Adronov, *J. Am. Chem. Soc.* **2009**, *131*, 2906–2916.
- [339] M. Malkoch, E. Malmström, A. Hult, *Macromolecules* **2002**, *35*, 8307–8314.
- [340] A. Carlmark, E. Malmström, M. Malkoch, *Chem. Soc. Rev.* **2013**, *42*, 5858.
- [341] T. Dutta, N. K. Jain, *Biochim. Biophys. Acta Gen. Subj.* **2007**, *1770*, 681–686.
- [342] N. L. Andon, D. Eckert, J. R. Yates, P. A. Haynes, *Proteomics* **2003**, *3*, 1270–1278.
- [343] J. H. Naismith, C. Emmerich, J. Habash, S. J. Harrop, J. R. Helliwell, W. N. Hunter, J. Raftery, A. J. Kalb, J. Yariv, *Acta Cryst.* **1994**, *D50*, 847–858.
- [344] M. Larvie, T. Shoup, W. C. Chang, L. Chigweshe, K. Hartshorn, M. R. White, G. L. Stahl, D. R. Elmaleh, K. Takahashi, *J. Biomed. Biotechnol.* **2012**, *2012*, 7–10.
- [345] B. H. Zimm, *J. Chem. Phys.* **1948**, *16*, 1099–1116.
- [346] J. C. Giddings, *Sep. Sci.* **1966**, *1*, 123–125.
- [347] M. E. Schimpf, K. Caldwell, J. C. Giddings, Eds. , *Field Flow Fractionation Handbook*, John Wiley & Sons, **2000**.
- [348] B. Chu, *Laser Light Scattering: Basic Principles and Practice*, Academic Press, **1991**.
- [349] B. J. Alder, T. E. Wainwright, *J. Chem. Phys.* **1959**, *31*, 459–466.
- [350] J. A. McCammon, B. R. Gelin, M. Karplus, *Nature* **1977**, *267*, 585–590.
- [351] H. Günther, *NMR Spectroscopy: Basic Principles, Concepts and Applications in Chemistry*, John Wiley & Sons, **2013**.
- [352] M. Biancalana, S. Koide, *Biochim. Biophys. Acta Proteins Proteom.* **2010**, *1804*, 1405–1412.
- [353] N. Amdursky, Y. Erez, D. Huppert, *Acc. Chem. Res.* **2012**, *45*, 1548–1557.
- [354] S. Noël, S. Cadet, E. Gras, C. Hureau, *Chem. Soc. Rev.* **2013**, *42*, 7747–7762.
- [355] G. Meisl, J. B. Kirkegaard, P. Arosio, T. C. T. Michaels, M. Vendruscolo, C. M. Dobson, S. Linse, T. P. J. Knowles, *Nat. Protoc.* **2016**, *11*, 252–272.
- [356] G. D. Fasman, Ed. , *Circular Dichroism and the Conformational Analysis of*

Biomolecules, Springer Science+Business Media, **1996**.

- [357] N. J. Greenfield, *Nat. Protoc.* **2007**, *1*, 2876–2890.
- [358] A. Micsonai, F. Wien, L. Kernya, Y. H. Lee, Y. Goto, M. Réfrégiers, J. Kardos, *Proc. Natl. Acad. Sci. U. S. A.* **2015**, *112*, E3095–E3103.
- [359] S. M. Kelly, T. J. Jess, N. C. Price, *Biochim. Biophys. Acta Proteins Proteom.* **2005**, *1751*, 119–139.
- [360] N. Sreerama, R. W. Woody, *Anal. Biochem.* **2000**, *287*, 252–260.
- [361] A. Micsonai, F. Wien, É. Bulyáki, J. Kun, É. Moussong, Y. H. Lee, Y. Goto, M. Réfrégiers, J. Kardos, *Nucleic Acids Res.* **2018**, *46*, W315–W322.
- [362] W. Gosal, S. Myers, S. Radford, N. Thomson, *Protein Pept. Lett.* **2006**, *13*, 261–270.
- [363] J. Mou, D. M. Czajkowsky, Y. Zhang, Z. Shao, *FEBS Lett.* **1995**, *371*, 279–282.
- [364] A. R. Kirby, A. P. Gunning, K. W. Waldron, V. J. Morris, A. Ng, *Biophys. J.* **1996**, *70*, 1138–1143.
- [365] B. P. Jena, J. K. H. Hörber, Eds., *Atomic Force Microscopy in Cell Biology*, Academic Press, **2002**.
- [366] F. S. Ruggeri, F. Benedetti, T. P. J. Knowles, H. A. Lashuel, S. Sekatskii, G. Dietler, *Proc. Natl. Acad. Sci. U. S. A.* **2018**, *115*, 7230–7235.
- [367] Tim Mosmann, *J. Immunol. Methods* **1983**, *65*, 55–63.
- [368] E. Chacon, D. Acosta, J. Lemasters, in *Vitr. Methods Pharm. Res.* (Eds.: J. V. Castell, M.J. Gómez-Lechón), Academic Press, **1996**, pp. 209–223.
- [369] R. Jevprasesphant, J. Penny, R. Jalal, D. Attwood, N. B. McKeown, A. D’Emanuele, *Int. J. Pharm.* **2003**, *252*, 263–266.
- [370] N. Jambunathan, in *Plant Stress Tolerance* (Ed.: R. Sunkar), Humana Press, **2010**, pp. 291–297.
- [371] S. I. Dikalov, D. G. Harrison, *Antioxidants Redox Signal.* **2014**, *20*, 372–382.
- [372] H. Pössel, H. Noack, W. Augustin, G. Keilhoff, G. Wolf, *FEBS Lett.* **1997**, *416*, 175–178.
- [373] C. R. b Istavan Vermes, Clemens Haanen, Helga Steffens-Nakken, *J. Immunol. Methods* **1995**, *184*, 39–51.
- [374] H. Ihre, A. Hult, *Macromolecules* **1998**, *31*, 4061–4068.
- [375] J. Song, B. K. Cho, *Bull. Korean Chem. Soc.* **2013**, *34*, 23–24.
- [376] D. Quémener, T. P. Davis, C. Barner-Kowollik, M. H. Stenzel, *Chem. Commun.* **2006**, 5051–5053.
- [377] P. O. Löwdin, *Adv. Quantum Chem.* **1970**, *5*, 185–199.
- [378] M. W. Schmidt, K. K. Baldrige, J. A. Boatz, S. T. Elbert, M. S. Gordon, J. H. Jensen,

- S. Koseki, N. Matsunaga, K. A. Nguyen, S. Su, et al., *J. Comput. Chem.* **1993**, *14*, 1347–1363.
- [379] P. Friedel, unpublished software RESMAIN, *version 0.3.2*, © **2019**.
- [380] D. Van Der Spoel, E. Lindahl, B. Hess, G. Groenhof, A. E. Mark, H. J. C. Berendsen, *J. Comput. Chem.* **2005**, *26*, 1701–1718.
- [381] H. J. C. Berendsen, J. P. M. Postma, W. F. Van Gunsteren, A. Dinola, J. R. Haak, *J. Chem. Phys.* **1984**, *81*, 3684–3690.
- [382] A. Perelman, C. Wachtel, M. Cohen, S. Haupt, H. Shapiro, A. Tzur, *Cell Death Dis.* **2012**, *3*, e430-7.
- [383] E. Malmström, M. Johansson, A. Hult, *Macromolecules* **1995**, *28*, 1698–1703.
- [384] E. Malmström, A. Hult, *Macromolecules* **1996**, *29*, 1222–1228.
- [385] Z. Wei, L. Huang, L. Cui, X. Zhu, *Biomed. Pharmacother.* **2020**, *129*, 110420B.
- [386] E. Hatami, Y. Mu, D. N. Shields, S. C. Chauhan, S. Kumar, T. J. Cory, M. M. Yallapu, *Biochem. Biophys. Rep.* **2019**, *17*, 197–207.
- [387] K. Sugawara, G. Hirabayashi, N. Kamiya, H. Kuramitz, *Talanta* **2006**, *68*, 1176–1181.
- [388] M. L. Wolfenden, M. J. Cloninger, *Bioconjug. Chem.* **2006**, *17*, 958–966.
- [389] M. Lo Conte, M. J. Robb, Y. Hed, A. Marra, M. Malkoch, C. J. Hawker, A. Dondoni, *Polym. Chem.* **2011**, *49*, 4468–4475.
- [390] R. Nelson, M. R. Sawaya, M. Balbirnie, A. Madsen, C. Riek, R. Grothe, D. Eisenberg, *Nature* **2005**, *435*, 773–778.
- [391] C. S. Goldsbury, S. Wirtz, S. A. Mu, P. Wicki, U. Aebi, P. Frey, **2000**, *231*, 217–231.
- [392] J. Drzewińska, D. Appelhans, B. Voit, M. Bryszewska, B. Klajnert, *Biochem. Biophys. Res. Commun.* **2012**, *427*, 197–201.
- [393] M. Johansson, E. Malmstrom, A. Hult, *J. Polym. Sci. A Polym. Chem.* **1993**, *31*, 619–624.
- [394] M. Geisler, Funktionalisierung Und Wechselwirkungsuntersuchungen von Dendritischen Hybridstrukturen Mit Alzheimer-Amyloiden, B.Sc. Thesis, HTW Dresden, **2015**.
- [395] E. Žagar, M. Žigon, *Macromolecules* **2002**, *35*, 9913–9925.
- [396] E. Žagar, M. Žigon, *Prog. Polym. Sci.* **2011**, *36*, 53–88.
- [397] R. J. Abraham, M. Mobli, *Modelling 1H NMR Spectra of Organic Compounds: Theory, Applications and NMR Prediction Software*, John Wiley & Sons, **2008**.
- [398] W. F. van Gunsteren, H. J. C. Berendsen, *Angew. Chem., Int. Ed. Engl.* **1990**, *29*, 992–1023.

- [399] H. J. C. Berendsen, *Simulating the Physical World: Hierarchical Modeling from Quantum Mechanics to Fluid Dynamics*, Cambridge University Press, **2007**.
- [400] B. A. Berg, *Eur. Phys. J. Spec. Top.* **2017**, *226*, 551–565.
- [401] J. Caballero, H. Poblete, C. Navarro, J. H. Alzate-Morales, *J. Mol. Graph. Model.* **2013**, *39*, 71–78.
- [402] Y. Kim, Y. Kwak, R. Chang, *J. Phys. Chem. B* **2014**, *118*, 6792–6802.
- [403] J. Wang, R. M. Wolf, J. W. Caldwell, P. A. Kollman, D. A. Case, *J. Comput. Chem.* **2004**, *25*, 1157–1174.
- [404] B. R. Brooks, R. E. Bruccoleri, B. D. Olafson, D. J. States, S. Swaminathan, M. Karplus, *J. Comput. Chem.* **1983**, *4*, 187–217.
- [405] S. L. Mayo, B. D. Olafson, W. A. Goddard, *J. Phys. Chem.* **1990**, *94*, 8897–8909.
- [406] S. Lifson, A. T. Hagler, P. Dauber, *J. Am. Chem. Soc.* **1979**, *101*, 5111–5121.
- [407] S. J. Weiner, P. A. Kollman, U. C. Singh, D. A. Case, C. Ghio, G. Alagona, S. Profeta, P. Weiner, *J. Am. Chem. Soc.* **1984**, *106*, 765–784.
- [408] S. Boye, H. Komber, P. Friedel, A. Lederer, *Polymer* **2010**, *51*, 4110–4120.
- [409] J. E. Gillam, C. E. Macphee, *J. Phys. Condens. Matter* **2013**, *25*, 373101.
- [410] M. Sunde, C. Blake, *Adv. Protein Chem.* **1997**, *50*, 129.
- [411] S. Giorgetti, C. Greco, P. Tortora, F. A. Aprile, *Int. J. Mol. Sci.* **2018**, *19*, 2677.
- [412] H. Levine, *Protein Sci.* **1993**, *2*, 404–410.
- [413] M. R. H. Krebs, E. H. C. Bromley, A. M. Donald, *J. Struct. Biol.* **2005**, *149*, 30–37.
- [414] B. Klajnert, M. Cortijo-Arellano, J. Cladera, J. P. Majoral, A. M. Caminade, M. Bryszewska, *Biochem. Biophys. Res. Commun.* **2007**, *364*, 20–25.
- [415] A. J. Dear, G. Meisl, T. C. T. Michaels, M. R. Zimmermann, S. Linse, T. P. J. Knowles, *J. Chem. Phys.* **2020**, *152*, 045101.
- [416] T. P. J. Knowles, C. A. Waudby, G. L. Devlin, S. I. A. Cohen, A. Aguzzi, M. Vendruscolo, E. M. Terentjev, M. E. Welland, C. M. Dobson, *Science* **2009**, *326*, 1533–1537.
- [417] A. K. Buell, C. Galvagnion, R. Gaspar, E. Sparr, M. Vendruscolo, T. P. J. Knowles, S. Linse, C. M. Dobson, *Proc. Natl. Acad. Sci. U. S. A.* **2014**, *111*, 7671–7676.
- [418] G. Meisl, J. B. Kirkegaard, P. Arosio, T. C. T. Michaels, M. Vendruscolo, C. M. Dobson, S. Linse, T. P. J. Knowles, *Nat. Protoc. SI* **2016**, *11*, 252–272.
- [419] G. Meisl, X. Yang, E. Hellstrand, B. Frohm, J. B. Kirkegaard, S. I. A. Cohen, C. M. Dobson, S. Linse, T. P. J. Knowles, *Proc. Natl. Acad. Sci. U. S. A.* **2014**, *111*, 9384–9389.
- [420] O. Klementieva, K. Willén, I. Martinsson, B. Israelsson, A. Engdahl, J. Cladera, P. Uvdal, G. K. Gouras, *Nat. Commun.* **2017**, *8*, 1–9.

- [421] A. Jabs, Jena Library of Biological Macromolecules, “Determination of Secondary Structure in Proteins by Fourier Transform Infrared Spectroscopy (FTIR),” http://jenalib.leibniz-fli.de/ImgLibDoc/ftir/IMAGE_FTIR.html, accessed on 23rd June 2022.
- [422] F. S. Ruggeri, G. Longo, S. Faggiano, E. Lipiec, A. Pastore, G. Dietler, *Nat. Commun.* **2015**, *6*, 1–9.
- [423] P. Hortschansky, V. Schroeckh, T. Christopeit, G. Zandomenighi, M. Fändrich, *Protein Sci.* **2005**, *14*, 1753–1759.
- [424] M. Dong, M. B. Hovgaard, W. Mamdouh, S. Xu, D. E. Otzen, F. Besenbacher, *Nanotechnology* **2008**, *19*, 384013.
- [425] N. Benseny-Cases, M. Cócera, J. Cladera, *Biochem. Biophys. Res. Commun.* **2007**, *361*, 916–921.
- [426] S. Linse, *Pure Appl. Chem.* **2019**, *91*, 211–229.
- [427] A. Munke, J. Persson, T. Weiffert, E. De Genst, G. Meisl, P. Arosio, A. Carnerup, C. M. Dobson, M. Vendruscolo, T. P. J. Knowles, et al., *Proc. Natl. Acad. Sci. U. S. A.* **2017**, *114*, 6444–6449.
- [428] S. M. Kelly, T. J. Jess, N. C. Price, *Biochim. Biophys. Acta Proteins Proteom.* **2005**, *1751*, 119–139.
- [429] F. S. Ruggeri, F. Benedetti, T. P. Knowles, H. A. Lashuel, S. Sekatskii, G. Dietler, *Proc. Natl. Acad. Sci. U. S. A.* **2018**, *115*, 7230–7235.
- [430] S. Krysiak, S. Liese, R. R. Netz, T. Hugel, *J. Am. Chem. Soc.* **2014**, *136*, 688–697.
- [431] J. Adamcik, J. M. Jung, J. Flakowski, P. De Los Rios, G. Dietler, R. Mezzenga, *Nat. Nanotechnol.* **2010**, *5*, 423–428.
- [432] W. Lee, S. W. Lee, G. Lee, D. S. Yoon, *J. Alzheimer’s Dis. Rep.* **2018**, *2*, 41–49.
- [433] J. S. Pedersen, C. B. Andersen, D. E. Otzen, *FEBS J.* **2010**, *277*, 4591–4601.
- [434] R. Khurana, C. Ionescu-Zanetti, M. Pope, J. Li, L. Nielson, M. Ramirez-Alvarado, L. Regan, A. L. Fink, S. A. Carter, *Biophys. J.* **2003**, *85*, 1135–1144.
- [435] M. Fändrich, J. Meinhardt, N. Grigorieff, *Prion* **2009**, *3*, 89–93.
- [436] L. D. Aubrey, B. J. F. Blakeman, L. Lutter, C. J. Serpell, M. F. Tuite, L. C. Serpell, W. F. Xue, *Commun. Chem.* **2020**, *3*, 1–10.
- [437] W. Close, M. Neumann, A. Schmidt, M. Hora, K. Annamalai, M. Schmidt, B. Reif, V. Schmidt, N. Grigorieff, M. Fändrich, *Nat. Commun.* **2018**, *9*, 1–7.
- [438] N. Malik, R. Wiwattanapatapee, R. Klopsch, K. Lorenz, H. Frey, J. W. Weener, E. W. Meijer, W. Paulus, R. Duncan, *J. Control. Release* **2000**, *65*, 133–148.

Appendix

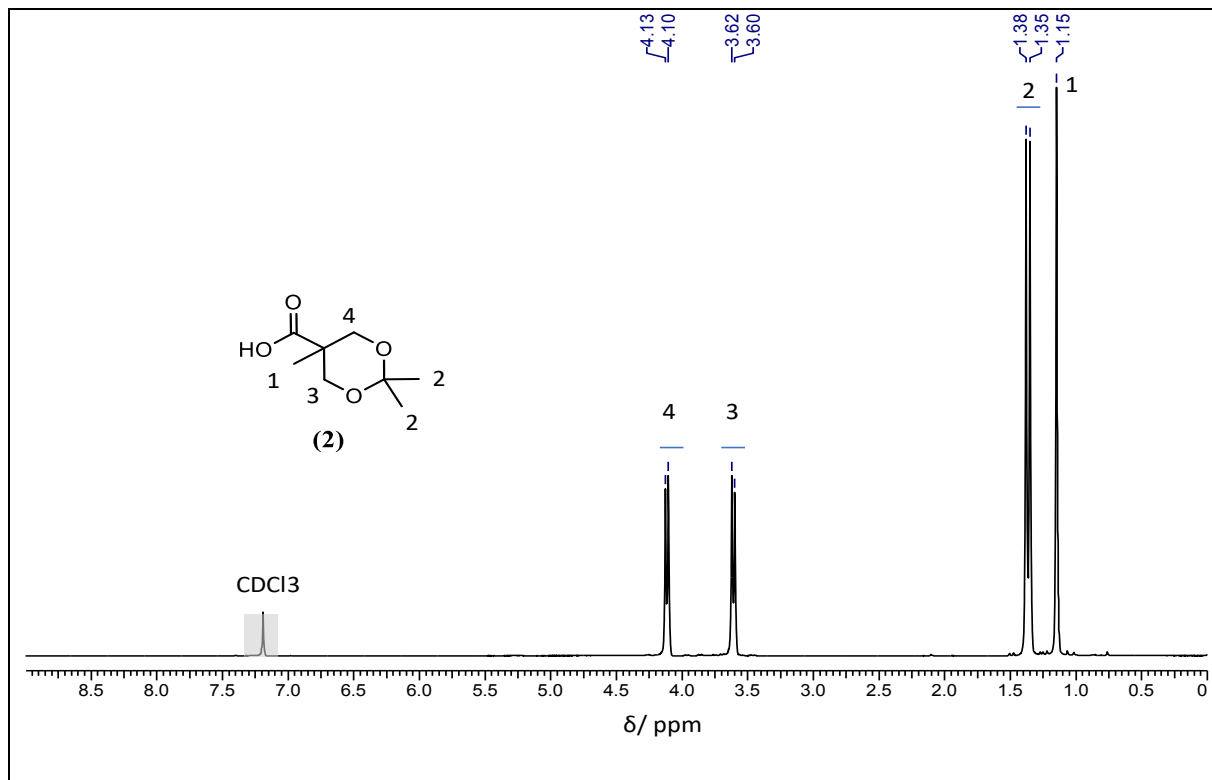


Figure 1: ^1H NMR spectrum of bis-MPA acetonide (2).

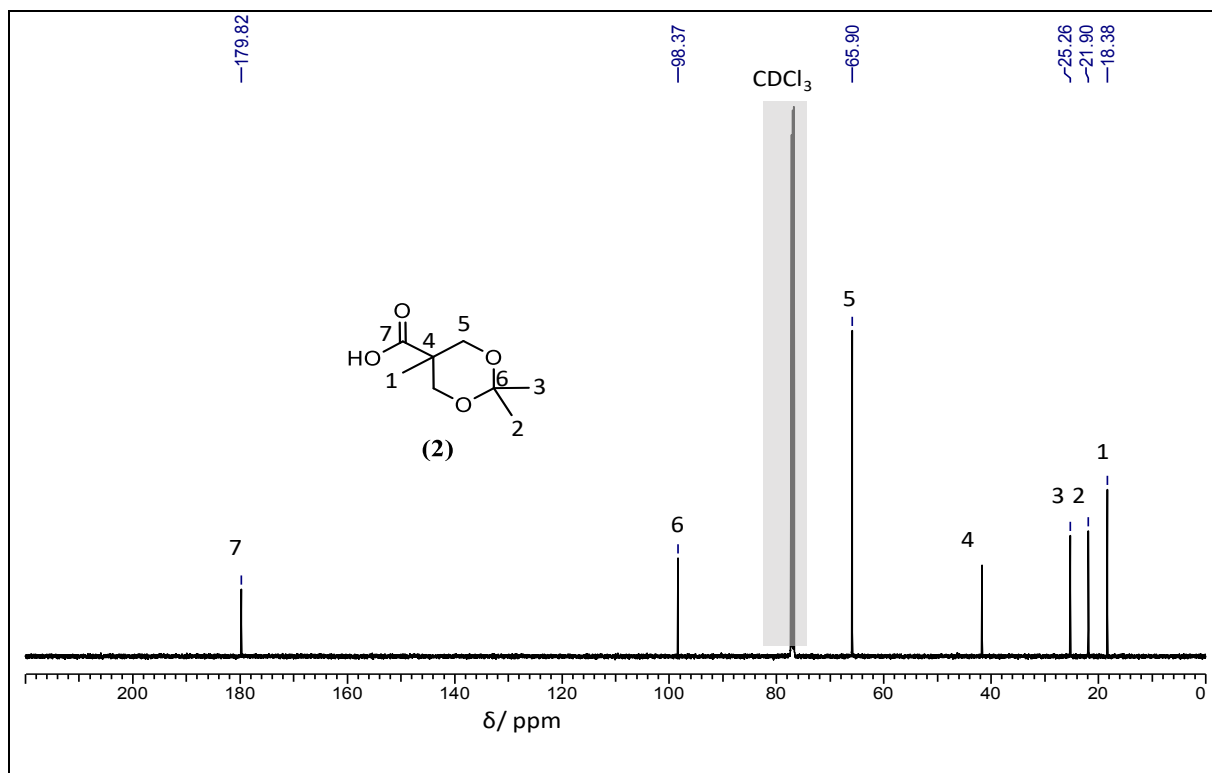
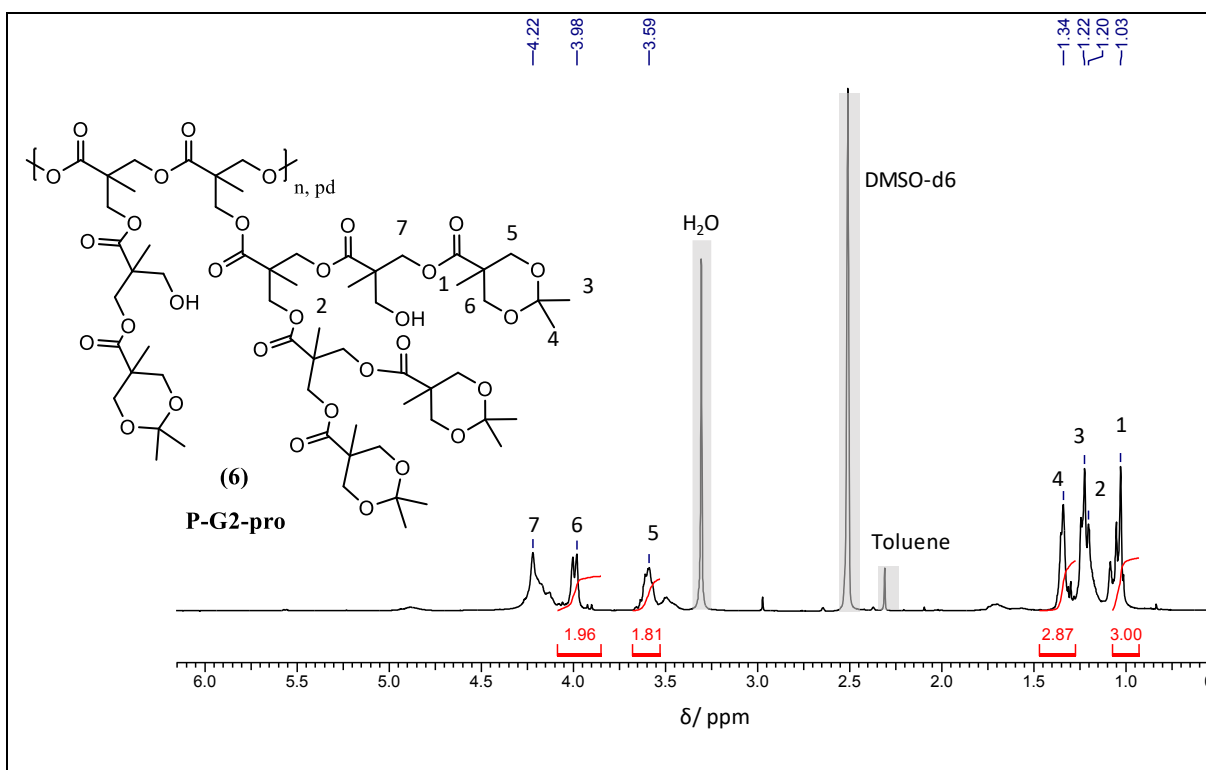
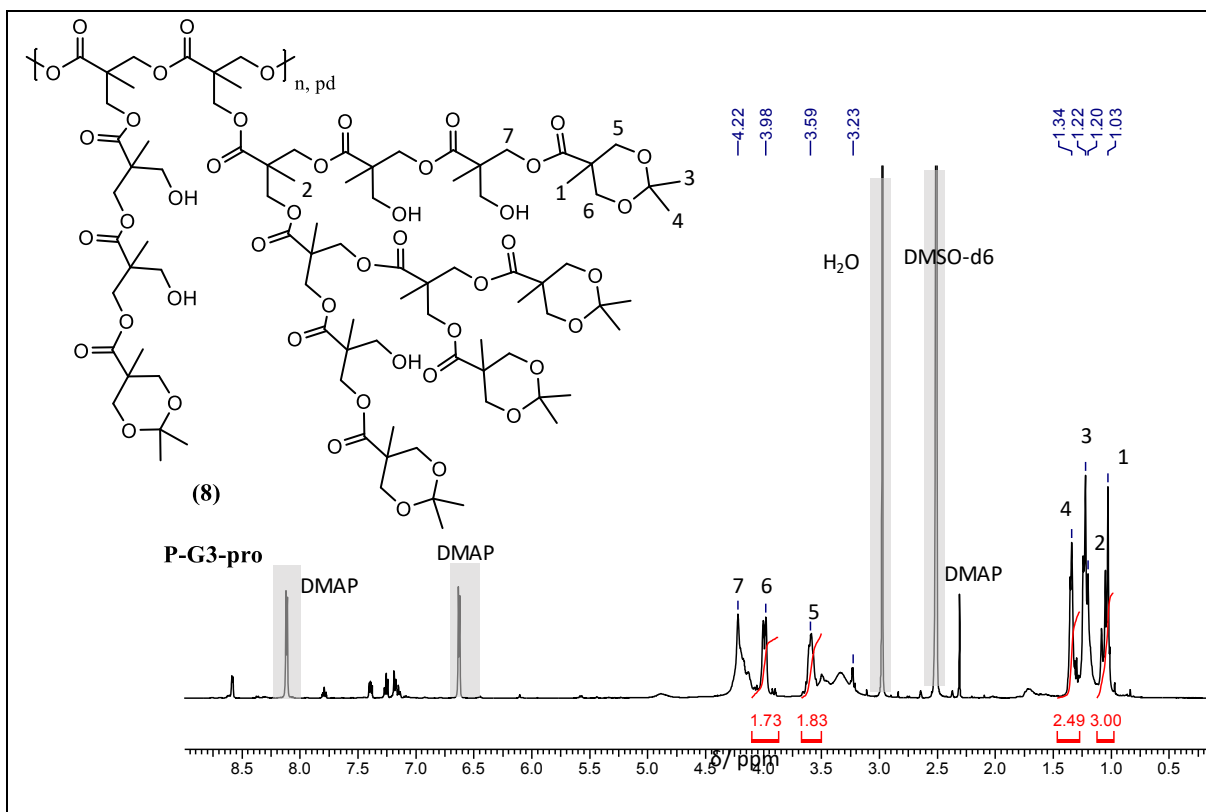


Figure 2: ^{13}C NMR spectrum of the bis-MPA acetonide (2).

**Figure 3:** ¹H NMR spectrum of P-G2-pro.**Figure 4:** ¹H NMR spectrum of P-G3-pro.

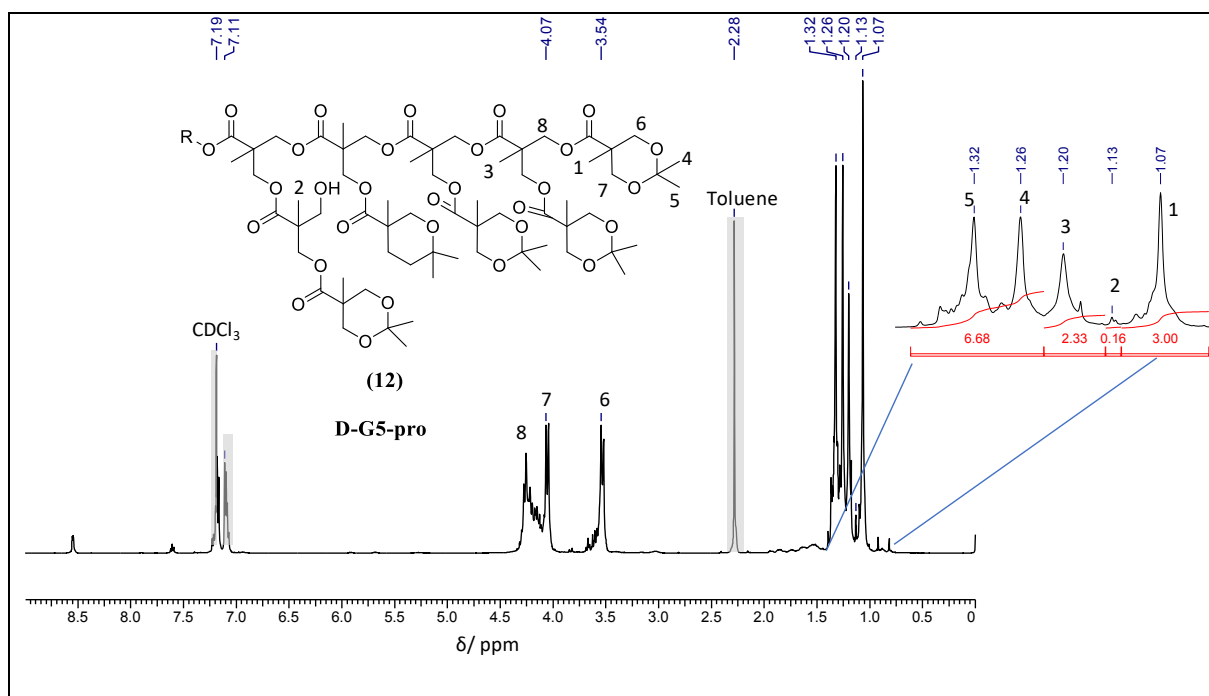


Figure 5: ^1H NMR spectrum of D-G5-pro.

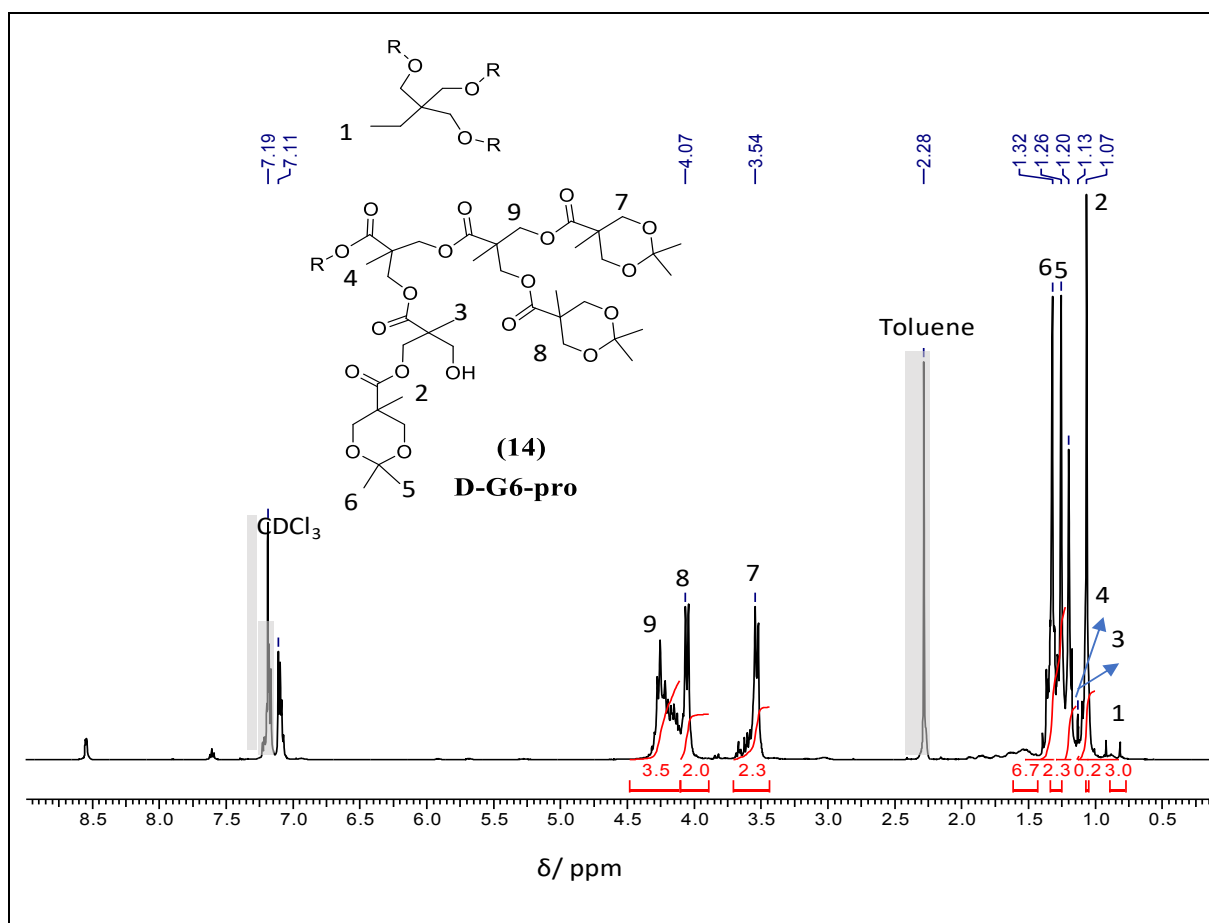


Figure 6: ^1H NMR spectrum of D-G6-pro.

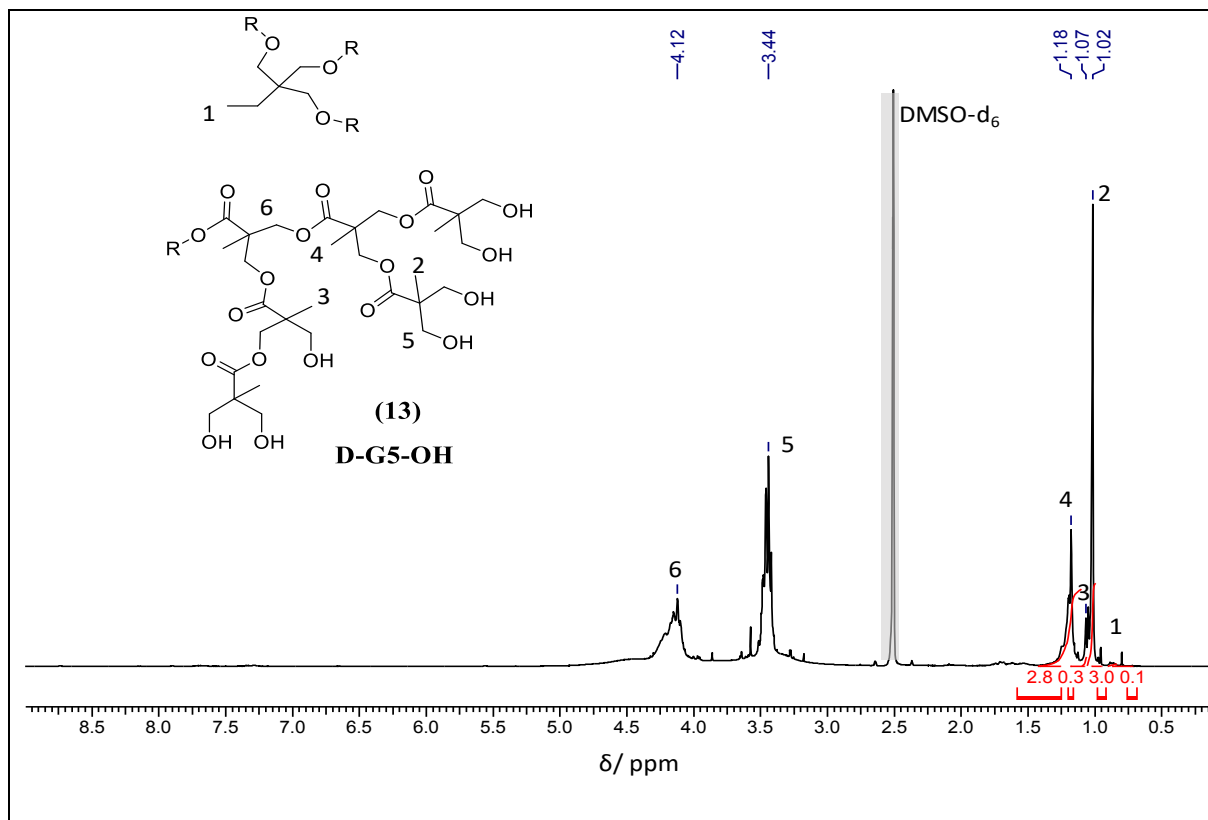


Figure 7: ^1H NMR spectrum of D-G5-OH.

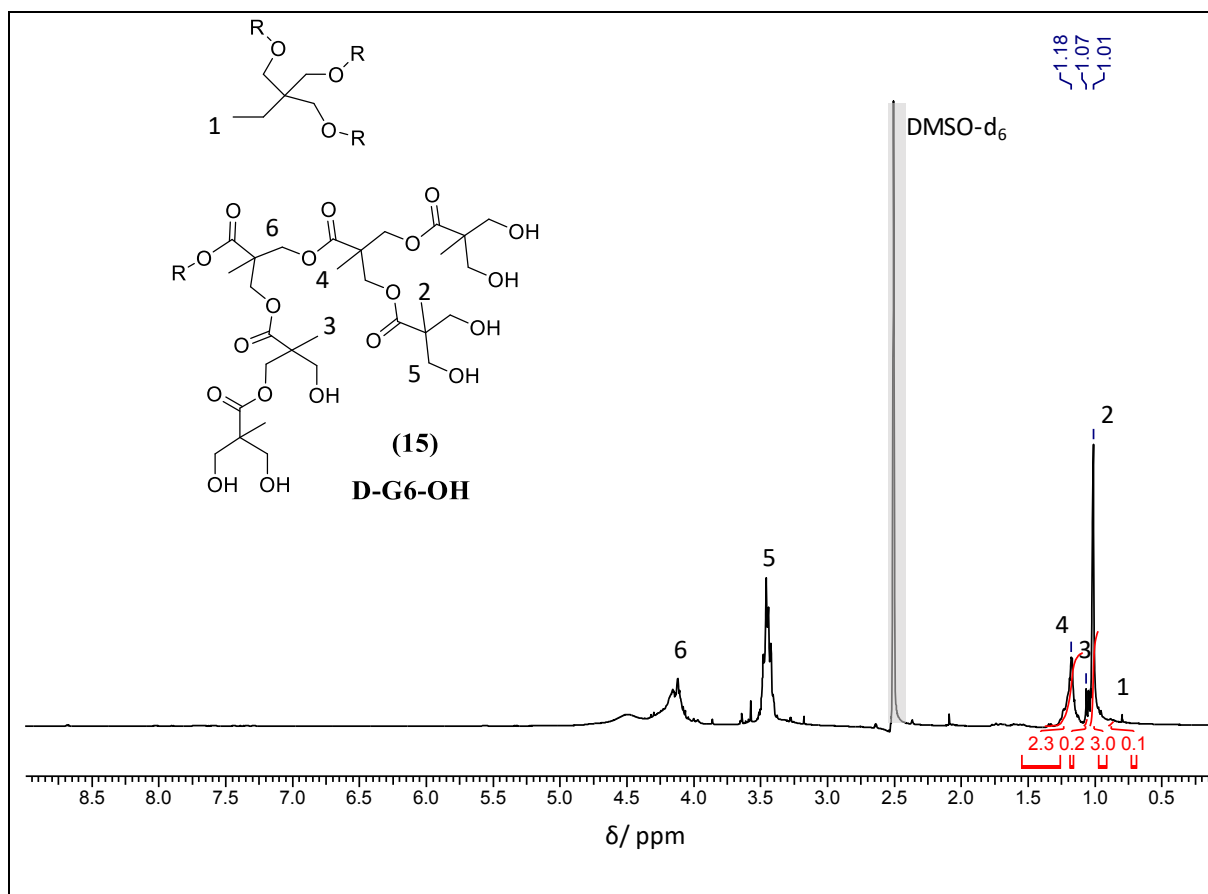


Figure 8: ^1H NMR spectrum of D-G6-OH.

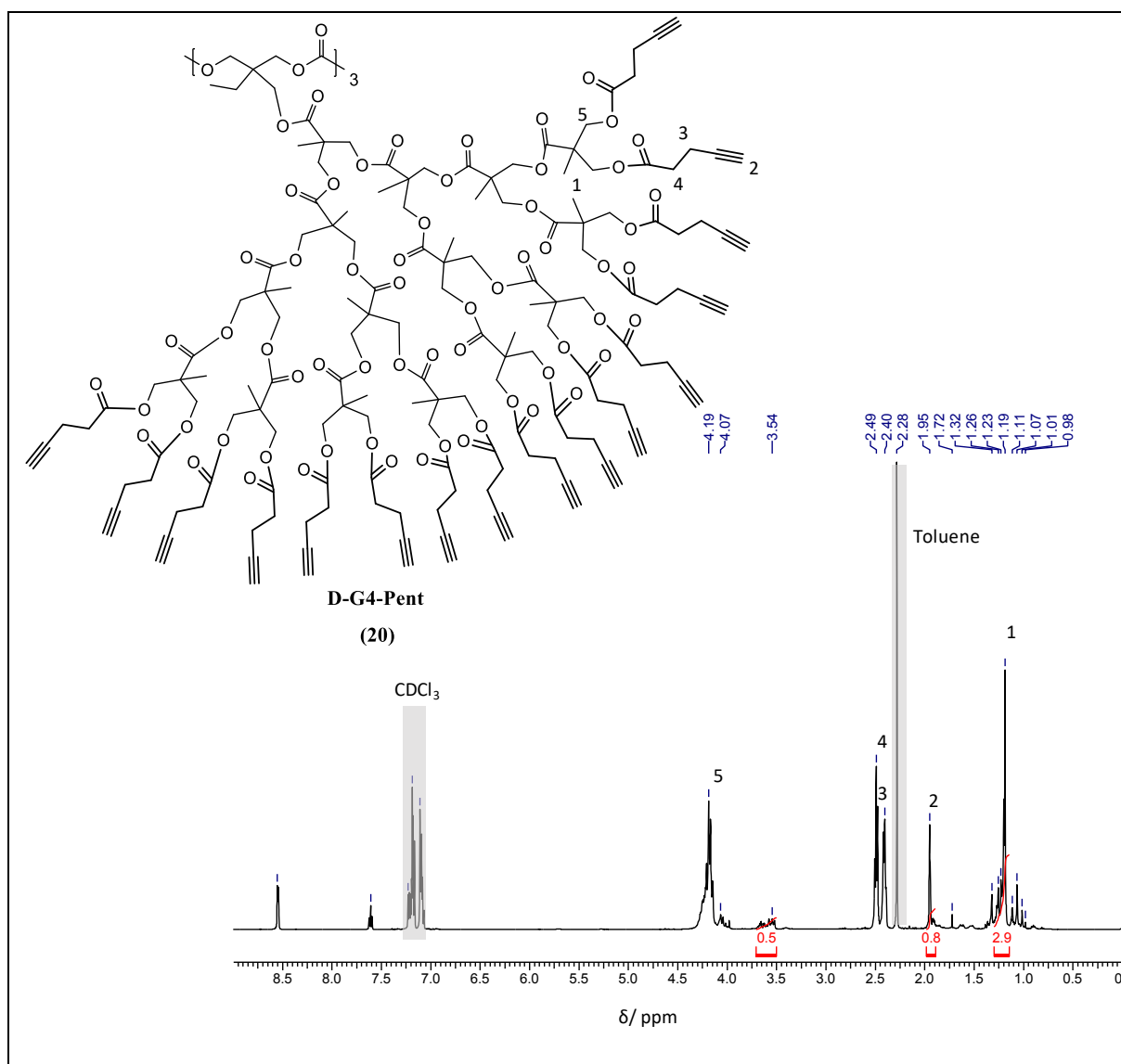


Figure 11: ¹H NMR spectrum of D-G4-pent.

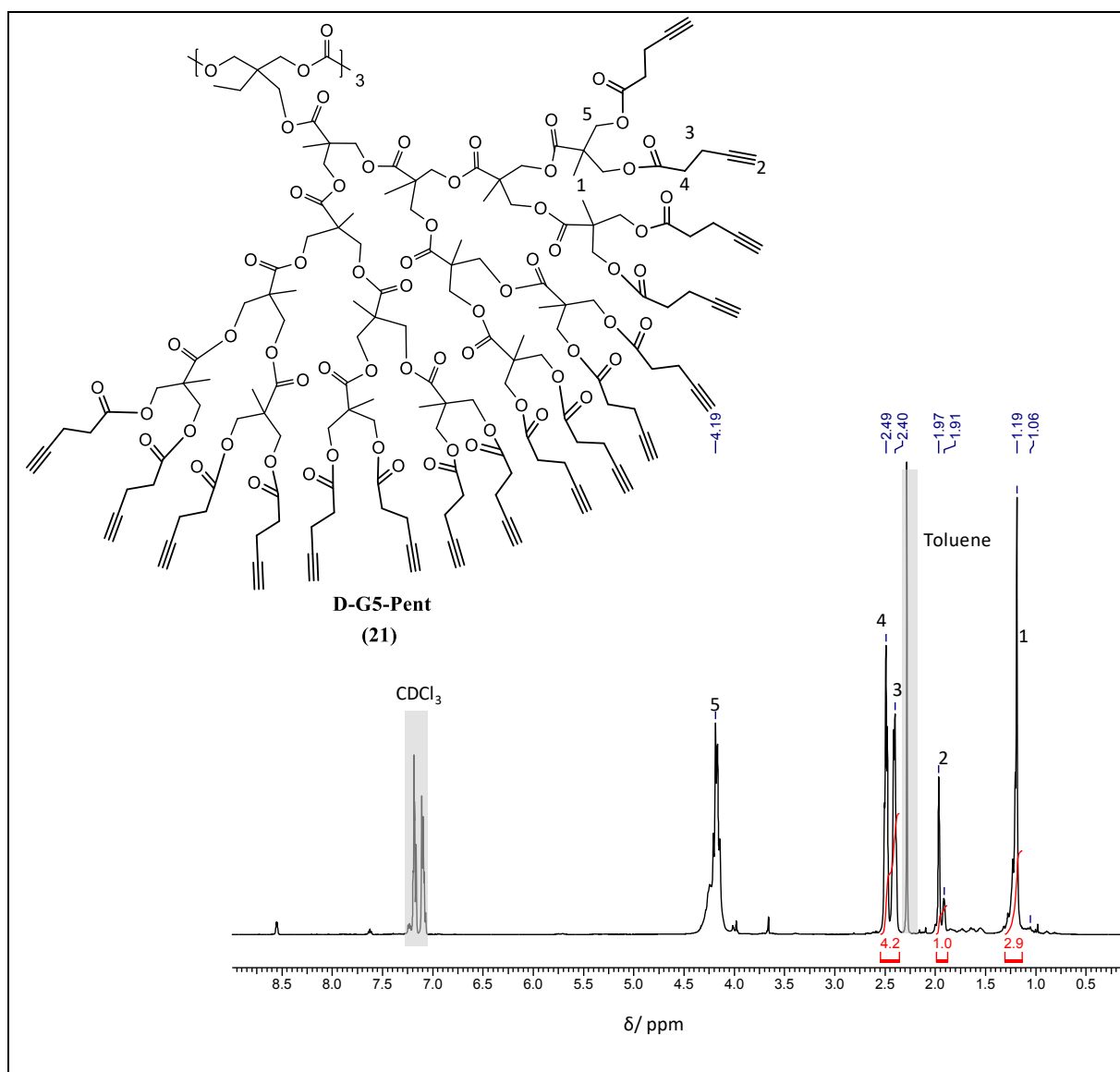


Figure 12: ¹H NMR spectrum of D-G5-pent.

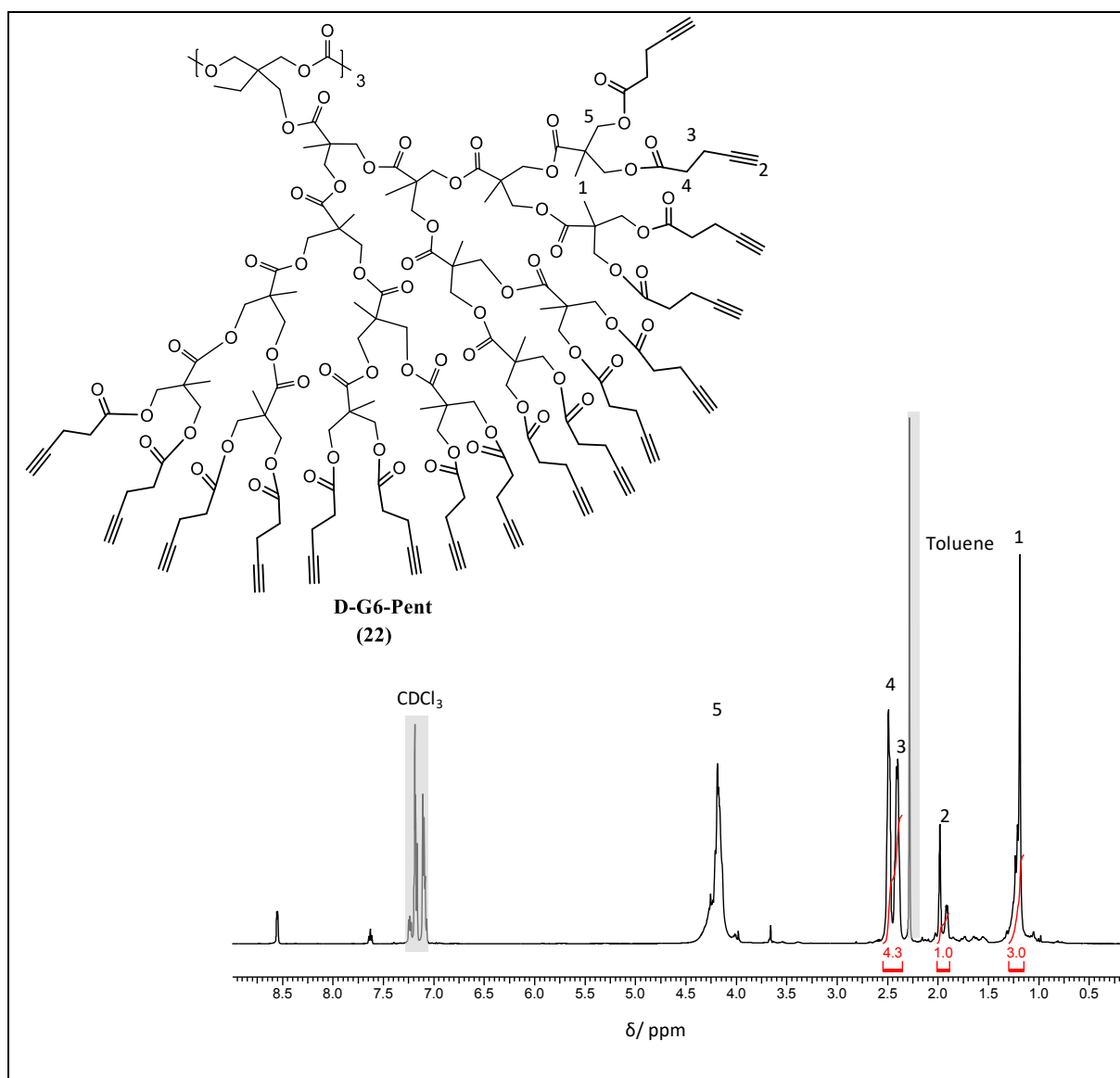


Figure 13: ¹H NMR spectrum of D-G6-pent.

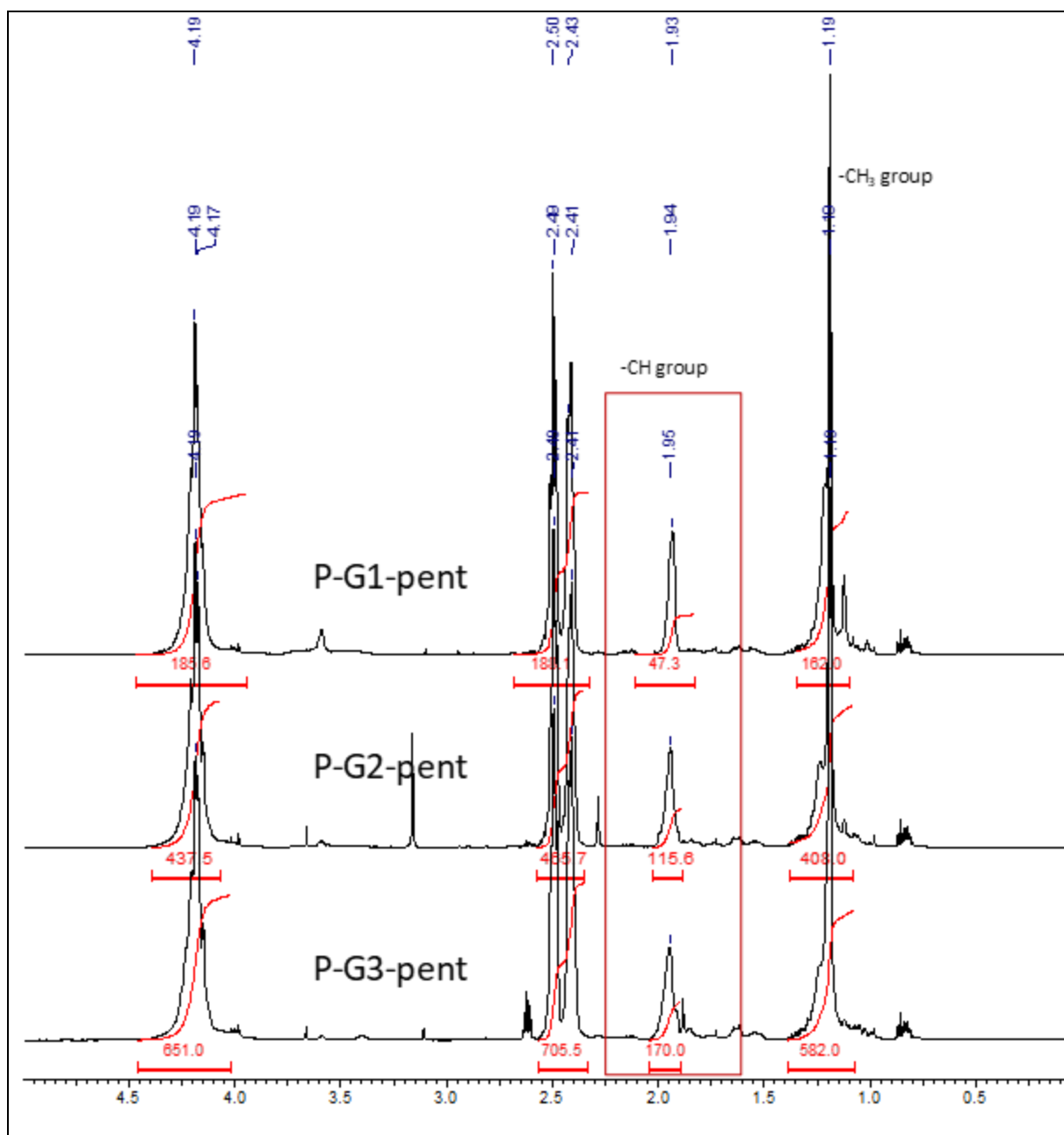


Figure 14: Calculation of degree of modification for P-G_x-pent (x=1, 2, 3).

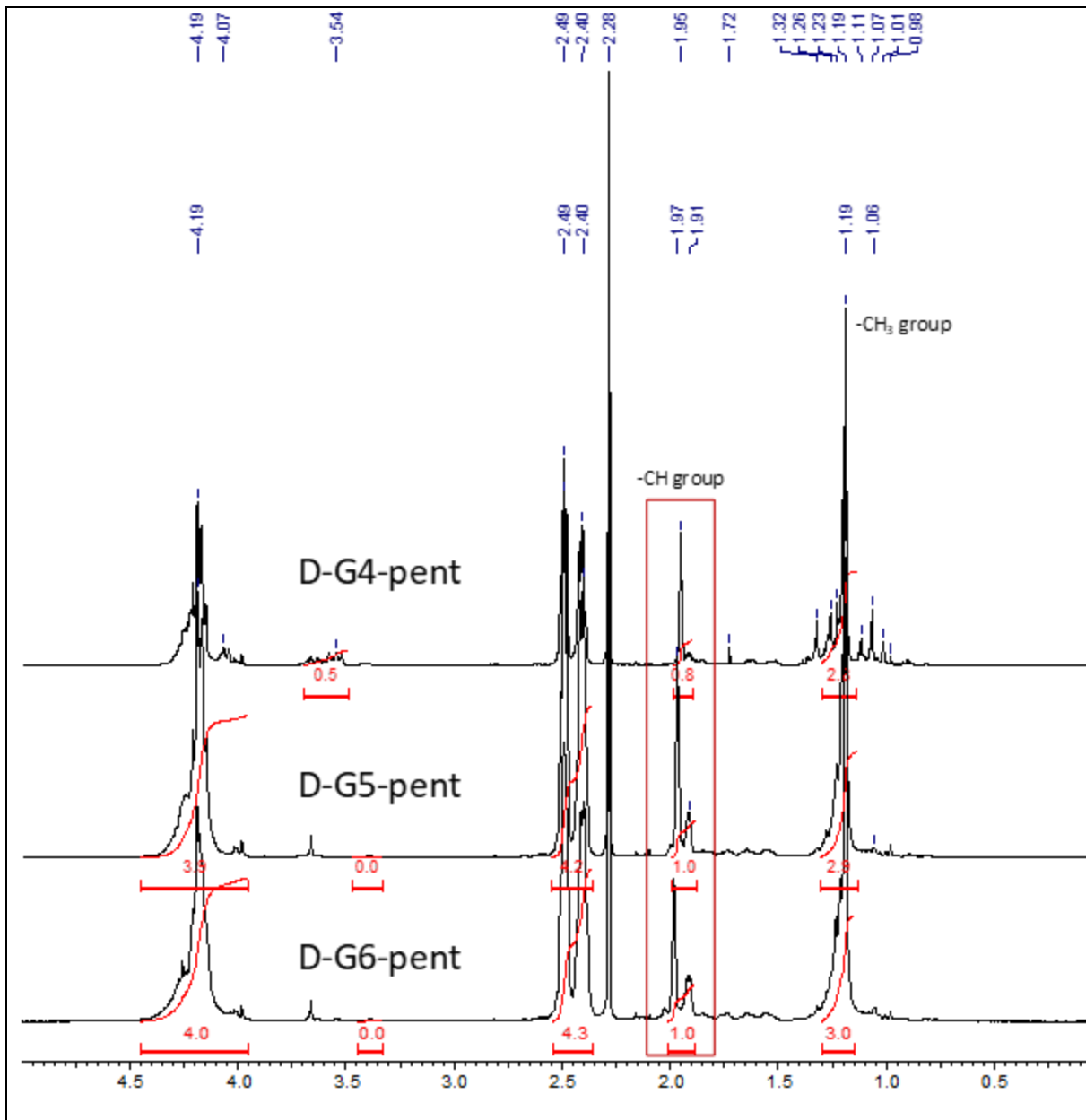
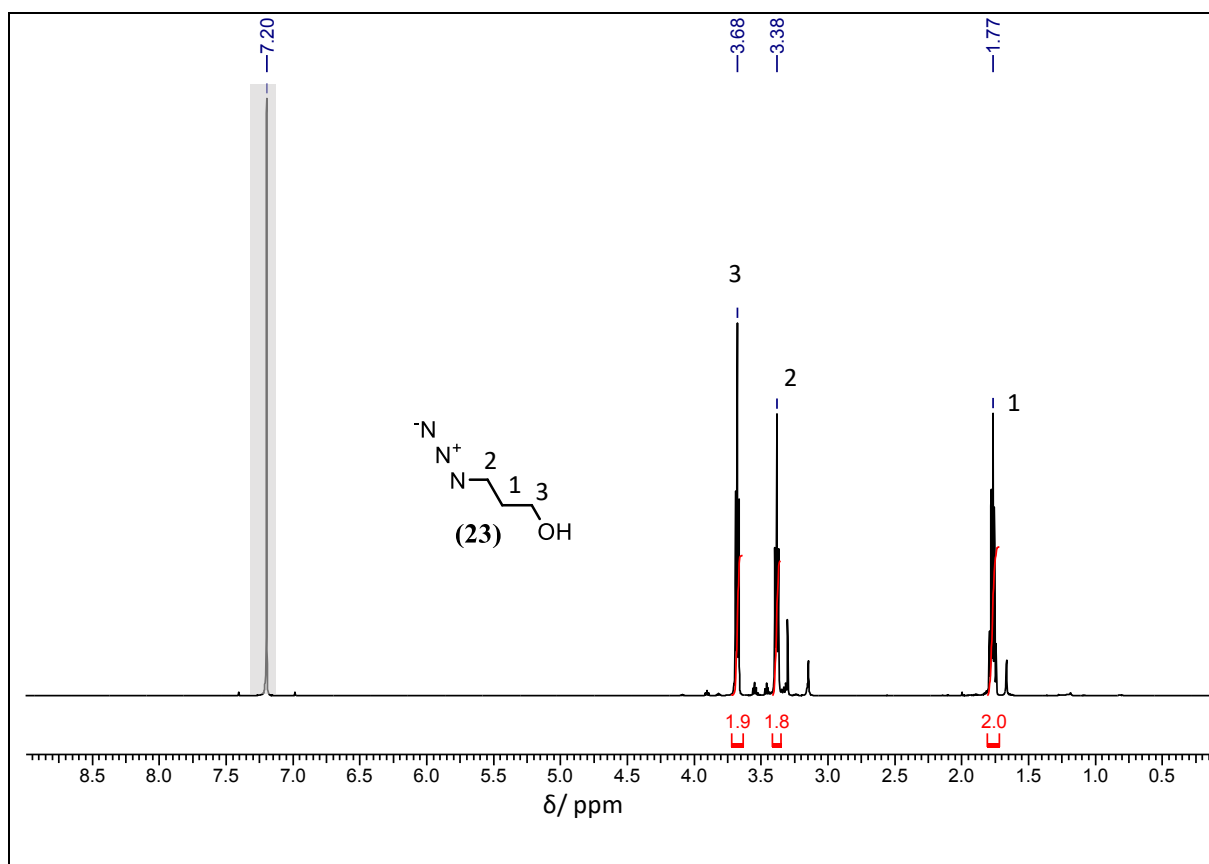
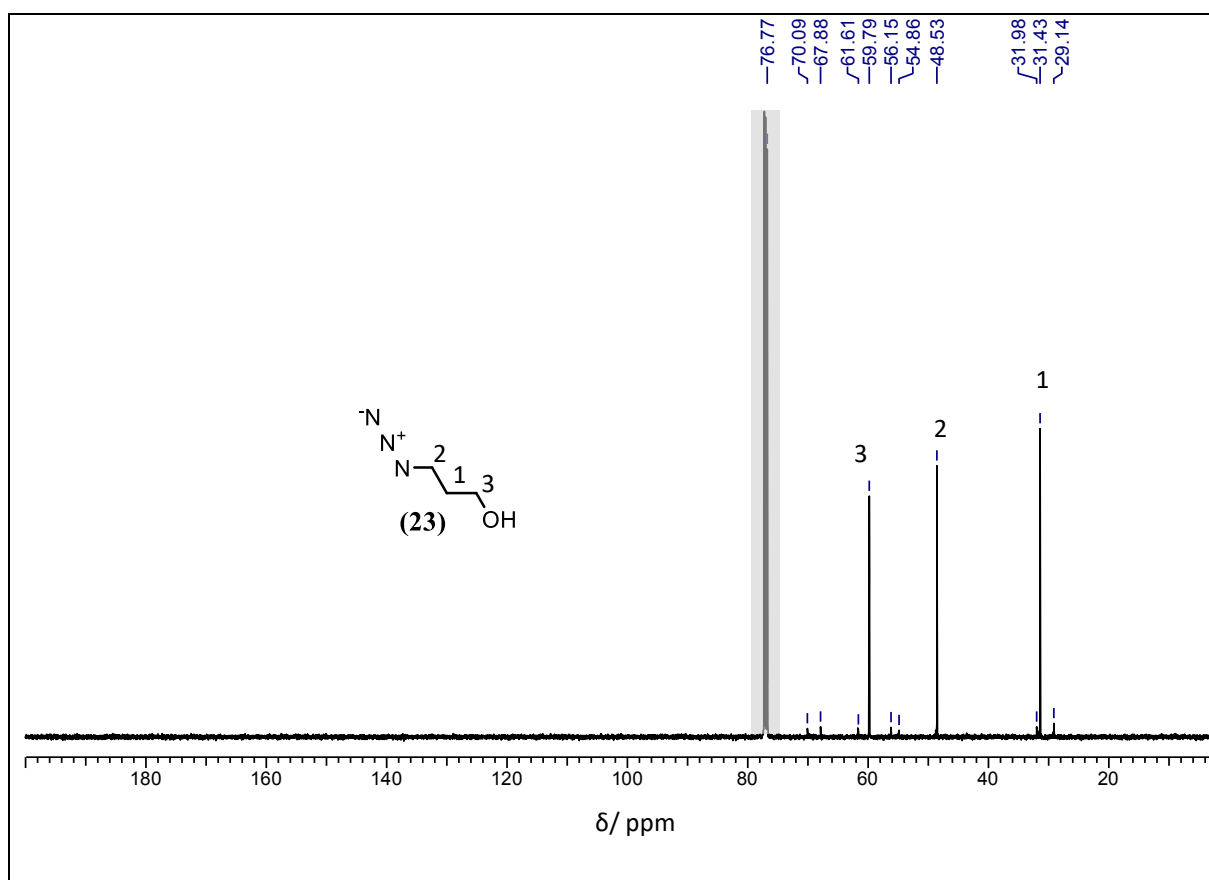


Figure 15: Calculation of degree of modification for D-G_x-pent (x=4, 5, 6).

**Figure 16:** ¹H NMR spectrum of azidopropanol.**Figure 17:** ¹³C NMR spectrum of azidopropanol.

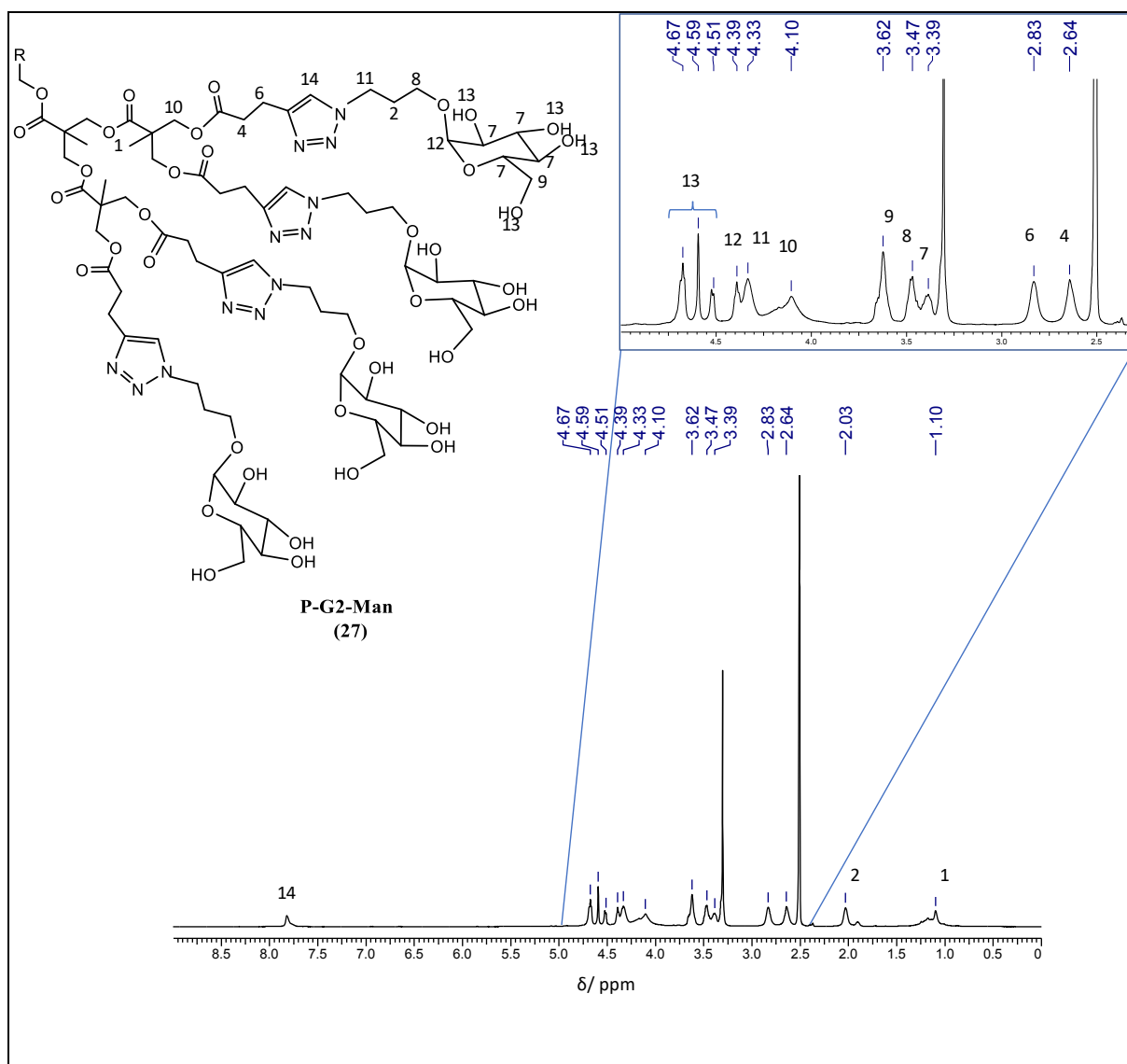


Figure 18: ¹H NMR spectrum of P-G2-Man.

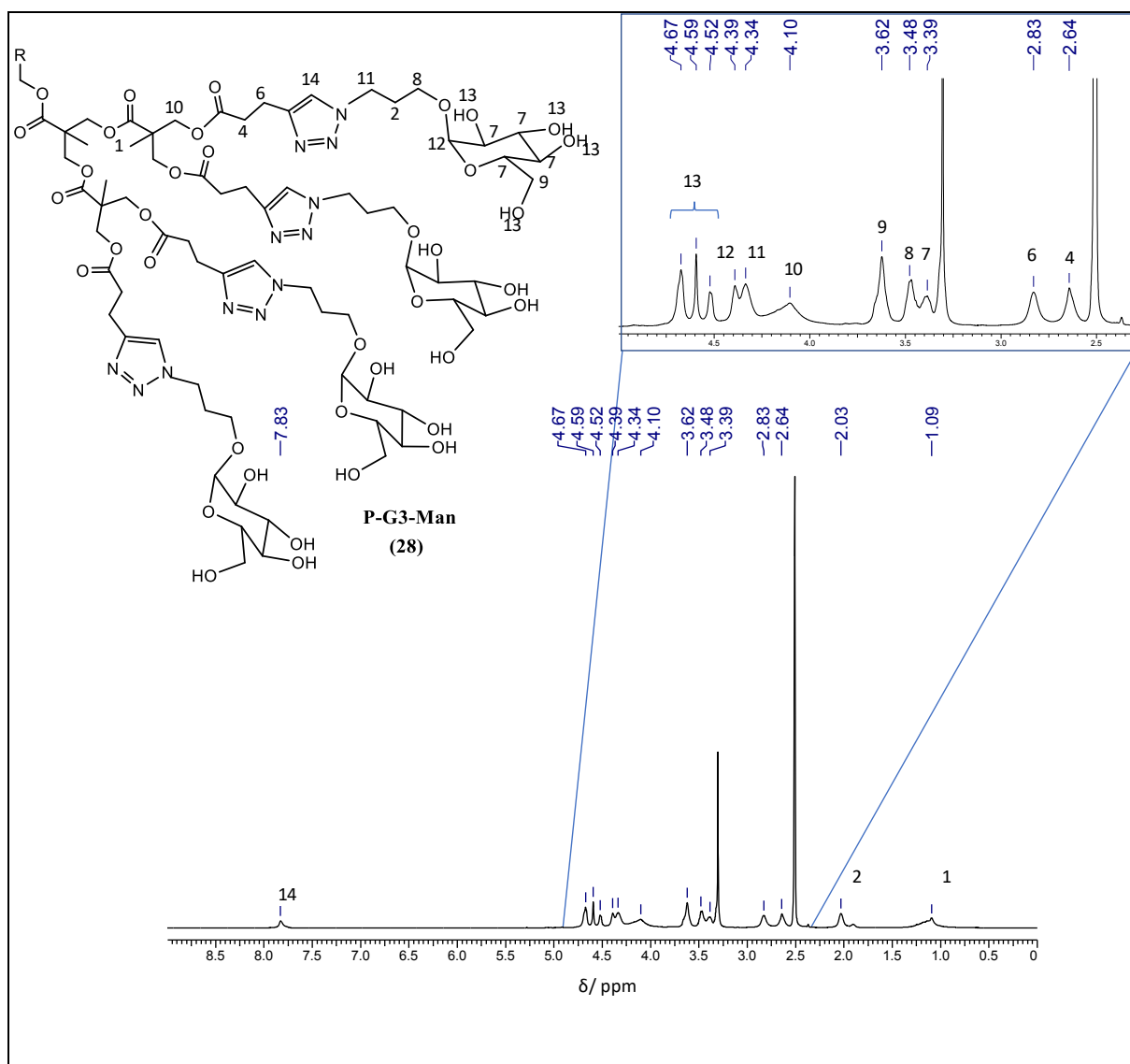


Figure 19: ¹H NMR spectrum of P-G3-Man.

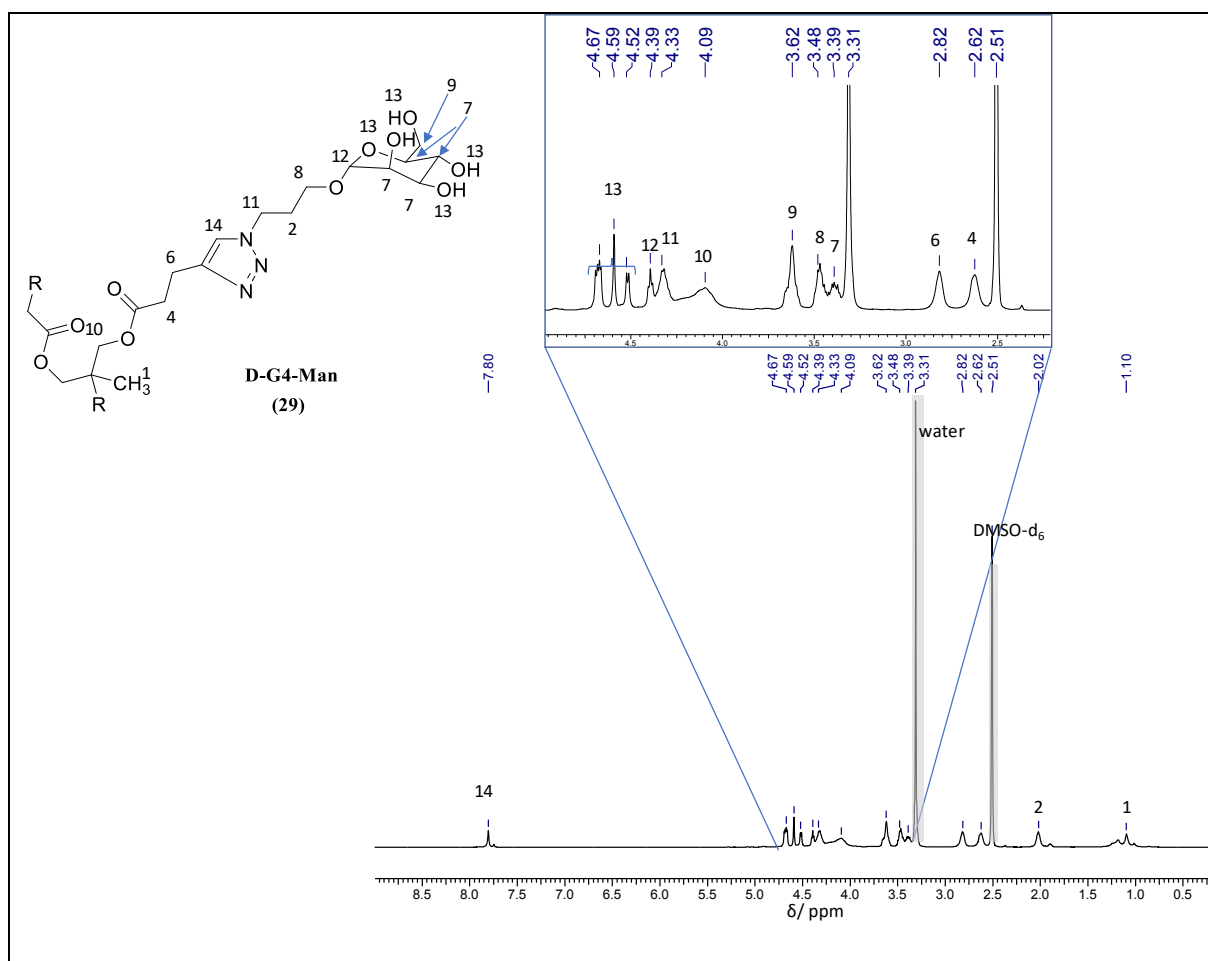


Figure 20: ¹H NMR spectrum of D-G4-Man.

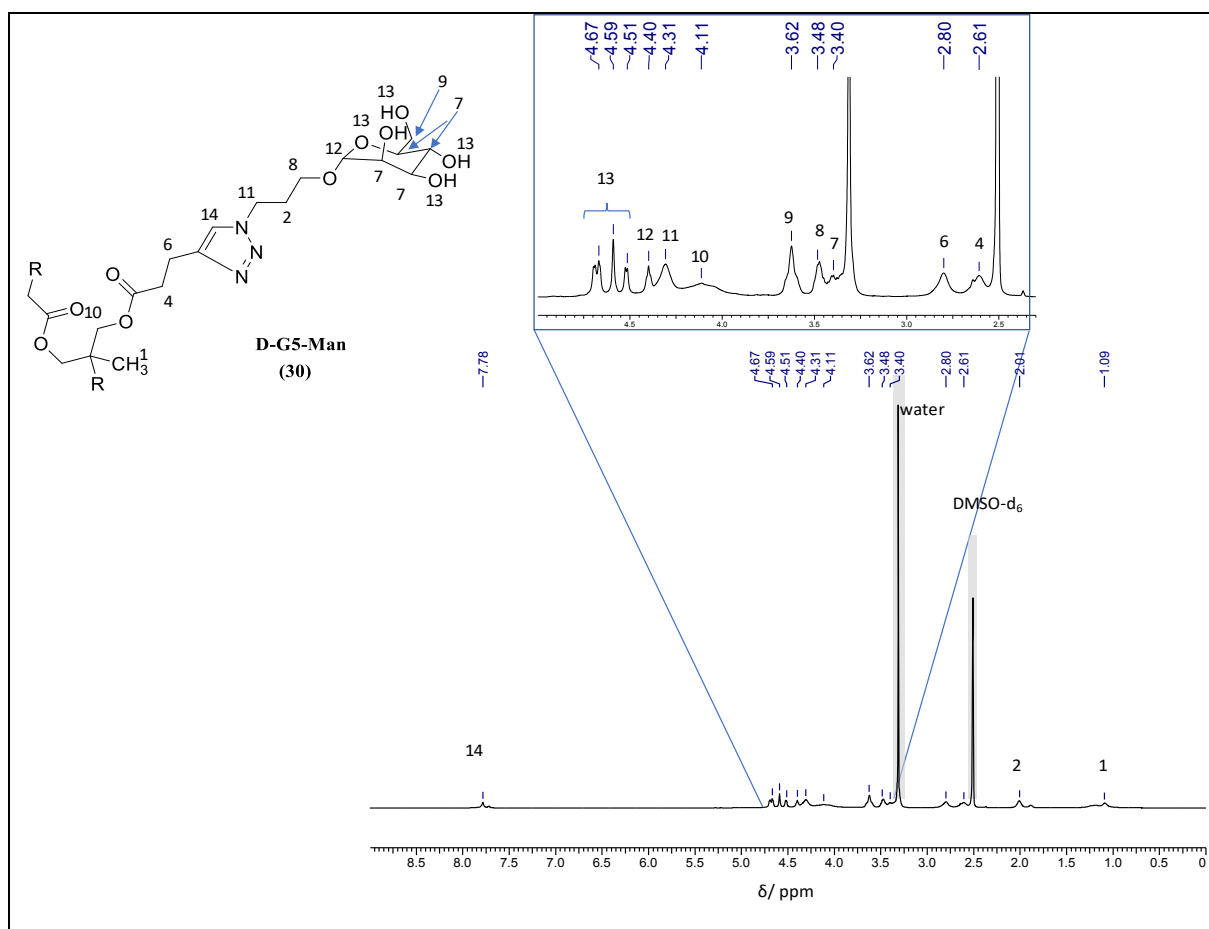
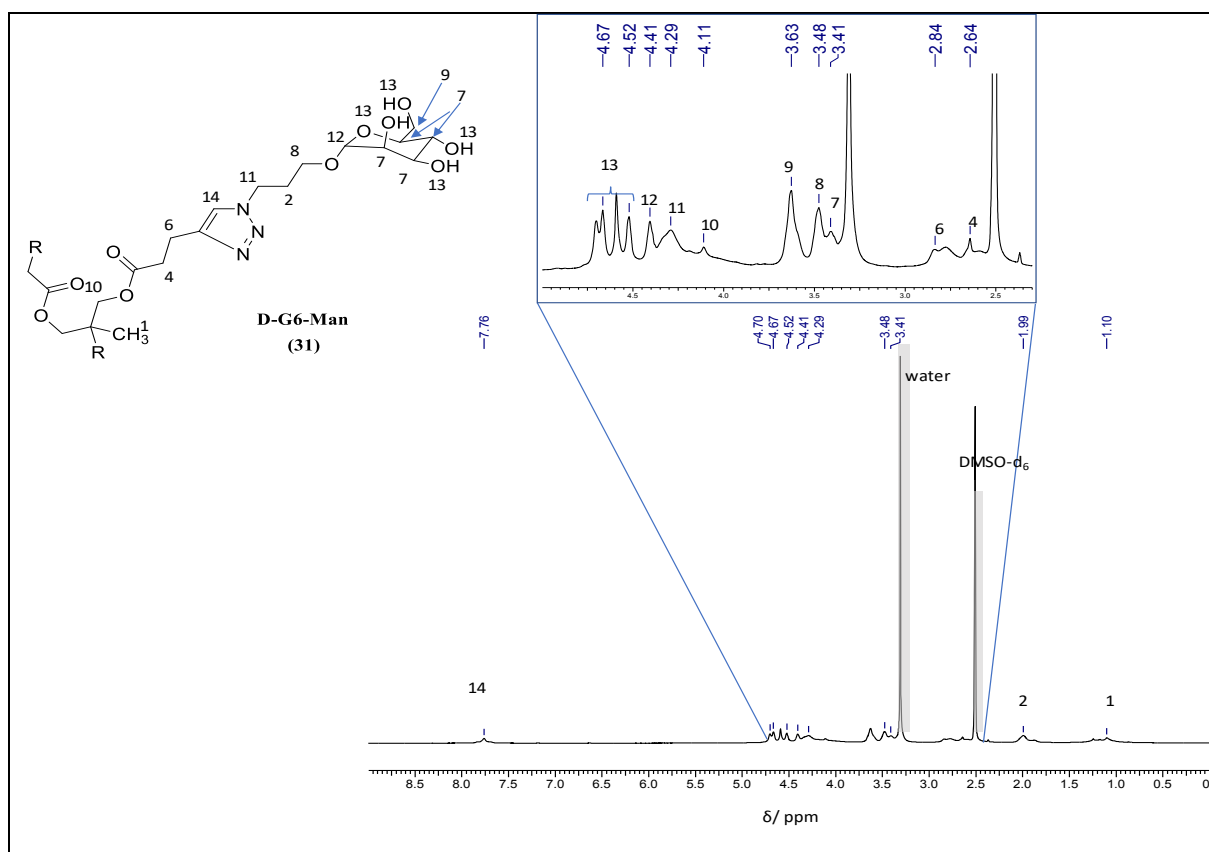
Figure 21: ^1H NMR spectrum of D-G5-Man.Figure 22: ^1H NMR spectrum of D-G6-Man.

Table 1: Mass fraction of aggregates determined from RI detector signals in AF4.

Aggregate mass fraction (%)								
Samples	0 h	2 h	5 h	7 h	10 h	16 h	18 h	20 h
A β 1-40 (control)	0	36	66	91	91	92	96	97
A β 1-40 + P-G1-Man	0	2	16	19	20	26	31	22
A β 1-40 + P-G2-Man	1	1	3	5	7	7	10	10
A β 1-40 + P-G3-Man	0	5	10	9	17	18	18	18
A β 1-40 + D-G4-Man	0	14	15	22	42	51	56	61
A β 1-40 + D-G5-Man	3	5	14	21	49	55	47	37
A β 1-40 + D-G6-Man	0	1	5	9	9	12	13	13

Table 2: Total number of atoms from MD simulations.

Samples	Total number of atoms
P-G1-OH	947
P-G2-OH	1907
P-G3-OH	3827
D-G4-OH	743
D-G5-OH	1511
D-G6-OH	3047
P-G1-Man	3647
P-G2-Man	4697
P-G3-Man	8777
D-G4-Man	2768
D-G5-Man	5831
D-G6-Man	11687

Acknowledgements

This work would not have been possible in this form without the support of many people. Firstly, I would like to thank Prof. Dr. Voit for the opportunity to do my work and dissertation at the Leibniz Institute of Polymer Research Dresden e.V. Special thanks to Prof. Dr. Alben Lederer, who continuously looked after and supported me scientifically and was always there for a good advice even during the most difficult of times. During my entire PhD she made a lot of efforts and opened up many new avenues for me. I would also like to thank Dr. Dietmar Appelhans. He always provided constructive suggestions with his expertise in the complex features of protein studies. I would like to thank Technische Universität Dresden for financing my studies and The Graduate Academy, TU Dresden for making this possible. I am also thankful to TU Dresden for providing me the funds to travel for various international conferences in Europe and South Africa.

I would also like to thank the entire Polymer Separation Group at Center Macromolecular Structure Analysis in IPF, who were always hands on to advice and help. Particularly, Christina Harnisch (ex-colleague) and Petra Treppe for their valuable knowledge with GPC and AF4, respectively. A big thanks goes to Susanne Boye for not only, her AF4 expertise but keeping a cheerful atmosphere during tedious experiments in AF4 studies. She always provided very constructive and critical suggestions. Further, I would like to thank Peter Friedel for his valuable discussions and support in the theoretical knowledge of dendrimers and pseudodendrimers. I would also like to thank Dr. Andreas Janke for helping me in planning and carrying out AFM experiments. A special thanks goes to Dr. Anna Janaszewska in Department of General Biophysics, Lodz for carrying out cytotoxic studies and providing me a comfortable time during my short research stay. I am extremely grateful to Dr. Georg Meisl for the scientific discussions about the kinetic data of ThT experiments. I am also thankful to Clemens Wirth, for carrying a part of the synthesis. I sincerely thank Beate Marchlewski for providing all the administrative help. I am also thankful to Martin, Mahmoud and many other students who helped in any way during the laboratory work. Furthermore, I would also like to thank Dr. Malanin to ensure “lunch time” is punctually followed and there is continuous supply of coffee as well as scientific and non-scientific discussions. I would also like to say thanks to current and former colleagues of Polymer Separation Group (2017-2022) –Laura, Andrea, Johanna, Upenyu, Zanelle and Franziska for their positive vibes throughout my time as PhD student. Throughout my work I was guided and supported by several colleagues who helped me push my work forward. My heartfelt thanks go to all of them.

I am thankful to Kajari and Maudood for their fun times outside work. I also thank Welcome center of TU Dresden for organizing several events to make my early days in Germany, slightly better. I also thank International Office of TU Dresden for giving me the opportunity to mentor DAAD-IIT-MSP students, with whom I made many memories and lifelong friendships. Despite

Acknowledgements

being far away, Nasreen, Neetu and Jyoti, I am grateful for the friendship that I share with each one of you.

I am very grateful to Omar, my husband, for always having faith in my abilities and for his constant support during the rough times. I thank both of our families for their incredible love and support even after sitting miles apart. Lastly, my little daughter Nura who has been so patient with my schedule during the last year of PhD.

And above all, I thank Allah.

Versicherung

Hiermit versichere ich, dass ich die vorliegende Arbeit ohne unzulässige Hilfe Dritter und ohne Benutzung anderer als der angegebenen Hilfsmittel angefertigt habe; die aus fremden Quellen direkt oder indirekt übernommenen Gedanken sind als solche kenntlich gemacht. Die Arbeit wurde bisher weder im Inland noch im Ausland in gleicher oder ähnlicher Form einer anderen Prüfungsbehörde vorgelegt.

Die vorliegende Arbeit wurde unter der wissenschaftlichen Betreuung von Frau Prof. Brigitte Voit und Frau Prof. Alben Lederer in der Zeit von November 2017 bis Juli 2022 an der Technischen Universität Dresden und am Leibniz-Institut für Polymerforschung Dresden e. V. angefertigt.

Bislang haben keine weiteren Promotionsverfahren stattgefunden.

Hiermit erkenne ich die Promotionsordnung dem Bereich Mathematik und Naturwissenschaften der Technischen Universität Dresden in geänderter Fassung vom 23.05.2018 an.

Dresden, den 7. Juli 2022

Shamila Firdaus